

Dissertation
submitted to the
Combined Faculty of Mathematics, Engineering and Natural Sciences
of the Ruprecht-Karls-Universität of Heidelberg, Germany
for the degree of
Doctor of Natural Sciences

Put forward by
Hannes Keppler
born in Magdeburg, Germany
Oral examination: July 23, 2025

Aspects of Tensor Models and Tensor Field Theories

Referees: Prof. Dr. Răzvan Gurău
Prof. Dr. Johannes Walcher

Abstract

This thesis investigates random tensor models and their applications across quantum field theory. Originating in quantum gravity studies, tensor models provide a framework for generating discrete random geometries and have connections to several other fields, including topology, conformal field theory, and constructive field theory. Their extension to d -dimensional quantum field theories constitutes tensor field theories. The most important feature of tensor models is their melonic large N limit. The $1/N$ expansion allows for non-trivial and systematic resummations of correlation functions, making them interesting quantum field theory models. Other methods that are used in this thesis include combinatorics, asymptotic series analysis, and two-particle irreducible effective action techniques.

Three main themes are developed throughout this work. First, the research on tensor models with symplectic symmetry broadens our understanding of tensor models with various symmetry groups. We establish a formal relation between orthogonal and symplectic random tensor models, demonstrating that tensor models with $O(N)$ symmetry are related to corresponding models with $Sp(N)$ symmetry through the replacement $N \rightarrow -N$. This duality extends to tensors transforming in arbitrary finite-dimensional representations of these groups and provides a framework for new fermionic models. Second, we analyze the zero-dimensional $O(N)$ vector model using constructive field theory techniques, particularly the Loop Vertex Expansion, establishing analyticity and Borel summability properties of the free energy. We derive transseries expansions that incorporate both perturbative and non-perturbative contributions. Third, we study a four-dimensional $O(N)^3$ tensor field theory exhibiting asymptotic freedom in the ultraviolet while developing strong correlations in the infrared. Through numerical solution of the Schwinger–Dyson equations, we demonstrate how quantum fluctuations significantly modify the propagator and identify a threshold mass below which the running coupling diverges at a finite infrared scale.

Zusammenfassung

Diese Dissertation untersucht Zufallstensoren und ihre Anwendungen in der Quantenfeldtheorie. Die Ursprünge der Zufallstensoren liegen in der Erforschung der Quantengravitation und bieten einen Ansatz zur Erzeugung diskreter Zufallsgeometrien mit Verknüpfungen zu verschiedenen anderen Fachrichtungen wie der Topologie, der konformen Feldtheorie und der konstruktiven Feldtheorie. Ihre Erweiterung auf d -dimensionale Quantenfeldtheorien führt zu Tensorfeldtheorien. Die wichtigste Eigenschaft von Tensormodellen ist ihr melonisches *Large N* -Limit. Die $1/N$ -Entwicklung ermöglicht eine nicht triviale und systematische Resummierung von Korrelationsfunktionen, was diese Modelle zu interessanten Feldtheorien macht. Weitere in dieser Arbeit verwendete Methoden umfassen Kombinatorik, die Analyse asymptotischer Reihen und die Methode der Zwei-Teilchen-irreduziblen effektiven Wirkung.

Diese Arbeit verfolgt drei Hauptthemen. Erstens erweitert die Forschung über Tensormodelle mit symplektischer Symmetrie unser Verständnis von Tensormodellen mit unterschiedlichen Symmetriegruppen. Wir stellen eine formale Beziehung zwischen orthogonalen und symplektischen Zufallstensoren her und zeigen, dass Tensormodelle mit $O(N)$ -Symmetrie mit entsprechenden Modellen mit $Sp(N)$ -Symmetrie durch die Substitution von $N \rightarrow -N$ in Beziehung stehen. Diese Dualität erstreckt sich auf Tensoren in beliebigen endlichdimensionalen Darstellungen dieser Gruppen und bietet einen methodischen Rahmen für neue fermionische Modelle. Zweitens analysieren wir das nulldimensionale $O(N)$ -Vektormodell mit Techniken der konstruktiven Feldtheorie, insbesondere der *Loop Vertex Expansion*, und zeigen Analytizitäts- und Borel-Summierbarkeitseigenschaften der freien Energie. Wir leiten Transreihenentwicklungen her, die sowohl perturbative als auch nicht perturbative Beiträge einbeziehen. Drittens untersuchen wir eine vierdimensionale $O(N)^3$ -Tensorfeldtheorie, die asymptotisch frei im Ultravioletten ist und starke Korrelationen im Infraroten entwickelt. Durch numerisches Lösen der Schwinger–Dyson-Gleichungen zeigen wir, wie Quantenfluktuationen den Propagator signifikant modifizieren und identifizieren eine Grenzmasse, unterhalb derer die laufende Kopplung bei einer endlichen Infrarotskala divergiert.

Table of Contents

Preface	iii
1 Introduction	1
1.1 General background on tensor models	2
1.2 Random tensor models	6
1.3 Quantum field theory context	13
1.4 Perturbative expansions and Borel summability	25
1.5 The BKAR forest formula	32
1.6 Overview of the remaining thesis content	38
2 Summary	39
2.1 Orthogonal and symplectic random tensor models	39
2.2 Zero-dimensional $O(N)$ model: constructive expansions and transseries	43
2.3 Four-dimensional asymptotically free tensor field theory	46
3 Duality of orthogonal and symplectic random tensor models	51
4 Duality of orthogonal and symplectic random tensor models: general invariants	97
5 Duality of $O(N)$ and $Sp(N)$ random tensor models: tensors with symmetries	113
6 The small-N series in the zero-dimensional $O(N)$ model: constructive expansions and transseries	137
7 Coupling renormalization flow in the strongly interacting regime of an asymp- totically free quantum field theory in four dimensions	201
8 Discussion and Outlook	213
8.1 Orthogonal and symplectic random tensor models	213
8.2 Zero-dimensional $O(N)$ model: constructive expansions and transseries	215
8.3 Four-dimensional asymptotically free tensor field theory	217
Acknowledgments	221
Bibliography	223

Preface

The research presented in this thesis was conducted predominantly at the Institute for Theoretical Physics at Heidelberg University in the years 2022 to 2025.

The content of Chapters 3–7 is the result of joint research efforts, and thus includes work from collaborators who contributed to different projects. A detailed description concerning the authors contribution to each paper is provided at the beginning of the chapter where the paper is reproduced. These statements have been agreed upon by all coauthors.

The corresponding publications are:

- *Duality of orthogonal and symplectic random tensor models* [1]
with Răzvan Gurău.
Published in *Ann. Inst. Henri Poincaré Comb. Phys. Interact.* **12** (2025) 2, 319–362.
Available as e-print: arXiv 2207.01993 [math-ph].
- *Duality of orthogonal and symplectic random tensor models: general invariants* [2]
with Thomas Muller.
Published in *Lett. Math. Phys.* **113** (2023) 4, 83.
Available as e-print: arXiv 2304.03625 [hep-th].
- *Duality of $O(N)$ and $Sp(N)$ random tensor models: tensors with symmetries* [3]
with Thomas Krajewski, Thomas Muller and Adrian Tanasa.
Published in *J. Phys. A: Math. Theor.* **56** (2023) 49, 495206.
Available as e-print: arXiv 2307.01527 [math-ph].
- *The small- N series in the zero-dimensional $O(N)$ model: constructive expansions and trans-series* [4]
with Dario Benedetti, Răzvan Gurău and Davide Lettera.
Published in *Ann. Henri Poincaré* **25** (2024), 5367–5428.
Available as e-print: arXiv 2210.14776 [hep-th].
- *Coupling renormalization flow in the strongly interacting regime of an asymptotically free quantum field theory in four dimensions* [5]
with Jürgen Berges, Răzvan Gurău and Thimo Preis.
Published in *Phys. Rev. D* **110** (2024) 3, 036007.
Available as e-print: arXiv 2405.08153 [hep-th].

This thesis contains reproductions of these published papers; only Chapter 5 contains the accepted manuscript and not the journal version of [3]. Chapters 1, 2, and 8 were checked for spelling, grammar, typographical errors and alternative sentence structures with assistance from DeepL and Claude 3.7 Sonnet. No content or entirely new text was generated by AI tools. Figures have been done using Inkscape, TikZ, Python and Mathematica.

Introduction

Our current understanding of the fundamental workings of nature is based on quantum field theory and the theory of relativity. As physical theories, their primary goal is to make quantitative predictions and provide a framework in which we can explain physical phenomena based on underlying principles. These principles are made manifest through mathematical structures and mathematics is central to a deeper understanding of physical phenomena.

In an idealized situation, one might hope that all predictions of a theory could be derived through pure mathematical machinery. In practice, however, the relationship between mathematics and physics is much more intricate. Different mathematical structures often emphasize different aspects or principles of a physical theory. Indeed, reconstructing physical theory based on new mathematical structures and concepts frequently leads to scientific progress. Even when the mathematical starting point seems clear, real physical systems generally lead to calculations of overwhelming complexity that resist exact solutions. For this reason, it is usually instructive to develop simplified models that capture essential aspects of actual systems while allowing for some degree of calculational control. These models serve as testbeds for new ideas and techniques that might later be applied to more complex systems. Furthermore, some supposedly mathematical structures used in physics still lack rigorous mathematical definitions and full understanding. In practice, one often implicitly introduces additional assumptions and employs approximations that may fail at the boundaries of their domains of applicability. It is at this interface where the field of mathematical physics flourishes. Mathematical rigor can provide new tools and a priori knowledge of their applicability, while physics provides inspiration, intuition, and creativity that can lead to unexpected connections and new developments in mathematics. In this context, model systems can help to advance our understanding by providing examples in which certain concepts can be made rigorous, eventually providing intuition for more general cases.

On the one hand, tensor models, which are the focus of this thesis, have their origins in quantum gravity research, which aims to resolve the discordance between quantum field theory and the theory of relativity, and would eventually provide a more fundamental understanding of nature. On the other hand, tensor models represent exactly such a class of model systems as discussed above. Crucially, they are equipped with a natural small expansion parameter—the reciprocal size of the tensors $1/N$ —and in the large N limit, non-trivial simplifications make them amenable to more rigorous analysis. In particular, their field-theoretic versions (tensor field theories) can allow for a systematic investigation of phenomena that would be inaccessible in more complicated systems. Moreover, some aspects of tensor models are different from other model systems, thus complementing and challenging our established customs.

1.1 General background on tensor models

The roots of random tensor models lie in quantum gravity and random geometry, and it is hoped that they can at some point parallel the success of random matrix models in two-dimensional quantum gravity. From these roots, tensor models grew and branched into a variety of topics, connecting combinatorics, discrete random geometry, statistical physics and quantum field theory (QFT). Although this thesis will not be directly about quantum gravity, we start with a survey of the historic developments which go deep into this area of research. Concrete details and definitions follow in the preceding sections.

Random tensor models arose in the 1990s [6–8] as a discrete/lattice approach to define a theory of quantum gravity that emphasizes the geometric nature inherent to the classical theory of general relativity. Random tensors¹ are probability measures for N^D random variables $T^{a_1 \dots a_D}$, which are invariant under the conjugation of T by the unitary (orthogonal or symplectic) group. The probability measures one studies are inspired by statistical physics and QFT, and thus mainly fall into the class of perturbed Gaussian measures. By means of a graphical expansion à la Feynman, random tensor models can be used to generate an ensemble of discrete spaces (gluings of simplices) endowed with a probability measure. Equipping these spaces with additional geometric data, e.g., fixed side lengths for the simplices (similar to a lattice spacing), one obtains a theory of discrete random geometries. Finally, one would like to find a continuum limit of these discrete spaces that is of relevance to quantum gravity.

The main motivation for this research program was the success of a similar effort for random matrices (see the extensive review [9] and references therein). Random matrices were introduced by Wishart [10] in the context of statistics and first used in physics by Wigner [11] to model the spectra of heavy nuclei. The moments and partition function of random matrix models can be expressed in a perturbative expansion as formal series indexed by ribbon graphs. These graphs are dual to two-dimensional surfaces, and starting with 't Hooft's seminal work [12], it became clear that the perturbative expansion of random matrix models can be reorganized as an expansion in the natural small parameter $1/N$. This series is a topological expansion and indexed by the genus of the ribbon graphs (or equivalently their dual surfaces). In the large N limit, planar graphs dominate. This family of graphs is summable and can be explicitly enumerated [13–16]. In turn, the $1/N$ expansion of matrix models sparked many applications in enumerative combinatorics [17, 18]. Tuning the coupling constants of the matrix model to some critical values, large planar graphs dominate and one obtains a theory of infinitely refined random surfaces [19–22], known in the mathematical literature as Brownian map² and shown to be equivalent to two-dimensional Liouville quantum gravity [23–27] (see also [28] for a pedagogical introduction, and Fig. 1.1). Moreover, matrix models also describe two-dimensional quantum gravity coupled to matter [29–36] and the critical behavior of matter on random surfaces is related to the one on a fixed geometry by the Knizhnik–Polyakov–Zamolodchikov (KPZ) correspondence [37]. The double scaling limit [38–40] enhances subleading terms in the $1/N$ expansion, thus allowing topology change, and corresponds to two-dimensional quantum gravity with fixed Newton's constant. In total, two-dimensional quantum gravity is the by now probably most rigorously understood quantum theory of gravity.

¹ We reserve the name tensor for $D > 2$ to distinguish it from the case of matrices ($D = 2$) and vectors ($D = 1$).

² A random metric space of Hausdorff dimension 4 and spectral dimension 2.

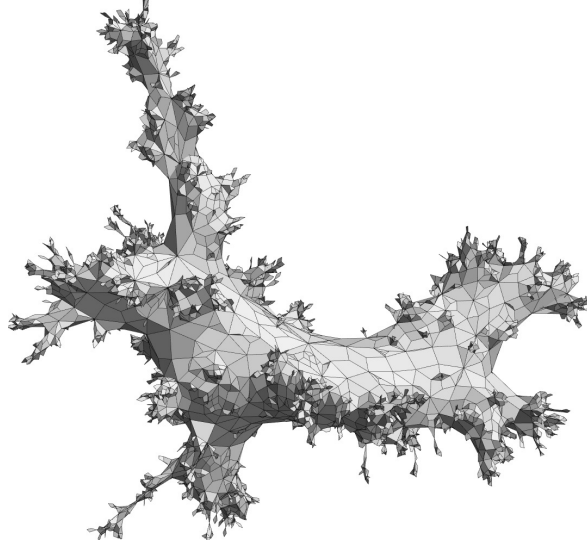


Figure 1.1. Illustration of a typical discrete spherical random geometry that can be obtained from matrix models. These geometries would converge to the Brownian map in a continuum limit. Courtesy of Timothy Budd, released under CC BY license.

The development of tensor models was hindered by the lack of a $1/N$ expansion until 2009 when Gurău introduced the so-called colored tensor models [41–47]. These models are fundamental to the modern theory of random tensors (see the book [48] and references therein). They possess a $1/N$ expansion organized by the Gurau degree ω that replaces the genus. The leading order graphs are so-called melonic graphs (see Fig. 1.2). The Feynman graphs of the colored tensor models have a dual description in terms of gluings of simplices and generate discrete manifolds as well as pseudomanifolds [49].³ The leading order melonic graphs are dual to certain triangulations of the D -dimensional sphere. Other triangulations of spheres appear at subleading orders. On the one hand, this shows that the $1/N$ expansion of random tensor models is not purely topological. On the other hand, there is no single and simple number that distinguishes different topologies in $D > 2$ dimensions. Based on the family of melonic graphs a continuum limit can be taken that is governed by the continuum random tree [50] and known as branched polymer⁴ phase in the physics literature [44, 51]. Tensor models also exhibit a double scaling limit [52–57]. In fact, the $1/N$ expansion of random tensor models has strong universality properties [58–69] and mostly leads to tree-like structures (transitions between a branched polymer phase and two-dimensional quantum gravity phase are also possible [70]). Up until now, finding a non-trivial random metric space with integer spectral dimension ≥ 3 remains an open problem (see also the literature on causal dynamical triangulations, e.g., the recent review [71] or [72, 73] for specific proposals to overcome this issue).

A further generalization of tensor models are group field theories, that aim to define a field theory of spacetime (see the reviews [74–76]). Prototypical examples are the Boulatov [77] and Ooguri [78] models. Their fields can be understood as elements $\phi \in L^2(G^D)$ where G is a Lie group. The

³ A pseudomanifold can have certain topological singularities such that the boundary of the neighborhood of a point is not homeomorphic to a sphere.

⁴ A random metric space of Hausdorff dimension 2 and spectral dimension $4/3$.

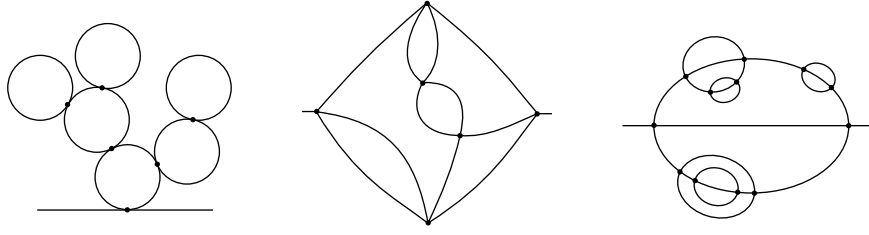


Figure 1.2. Graphical representation of leading order Feynman graphs in the large N limits of vector, matrix and tensor models (from left to right).

Feynman graphs of group field theories are like the ones of tensor models, but decorated with group elements. The amplitudes of these Feynman graphs include an integral over the group G . For example, in the case $D = 3$ and $G = SU(2)$ these models can be interpreted as three-dimensional Euclidean quantum gravity path integrals, whereby the metric is encoded by its holonomies. The discovery of the melonic large N limit of tensor models had significant impact on group field theories (see, e.g., [79]); yet, until now, the metric properties of their continuum limit are not well understood. In a different approach, a theory of renormalization was developed for group field theories [80, 81]. This is a quite non-trivial generalization of the renormalization of local QFTs, as these theories are non-local and do not have an a priori notion of scale.⁵

In 2015, it was recognized that the Sachdev–Ye–Kitaev (SYK) model [82, 83] provides a nearly conformal dual to two-dimensional Jackiw–Teitelboim gravity [84, 85] in nearly Anti-de-Sitter space, that describes the near horizon dynamics of near-extremal black holes and exhibits chaotic quantum behavior [86–89]. The fact, that both sides of this holographic duality can be studied analytically to a large extent led to several advancements in the field of holography/gauge-gravity duality and the black hole information paradox (see, e.g., the review [90]). Shortly after, Witten [91] noted that the melonic large N limit—resulting from a disorder average in the SYK model—occurs naturally in quantum mechanical tensor models without requiring disorder. In subsequent work, tensor models have been used to construct a new family of large N field theories [92–95] that—because of the melonic large N limit—are amenable to analytic studies. Thus, while the melonic large N limit seems to be a hurdle in the random geometry context, it is very fortunate in the field theory context, because it is at the same time richer than the large N limit of vector-like theories, but simpler than the one of matrices (Fig. 1.2). In particular, these models have been used to construct many new (melonic) conformal field theories (CFTs) through renormalization group (RG) analysis. Among the most studied models is the $O(N)^3$ tensor field theory [92, 96].⁶ In $d = 4 - \epsilon$ dimensions, it was shown to exhibit a fixed point with (complex) couplings of order $\sqrt{\epsilon}$ [97], but the resulting CFT is unstable [98]. In contrast, a version of the model with a long-range propagator⁷ exhibits an infrared RG fixed point that corresponds to a unitary and stable large N CFT [99–102].

⁵ The terms tensor(-ial) field theories and tensorial group field theories appear in this context. The former shall not be confused with the local QFTs with tensorial degrees of freedom that will be introduced below and an example of which is studied in Chapter 7. Both are characterized by a kinetic term that includes the Laplace–Beltrami operator on the group manifold.

⁶ Sometimes called Carrozza–Tanasa–Klebanov–Tarnopolsky (CTKT) model.

⁷ This means that the kinetic term is defined by a fractional Laplacian $(-\Delta)^\zeta$, with $\zeta < 1$. The choice $\zeta = d/4$ makes the quartic interaction marginal. Because of the long-range propagator, there is no wave function renormalization.

In [103] it was noted that the $O(N)^3$ tensor model with purely imaginary tetrahedral coupling can be asymptotically free in the ultraviolet, and this result laid the ground for the research presented in Chapter 7 of this thesis. Other work on tensor field theories and quantum mechanical tensor models includes [104–122]. For other recent reviews and theses on tensor models see [74, 95, 102, 123].

1.2 Random tensor models

After surveying the history of random tensor models, in this section we give a slightly more detailed introduction to this topic. For concreteness, we consider a real tensor model with $O(N)^D$ symmetry. In the context of random geometry, complex tensor models, invariant under conjugation with the unitary group, are more common, and it was for these models that the existence of the $1/N$ expansion was first shown. However, the real tensor model with orthogonal symmetry is much more relevant for tensor models as QFTs, and for the work presented in this thesis.

Tensors. We take as tensors the D -linear forms on $\bigotimes_{c=1}^D \mathbb{R}^N$, choosing a tensor product basis $\{e_{a_1} \otimes e_{a_2} \otimes \cdots \otimes e_{a_D} \mid (a_1, a_2, \dots, a_D) \in N^D\}$, a tensor T writes

$$T = \sum_{a_1, a_2, \dots, a_D} T^{a_1 a_2 \dots a_D} e_{a_1} \otimes e_{a_2} \otimes \cdots \otimes e_{a_D} . \quad (1.2.1)$$

In the following, we always denote a tensor by its components $T^{a_1 a_2 \dots a_D}$. Each \mathbb{R}^N is equipped with a real symmetric scalar product and we take all basis vectors to be orthonormal: $(e_{a_c}, e_{b_c}) = \delta_{a_c b_c}$, with the Kronecker symbol δ . The induced scalar product between two tensors \tilde{T}, T is

$$(\tilde{T}, T) = \sum_{a_1, a_2, \dots, a_D} \tilde{T}^{a_1 a_2 \dots a_D} T^{a_1 a_2 \dots a_D} . \quad (1.2.2)$$

Now, consider tensors transforming in the tensor product of D fundamental representations of $O(N)$

$$T^{a_1 a_2 \dots a_D} \mapsto \sum_{b_1, b_2, \dots, b_D} M_{(1) b_1}^{a_1} M_{(2) b_2}^{a_2} \cdots M_{(D) b_D}^{a_D} T^{b_1 b_2 \dots b_D} , \quad (1.2.3)$$

with $M_{(c)}$ an orthogonal transformation. Note that each index transforms independently. Because of this, the position $c = 1, 2, \dots, D$ of an index is fixed and in view of the graphical representation introduced below (Fig. 1.3) c is called the color of the index. In particular, the tensors have no symmetry properties under permutation of indices.

Invariants and colored graphs. By averaging over the orthogonal group, it can be shown that the invariants that are polynomial in the tensor components are linear combinations of trace invariants [48].⁸ These are built by contracting, in all possible ways, the indices in products of $T^{a_1 a_2 \dots a_D}$. Trace invariants have a graphical representation in terms of edge D -colored regular graphs, or colored graphs for short.

Definition 1 (colored graph). A edge D -colored regular graph is a graph $\mathcal{B} = (\mathcal{V}(\mathcal{B}), \mathcal{E}(\mathcal{B}))$ with finite vertex set $\mathcal{V}(\mathcal{B})$ and edge set $\mathcal{E}(\mathcal{B}) \subset \mathcal{V}(\mathcal{B}) \times \mathcal{V}(\mathcal{B})$ such that:

- (edge D -colored): The edge set is partitioned into D disjoint subsets $\mathcal{E}(\mathcal{B}) = \bigcup_{c=1}^D \mathcal{E}^c(\mathcal{B})$, where $\mathcal{E}^c(\mathcal{B})$ is the set of edges of color c .
- (regular): All vertices are D -valent with exactly one edge of each color incident to every vertex.

⁸ Trace invariants are a complete set for all $O(N)^D$ invariants, but they only form a basis as long as their order as a polynomial in the tensors does not exceed N .

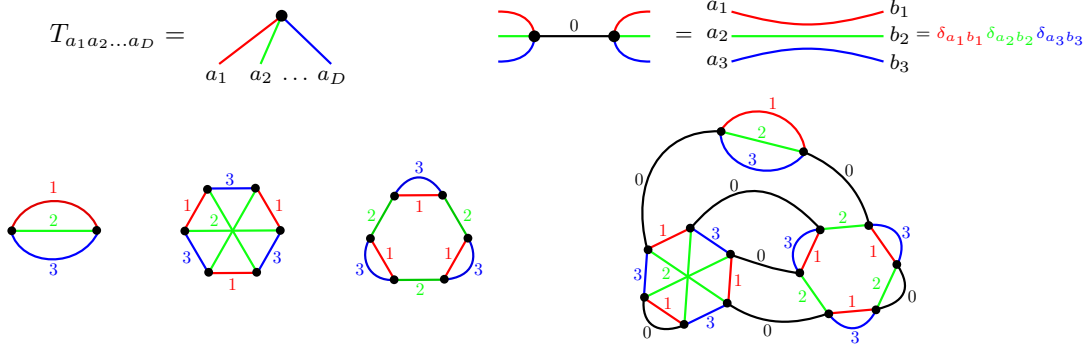


Figure 1.3. Graphical representation of tensor model invariants and Feynman graphs as colored graphs for $D = 3$.

Notice that a colored graph needs to have an even number of vertices. A very important notion is the one of colored faces. We call a face of colors (i, j) a cycle of alternating colors $i \neq j$ in the graph. We denote their number by $F_{i,j}(\mathcal{B})$ and the total number of colored faces by $F(\mathcal{B})$.

The trace invariant associated to a colored graph \mathcal{B} is defined as

$$I_{\mathcal{B}}(T) = \sum_{\text{all indices}} \prod_{v \in \mathcal{V}(\mathcal{B})} T^{a_1^v a_2^v \dots a_D^v} \prod_{c=1}^D \left(\prod_{(v,w) \in \mathcal{E}^c(\mathcal{B})} \delta_{a_c^v a_c^w} \right). \quad (1.2.4)$$

The graphical representation of trace invariants and tensor model Feynman graphs is shown in Fig. 1.3. Tensors are represented as vertices and a contraction between two vertices of color c by an edge of that color. In complex tensor models, contraction only happens between tensors and their complex conjugates. As a result, the associated colored graphs are bipartite, i.e., they have black and white vertices and edges only connect vertices of different types.

Probability measures and Feynman graphs. A random tensor model is a probability measure of the form

$$d\mu(T) = dT e^{-\frac{1}{2}(T,T) - V(T)}, \quad dT = \prod_{a_1, a_2, \dots, a_D} \frac{dT^{a_1 a_2 \dots a_D}}{\sqrt{2\pi}}, \quad (1.2.5)$$

where $V(T)$ is a perturbation of the Gaussian measure by trace invariants

$$V(T) = \sum_{\mathcal{B}} \frac{g_{\mathcal{B}}}{N^{\alpha_{\mathcal{B}}}} I_{\mathcal{B}}(T), \quad (1.2.6)$$

and the sum runs over some (finite) set of colored graphs. In analogy to QFT the terms in $V(T)$ are called interactions and $S(T) = \frac{1}{2}(T, T) + V(T)$ the action. We explicitly included a scaling of the coupling constants $g_{\mathcal{B}}$ with N . The powers $\alpha_{\mathcal{B}}$ influence the large N limit. If the interactions are too strongly suppressed in $1/N$, the limit will be Gaussian, and if the suppression is too weak, there will be no well-defined large N limit. This generalizes the 't Hooft scaling in matrix models. The minimal values $\alpha_{\mathcal{B}}$, such that a large N limit exists are called optimal scaling [66]. In the models at hand, taking

$$\alpha_{\mathcal{B}} = \frac{D(D-1)}{4} + \frac{F(\mathcal{B}) - \frac{D(D-1)}{2}}{D-1}, \quad (1.2.7)$$

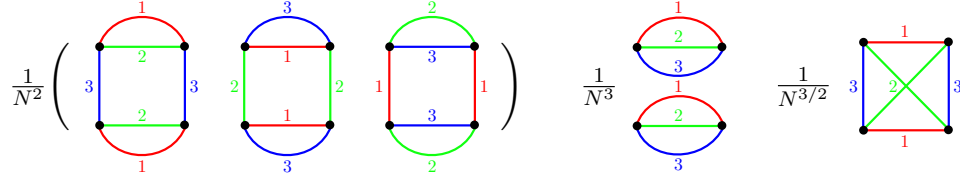


Figure 1.4. Pillow (three color permutations), double-trace, tetrahedron and their optimal scaling.

leads to a non-trivial large N limit. In general, it is difficult to find the optimal scaling for a particular interaction—if it exists at all.⁹ For $D = 3$, Fig. 1.4 shows the trace invariants at quartic order, together with their optimal scaling (which is given by Eq. (1.2.7) in these cases). They are called tetrahedron, pillow and double-trace, respectively.

The partition function, free energy and expectation value of an invariant of a random tensor model are defined as

$$Z(\{g_B\}, N) = \int d\mu(T) , \quad F(\{g_B\}, N) = \ln Z(\{g_B\}, N) , \quad \langle I_B \rangle = \frac{1}{Z} \int d\mu(T) I_B(T) . \quad (1.2.8)$$

These quantities can be evaluated in a formal perturbative expansion in terms of Feynman graphs. This expansion is derived by expanding $e^{-V(T)}$ in a Taylor series and exchanging the order of integration and summation. For this reason, the expansion is in most cases only asymptotic. Section 1.4 discusses this issue in more detail. For example, for the free energy

$$F(\{g_B\}, N) = \ln \left\{ \sum_{n=0}^{\infty} \frac{1}{n!} \int dT e^{-\frac{1}{2}(T,T)} [V(T)]^n \right\} . \quad (1.2.9)$$

Gaussian expectation values can be expressed by a sum over (Wick) pairings and for this reason, the Gaussian integral can be written as the action of a second order derivative operator $(\partial_T, \partial_T) = \sum_{a_1, \dots, a_D} \frac{\partial}{\partial T^{a_1 a_2 \dots a_D}} \frac{\partial}{\partial T^{a_1 a_2 \dots a_D}}$ as follows (see also Section 1.5)

$$F(\{g_B\}, N) = \ln \left\{ \sum_{n=0}^{\infty} \frac{1}{n!} \left[e^{\frac{1}{2}(\partial_T, \partial_T)} [V(T)]^n \right]_{T=0} \right\} . \quad (1.2.10)$$

This reformulation makes the graphical representation of Feynman graphs most transparent. The interactions in $V(T)$ are represented by colored graphs with colors $c = 1, 2, \dots, D$, such that each monomial in the product $[V(T)]^n$ corresponds to a disjoint union of D -colored graphs. The derivative operator (∂_T, ∂_T) acts by contracting two tensors in such a monomial and the result is a product of Kronecker deltas

$$(\partial_T, \partial_T) T^{a_1 a_2 \dots a_D} T^{b_1 b_2 \dots b_D} = \prod_{c=1}^D \delta_{a_c b_c} . \quad (1.2.11)$$

Graphically this is represented by a new edge of color 0 joining the vertices that correspond to $T^{a_1 a_2 \dots a_D}$ and $T^{b_1 b_2 \dots b_D}$. These edges are exactly the propagator lines in normal QFT Feynman

⁹ If an interaction vertex can appear an arbitrary number of times in Feynman graphs at fixed order in the $1/N$ expansion, the scaling for that vertex is necessarily optimal.

graphs. In this language the QFT interaction vertices correspond to the D -colored graphs with colors $c = 1, 2, \dots, D$. The condition $T = 0$ makes sure that only those terms contribute where all tensors have been contracted. As the disconnected contributions factorize, taking the logarithm restricts to connected diagrams. In total, the free energy can be represented as a formal sum over $(D+1)$ -colored graphs \mathcal{G} that are build by joining the D -colored graphs \mathcal{B} in $V(T)$ with new edges of color 0, such that the resulting graph is connected. In the tensor model literature, the D -colored subgraphs with colors $1, 2, \dots, D$ are called bubbles. We obtain

$$F(\{g_{\mathcal{B}}\}, N) = \sum_{\mathcal{G}} \prod_{\mathcal{B} \subset \mathcal{G}} (-g_{\mathcal{B}})^{n(\mathcal{B})} \mathcal{A}(\mathcal{G}), \quad (1.2.12)$$

where the product runs over the bubbles in \mathcal{G} , $n(\mathcal{B})$ denotes the number of bubbles \mathcal{B} in \mathcal{G} , and $\mathcal{A}(\mathcal{G})$ contains numerical factors and, crucially, the dependence on N . The whole term labeled by \mathcal{G} in the expansion above is often called the amplitude of the graph. Analogous expansions hold for the expectation values of invariants $\langle I_{\mathcal{B}'} \rangle$, where the sum is over graphs \mathcal{G} that contain \mathcal{B}' as a marked subgraph.

Now let us count the powers of N in $\mathcal{A}(\mathcal{G})$ using the graphical representation in Fig. 1.3. Every vertex includes a sum over the attached tensor indices, an edge of color $c \neq 0$ is a Kronecker delta of two indices with the same color, and each edge of color 0 contracts all indices it is joining, respecting their color. In total, each cycle of edges of alternating colors 0 and $c \neq 0$ will lead to a cyclic contraction of Kronecker deltas and thus a free sum, that gives one power of N . These are exactly the faces of colors $(0, c)$. Including the explicit scaling factor $N^{-\alpha_{\mathcal{B}}}$ we have

$$\mathcal{A}(\mathcal{G}) \propto N^{\sum_{c=1}^D F_{0,c} - \sum_{\mathcal{B} \subset \mathcal{G}} \alpha_{\mathcal{B}}} = N^{\frac{D(D-1)}{2} - \omega(\mathcal{G})}, \quad (1.2.13)$$

where on the right, we introduced the (Gurau) degree $\omega(\mathcal{G})$. For the model at hand, with the scaling in Eq. (1.2.7), the degree is a non-negative half-integer [96, 102]. Showing the non-negativity of the degree is the most important step in order to establish a large N limit and is usually done by expressing ω in terms of other, manifestly non-negative, combinatorial quantities.¹⁰ As a result, the powers of N are bounded from above and the model has a well-defined large N expansion of the form

$$N^{-\frac{D(D-1)}{2}} F(\{g_{\mathcal{B}}\}, N) = \sum_{\omega \geq 0} \sum_{\mathcal{G} \text{ of degree } \omega} N^{-\omega} \prod_{\mathcal{B} \subset \mathcal{G}} (-g_{\mathcal{B}})^{n(\mathcal{B})} a(\mathcal{G}), \quad (1.2.14)$$

where $a(\mathcal{G})$ includes the remaining numerical factors.

There exist a refined graphical representation where the color 0 edges are replaced by D parallel edges (strands) of colors $1, 2, \dots, D$. The resulting graphs are called stranded graphs and in this representation each strand corresponds directly to a chain of Kronecker deltas with a fixed color, such that (up to the explicit scaling) the power of N is equal to the number of closed strands. This representation is needed if the tensors have symmetry properties under permutation of their indices, because in this case different colors can mix (see [61, 68, 124] and Chapter 5).

¹⁰ In most proofs (e.g., [42, 96]) certain embedded ribbon graphs with only two colors are used, because their genus is manifestly non-negative.

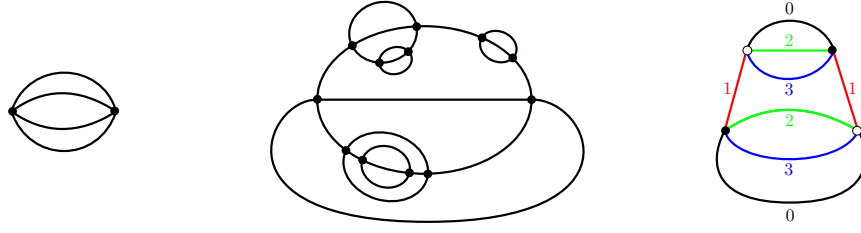


Figure 1.5. Melonic graphs. From left to right: elementary melon with four edges; melonic graph build from five iterative insertions; bipartite four-colored melonic graph of the type that dominate the complex colored tensor models.

Melonic graphs. Melonic graphs dominate (with varying combinatorial details) most of the large N limits of tensor models.

Definition 2 (Melonic graphs). For fixed $k \in \mathbb{N}$, $k \geq 3$, the elementary melon is the unique graph with two vertices connected by k edges. Every other melonic graph is a regular graph that can be built by recursively inserting pairs of vertices connected by $(k - 1)$ edges on any of the available edges. If the graph is in addition an edge k -colored regular graph (Def. 1), we call it k -colored melonic graph.

Illustrations can be found in Fig. 1.5. Because of their recursive nature, melonic graphs are in bijection with combinatorial k -ary trees and can be explicitly enumerated [44].

Melonic graphs constitute the large N limit of random tensor models in different ways: In the complex colored tensor models of [41, 44] and the ones with $U(N)^D$ symmetry [45] the leading order graphs are exactly the (bipartite) colored melonic graphs with $(D + 1)$ edges. For $D = 3$ the leading order graphs of the $O(N)^3$ symmetric tensor field theory with only quartic interactions (tetrahedron, pillow and double-trace; Fig. 1.4) are melonic after:

1. replacing each pillow and double-trace bubble with their minimal resolution in terms of tetrahedral bubbles.
2. contracting all tetrahedral bubbles to four-valent vertices.

See Fig. 1.6 for illustration. Thus, in this sense, the graphs are melonic with respect to the color 0 propagator edges. Keeping the pillow and double-trace bubbles unresolved, the leading order graphs are so-called melontadpole graphs, that are built from iterative melon (having tetrahedral bubbles as their vertices) and tadpole insertions (having pillow or double-trace bubbles) on the color 0 edges. Such a graph is shown in Fig. 2.4 in Section 2.3, where the paper of Chapter 7, that deals in depth with the $O(N)^3$ symmetric tensor field theory, is summarized.

Dual triangulation. Edge $(D + 1)$ -colored regular graphs are Poincaré dual to vertex colored D -dimensional triangulations [48]. Although we do not deal with the geometric interpretation of random tensor models in this thesis, we briefly mention this aspect as it is fundamental to the original motivation for these models in quantum gravity.

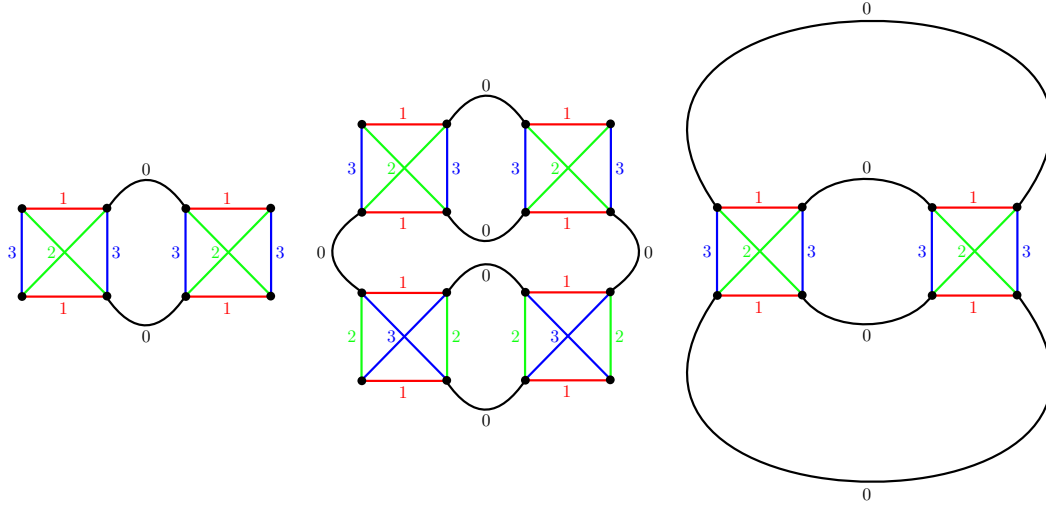


Figure 1.6. Minimal resolution of a pillow (left) and the double-trace (middle) in terms of tetrahedra. Melonic graph with tetrahedral interaction vertices (right).

Definition 3 (colored D -dimensional triangulation). A vertex colored D -dimensional triangulation is a gluing of D -simplices, such that

- only pairs of D -simplices are glued along $(D - 1)$ -simplices.
- all the vertices (0 -simplices) have a label (color) $0, 1, \dots, D$, such that all the $D + 1$ vertices belonging to the same D -simplex have distinct labels.

A vertex colored D -dimensional triangulation is called bipartite if it has positive and negative oriented D -simplices and only pairs of those are glued together according to the first item.

The condition of bipartiteness ensures that the resulting triangulations are orientable. This is the case for complex tensor models. In turn, the Feynman graphs of real tensor models, like the $O(N)^D$ symmetric ones, allow for non-orientable gluings of simplices. Starting from a (bipartite) edge $(D + 1)$ -colored regular graph \mathcal{G} , the (bipartite) vertex colored D -dimensional triangulation is obtained as follows [48, 123]:

- for each (black/white) vertex of \mathcal{G} one draws a (positive/negative oriented) D -simplex and labels its triangulation vertices with $1, 2, \dots, D$.
- for each edge of color c connecting two vertices in \mathcal{G} , glue the two corresponding simplices along the $(D - 1)$ -simplex not containing the triangulation vertex with label c by identifying the vertices with the same label.

Starting from the triangulation:

- draw the connectivity graph of the D -simplices, i.e., draw a vertex for each D -simplex, and connect two vertices by an edge if the corresponding simplices share a $(D - 1)$ -simplex.
- color each edge of this graph by the label of the triangulation vertex that is not contained in the $(D - 1)$ -simplex it represents.

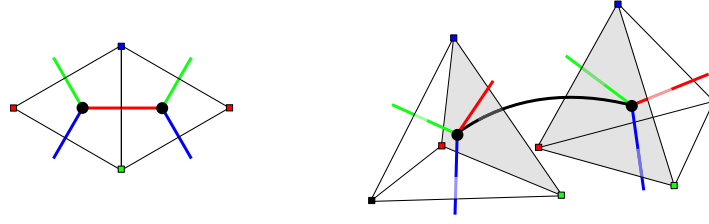


Figure 1.7. D -dimensional triangulation dual to a $(D + 1)$ -colored graph. Left: gluing of triangles in $D = 2$. Right: gluing of tetrahedra in $D = 3$.

This duality is illustrated in Fig. 1.7

The D -dimensional triangulations one obtains from the $(D + 1)$ -colored graphs are not only simplicial manifolds, but also simplicial pseudomanifolds are generated. For a manifold, the neighborhood of a triangulation vertex (the star) has to be a D -ball, and thus its boundary (the link) has to be a $(D - 1)$ -dimensional sphere. But for a pseudomanifold this does not have to be true and the link is allowed to have a different topology (see [49] for more details).

1.3 Quantum field theory context

Quantum field theory is the foundation of modern fundamental physics. It is the framework in which the Standard Model of particle physics—probed with high precision, e.g., at particle colliders—is formulated, and at the same time it can describe critical phenomena in statistical physics. Even if a different, more fundamental theory is eventually discovered, QFT will almost surely remain an effective and efficient description of nature on a vast range of energy scales.

We assume that the reader is familiar with the subject and focus on aspects that may be less standard and are relevant for the rest of the thesis. Moreover, we focus on QFTs in d -dimensional Euclidean spacetime and study partition functions and correlation functions defined by path integrals. On the one hand, they are used to describe thermal properties and are sometimes rather called statistical field theories. On the other hand, if the correlation functions of a QFT obey the Osterwalder–Schrader axioms [125, 126], these functions can be analytically continued to the correlation functions of a Lorentzian QFT obeying the Wightman axioms [127, 128], and in this way a Hilbert space of quantum states can be reconstructed. From this perspective, a Euclidean QFT model is a probability measure for random functions (distributions) and as such is used to compute expectation values (moments, cumulants, correlation/ n -point functions, ...)

$$\langle \phi(x_1) \dots \phi(x_n) \rangle = \int \mathcal{D}\phi \phi(x_1) \dots \phi(x_n) e^{-S(\phi)} . \quad (1.3.1)$$

The quantum fields¹¹ are an assignment of a random variable to every point of spacetime $x \mapsto \phi(x)$, and the action $S(\phi)$ is usually split into a quadratic (Gaussian) part and an interacting part

$$S(\phi) = \frac{1}{2}(\phi, C^{-1}\phi) + V(\phi) , \quad (1.3.2)$$

where (\cdot, \cdot) is an appropriate inner product on the vector space of fields, C is the covariance (free/classical propagator). Usually for a bosonic scalar field theory $C^{-1}\phi(x) = -\Delta\phi(x) + m^2\phi(x)$. Because the set of spacetime points is uncountable, generic probability measures for these random variables are ill-defined.¹² This problem manifests itself in the ultraviolet (high energy) divergences encountered in QFT. The mathematical construction of such probability measures is the aim of the constructive field theory program [129–135]. One way to overcome these issues is to regularize the theory by placing it on a spacetime lattice, or regulating the covariance by a cutoff Λ in Fourier (momentum) space. One can then make the parameters (coupling constants) of the action cutoff-dependent and search for a limit $\Lambda \rightarrow \infty$ (or vanishing lattice spacing). The theory of renormalization, as developed by Wilson [136–139], following work by Kadanoff [140], treats the problem by using effective actions¹³ $W^{\Lambda', \Lambda}(\phi)$ at scale Λ' that are obtained by integrating the field modes with momenta higher than Λ'

$$e^{W^{\Lambda', \Lambda}(\phi)} = \int_{\phi(p), \Lambda' < |p| < \Lambda} \mathcal{D}\phi e^{-S^\Lambda(\phi)} , \quad (1.3.3)$$

¹¹ In this introduction, we write equations for the case of real bosonic scalar fields and use a quite condensed notation that omits several details, which, in the end, depend on the precise model under consideration.

¹² Gaussian measures do make sense in infinite-dimensional Banach spaces.

¹³ These effective actions should not be confused with the (1PI) effective action $\Gamma(\phi)$ that is discussed in Section 1.3.2.

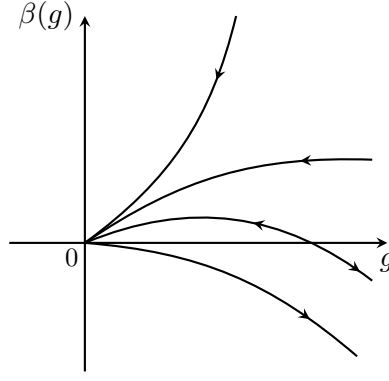


Figure 1.8. Schematic representation of possible kinds of behavior of the beta function for a single coupling. By convention arrows point towards lower energy scales. As $\mu \rightarrow \infty$ the coupling $g(\mu)$ would (from top to bottom): diverge at a finite value of μ ; continue growing towards infinity; approach a finite value (fixed point); approach zero (asymptotic freedom).

and thus $W^{\Lambda',\Lambda}(\phi)$ describes the effective distribution of fields with momenta $|p| < \Lambda'$. In this way one can study the dependence on both scales, integrate over momentum shells iteratively, and potentially remove the cutoffs. The RG flow is the map $\Lambda' \mapsto W^{\Lambda',\Lambda}$ and describes the change of physics with scale.¹⁴ Conventionally the flow goes from high to low energies, i.e., short to long distances. In fact, the scale dependence of effective correlation functions is closely related to their actual physical momentum dependence.¹⁵ Projecting the scale dependent functional $W^{\Lambda',\Lambda}$ down to its local parts, one can define scale dependent/renormalized coupling constants $g(\Lambda', \Lambda)$. The differential equations that describe the change of these coupling constants with respect to Λ' are called beta functions and play an important role in describing the asymptotic behavior of a field theory.

1.3.1 Asymptotic freedom

As just mentioned, the behavior of a QFT across different energy scales is described by the RG flow and encapsulated in the beta functions, which govern the scale dependence of the coupling constants.¹⁶ For a theory with a single coupling constant g , the beta function is defined as

$$\beta(g) = \mu \frac{dg}{d\mu}, \quad (1.3.4)$$

where we denote by μ some energy/renormalization scale. Depending on the renormalization scheme this scale can, e.g., be a regulator scale like the momentum cutoff Λ' , or the energy scale that is introduced in dimensional regularization. Generally, one rescales the couplings by an appropriate power of μ to define the dimensionless renormalized couplings. In perturbation theory, the beta function can typically be expanded as

$$\beta(g) = \beta_1 g + \beta_2 g^2 + \beta_3 g^3 + \mathcal{O}(g^4), \quad (1.3.5)$$

¹⁴ As the RG is defined by integrating out modes, it is a semi-group rather than a group.

¹⁵ In general, the momentum dependence is of course more complicated than the dependence on a single scale parameter.

¹⁶ A detailed discussion of the different kinds of asymptotic behavior can be found in the classical book [141].

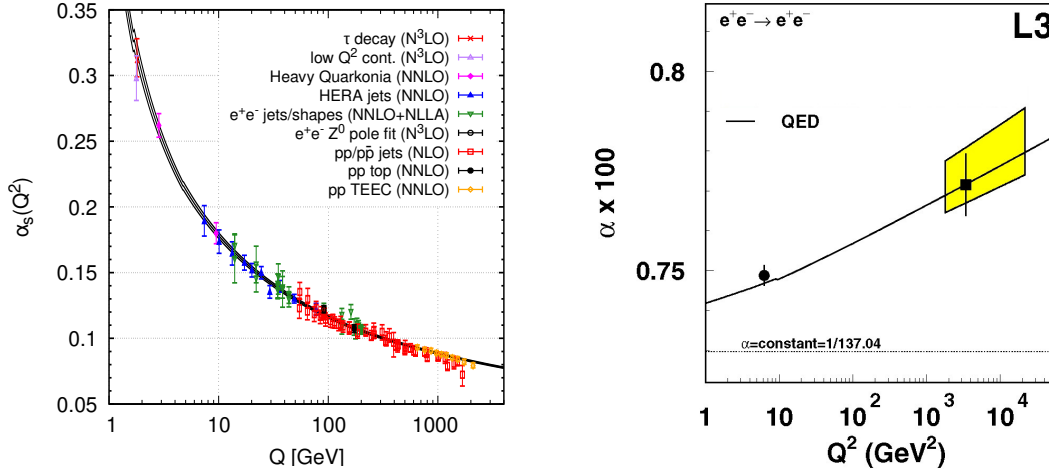


Figure 1.9. Measurements of the QCD running coupling (left) and QED running coupling (right) as a function of the energy scale. Left figure adapted from [144] licensed under CC BY-NC 4.0. Right figure adapted from [145] licensed under CC BY 3.0.

where the coefficients β_n depend on the specific theory under consideration and β_1 is minus the mass dimension of the coupling. Assuming $g \geq 0$, asymptotic freedom occurs in the ultraviolet when $\beta(g) < 0$ for small enough g , causing the coupling to decrease as the energy scale μ increases. This behavior can be seen by integrating the beta function for a marginal ($\beta_1 = 0$) coupling at leading (quadratic) order, which yields

$$g(\mu) = \frac{g(\mu_0)}{1 - \beta_2 g(\mu_0) \ln(\mu/\mu_0)} , \quad (1.3.6)$$

where μ_0 is a reference energy scale. As $\mu \rightarrow \infty$, the coupling $g(\mu) \rightarrow 0$, justifying the term asymptotic freedom—at asymptotically high energies, the interaction strength effectively vanishes. See also Fig. 1.8 for a schematic representation.

The discovery of asymptotic freedom in non-Abelian gauge theories by Gross, Wilczek, and Politzer [142, 143] was crucial for the development of QFT in general, and earned them the 2004 Nobel Prize in Physics. This discovery was also very important to establish quantum chromodynamics (QCD) as the theory of the strong interaction, explaining why quarks appear to behave as nearly free particles in high-energy scattering experiments despite being strongly bound in hadrons at lower energies. This has to be contrasted with theories like quantum electrodynamics (QED), where the coupling strength increases with energy (see Fig. 1.9). For QCD with N_c colors and N_f flavors of quarks, the leading coefficient of the beta function is given by

$$\beta_2 = -\frac{11N_c - 2N_f}{3(4\pi)^2} , \quad (1.3.7)$$

which is negative for the physical case of $N_c = 3$, as long as there are fewer than 17 quark flavors—a condition safely satisfied in nature with six known quark flavors.

From a theoretical perspective, asymptotic freedom has important consequences for the consistency of QFTs. In the context of the RG, asymptotic freedom represents a special case where the RG flow drives the theory towards the free (Gaussian) fixed point. RG fixed points are points where

the beta functions vanish, and they can provide initial conditions for the RG method described in the previous section. At these points the theory becomes scale independent and one has the chance to remove the ultraviolet regulator/cutoff. In principle, theories can also flow towards interacting (non-Gaussian) fixed points, which often describe critical phenomena in statistical physics; but if the interacting fixed point is far from the Gaussian one, it is hard to study it rigorously, because methods that rely on expanding in a small coupling parameter are usually not applicable. This is a general problem, since theories that are asymptotically free in the ultraviolet typically become strongly interacting in the infrared. At this point, large N field theories, having a well-defined $1/N$ expansion, offer the chance to obtain results that do not rely on small couplings, as $1/N$ can play the role of an alternative small expansion parameter.

The rigorous mathematical understanding of asymptotic freedom beyond perturbation theory remains an active area of research. Simpler models that exhibit asymptotically free behavior, such as the two-dimensional Gross–Neveu model [146–151], have been successfully constructed and provide valuable testing grounds for rigorous renormalization. Different methods, such as random walk representations have been the basis of proving that ϕ^4 theory is trivial, i.e., asymptotically free in the infrared in ≥ 4 dimensions [133, 152–154]. Extending such results to non-Abelian gauge theories represents a significant challenge and is part of one of the Millenium Prize Problems by the Clay Mathematics Institute [155–157]. This area bridges theoretical physics and geometry, and is also particularly relevant for pure mathematics since Witten related Donaldson invariants of four manifolds to functional integrals of supersymmetric Yang–Mills theory [158].

In Chapter 7 of this thesis, we propose the $O(N)^3$ tensor field theory as another model for an asymptotically free QFT in four dimensions. The RG flow of this model has been studied using perturbative and large N techniques, and in [103] it was noted that the large N theory is asymptotically free. In the work reproduced in Chapter 7, we used numerical techniques to investigate the physical behavior of the theory in the strongly correlated infrared regime. We refer the reader to that chapter and Sections 2.3 and 8.3 for more details.

1.3.2 Generating functions and effective action

We introduce the shorthand notation $a = (A, x)$ and $\phi_A(x) = \phi_a$, where A are internal indices. The partition function in the presence of sources J is the generating function of moments/ n -point functions

$$Z(J) = \int \mathcal{D}\phi e^{-S(\phi) + \sum_a J_a \phi_a}, \quad \langle \phi_{a_1} \dots \phi_{a_n} \rangle = \frac{1}{Z(0)} \left[\frac{\delta^n Z(J)}{\delta J_{a_1} \dots \delta J_{a_n}} \right]_{J=0}, \quad (1.3.8)$$

and has an interpretation as a sum over possibly disconnected (Feynman) graphs. It is a combinatorial fact, that $W(J) = \ln Z(J)$ is the same sum restricted to connected graphs, and therefore the Schwinger functional $W(J)$ is the generating function of cumulants/connected n -point functions

$$\langle \phi_{a_1} \dots \phi_{a_n} \rangle_{\text{conn.}} = \left[\frac{\delta^n W(J)}{\delta J_{a_1} \dots \delta J_{a_n}} \right]_{J=0}. \quad (1.3.9)$$

For vanishing sources, $W(0)$ is the free energy and the connected two-point function $\langle \phi_a \phi_b \rangle_{\text{conn.}}$ is also called the (full) propagator. If the source J is not set to zero we sometimes indicate that with

a J superscript $\langle \dots \rangle^J$. Moments and cumulants are related by

$$\langle \phi_{a_1} \dots \phi_{a_n} \rangle = \sum_{\pi \in \Pi_n} \prod_{B \in \pi} \left\langle \prod_{a_i \in B} \phi_{a_i} \dots \phi_{a_n} \right\rangle_{\text{conn.}}, \quad (1.3.10)$$

where the sum is over partitions $\pi \in \Pi_n$ of $\{a_1, \dots, a_n\}$ and $B \in \pi$ denotes the blocks in π . In the fermionic case one has to include a sign coming from reordering the fields.

Denote the connected one-point function in presence of the source by $W_a^{(1)}(J) = \frac{\delta W(J)}{\delta J_a} = \langle \phi_a \rangle_{\text{conn.}}^J$. Assuming that its inverse functional $\mathcal{J}_a(\Phi)$ exists, the (1PI) effective action $\Gamma(\Phi)$ is defined as the Legendre transform

$$\Gamma(\Phi) = \left[\sum_a \Phi_a J_a - W(J) \right]_{J_a = \mathcal{J}_a(\Phi)}. \quad (1.3.11)$$

Going on shell means setting $\Phi_a = \Phi_a^*$, the solution of $\delta\Gamma/\delta\Phi_a = 0$. In particular, the on shell effective action equals minus the free energy $\Gamma(\Phi^*) = -W(0)$.

The effective action can be written as a functional integral over fluctuations ψ around the background Φ

$$e^{-\Gamma(\Phi)} = \int \mathcal{D}\phi e^{-S(\phi) + \sum_a (\mathcal{J}_a(\Phi)\phi_a - \Phi_a \mathcal{J}_a(\Phi))} = \int \mathcal{D}\psi e^{-S(\Phi + \psi) + \sum_a \mathcal{J}_a(\Phi)\psi_a}, \quad (1.3.12)$$

and since \mathcal{J}_a is the inverse of $W_a^{(1)}$, i.e., $W_a^{(1)}(\mathcal{J}(\Phi)) = \Phi_a$, it is exactly the source that ensures that the (connected) one-point function is Φ and thus it ensures that the expectation value of the fluctuation in presence of the source is zero $\langle \psi \rangle^{\mathcal{J}} = 0$. Thus, the effective action can also be defined as a conditioned functional integral

$$e^{-\Gamma(\Phi)} = \int_{\langle \psi \rangle^{\mathcal{J}} = 0} \mathcal{D}\psi e^{-S(\Phi + \psi) + \sum_a \mathcal{J}_a(\Phi)\psi_a}. \quad (1.3.13)$$

Note that this formula for the effective action might be well-defined even when the action is not convex.¹⁷ In fact, the condition $\langle \psi \rangle_{\mathcal{J}(\Phi)} = 0$ ensures that only one-particle irreducible (1PI) graphs (those that stay connected after cutting one edge) contribute to the Feynman graph expansion of $\Gamma(\Phi)$, and $\sum_a \mathcal{J}_a(\Phi)\psi_a$ acts as a counterterm. Thus, the effective action takes the form $\Gamma(\Phi) = S(\Phi) + \Gamma^{\text{1PI}}(\Phi)$, where Γ^{1PI} is the sum over non-trivial 1PI graphs (that is graphs with at least one edge). The 1PI correlation functions (also called vertex functions) $\Gamma_{a_1, \dots, a_n}^{(n)}$ are defined by

$$\Gamma_{a_1, \dots, a_n}^{(n)} = \frac{\delta^n \Gamma(\Phi)}{\delta \Phi_{a_1} \dots \delta \Phi_{a_n}}, \quad (1.3.14)$$

and in particular the inverse 1PI two-point function equals the connected two-point function

$$\left[\Gamma^{(2)} \right]_{ab}^{-1}(\Phi) = \left[\frac{\delta^2 W(J)}{\delta J_a \delta J_b} \right]_{J = \mathcal{J}(\Phi)} = \langle \phi_a \phi_b \rangle_{\text{conn.}}^{J = \mathcal{J}(\Phi)}. \quad (1.3.15)$$

¹⁷ A subtlety arises when there are several on shell solutions, i.e., the action has a complex landscape of minima. In this case, the effective action should be thought of as a patchwork of cells in configuration/field space, such that each cell is centered around a distinct minimum. This typically occurs in spin glass models where the effect is quantified by the Thouless–Anderson–Palmer complexity.

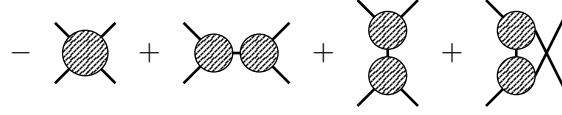


Figure 1.10. Graphical representation of Eq. (1.3.18) for the connected four-point function. The filled vertices represent 1PI correlation functions and the edges connected two-point functions.

Noting that the covariance of the fluctuation field is $(\frac{\delta^2 S}{\delta\Phi_a\delta\Phi_b})^{-1}$, the 1PI two-point function can be written as

$$\Gamma_{ab}^{(2)}(\Phi) = \frac{\delta^2 S}{\delta\Phi_a\delta\Phi_b} - \Sigma(\Phi), \quad \Sigma(\Phi) = -\frac{\delta^2 \Gamma^{1\text{PI}}}{\delta\Phi_a\delta\Phi_b}, \quad (1.3.16)$$

where $\Sigma_{ab}(\Phi)$ is called the self-energy and it is equal to the sum over all 1PI graphs contributing to the two-point function. This equation is called the Schwinger–Dyson equation. The higher $n > 2$ 1PI correlation functions are also related to the connected correlation functions: every $\langle\phi_{a_1} \dots \phi_{a_n}\rangle_{\text{conn.}}$ can be written as a sum over trees with n leaves, propagators $\langle\phi_a\phi_b\rangle_{\text{conn.}}$ at their edges and non-leaf vertices of degree $v > 2$ that represent minus $\Gamma_{b_1\dots b_v}^{(v)}$. For example the connected three and four-point functions write

$$\langle\phi_{a_1}\phi_{a_2}\phi_{a_3}\rangle_{\text{conn.}} = -\left(\prod_{i=1}^3 \langle\phi_{a_i}\phi_{b_i}\rangle_{\text{conn.}}\right) \Gamma_{b_1 b_2 b_3}^{(3)}, \quad (1.3.17)$$

and

$$\begin{aligned} \langle\phi_{a_1}\phi_{a_2}\phi_{a_3}\phi_{a_4}\rangle_{\text{conn.}} = & -\left(\prod_{i=1}^4 \langle\phi_{a_i}\phi_{b_i}\rangle_{\text{conn.}}\right) \Gamma_{b_1 b_2 b_3 b_4}^{(4)} \\ & + \left(\prod_{i=1}^4 \langle\phi_{a_i}\phi_{b_i}\rangle_{\text{conn.}}\right) \Gamma_{b_1 b_2 c}^{(3)} \langle\phi_c\phi_{c'}\rangle_{\text{conn.}} \Gamma_{c' b_3 b_4}^{(3)} \\ & + \left(\prod_{i=1}^4 \langle\phi_{a_i}\phi_{b_i}\rangle_{\text{conn.}}\right) \Gamma_{b_1 b_4 c}^{(3)} \langle\phi_c\phi_{c'}\rangle_{\text{conn.}} \Gamma_{c' b_2 b_3}^{(3)} \\ & + \left(\prod_{i=1}^4 \langle\phi_{a_i}\phi_{b_i}\rangle_{\text{conn.}}\right) \Gamma_{b_1 b_3 c}^{(3)} \langle\phi_c\phi_{c'}\rangle_{\text{conn.}} \Gamma_{c' b_2 b_4}^{(3)}, \end{aligned} \quad (1.3.18)$$

which is represented graphically in Fig. 1.10.

The next section takes the construction of effective actions and generating functions one step further by introducing the two-particle irreducible (2PI) effective action, that is of great use for the large N expansion of tensor models.

1.3.3 2PI formalism

The 2PI formalism [159–161] implements a selective resummation of infinitely many Feynman graphs. The resulting 2PI graphs stay connected after cutting two edges. This formalism is of

great use as a nonperturbative expansion scheme,¹⁸ plays a crucial role in understanding the out-of-equilibrium dynamics of quantum fields [160, 164–166]—as it provides approximation schemes which are uniform in time—and is well suited for $1/N$ expansions in the $O(N)$ vector model [167, 168], SYK-model, and tensor models [119]. The usefulness of resumming 2PI graphs in the context of tensor models becomes immediately clear, since melonic graphs are generated by insertions which are themselves two-particle reducible (can be removed by cutting two edges). In other words, the only melonic 2PI graph is the elementary melon itself. Thus, 2PI methods resum the class of graphs that is most relevant for large N tensor models.

In the following we derive the 2PI effective action for a bosonic field ϕ_a , partially following [119]. As before, the index a is understood as a multiindex, including reference to a spacetime point, and repeated indices are summed/integrated over spacetime. Further below we will describe the 2PI effective action for the $O(N)^3$ model as a concrete example, which is particularly relevant for this work. To start the derivation, we add a bilocal source $K_{ab}(x, y)$ to the action, such that

$$W(J, K) = \ln \int \mathcal{D}\varphi e^{-S(\varphi) + \int d^d x J_a(x) \varphi_a(x) + \int d^d x d^d y \frac{1}{2} \varphi_a K_{ab} \varphi_b} \quad (1.3.19)$$

depends on two sources J and K . $W(J, K)$ depends only on the symmetric part of K , which is therefore assumed to be symmetric in its indices. Thus

$$\frac{\delta K_{ab}}{\delta K_{cd}} = \frac{1}{2} (\delta_{ac} \delta_{bd} + \delta_{ad} \delta_{bc}) \equiv \mathcal{S}_{ab;cd}, \quad (1.3.20)$$

where we defined the projector on symmetric matrices \mathcal{S} .¹⁹ We denote $W_a^{(1)}(J, K)$ and $W_{ab}^{(2)}(J, K)$ the connected one and two-point functions in presence of the sources

$$\begin{aligned} W_a^{(1)}(J, K) &= \langle \varphi_a \rangle_{\text{conn.}}^{J, K} = \frac{\delta W(J, K)}{\delta J_a}, \\ W_{ab}^{(2)}(J, K) &= \langle \varphi_a \varphi_b \rangle_{\text{conn.}}^{J, K} = \frac{\delta^2 W(J, K)}{\delta J_a \delta J_b} = 2 \frac{\delta W(J, K)}{\delta K_{ab}} - W_a^{(1)}(J, K) W_b^{(1)}(J, K), \end{aligned} \quad (1.3.21)$$

and we denote by $(\mathcal{J}_a(\Phi, G), \mathcal{K}_{ab}(\Phi, G))$ the inverse functionals of $(W_a^{(1)}(J, K), W_{ab}^{(2)}(J, K))$, assuming they exist. The 2PI effective action $\Gamma(\Phi, G)$ is the double Legendre transform

$$\Gamma(\Phi, G) = \left[\Phi_a J_a + \frac{1}{2} K_{ab} (G_{ab} + \Phi_a \Phi_b) - W(J, K) \right]_{\substack{J_a = \mathcal{J}_a(\Phi, G) \\ K_{ab} = \mathcal{K}_{ab}(\Phi, G)}}. \quad (1.3.22)$$

In general, it has the following compelling features:

1. The connected one and two-point functions for vanishing sources are the solutions Φ_a^*, G_{ab}^* to the equations of motion

$$0 = \frac{\delta \Gamma(\Phi, G)}{\delta \Phi_a} = \mathcal{J}_a(\Phi, G) + \mathcal{K}_{ab}(\Phi, G) \Phi_b, \quad 0 = \frac{\delta \Gamma(\Phi, G)}{\delta G_{ab}} = \frac{1}{2} \mathcal{K}_{ab}(\Phi, G). \quad (1.3.23)$$

¹⁸ Loop expansions of the 2PI effective action are sometimes called “ Φ -derivable” approximations [162, 163].

¹⁹ For anticommuting fermionic/Graßmann fields one would obtain the projector on antisymmetric matrices.

2. The on shell 2PI effective action equals minus the free energy $\Gamma(\Phi^*, G^*) = -W(0, 0)$. Going partially on shell $\Gamma(\Phi, G^*(\Phi))$ is the (1PI) effective action from Eq. (1.3.11). Going partially on shell in Φ yields the 2PI effective action for an even theory in a symmetric phase²⁰

$$\Gamma(G) = \left[\frac{1}{2} K_{ab} G_{ab} - W(0, K) \right]_{K_{ab} = \mathcal{K}_{ab}(G)} . \quad (1.3.24)$$

3. The 2PI effective action can be expressed as a conditioned functional integral over a fluctuation field ψ_a (analogous to Eq. (1.3.13))

$$e^{-\Gamma(\Phi, G)} = e^{-\frac{1}{2} \text{Tr}[\mathcal{K}G]} \int_{\substack{\langle \psi_a \rangle^{\mathcal{J}, \mathcal{K}} = 0 \\ \langle \psi_a \psi_b \rangle^{\mathcal{J}, \mathcal{K}} = G_{ab}}} \mathcal{D}\psi e^{-S(\Phi + \psi) + \frac{1}{2} \psi_a \mathcal{K}_{ab} \psi_b + \psi_a (\mathcal{J}_a + \mathcal{K}_{ab} \Phi_b)} . \quad (1.3.25)$$

As for the 1PI effective action, the condition $\langle \psi_a \rangle^{\mathcal{J}, \mathcal{K}} = 0$ ensures that only 1PI graphs contribute to the Feynman graph expansion—the term $\psi_a (\mathcal{J}_a + \mathcal{K}_{ab} \Phi_b)$ acts as a counterterm. The second condition $\langle \psi_a \psi_b \rangle^{\mathcal{J}, \mathcal{K}} = G_{ab}$ ensures that the sources are tuned such that G_{ab} equals the full two-point function of the fluctuation field.

4. The self-energy $\Sigma(\Phi, G)$ is a sum over non-trivial 2PI graphs with G_{ab} associated to their edges. In this case, non-trivial refers to graphs having at least one vertex, and at least two loops. Noting that the covariance of the fluctuation field is $(\frac{\delta^2 S}{\delta \Phi_a \delta \Phi_b} - \mathcal{K}_{ab})^{-1}$, the Schwinger–Dyson equation writes

$$G_{ab}^{-1} = \frac{\delta^2 S(\Phi)}{\delta \Phi_a \delta \Phi_b} - \mathcal{K}_{ab}(\Phi, G) - \Sigma_{ab}(\Phi, G) , \quad (1.3.26)$$

where the self-energy $\Sigma(\Phi, G)$ is a priori the sum over 1PI graphs contributing to the two-point function, but the constraint that the full two-point function is G_{ab} leads to a resummation of two-point insertions, such that $\Sigma(\Phi, G)$ is a sum over graphs with the full G_{ab} associated to their edges and no more two-point insertions, i.e., they can not be disconnected by cutting two edges (that is the 2PI property). Denoting $\Gamma^{2\text{PI}}(\Phi, G)$ the generating function of non-trivial 2PI graphs with G_{ab} associated to the edges and vertices $\frac{\delta^n S}{\delta \Phi^n}$, $n \geq 2$, we have

$$\Sigma_{ab}(\Phi, G) = -2 \frac{\delta \Gamma^{2\text{PI}}(\Phi, G)}{\delta G_{ab}} . \quad (1.3.27)$$

5. The 2PI effective action can be written as

$$\Gamma(\Phi, G) = S(\Phi) + \frac{1}{2} \frac{\delta^2 S(\Phi)}{\delta \Phi_a \delta \Phi_b} G_{ab} - \frac{1}{2} \text{Tr} \ln(G) + \Gamma^{2\text{PI}}(\Phi, G) . \quad (1.3.28)$$

Together, the last two terms are the generating function of all 2PI graphs. $\frac{1}{2} \text{Tr} \ln(G^{-1})$ is represented by the ring graph with one edge and no vertex. The above formula can be shown by formally integrating the last equation in Eq. (1.3.23), using Eqs. (1.3.26), (1.3.27), and fixing the integration constant by adopting the functional integral representation.

²⁰ For an even theory $S(\varphi) = S(-\varphi)$, and in a symmetric phase, the vacuum $\varphi = 0$ is stable. As a consequence all odd correlations functions are zero and stay so in presence of the bilocal source K .

Schwinger–Dyson equation. What one gains from the 2PI effective action is an expression of the Schwinger–Dyson equation as a self-consistent (fixed point) equation for the connected two-point function G_{ab} in the absence of sources. Deriving Eq. (1.3.28) with respect to G_{ab} leads to

$$G_{ab}^{-1} = \frac{\delta^2 S(\Phi)}{\delta \Phi_a \delta \Phi_b} + 2 \frac{\delta \Gamma^{2\text{PI}}(\Phi, G)}{\delta G_{ab}}. \quad (1.3.29)$$

Bethe–Salpeter kernel. We define the Bethe–Salpeter kernel by²¹

$$\kappa_{ab;cd} = -2 \frac{\delta \Sigma_{ab}(\Phi, G)}{\delta G_{cd}} = 4 \frac{\delta^2 \Gamma^{2\text{PI}}(\Phi, G)}{\delta G_{ab} \delta G_{cd}}. \quad (1.3.30)$$

This kernel is of great interest because it allows one to compute four point correlations in terms of a ladder expansion where the rungs consist of kernels that are connected by propagators. The Bethe–Salpeter kernel is important to obtain resummed four-point functions in the 2PI formalism, it is used to study two particle bound states [169, 170], and it is a useful tool in CFT (see, e.g., the review [171]), since conformal three-point functions are eigenfunctions of the kernel.

Introducing the four-point function that is 2PI in the channel $(ab)-(cd)$, i.e. that is 2PI after connecting a with b and c with d ,

$$V_{(ab)-(cd)}^{(4)} = \Gamma_{abcd}^{(4)} - \Gamma_{ace}^{(3)} G_{ef} \Gamma_{fbd}^{(3)} - \Gamma_{ade}^{(3)} G_{ef} \Gamma_{fbc}^{(3)}, \quad (1.3.31)$$

this function is determined by the Bethe–Salpeter kernel through the following self-consistency equation

$$V_{(ab)-(cd)}^{(4)} = \kappa_{ab;cd} - \frac{1}{2} \kappa_{ab;a'b'} G_{a'c'} G_{b'd'} V_{(c'd')-(cd)}, \quad (1.3.32)$$

called the (inhomogeneous) Bethe-Salpeter equation (see, e.g., [161, 162, 172]). It has the graphical representation

$$\text{Diagram of } V_{(ab)-(cd)}^{(4)} = \text{Diagram of } \kappa_{ab;cd} - \frac{1}{2} \kappa_{ab;a'b'} G_{a'c'} G_{b'd'} V_{(c'd')-(cd)}, \quad (1.3.33)$$

where the edges represent full propagators G_{ab} . Note that for a theory in the symmetric phase $V_{(ab)-(cd)}^{(4)} = \Gamma_{abcd}^{(4)}$.

In the following we briefly explain how this equation can be derived. One starts by taking two derivatives of $\Gamma(\Phi, G)$

$$\frac{\delta^2 \Gamma(\Phi, G)}{\delta G_{ab} \delta G_{cd}} = \frac{1}{2} G_{aa'}^{-1} G_{bb'}^{-1} \mathcal{S}_{a'b';cd} + \frac{1}{4} \kappa_{a'b';cd}, \quad (1.3.34)$$

and the aim will be to express the left hand side in terms of four point correlation functions. Since $(W_a^{(1)}(\mathcal{J}(\Phi, G), \mathcal{K}(\Phi, G)), W_{ab}^{(2)}(\mathcal{J}(\Phi, G), \mathcal{K}(\Phi, G))) = (\Phi_a, G_{ab})$ the Jacobian matrices fulfill

$$\mathbb{1} = \begin{pmatrix} \frac{\delta W^{(1)}}{\delta \mathcal{J}} & \frac{\delta W^{(1)}}{\delta \mathcal{K}} \\ \frac{\delta W^{(2)}}{\delta \mathcal{J}} & \frac{\delta W^{(2)}}{\delta \mathcal{K}} \end{pmatrix} \begin{matrix} J=\mathcal{J}(\Phi, G) \\ K=\mathcal{K}(\Phi, G) \end{matrix} \begin{pmatrix} \frac{\delta \mathcal{J}}{\delta \Phi} & \frac{\delta \mathcal{J}}{\delta G} \\ \frac{\delta \mathcal{K}}{\delta \Phi} & \frac{\delta \mathcal{K}}{\delta G} \end{pmatrix}, \quad (1.3.35)$$

²¹ The sign and factors of 2 in the definition of $\kappa_{ab;cd}$ are conventional. Our definition agrees with [162].

focusing on the lower right element in the second Jacobian $\frac{\delta \mathcal{K}_{ab}(\Phi, G)}{\delta G_{cd}} = 2 \frac{\delta^2 \Gamma(\Phi, G)}{\delta G_{ab} \delta G_{cd}}$, inverting the first Jacobian, and evaluating the derivatives of $W(J, K)$ one can deduce

$$\begin{aligned} \left(\frac{\delta^2 \Gamma(\Phi, G)}{\delta G \delta G} \right)_{ab, cd}^{-1} &= 2 \frac{\delta W_{ab}^{(2)}}{\delta K_{cd}} - 2 \frac{\delta W_{ab}^{(2)}}{\delta J_e} G_{ef}^{-1} \frac{\delta W_f^{(1)}}{\delta K_{cd}} \\ &= F_{(ab)-(cd)}^{(4)} - F_{(ab)-(e)}^{(3)} G_{ef}^{-1} F_{(f)-(cd)}^{(3)}, \end{aligned} \quad (1.3.36)$$

where we abbreviated

$$F_{(ab)-(cd)}^{(4)} = 4 \frac{\delta^2 W(J, K)}{\delta K_{ab} \delta K_{cd}} = \langle \phi_a \phi_b \phi_c \phi_d \rangle^{J, K} - \langle \phi_a \phi_b \rangle^{J, K} \langle \phi_c \phi_d \rangle^{J, K}, \quad (1.3.37)$$

that is the four-point function that is connected in the channel $(a, b)-(c, d)$, i.e., it is connected after joining a with b and c with d , and

$$F_{(ab)-(c)}^{(3)} = F_{(c)-(ab)}^{(3)} = 2 \frac{\delta^2 W(J, K)}{\delta K_{ab} \delta J_c} = \langle \phi_a \phi_b \phi_c \rangle^{J, K} - \langle \phi_a \phi_b \rangle^{J, K} \langle \phi_c \rangle^{J, K}, \quad (1.3.38)$$

the three-point function that is connected in the channel $(a, b)-(c)$, i.e., it is connected after joining a with b . Thus the right hand side of Eq. (1.3.36) can be recognized as the four-point function that is 1PI in the channel $(ab)-(cd)$. Next, we rewrite Eq. (1.3.36) in terms of 1PI correlation functions (as in Eqs. (1.3.17) and (1.3.18)) and obtain

$$\begin{aligned} \left(\frac{\delta^2 \Gamma(\Phi, G)}{\delta G \delta G} \right)_{ab, cd}^{-1} &= G_{aa'} G_{bb'} G_{cc'} G_{dd'} \left(-\Gamma_{a'b'c'd'}^{(4)} + \Gamma_{a'e'c'e}^{(3)} G_{ef} \Gamma_{fb'd'}^{(3)} + \Gamma_{a'd'e}^{(3)} G_{ef} \Gamma_{fb'c'}^{(3)} \right) \\ &\quad + G_{ac} G_{bd} + G_{ad} G_{bc} \\ &= -G_{aa'} G_{bb'} V_{(a'b')-(c'd')}^{(4)} G_{c'e} G_{d'd} + G_{ac} G_{bd} + G_{ad} G_{bc}. \end{aligned} \quad (1.3.39)$$

Finally, Eq. (1.3.32) is obtained from multiplying Eq. (1.3.34) with Eq. (1.3.39) from the right and amputating the external propagators.

2PI effective action of the $O(N)^3$ tensor model. As an example, we now derive the 2PI effective action of the $O(N)^3$ tensor model at large N and in the symmetric phase. We use a multi-index notation for the tensor indices $\mathbf{a} = (a_1, a_2, a_3) \in \{1, \dots, N\}^3$ and repeated indices are summed respecting their color. The model's fundamental fields $\varphi_{\mathbf{a}}$, transform as real 3-index tensors in the trifundamental representation of $O(N)^3$. The model is defined by the action

$$\begin{aligned} S(\varphi) &= \int d^d x \left[\frac{1}{2} \varphi_{\mathbf{a}}(x) (-\Delta + m^2) \varphi_{\mathbf{a}}(x) \right. \\ &\quad \left. + \frac{1}{4} \left(g_1 \hat{P}_{\mathbf{ab}; \mathbf{cd}}^{(1)} + g_2 \hat{P}_{\mathbf{ab}; \mathbf{cd}}^{(2)} + ig \hat{\delta}_{\mathbf{abcd}}^t \right) \varphi_{\mathbf{a}}(x) \varphi_{\mathbf{b}}(x) \varphi_{\mathbf{c}}(x) \varphi_{\mathbf{d}}(x) \right], \end{aligned} \quad (1.3.40)$$

which is invariant under the global $O(N)^3$ symmetry. The three interaction terms in the action correspond to the three $O(N)^3$ -invariant contraction patterns: pillow, double-trace and tetrahedron (Fig. 1.4). Note that we have chosen to write the coupling of the tetrahedral interaction as ig , such that it is purely imaginary for real g . This will be important for the research presented in Chapter 7,

but can be ignored for the purpose of this section. Instead of using directly the pillow and double-trace interactions, it is useful to introduce the new couplings g_1 and g_2 , and their associated index contraction operators $\hat{P}^{(1)}$ and $\hat{P}^{(2)}$, that are linear combinations of the pillow $\hat{\delta}^p$ and double-trace $\hat{\delta}^d$ contraction operators

$$\begin{aligned}
 \hat{\delta}_{\mathbf{ab};\mathbf{cd}}^p &= \frac{1}{3N^2} \sum_{i=1}^3 \delta_{a_i c_i} \delta_{b_i d_i} \prod_{j \neq i} \delta_{a_j b_j} \delta_{c_j d_j} , & \hat{P}^{(1)} &= 3(\hat{\delta}^p - \hat{\delta}^d) , \\
 \hat{\delta}_{\mathbf{ab};\mathbf{cd}}^d &= N^{-3} \prod_{i=1}^3 \delta_{a_i b_i} \prod_{j=1}^3 \delta_{c_j d_j} , & \hat{P}^{(2)} &= \hat{\delta}^d , \\
 \hat{\delta}_{\mathbf{abcd}}^t &= N^{-3/2} \delta_{a_1 b_1} \delta_{c_1 d_1} \delta_{a_2 c_2} \delta_{b_2 d_2} \delta_{a_3 d_3} \delta_{b_3 c_3} , & g_1 &= \frac{g_p}{3} , \\
 & & g_2 &= g_p + g_d .
 \end{aligned} \tag{1.3.41}$$

This rewriting is useful, because the new contraction operators are orthogonal $\hat{P}_{\mathbf{ab};\mathbf{cd}}^{(1)} \hat{P}_{\mathbf{cd};\mathbf{ef}}^{(2)} = 0$.

As we consider a symmetric phase all odd correlation functions vanish, the 2PI effective action $\Gamma(G)$ only depends on the propagator $G_{\mathbf{ab}}(x, y)$, and can be defined by the Legendre transform in Eq. (1.3.24). The non-trivial part of the 2PI effective action is the generating function of non-trivial 2PI graphs $\Gamma^{2PI}(G)$. In general it contains an infinite number of graphs, but exploiting the large N limit (discussed on p. 10 in Section 1.2), only a finite number of diagrams contribute to $\Gamma^{2PI}(G)$ at leading order in $1/N$. These are:

1. a double-tadpole with the g_1 interaction and one with the g_2 interaction

$$\frac{g_1}{4} \int d^d x G_{\mathbf{ab}}(x, x) \hat{P}_{\mathbf{ab};\mathbf{cd}}^{(1)} G_{\mathbf{cd}}(x, x) + \frac{g_2}{4} \int d^d x G_{\mathbf{ab}}(x, x) \hat{P}_{\mathbf{ab};\mathbf{cd}}^{(2)} G_{\mathbf{cd}}(x, x) . \tag{1.3.42}$$

(As before, the edges represent full propagators $G_{\mathbf{ab}}(x, y)$, but we omit the detailed structure of the tensor interactions.)

2. a melonic graph with two tetrahedral interactions

$$\frac{g^2}{8} \int d^d x d^d y \hat{\delta}_{\mathbf{abcd}}^t G_{\mathbf{aa}'}(x, y) G_{\mathbf{bb}'}(x, y) G_{\mathbf{cc}'}(x, y) G_{\mathbf{dd}'}(x, y) \hat{\delta}_{\mathbf{a'b'c'd'}}^t . \tag{1.3.43}$$

1 Introduction

$\Gamma^{2PI}(G)$ is the sum of these contributions. Taking derivatives, the self-energy is

$$\begin{aligned} \Sigma_{\mathbf{ab}}(x, y) &= -g_1 \delta(x - y) \hat{P}_{\mathbf{ab};\mathbf{cd}}^{(1)} G_{\mathbf{cd}}(x, x) - g_2 \delta(x - y) \hat{P}_{\mathbf{ab};\mathbf{cd}}^{(2)} G_{\mathbf{cd}}(x, x) \\ &\quad - g^2 \hat{\delta}_{\mathbf{a}\mathbf{c}_1\mathbf{c}_2\mathbf{c}_3}^t G_{\mathbf{c}_1\mathbf{d}_1}(x, y) G_{\mathbf{c}_2\mathbf{d}_2}(x, y) G_{\mathbf{c}_3\mathbf{d}_3}(x, y) \hat{\delta}_{\mathbf{d}_1\mathbf{d}_2\mathbf{d}_3\mathbf{b}}^t \\ &= -g_1 \text{---}\bigcirc\text{---} - g_2 \text{---}\bigcirc\text{---} - g^2 \text{---}\bigcirc\text{---}, \end{aligned} \quad (1.3.44)$$

and the Bethe–Salpeter kernel writes

$$\begin{aligned} \kappa_{\mathbf{ab};\mathbf{cd}}(x, y; w, z) &= \left[2g_1 \hat{P}_{\mathbf{ab};\mathbf{cd}}^{(1)} + 2g_2 \hat{P}_{\mathbf{ab};\mathbf{cd}}^{(2)} \right] \delta(x - y) \delta(x - w) \delta(x - z) \\ &\quad + 2g^2 \hat{\delta}_{\mathbf{a}\mathbf{c}\mathbf{e}_1\mathbf{e}_2}^t G_{\mathbf{e}_1\mathbf{f}_1}(x, y) G_{\mathbf{e}_2\mathbf{f}_2}(x, y) (x, y) \hat{\delta}_{\mathbf{f}_1\mathbf{f}_2\mathbf{b}\mathbf{d}}^t \\ &\quad \cdot \frac{1}{2} \left[\delta(x - w) \delta(y - z) + \delta(x - z) \delta(y - w) \right] \\ &= 2g_1 \text{---}\times\text{---} + 2g_2 \text{---}\times\text{---} + 2g^2 \cdot \frac{1}{2} \left[\text{---}\bigcirc\text{---} + \text{---}\bigcirc\text{---} \right]. \end{aligned} \quad (1.3.45)$$

In the following we are interested in on-shell quantities. As a consequence of the unbroken $O(N)^3$ symmetry, the index structure of the propagator is fixed on-shell and it can be decomposed as

$$G_{\mathbf{ab}}(x, y) = \delta_{\mathbf{ab}} G(x, y) = \delta_{\mathbf{ab}} \int \frac{d^d p}{(2\pi)^d} e^{ip \cdot (x-y)} G(p), \quad (1.3.46)$$

where $G(x, y)$ and $G(p)$ are just functions that transform as a scalar under $O(N)^3$. By abuse of notation, we use the same symbol for these objects and distinguish them by their arguments as functions on position or momentum space, and by the presence of indices. Performing the sums over indices, the on-shell 2PI effective action, i.e., minus the free energy, writes

$$\begin{aligned} \frac{\Gamma(G)}{N^3} &= \frac{1}{2} \int d^d x d^d y (-\Delta + m^2) G(x, y) \delta(x - y) - \frac{1}{2} \frac{\text{Tr} \ln(G)}{N^3} \\ &\quad + \frac{g_2}{4} \int d^d x [G(x, x)]^2 + \frac{g^2}{8} \int d^d x d^d y [G(x, y)]^4. \end{aligned} \quad (1.3.47)$$

Notice that the g_1 term vanishes because $\sum_{\mathbf{c}}, \hat{P}_{\mathbf{ab};\mathbf{cc}}^{(1)} = 0$. The Schwinger–Dyson equation can be reduced to an equation for $G(p)$, and writes

$$G^{-1}(p) = p^2 + m^2 + g_2 \int \frac{d^d q}{(2\pi)^d} G(q) + g^2 \int \frac{d^d q}{(2\pi)^d} \frac{d^d k}{(2\pi)^d} G(q) G(k) G(p + q + k). \quad (1.3.48)$$

This is a closed equation for the function $G(p)$ and the basis for the results presented in Chapter 7.

1.4 Perturbative expansions and Borel summability

In practice, perturbation theory methods allow for extremely precise calculations of physical observables that can be accessed by experiments. Two examples are the anomalous magnetic dipole moment of the electron (calculated up to tenth order in the coupling [173–175]) and critical exponents of the $O(N)$ -symmetric ϕ^4 vector model (calculated up to sixth order [176]).²² However, in most cases the perturbative series is only an asymptotic series with zero radius of convergence, and non-analytic terms are absent in perturbation theory—for example, the Taylor series of $e^{-1/g}$ at $g = 0$ is identically zero. Such contributions typically arise from instantons, i.e., critical points of the action at which the latter is finite. In a semiclassical approximation, the path integral is dominated by its critical points and evaluated by a saddle point (Laplace) approximation. Schematically

$$\int \mathcal{D}\phi e^{-S(\phi)} \simeq \sum_c e^{-S_c} A_c, \quad (1.4.1)$$

where the sum is over the different critical points, S_c is the action at the critical points, and A_c captures the contribution from fluctuations around them. The action at the critical points S_c depends on the coupling constants and typically leads to the mentioned non-analytic terms.

An example for an instanton effect in QFT is the Schwinger effect [178, 179], i.e., the creation of positron-electron pairs in a strong electric field E . At leading one-loop order, the production rate in a constant field is

$$\Gamma = \frac{(eE)^2}{(2\pi)^3} \sum_{n=1}^{\infty} \frac{1}{n^2} e^{-\frac{\pi m^2}{eE} n}, \quad (1.4.2)$$

and is clearly non-analytic in e . This formula can be obtained from a saddle point approximation around an instanton configuration that can be interpreted as charged particles traveling in circles [180].

In QFT, so-called renormalons are another typical source of non-analytic contributions. Here, the focus is on instanton-like effects. The renormalon singularities are different and stem from the factorial growth of the renormalized amplitude of a family of Feynman diagrams.

In the following, we will discuss some techniques that can be used to resum the perturbative series (which is necessary to obtain accurate predictions for physical observables) and to shed light on the effect of instantons in the perturbative series. In doing so, we will work with zero-dimensional toy model field theories, which can be thought of as a field theory living at a single spacetime point, and thus the path integral is just an ordinary integral. In this setting, renormalization is absent, and the calculation of the amplitudes of Feynman graphs is a pure combinatorics problem (see also the book [181]). Still, the perturbative series is divergent because of the factorial growth of the number of Feynman graphs. For concreteness, consider a function $Z(g)$ of the variable $g \in \mathbb{C}$, defined by the integral

$$Z(g) = \int_{-\infty}^{+\infty} \frac{dx}{\sqrt{2\pi}} e^{-S(g,x)}, \quad S(g,x) = \frac{1}{2}x^2 + \frac{g}{4!}x^4. \quad (1.4.3)$$

²² To study critical phenomena, a widely used method is the ϵ -expansion, which also relies on RG and perturbative methods, but works in $d = 4 - \epsilon$ dimensions. Similar to the coupling expansion, the ϵ -expansion is divergent, but very precise critical exponents can be calculated with resummation methods [177].

1 Introduction

In this example, it is easy to see that the perturbative series of $Z(g)$ (its Taylor expansion around $g = 0$) will be problematic because the integral is convergent for $\Re(g) > 0$ but divergent for $\Re(g) < 0$. Since the integral is convergent in the right half of the complex plane, $Z(g)$ can be analytically continued to a larger domain, but $g = 0$ is a branch point and will stay on the boundary of the domain of analyticity. In Chapter 6, a generalization of this model to an N component vector is discussed.

The perturbative series of $Z(g)$ around the critical point $x = 0$ is

$$A_0(g) = \sum_{n=0}^{\infty} \frac{1}{n!} \frac{(-g)^n}{(4!)^n} \int_{-\infty}^{+\infty} \frac{dx}{\sqrt{2\pi}} e^{-\frac{1}{2}x^2} x^{4n} = \sum_{n=0}^{\infty} a_{0,n} g^n, \quad (1.4.4)$$

$$a_{0,n} = \frac{(-1)^n (4n)!}{n! (2n)! 2^{6n}} \left(\frac{2}{3}\right)^n,$$

and one can see²³ that the coefficients $|a_{0,n}|$ grow factorially as $n \rightarrow \infty$. The instantons are the two non-trivial solutions to the equation $dS/dx = 0$. Writing $g = |g|e^{i\varphi}$ they are

$$x_{\pm} = \pm i e^{-i\frac{\varphi}{2}} \sqrt{\frac{6}{|g|}}, \quad S(x_{\pm}) = -\frac{3}{2g}, \quad (1.4.5)$$

and for real g the instantons are purely imaginary. We analytically continue the function $Z(g)$, $g = |g|e^{i\varphi}$ to $|\varphi| > \pi/2$ by tilting the integration contour. We distinguish the counterclockwise continuation $Z_+(g)$ for $\varphi > \pi/2$ and the clockwise continuation $Z_-(g)$ for $\varphi < -\pi/2$. To keep the integral convergent, the integration contour is rotated in the opposite direction by an angle θ

$$Z_{\pm}(g) = \int_{e^{\mp i\theta}\mathbb{R}} \frac{dx}{\sqrt{2\pi}} e^{-\frac{1}{2}x^2 - \frac{1}{4!}|g|e^{i\varphi}x^4} = e^{\mp i\theta} \int_{\mathbb{R}} \frac{dx}{\sqrt{2\pi}} e^{-e^{\mp 2i\theta}\frac{1}{2}x^2 - \frac{1}{4!}|g|e^{i(\varphi \mp 4\theta)}x^4}. \quad (1.4.6)$$

Fixing the tilting angle θ by $\varphi \mp 4\theta = \pi/2$, the quartic term in the action is purely imaginary and the integral is convergent as long as $-\pi/4 < \theta < \pi/4$. Thus, we obtained an analytic continuation of $Z(g)$ up to $|\varphi| < 3\pi/2$. The clockwise and counterclockwise continuations do not agree for $|\varphi| > \pi$, and one should think of $Z(g)$ as a function on a Riemann surface where the regions $|\varphi| > \pi$ belong to the adjacent Riemann sheets. In the right half of the complex plane the different continuations agree. Moreover, the perturbative expansion of $Z_{\pm}(g)$ at $g = 0$ is given by $A_0(g)$ (Eq. (1.4.4)), the same formula as for $Z(g)$.

Borel summation. Let us now return to the problem of resumming the perturbative series in Eq. (1.4.4). More generally, inside its domain of analyticity, an analytic function is the sum of its Taylor series. Ordinary summation provides a one-to-one correspondence (inside the radius of convergence) between convergent power series and analytic functions. Borel summation [182] is a method to extend this correspondence (under certain conditions) to analytic functions that have been Taylor expanded on the boundary of their domain of analyticity, which causes the Taylor series to not be summable in the ordinary sense. See [130] and the appendix of [48] for Borel summability in the context of constructive QFT.

One has to distinguish two notions that will be defined in a moment: Borel summable function and Borel summable series. They have the following properties and relations:

²³ Using Stirling's formula $n! \sim \sqrt{2\pi n} n^{n+1/2} e^{-n}$ for $n \rightarrow \infty$.

1. the Borel sum of a Borel summable series is unique.
2. if a series is the (possibly divergent) Taylor expansion of a Borel summable function at a point $z \in \mathbb{C}$, then that function is the unique Borel summable function with the given Taylor series.
3. the (possibly divergent) Taylor expansion of a Borel summable function is a Borel summable series and that function is the Borel sum of its Taylor series.

So in principle, the strategy to handle the perturbative series is to prove a priori that the function of interest (e.g., the partition function or free energy) is Borel summable, and then try to Borel sum the perturbative series. The last step is generically very hard, because it involves constructing an analytic continuation. However, proving the Borel summability of the original function guarantees that the resummation must in principle work. In numerical applications where one does not have access to the full perturbative series, there exist the Páde–Borel method (see, e.g., the review [183]) to construct an approximation of the Borel sum.

Now we turn to the definitions and details.

Definition 4 (Borel summable series). A power series $A(z) = \sum_{n=0}^{\infty} a_n z^n$ is called Borel summable if: (1.) the series

$$B(t) = \sum_{n=0}^{\infty} \frac{a_n}{n!} t^n, \quad (1.4.7)$$

called its Borel transform, has a non-zero radius of convergence r_B , (2.) $\exists \sigma$ with $0 < 1/\sigma < r_B$, such that $B(t)$ can be analytically continued inside the strip-like region $S_\sigma \equiv \{t \mid \text{dist}(t, \mathbb{R}_+) < 1/\sigma\}$, and (3.) $B(t) \leq K e^{|t|/R}$, $\forall t \in S_\sigma$ and real positive constants K and R .

The crucial point is, that the radius of convergence of $B(t)$ can be non-zero even if the radius of convergence of $A(z)$ is zero. The complex t -plane is often called the Borel plane. The Borel sum of the series $A(z)$ is defined by the integral

$$f(z) = \frac{1}{z} \int_0^{\infty} dt B(t) e^{-t/z}. \quad (1.4.8)$$

Constructing the necessary analytic continuation of the Borel transform $B(t)$ is usually very difficult.

Definition 5 (Borel summable function). A function $f(z)$ is Borel summable in z at the origin if: (1.) it is analytic in a disk $D_R \equiv \{z \in \mathbb{C} \mid \Re(1/z) > 1/R\}$ of some fixed radius $R > 0$ and tangent in $z = 0$ to the imaginary axis, (2.) it admits a Taylor expansion at $z = 0$ with factorial bound on the Taylor remainder

$$f(z) = \sum_{n=0}^{r-1} a_n z^n + R_r(z), \quad |R_r(z)| \leq K \sigma^r r! |z|^r \quad \forall z \in D_R, \quad (1.4.9)$$

for positive real constants K and σ .

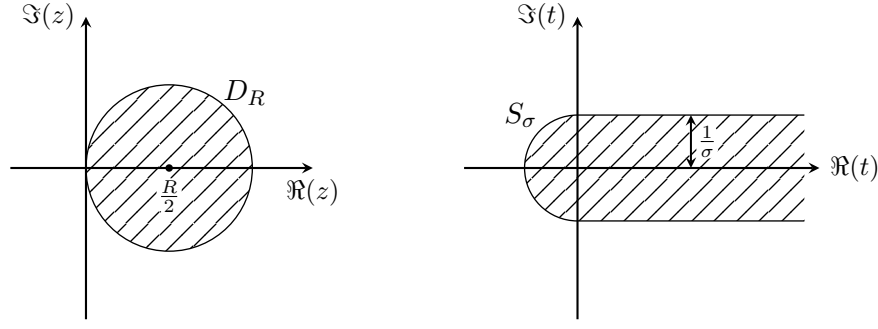


Figure 1.11. The disk D_R in the complex z plane (left) and the strip S_σ in the Borel plane (right).

The Borel sum of a Borel summable series is a Borel summable function with the same constants R , K , and σ in both definitions. The sets S_σ and D_R are illustrated in Fig. 1.11.

The Borel sum of the series $A(z)$ is not the unique function analytic in D_R whose asymptotic expansion is the original series. For example the unique Borel sum of the series that is identically zero is the function that is identically zero, but the function $e^{-1/z}$ is analytic in D_R (which does not include the origin) and its Taylor series at $z = 0$ is also identically zero. In fact, $e^{-1/z}$ is not Borel summable at the origin and thus the uniqueness breaks down.

The following theorem states the relation between a Borel summable function and the Borel sum of its Taylor series. It is due to A. Sokal [184] and was, in fact, a rediscovery of a theorem by F. Nevanlinna [185].

Theorem (Nevanlinna–Sokal). *Let $f(z) = \sum_{n=0}^{r-1} a_n z^n + R_r(z)$ be a Borel summable function, then the following holds true:*

1. *the Taylor series of $f(z)$ at the origin is a Borel summable series, i.e., the Borel transform of the Taylor series $B(t) = \sum_{n=0}^{\infty} \frac{a_n}{n!} t^n$ is an analytic function for $|t| < 1/\sigma$ and admits an analytic continuation in the strip S_σ , such that $|B(t)| \leq K e^{|t|/R}$, $\forall t \in S_\sigma$.*
2. *for $z \in D_R$, $f(z)$ is given by the Borel sum of its Taylor series $f(z) = \frac{1}{z} \int_0^\infty dt B(t) e^{-t/z}$, and the integral converges absolutely in that disk.*

This theorem is not optimal, in the sense that it does not reconstruct the maximal domain of analyticity of the Borel sum, and there are modifications that allow the summation of series that diverge even faster. For example, for the problem in Chapter 6 one already needs a generalization where the bound on $|R_r(z)|$ can grow proportional to $r! r^\beta$, $\beta > 0$. More generally, there exist extensions of Borel summation to series whose coefficients a_n diverge as fast as $\Gamma(kn + 1)$, for rational $k \geq 1$, and even as fast as $\Gamma(kn + 1) e^{\alpha n^2/4}$, for suitable positive constants k and α [183, 186, 187].

As can be seen from the formula of the Borel sum, Borel summation is directional (as stated, along the positive real axis). Tilting z and t in the complex plane leads to Borel summation along different directions.

Now, let us continue with the example given in Eq. (1.4.3) and apply the method of Borel summation and in particular the Nevanlinna–Sokal theorem. In order to not confuse the reader with the small technical calculations we summarize the results first:

1. $Z_{\pm}(g)$ is a Borel summable function in g for all directions in the upper (respectively lower) half of the complex plane.
2. The Borel transform $B(t)$ of the perturbative series $A_0(g)$ of $Z(g)$ and $Z_{\pm}(g)$ has a leading singularity at $t = -3/2$ on the negative real axis.

We focus on $Z_+(g)$, as the calculation for $Z_-(g)$ is completely analogous, and first check the Borel summability of $Z_+(g)$ in g . As $Z_+(g)$ is analytic in a plane with a cut on the negative imaginary axis it is in particular analytic inside tilted disks D_R , $R > 0$, that are tangent to the imaginary axis tilted counterclockwise by $\pi/2 + \varphi$ for $\varphi < \pi$. Therefore $Z_+(g)$ can at most be Borel summable in the upper half of the complex plane ($0 \leq \varphi < \pi$). It remains to calculate the Taylor remainder

$$\begin{aligned} R_r(g) &= \frac{1}{(r-1)!} \int_0^1 du (1-u)^{r-1} \frac{d^r Z_+(ug)}{du^r} \\ &= \frac{g^r}{(r-1)!(4!)^r} \int_0^1 du (1-u)^{r-1} \int_{e^{-i\theta}\mathbb{R}} \frac{dx}{\sqrt{2\pi}} e^{-\frac{1}{2}x^2 - \frac{1}{4!}gx^4} x^{4r}. \end{aligned} \quad (1.4.10)$$

Taking the absolute value, remembering that we fixed $\theta = \varphi/4 - \pi/8$ such that the quartic term is purely imaginary and thus uniformly bounded by 1, and integrating over u , we obtain a bound on the Taylor remainder

$$\begin{aligned} |R_r(g)| &\leq \frac{|g|^r}{r!(4!)^r} \int_{\mathbb{R}} \frac{dx}{\sqrt{2\pi}} e^{-\frac{1}{2}\cos(\phi/2 - \pi/4)x^2} x^{4r} \\ &= \frac{|g|^r}{r!(4!)^r} \frac{(4r)!}{2^{2r}(2r)!} \frac{1}{[\cos(\phi/2 - \pi/4)]^{4r+1/2}}, \end{aligned} \quad (1.4.11)$$

which is a factorial bound for the range $-\pi/2 < \varphi < 3\pi/2$. Thus, as stated above, $Z_+(g)$ is Borel summable along all the directions in the upper half of the complex plane. For the second claim we look at the asymptotic behavior of the Borel transform of the perturbative series

$$\begin{aligned} B(t) &= \sum_{n=0}^{\infty} b_n t^n = \sum_{n=0}^{\infty} \frac{a_{0,n} t^n}{n!}, \\ b_n &= \frac{(-1)^n (4n)!}{(n!)^2 (2n)! 2^{6n}} \left(\frac{2}{3}\right)^n \underset{n \rightarrow \infty}{\sim} \frac{1}{\sqrt{2\pi}} \frac{1}{n} \left(-\frac{2}{3}\right)^n. \end{aligned} \quad (1.4.12)$$

Summing the asymptotic behavior of the coefficients, one can recover the position of the leading singularity (the one closest to the origin)

$$\sum_{n=0}^{\infty} \frac{1}{n} \left(-\frac{2t}{3}\right)^n = -\ln \left(1 + \frac{2t}{3}\right), \quad (1.4.13)$$

which is at $t = -3/2$ on the negative real axis. Because of this singularity, $Z_{\pm}(g)$ ceases to be Borel summable past $|\varphi| = \pi$, and this explains why the Borel sums coming from above and below, i.e., $Z_+(g)$ and $Z_-(g)$, will not agree past the negative real axis.

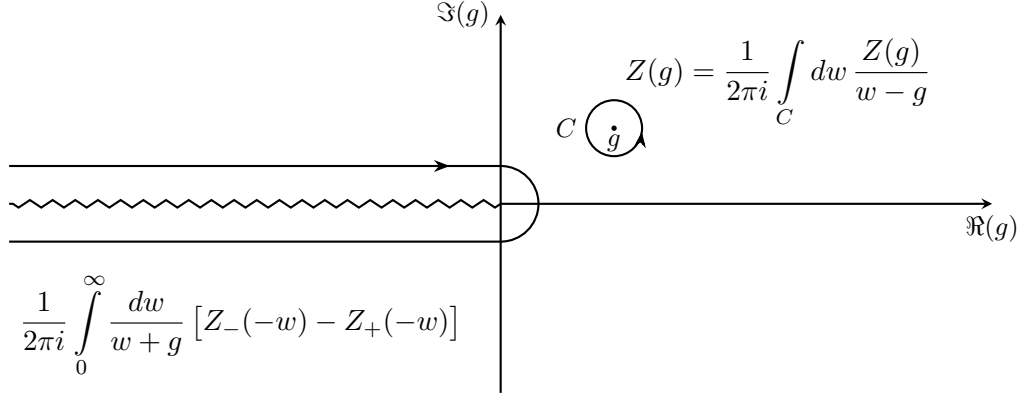


Figure 1.12. Contours in the complex g plane. Using Cauchy's integral formula, the value of $Z(g)$ can be expressed as a contour integral along the small circle C . The contour C can be deformed to a contour around the cut along the negative real axis and this integral can be expressed using the difference between Z_+ and Z_- .

The singularities in the Borel plane capture a lot of information about the original function. For example, it is no accident that the exponential in the integrand of the Borel sum formula in Eq. (1.4.8) recovers the instanton contribution $e^{3/(2g)}$. On the contrary, the instanton can be seen as the reason for this singularity in the Borel plane, since for $\varphi \rightarrow \pm\pi$ the instantons $x_\pm(-|g|) = \pm\sqrt{6/|g|}$ approach the real axis and thus cross the original integration contour. This behavior can also be understood by using complex Morse theory and the method of Lefschetz thimbles (see, e.g., [188, 189]). In this framework, each integration contour in the complex x plane is decomposed into a sum of more convenient contours, called thimbles. The point is that the number of contributing thimbles can change when some parameter, like g , is changed. In our example, this happens when the instantons cross the real axis. More details on this point of view can be found in Appendix A of Chapter 6.

Much more information about the instantons is encoded in the perturbative series. In fact, as explained pictorially in Fig. 1.12, $Z(g)$ can be related, using the Cauchy formula, to the discontinuity of the counterclockwise and clockwise analytic continuations for negative $g = -|g|$, $Z_+(-|g|) - Z_-(-|g|)$. Denote the perturbative expansion of $Z_\pm(-g)$ around the instanton as

$$\pm i e^{-\frac{3}{2g}} A_I(-g), \quad A_I(-g) = \sum_{n=0}^{\infty} a_{I,n} (-g)^n, \quad (1.4.14)$$

where the coefficients $a_{I,n}$ are real. Expanding $Z(g)$ and the discontinuity in Fig. 1.12 in their perturbative series and comparing coefficients of g , one can deduce a formal relation between the series coefficients

$$a_{0,n} = \left(-\frac{2}{3}\right)^n \sum_{k=0}^{\infty} \left(-\frac{3}{2}\right) \frac{\Gamma(n-k)}{\pi} a_{I,k}. \quad (1.4.15)$$

This shows that the expansion around the instanton configuration is captured by the large n behavior of the coefficients of the perturbative expansion around the $x = 0$ configuration.

In general, the study of the relations between perturbative and nonperturbative (like the instantons) sectors goes under the name of resurgence. This entails the general study of singularities

in the Borel plane, as these singularities govern the discontinuities of the analytical continuations. More on this topic and similar calculations in a more complicated but still zero-dimensional model can be found in the paper reproduced in Chapter 6.

1.5 The BKAR forest formula

This section is devoted to introducing the Brydges–Kennedy–Abdesselam–Rivasseau (BKAR) forest formula [190, 191]. It is a combinatorial formula that can be used for cluster expansions, that are common in statistical physics. Due to its symmetry and positivity properties, this formula is well suited for rigorous nonperturbative methods and applied in constructive QFT, e.g., to prove Borel summability in ϕ^4 theory and vector models [192–195], and also in random matrix and tensor models [47, 196–201].

In Chapter 6, we use it to write down a convergent series expansion for the free energy, therefore enabling the proofs of analyticity and Borel summability that would not have been possible with a formal expansion in Feynman graphs.

Despite being used predominantly in constructive QFT, the formula itself is very general and in essence a Taylor expansion formula for functions of several variables. Therefore, it can be understood without knowing about these subjects. In the second half of this section, we will outline how the forest formula is useful in the QFT context. We closely follow Appendix D in Chapter 6 and the review [202] but add some details and illustrations.

Let us consider a set of n points labeled $i = 1 \dots n$, which we identify with the set of vertices of the complete graph \mathcal{K}_n . The set of unordered pairs of such points has $n(n-1)/2$ elements $e = (i, j)$ for $1 \leq i, j \leq n$, $i \neq j$ and can be identified with the set of edges of \mathcal{K}_n . Let us consider a smooth function $f : [0, 1]^{n(n-1)/2} \rightarrow \mathbb{R}$ depending on the edge variables $x_e \equiv x_{ij}$.

We define a forest \mathcal{F} as an edge-subgraph of the complete graph \mathcal{K}_n having no cycles (loops). Every forest is a disjoint union of trees. We denote by $|\mathcal{F}|$ the number of edges of \mathcal{F} . See Fig. 1.13 for illustration.

Theorem (BKAR forest formula). *We have (with the convention that empty products are 1):*

$$f(1, \dots, 1) = \sum_{\mathcal{F}} \underbrace{\int_0^1 \cdots \int_0^1}_{|\mathcal{F}| \text{ times}} \left(\prod_{e \in \mathcal{F}} du_e \right) \left[\left(\prod_{e \in \mathcal{F}} \frac{\partial}{\partial x_e} \right) f \right] \left(w_{kl}^{\mathcal{F}}(u_{\mathcal{F}}) \right), \quad (1.5.1)$$

where:

- the sum runs over the forests \mathcal{F} drawn over the labeled vertices $i = 1, \dots, n$, including the empty forest (having no edge). To each edge $e \in \mathcal{F}$ we attribute a variable u_e that is integrated from 0 to 1 and we denote $u_{\mathcal{F}} = \{u_e \mid e \in \mathcal{F}\}$.
- the derivative $\left(\prod_{e \in \mathcal{F}} \frac{\partial}{\partial x_e} \right) f$ is evaluated at the point:

$$w_{kl}^{\mathcal{F}}(u_{\mathcal{F}}) = \inf_{e' \in P_{k-l}^{\mathcal{F}}} \{u_{e'}\}, \quad (1.5.2)$$

where $P_{k-l}^{\mathcal{F}}$ denotes the unique path in the forest \mathcal{F} joining the vertices k and l , and the infimum is set to zero if such a path does not exist.

Setting by convention $w_{kk}^{\mathcal{F}}(u_{\mathcal{F}}) \equiv 1$, for any assignment of tree edge variables $0 \leq u_{\mathcal{F}} \leq 1$ the symmetric $n \times n$ matrix $W^{\mathcal{F}}(u_{\mathcal{F}}) = (w_{kl}^{\mathcal{F}}(u_{\mathcal{F}}))_{1 \leq k, l \leq n}$ is positive.

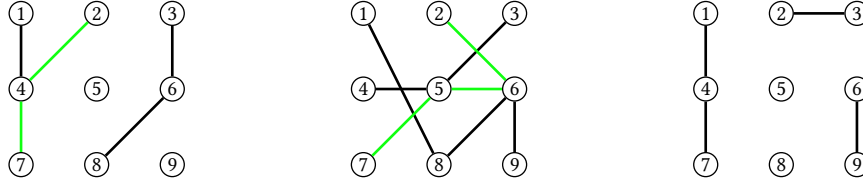


Figure 1.13. Three forests on the set of vertices labeled $1, 2, \dots, 9$. The unique path in the forest between the vertices 2 and 7 is drawn in green if it exists.

Proof idea. A full proof can be found in [202]. Here we briefly describe the idea of the proof and explain the positivity of $W^{\mathcal{F}}(u_{\mathcal{F}})$. Let \mathcal{F} be a forest, $u_e \in [0, 1]$ a variable for each edge $e \in \mathcal{F}$ and define the symmetric $n \times n$ matrix

$$W_{kl}^{\mathcal{F}}(u_{\mathcal{F}}; t) = \begin{cases} \inf_{e \in P_{k-l}^{\mathcal{F}}} \{u_e\}, & k \neq l \text{ and } P_{k-l}^{\mathcal{F}} \text{ exists} \\ t, & k \neq l \text{ and } k \text{ and } l \text{ are not connected in } \mathcal{F} \\ 1, & k = l \end{cases} \quad (1.5.3)$$

Note that $W^{\mathcal{F}}(u_{\mathcal{F}}; 0) = W^{\mathcal{F}}(u_{\mathcal{F}})$ and for the empty forest $W^{\emptyset}(u_{\emptyset}; t)$ is the matrix with 1 on the diagonal and t everywhere else. Let now $f : [0, 1]^{n(n-1)/2} \rightarrow \mathbb{R}$ be a function of the edge variable $x_e \equiv x_{ij}$, $e = (i, j)$, that we encode as the off-diagonal elements of a symmetric matrix. The crucial point is that

$$\frac{d}{dt} \left[f \left(W^{\mathcal{F}}(u_{\mathcal{F}}; t) \right) \right] = \sum_{\substack{\text{edges } e \text{ s.t.} \\ e \cup \mathcal{F} \text{ is a forest}}} \left(\frac{\partial}{\partial x_e} f \right) \left(W^{\mathcal{F}}(u_{\mathcal{F}}; t) \right), \quad (1.5.4)$$

because the variable t is associated to edges e that do not connect vertices that are already connected in \mathcal{F} and thus $e \cup \mathcal{F}$ is still a forest. The forest formula is then proven by iterated Taylor expansion. At first order

$$\begin{aligned} f(1, \dots, 1) &= f \left(W^{\emptyset}(u_{\emptyset}; 0) \right) + \int_0^1 dt \frac{d}{dt} \left[f \left(W^{\emptyset}(u_{\emptyset}; t) \right) \right] \\ &= f \left(W^{\emptyset}(u_{\emptyset}) \right) + \sum_e \int_0^1 dt \left(\frac{\partial}{\partial x_e} f \right) \left(W^{\emptyset}(u_{\emptyset}; t) \right) \\ &= f \left(W^{\emptyset}(u_{\emptyset}) \right) + \sum_e \int_0^1 du_e \left(\frac{\partial}{\partial x_e} f \right) \left(W^{\emptyset}(u_{\emptyset}; t = u_e) \right), \end{aligned} \quad (1.5.5)$$

where in the last step we relabeled the integration variable. The sum over e is equivalent to a sum over forests with one edge. In order to iterate, for each forest $\mathcal{F} = \{e\}$ we set $W^{\emptyset}(u_{\emptyset}; t = u_e) = W^{\{e\}}(u_{\{e\}}; t = u_e)$, i.e., we keep the variable u_e at the edge e fixed and let all the others be inter-

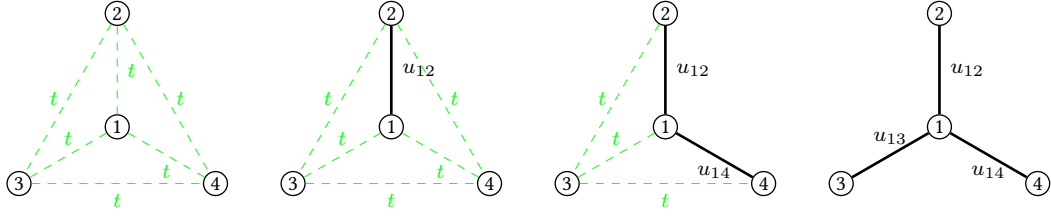


Figure 1.14. Illustration of how a forest (in this example a maximal forest on four vertices) is generated, as described in the proof of the BKAR forest formula. The forest grows by successively selecting edges e with interpolation parameter t and fixing this parameter to u_e . Note that in the third step the edge $(2, 4)$ is missing, since it cannot be added without forming a cycle.

polated by a second Taylor expansion in t . Iterating this process a second time gives

$$\begin{aligned}
 f(W^\emptyset(u_\emptyset)) &+ \sum_{\mathcal{F}=\{e\}} \int_0^1 du_e \left(\frac{\partial}{\partial x_e} f \right) (W^{\{e\}}(u_{\{e\}})) \\
 &+ \sum_{\mathcal{F}=\{e_1, e_2\}} \int_0^1 du_{e_1} \int_0^{u_{e_1}} du_{e_2} \left[\left(\frac{\partial^2}{\partial x_{e_2} \partial x_{e_1}} f \right) \right] (W^{\{e_1, e_2\}}(u_{\{e_1, e_2\}}; t = u_{e_2})) .
 \end{aligned} \tag{1.5.6}$$

In this way, one builds up all possible forests on the set of n labeled vertices, edge by edge. Fig. 1.14 should help to visualize this process. The same forest appears $|\mathcal{F}|!$ times, corresponding to different orderings of its edges. The process stops at a maximal forest with $|\mathcal{F}| = n - 1$ edges, where all vertices are connected.

The most subtle point in the forest formula is that $W^{\mathcal{F}}(u_{\mathcal{F}})$ is a positive matrix. To see this, we proceed as follows. A forest \mathcal{F} divides the set of vertices $\{1, \dots, n\}$ into several connected components (blocks) corresponding to the trees in the forest. If \mathcal{F} is the empty forest, the blocks are all singletons consisting in a unique vertex per block. For any forest \mathcal{F} , the matrix:

$$B_{kl}^{\mathcal{F}} = \begin{cases} 1, & \text{if } k, l \text{ belong to the same block of } \mathcal{F} \\ 0, & \text{otherwise} \end{cases}, \tag{1.5.7}$$

is positive. Indeed, denoting $b \subset \mathcal{F}$ the blocks of \mathcal{F} and $k \in b$ the vertices in the block b :

$$\sum_{k, l} B_{kl}^{\mathcal{F}} a_k a_l = \sum_{b \subset \mathcal{F}} \left(\sum_{k \in b} a_k \right)^2. \tag{1.5.8}$$

Let us denote the number of edges in \mathcal{F} by $q \equiv |\mathcal{F}|$. We order the edges of \mathcal{F} in decreasing order of their parameters u :

$$1 \geq u_{e_1} \geq u_{e_2} \geq \dots u_{e_q} \geq 0. \tag{1.5.9}$$

Adding edges one by one, starting from the highest edge, we obtain a family of subforests of \mathcal{F} (see also Fig. 1.15):

$$\mathcal{F}^0 = \emptyset, \quad \mathcal{F}^1 = \{e_1\}, \quad \mathcal{F}^2 = \{e_1, e_2\}, \dots, \quad \mathcal{F}^q = \{e_1, \dots, e_q\} = \mathcal{F}, \tag{1.5.10}$$

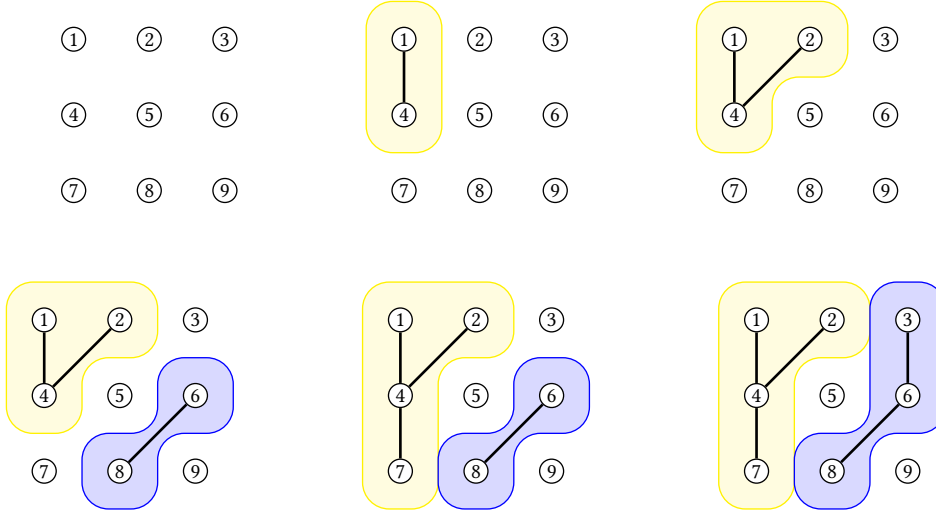


Figure 1.15. The subforests $\mathcal{F}^0, \mathcal{F}^1, \dots, \mathcal{F}^5$ of the first forest in Fig. 1.13 for the ordering $1 \geq u_{12} \geq u_{24} \geq u_{68} \geq u_{36} \geq 0$ of edge parameters. The non-singleton blocks of the forests are highlighted.

and the matrix $W^{\mathcal{F}}(u_{\mathcal{F}})$ writes as:

$$W^{\mathcal{F}}(u_{\mathcal{F}}) = (1 - u_{e_1})B^{\mathcal{F}^0} + (u_{e_1} - u_{e_2})B^{\mathcal{F}^1} + \dots + u_{e_q}B^{\mathcal{F}^q}. \quad (1.5.11)$$

Indeed, if i and j do not belong to the same block of $\mathcal{F}^q = \mathcal{F}$, then they do not belong to the same block in any of the \mathcal{F}^s , $s \leq q$ and none of the terms above contribute, hence $w_{ij}^{\mathcal{F}}(u_{\mathcal{F}}) = 0$. If, on the other hand, i and j belong to the same block of \mathcal{F} , then:

$$\left[(1 - u_{e_1})B^{\mathcal{F}^0} + (u_{e_1} - u_{e_2})B^{\mathcal{F}^1} + \dots + u_{e_q}B^{\mathcal{F}^q} \right]_{ij} = u_{e_s}, \quad (1.5.12)$$

where s is such that i and j belong to the same block of \mathcal{F}^s , but belong to two different blocks of \mathcal{F}^{s-1} . As $u_{e_s} \leq u_{e_{s-1}} \leq u_{e_{s-2}} \leq \dots$ it follows that u_{e_s} is the infimum of the u_e in the unique path in \mathcal{F}^s joining i and j , hence it is also the infimum of the u_s in the unique path in \mathcal{F} joining i and j . The matrix $W^{\mathcal{F}}(u_{\mathcal{F}})$ is a convex combination of positive matrices, hence it is itself positive. \square

Computing cumulants. The BKAR forest formula is used in the constructive QFT context to compute the generating function $W(J)$ of cumulants of a perturbed Gaussian measure with action $S(\phi) = \frac{1}{2}(\phi, C^{-1}\phi) + V(\phi)$. The source term $J\phi$ plays no special role and we absorb it in the interaction. We reuse the notation in Section 1.3. Moreover, we will use the derivative representation of the Gaussian integral (see [203] for a detailed discussion), which essentially follows from the fact that moments of a normalized Gaussian measure can be computed by (Wick) contractions and these contractions can be implemented by a derivative operator. Thus, for every polynomial

$$\int \frac{d\phi}{\mathcal{N}} e^{-\frac{1}{2}(\phi, C^{-1}\phi)} f(\phi) = \left[e^{\frac{1}{2}(\delta_{\phi}, C\delta_{\phi})} f(\phi) \right]_{\phi=0}, \quad (1.5.13)$$

where we denote $(\delta_{\phi}, C\delta_{\phi}) \equiv \frac{\delta}{\delta\phi_a} C_{ab} \frac{\delta}{\delta\phi_b}$ and \mathcal{N} is the constant that normalizes the Gaussian integral.

1 Introduction

In order to apply the forest formula, one starts as in naive perturbation theory by expanding the interaction

$$Z(J) = e^{W(J)} = \left[e^{\frac{1}{2}(\delta_\phi, C\delta_\phi)} e^{-V(\phi)} \right]_{\phi=0} = \sum_{n=0}^{\infty} \frac{(-1)^n}{n!} \left[e^{\frac{1}{2}(\delta_\phi, C\delta_\phi)} [V(\phi)]^n \right]_{\phi=0} \quad (1.5.14)$$

The difference is that instead of computing the Gaussian integral directly, we now use a replica trick, i.e., we substitute $[V(\phi)]^n = \prod_{i=1}^n V(\phi^{(i)}) \Big|_{\phi^{(i)}=\phi}$ and use a covariance that is degenerate between all copies $\phi^{(i)}$. With this trick one can now introduce fictitious link parameters $x_{ij} = x_{ji} = 1$, and obtain

$$\begin{aligned} & \sum_{n=0}^{\infty} \frac{(-1)^n}{n!} \left[e^{\frac{1}{2} \sum_{i,j=1}^n (\delta_{\phi^{(i)}}, C\delta_{\phi^{(j)}})} \prod_{i=1}^n V(\phi^{(i)}) \right]_{\phi^{(i)}=0} \\ &= \sum_{n=0}^{\infty} \frac{(-1)^n}{n!} \left[e^{\frac{1}{2} \sum_{i,j=1}^n x_{ij} (\delta_{\phi^{(i)}}, C\delta_{\phi^{(j)}})} \prod_{i=1}^n V(\phi^{(i)}) \right]_{\phi^{(i)}=0, x_{ij}=1}. \end{aligned} \quad (1.5.15)$$

We keep $x_{ii} = 1 \forall i$ and want to apply the forest formula to the $n(n-1)/2$ link variables $x_{ij} = x_{ji}$, $i \neq j$. Without loss of generality, take $k < l$ and consider

$$\begin{aligned} & \frac{\partial}{\partial x_{kl}} \left[e^{\frac{1}{2} \sum_{i,j=1}^n x_{ij} (\delta_{\phi^{(i)}}, C\delta_{\phi^{(j)}})} \right] = \frac{\partial}{\partial x_{kl}} \left[e^{\frac{1}{2} \sum_{i=1}^n x_{ii} (\delta_{\phi^{(i)}}, C\delta_{\phi^{(i)}}) + \sum_{i < j} x_{ij} (\delta_{\phi^{(i)}}, C\delta_{\phi^{(j)}})} \right] \\ &= e^{\frac{1}{2} \sum_{i,j=1}^n x_{ij} (\delta_{\phi^{(i)}}, C\delta_{\phi^{(j)}})} (\delta_{\phi^{(k)}}, C\delta_{\phi^{(l)}}). \end{aligned} \quad (1.5.16)$$

Applying now the forest formula, we obtain

$$\begin{aligned} Z(J) &= \sum_{n=0}^{\infty} \frac{(-1)^n}{n!} \sum_{\mathcal{F}_n} \int_0^1 \cdots \int_0^1 \left(\prod_{(i,j) \in \mathcal{F}_n} du_{ij} \right) \\ &\cdot \left\{ e^{\frac{1}{2} \sum_{i,j=1}^n w_{ij}^{\mathcal{F}_n}(u_{\mathcal{F}_n}) (\delta_{\phi^{(i)}}, C\delta_{\phi^{(j)}})} \left[\prod_{(i,j) \in \mathcal{F}_n} (\delta_{\phi^{(i)}}, C\delta_{\phi^{(j)}}) \right] \prod_{i=1}^n V(\phi^{(i)}) \right\}_{\phi^{(i)}=0}, \end{aligned} \quad (1.5.17)$$

where the sum runs over forests \mathcal{F}_n over n labeled vertices. The contribution of each forest factors over its blocks, thus taking the logarithm amounts to summing over connected forests, i.e., trees. Reinstating the source term, we obtain

$$\begin{aligned} W(J) &= \sum_{n=0}^{\infty} \frac{(-1)^n}{n!} \sum_{\mathcal{T}_n} \int_0^1 \cdots \int_0^1 \left(\prod_{(i,j) \in \mathcal{T}_n} du_{ij} \right) \\ &\cdot \left\{ e^{\frac{1}{2} \sum_{i,j=1}^n w_{ij}^{\mathcal{T}_n}(u_{\mathcal{T}_n}) (\delta_{\phi^{(i)}}, C\delta_{\phi^{(j)}})} \left[\prod_{(i,j) \in \mathcal{T}_n} (\delta_{\phi^{(i)}}, C\delta_{\phi^{(j)}}) \right] \prod_{i=1}^n [V(\phi^{(i)}) + J\phi^{(i)}] \right\}_{\phi^{(i)}=0}, \end{aligned} \quad (1.5.18)$$

where the sum runs over trees \mathcal{T}_n over n labeled vertices. Several remarks are in order:

- crucially, $C \otimes w^{\mathcal{F}_n}(u_{\mathcal{F}_n})$ is a positive matrix, hence the integral is a normalized Gaussian integral with positive covariance.

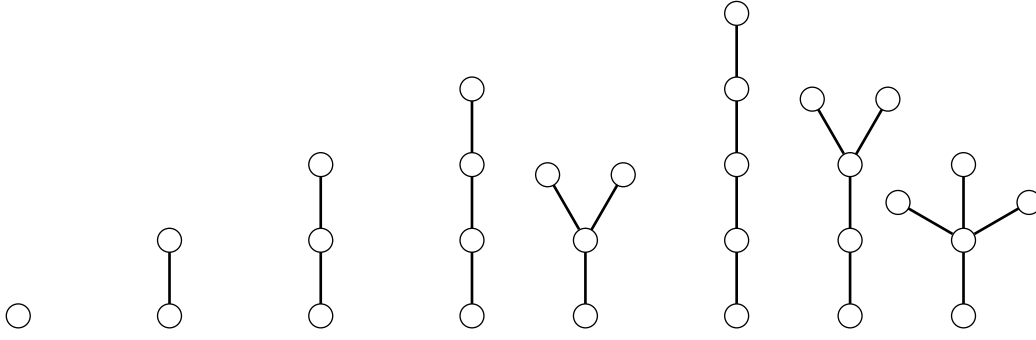


Figure 1.16. The first topologically distinct trees for a small number $n \leq 5$ of vertices. They correspond (from left to right) to 1, 1, 3, 12, 4, 60, 60, 5 distinct labeled trees.

- there are n^{n-2} trees with n labeled vertices (see also Fig. 1.16), thus, asymptotically, their number grows like $n!$. This is slower than the typical number of Feynman graphs, whose number grows like $(2n)!$ in the usual ϕ^4 model. Combined with the $1/n!$ prefactor this series has a better chance of being summable.
- one can give a graphical interpretation to this formula. For each tree \mathcal{T}_n , we interpret the n interaction terms as vertices. The derivatives $\left[\prod_{(i,j) \in \mathcal{T}_n} (\delta_{\phi^{(i)}}, C \delta_{\phi^{(j)}}) \right]$ act on them and generate the tree edges with covariance C . Afterwards, the Gaußian integral creates more pairings between the vertices and thus produces loop edges. In this sense, the sum over Feynman graphs is reorganized as an expansion in spanning trees²⁴

$$W(J) = \sum_{n=0}^{\infty} \frac{(-1)^n}{n!} \sum_{\mathcal{T}_n} \sum_{G \supset \mathcal{T}_n} w(G, \mathcal{T}_n) A(G), \quad (1.5.19)$$

where for each tree the second sum is over Feynman graphs (built according to the procedure above) that have this tree as a spanning tree, $w(G, \mathcal{T})$ is a combinatorial weight²⁵ and we collect the rest, e.g., the dependence on coupling constants, inside the amplitude $A(G)$ of the graph G .

Unfortunately, for a $O(N)$ vector model with quartic interaction $g(\phi^2)^2$ the procedure described above is not sufficient to obtain a convergent expression, because for each tree the contribution of the Gaußian integral is of order $n!$. For the vector model, one can overcome this issue by using the intermediate field/Hubbard–Stratonovich representation. This effectively repackages the degrees of freedom and keeps some of the coupling constants g unexpanded. Analyzing the resulting convergent expression for the free energy $W(0)$ is the content of Chapter 6.

²⁴ A tree inside a connected graph G is said to be spanning if it has the same number of vertices, i.e., it connects all vertices in G .

²⁵ The weights $w(G, \mathcal{T})$ are defined from the forest formula and have a combinatorial interpretation as the percentage of so-called Hepp sectors of G in which the tree \mathcal{T} is leading. See Appendix D of Chapter 6 for more details.

1.6 Overview of the remaining thesis content

The main part of this thesis revolves around five research papers by the author, which are reproduced here in Chapters 3–7. These papers are concerned with three different topics: orthogonal and symplectic random tensor models; constructive field theory methods and so-called transseries expansions in a zero-dimensional $O(N)$ model; and a four-dimensional tensor field theory that is asymptotically free in the ultraviolet but strongly correlated in the infrared. We start with summaries of these papers in Chapter 2, providing accessible overviews with fewer technical details and focusing on key results. For full details and proofs, we refer to the reproductions of the papers themselves. We conclude with a detailed discussion of the five papers in Chapter 8, expanding on their motivation, reviewing their implications, relating them to the existing literature, and highlighting how the work presented in these papers contributes to the field. This final chapter also addresses open questions and outlines potential extensions.

We will now briefly describe how the different topics of the introduction relate to the research work reproduced in the following chapters:

- Sections 1.1 and 1.2 on tensor models provide the necessary background for the papers on orthogonal and symplectic random tensor models in Chapters 3–5, as well as for understanding the $O(N)^3$ tensor field theory in Chapter 7. These sections introduce the concept of tensor models, their graphical representation, and the combinatorial structures that appear in their perturbative expansions.
- The 2PI formalism in Section 1.3.3 is foundational to the work on the large N $O(N)^3$ tensor field theory in Chapter 7. The discussion of asymptotic freedom in Section 1.3.1 provides extended context for the same paper, which studies a four-dimensional model that is asymptotically free in the ultraviolet but strongly correlated in the infrared.
- The $O(N)^3$ tensor field theory is a tensor model with orthogonal symmetry and thus falls into the class of models that are considered in Chapters 3–5, but otherwise the specific model is not of special importance to the content of these chapters.
- Section 1.4 on perturbative expansions and Borel summability is directly relevant to the work in Chapter 6, which investigates questions of analyticity, Borel summability, and transseries expansions in a zero-dimensional $O(N)$ model.
- The BKAR forest formula, introduced in Section 1.5, is a central mathematical tool from constructive field theory and crucial in Chapter 6 to obtain a convergent expansion for the free energy.

Summary

In the following, we summarize the respective publications that are reproduced in the subsequent chapters. The series of papers of Chapters 3–5 is presented in a single section.

2.1 Orthogonal and symplectic random tensor models

The first part of this thesis deals with a generalization of random tensor models to tensors that transform in representations of the real symplectic group $Sp(N)$ (in all that follows, N is an even integer). In certain cases, this generalization inevitably leads to tensors whose components are anticommuting Grassmann numbers and, in this sense, some of these models are fermionic. The need for anticommuting Grassmann numbers can already be seen by considering a real vector v^a , $a = 1, \dots, N$, transforming in the fundamental representation of the symplectic group, $v^a \mapsto M^a_b v^b$, with $M \in Sp(N)$. Invariants under this group action are built by contracting vectors with the symplectic form ω_{ab} . The unique quadratic invariant is

$$v^a \omega_{ab} v^b \mapsto v^c (M^T)_c^a \omega_{ab} M^b_d v^d = v^c \omega_{cd} v^d \quad \forall M \in Sp(N), \quad (2.1.1)$$

and the invariance follows directly from the defining property of $Sp(N)$ as the group of real $N \times N$ matrices preserving the symplectic form. Note that, because of the antisymmetry of ω_{ab} we have

$$v^a \omega_{ab} v^b = -v^a \omega_{ba} v^b = \begin{cases} -v^b \omega_{ba} v^a = 0 & \text{if } v^a \text{ and } v^b \text{ commute} \\ v^b \omega_{ba} v^a & \text{if they anticommute} \end{cases}. \quad (2.1.2)$$

Thus, only if v^a and v^b anticommute, the quadratic invariant is nonvanishing. The vector model mentioned here is known in the field theory context as symplectic fermions.

The connections between the representations of $O(N)$ and $Sp(N)$ have been extensively studied in the literature. King [204] demonstrated that the dimensions of irreducible representations of these two groups coincide when symmetrization and antisymmetrization are interchanged, and N is replaced by $-N$. The so-called negative dimension theorems, or N to $-N$ dualities, which establish a formal relationship between the orthogonal and symplectic groups via $SO(-N) \simeq Sp(N)$, are well known in the context of matrix and vector models [205–210].

Various manifestations of this relationship appear in the literature: $SO(N)$ and $Sp(N)$ gauge theories are related by substituting N with $-N$ [211]; a vector model involving symplectic fermions in three space-time dimensions has been explored in [212, 213]; and an instance of $SO(N)$ and

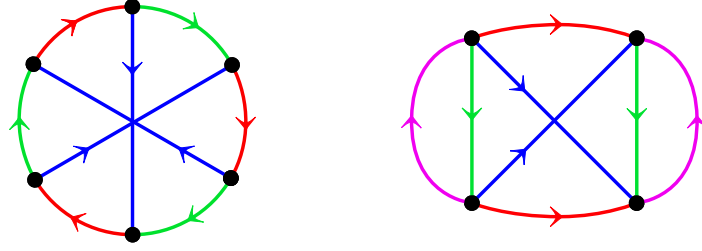


Figure 2.1. Directed edge colored graphs representing a sextic (left) and quartic (right) invariant in the tensor models with symplectic symmetry. Note that in the left graph the tensors are order three and in the right they are order four. This is a colored version of Fig. 1 in [2].

$Sp(N)$ gauge theories featuring matter fields and Yukawa interactions is discussed in [214]. Additionally, a duality between orthogonal and symplectic matrix ensembles (the so-called $\beta = 1, 4$ ensembles) has been established in [215]. From a supergeometric or supersymmetric perspective, such relations emerge naturally [216].

In a series of papers [1–3] (reproduced in Chapters 3–5), we constructed tensor models that showcase such an N to $-N$ duality. The first two papers consider tensors with no permutation symmetry among their indices. In other words, the tensors transform in representations which are products of distinct copies of the fundamental representation of $O(N)$ and $Sp(N)$. We denote by $T^{a_1 \dots a_D}$ the components of a tensor of order D that transform according to

$$T^{a_1 \dots a_D} \mapsto M_{(1) b_1}^{a_1} \dots M_{(D) b_D}^{a_D} T^{b_1 \dots b_D}, \quad (2.1.3)$$

where each $M_{(c)}$ is either an element of $O(N_c)$ or $Sp(N_c)$ for $c \in \{1, \dots, D\}$. The number c , indicating the position of the tensor indices, is called color. For bookkeeping, a parity is assigned to each color: $|c| = 0$ iff the corresponding index transforms under $O(N_c)$ and $|c| = 1$ iff it transforms under $Sp(N_c)$. The tensor components are fermionic (anticommuting Grassmann numbers) iff $\sum_{c=1}^D |c|$ is odd. This means that an odd number of symplectic matrices appear in the transformation rule Eq. (2.1.3).

Invariants are built by contracting several tensors with the bilinear form $g_{a_c b_c}^c$ that is equal to the symmetric $\delta_{a_c b_c}$, iff $|c| = 0$, or the antisymmetric symplectic form $\omega_{a_c b_c}$, iff $|c| = 1$. These invariants can be represented as edge D -colored and directed graphs (Fig. 2.1). The vertices represent tensors and an edge of color c indicates the contraction of two indices having that color. Because of the antisymmetry of ω_{ab} , it is necessary to indicate the order of indices. This is done by directing the graph edges from the second to the first index and adding a small arrow in the graphical notation. Reversing the direction of an edge of color c gives a factor of -1 iff $|c| = 1$.

Now, consider a random tensor model defined as a probability measure

$$d\mu[T] = e^{-S[T]} \mathcal{N} \prod_{a_1 \dots a_D} dT^{a_1 \dots a_D}, \quad (2.1.4)$$

$$S[T] = \frac{1}{2} \left(T^{a_1 \dots a_D} T^{b_1 \dots b_D} \prod_{c=1}^D g_{a_c b_c}^c \right) + \sum_{\substack{\mathcal{B} \text{ connected,} \\ |\mathcal{V}(\mathcal{B})| > 2}} \frac{\lambda_{\mathcal{B}}}{|\mathcal{V}(\mathcal{B})|} I_{\mathcal{B}}(T), \quad (2.1.5)$$

where \mathcal{N} is some normalization constant and the sum runs over connected edge colored graphs \mathcal{B}

with $|\mathcal{V}(\mathcal{B})| > 2$ vertices.²⁶ These graphs encode all the possible different invariants $I_{\mathcal{B}}$ and the prefactors $\lambda_{\mathcal{B}}$ are called coupling constants. The model is invariant under the symmetry transformation Eq. (2.1.3) and for this reason, we have called these models *real graded tensor models*.

The partition function Z and the expectation value of an invariant $\langle I_{\mathcal{B}}(T) \rangle$ are defined by

$$Z = \int d\mu[T], \quad \text{and} \quad \langle I_{\mathcal{B}}(T) \rangle = \frac{1}{Z} \int d\mu[T] I_{\mathcal{B}}(T), \quad (2.1.6)$$

and can be evaluated in a perturbative expansion in the couplings. In other words, these objects are treated as formal power series in the couplings.

The main result of Chapter 3 and 4 can be summarized in the following theorem:

Theorem (N to $-N$ in tensor models with $O(N)$ and $Sp(N)$ symmetry). *The perturbative series of the partition function Z and expectation values of invariants $\langle I_{\mathcal{B}}(T) \rangle$ can be expressed as a formal sum over edge $(D+1)$ -colored undirected graphs \mathcal{G} . Each summand, corresponding to a specific graph \mathcal{G} , writes as a product:*

$$K(\{\lambda_{\mathcal{B}}\}, \mathcal{G}) \cdot \prod_{c=1}^D \left((-1)^{|c|} N_c \right)^{F_{c/0}(\mathcal{G})} \quad (2.1.7)$$

of a term K , encoding the dependence on the coupling constants $\lambda_{\mathcal{B}}$ and some combinatorial numbers associated to \mathcal{G} , and a term depending on N_1, N_2, \dots, N_D (see Chapter 4 for the precise definitions and exact form of the series).

Whereas the work in Chapter 3 proves this theorem for tensor models having only quartic interactions, Chapter 4 extends the proof, using different methods, to interactions of arbitrary order.

The essential remark is that all factors of N_c come in the form $(-1)^{|c|} N_c$; hence, each term is mapped into itself by exchanging $O(N_c) \leftrightarrow Sp(N_c)$ and $N_c \leftrightarrow -N_c$. Because graphically the factors of N_c are associated to certain loops of alternating colors c and 0 , the result can be interpreted as a generalization of the usual minus sign for fermionic loops in a QFT. But one should keep in mind that the full tensor does not necessarily need to be fermionic.

The idea of the proof is to first define some canonical ordering of the invariants. This is necessary in order to compare models with different symmetry groups. For example, an invariant of a $O(N_1) \otimes O(N_2) \otimes O(N_3)$ invariant tensor model is invariant under commuting the tensor components and redirecting edges in the graphical representation, but the overall sign of the same invariant in a (fermionic) $Sp(N_1) \otimes O(N_2) \otimes O(N_3)$ model changes under these manipulations. In order to compare both models, the invariants are treated as class functions that only depend on undirected graphs, but a certain canonical representative of each class is chosen to define the corresponding interaction term in the action $S[T]$ with an unambiguous sign. Note that an overall sign can be absorbed in a change of sign of the coupling constant $\lambda_{\mathcal{B}}$. After fixing the representation of the interaction terms and invariants, the remaining part of the proof consists in carefully keeping track of all the different signs coming from: redirecting arrows in the graphical representation; and the fermionic or bosonic variant of Wick's theorem used to evaluate Gaußian expectation values of monomials in the $T^{a_1 \dots a_D}$.

²⁶ In the papers reproduced in Chapters 4 and 5, the set of vertices of a graph \mathcal{B} is denoted by $V(\mathcal{B})$. In this summary, we stay consistent with the notation in the introduction and in the paper of Chapter 3.

In Chapter 3, which contains the chronologically first paper and deals with quartic interactions only, a Hubbard–Stratonovic transformation is used to obtain a model with purely bosonic, but symmetric, respectively, antisymmetric tensors. In the case $D = 2$ (matrices) the Feynman diagrams of the model are so-called ribbon graphs. Classifying these ribbon graphs according to their topology allows us to calculate the sign accompanying N_c in each case. For tensors of order $D > 2$, the calculation of the sign could be reduced to the matrix case.

In the third paper (reproduced in Chapter 5), we extended the relation between tensor models with orthogonal and symplectic symmetry to tensors that transform in arbitrary finite-dimensional representations of $O(N)$ or $Sp(N)$. Let $V = \mathbb{R}^N$. $O(N)$ and $Sp(N)$ act on the tensor product space $V^{\otimes D}$. A representation $R \subset V^{\otimes D}$ can be obtained from a suitable projector. For a tensor model with tensors in R the covariance is then proportional to this projector.

As a simple example, consider $D = 2$ (a matrix). It can be decomposed according to the irreducible representations of $O(N)$ into: an antisymmetric matrix, a symmetric traceless matrix and a matrix that is proportional to the identity (the trace part). The covariance of the matrix model would then be, e.g., proportional to the projector on antisymmetric matrices. The last case (the trace representation) would merely be a scalar theory in disguise, as all matrices are proportional to the identity.

It should be stressed that, in this context traces mean the contraction of indices of the same tensor by either the symmetric form δ_{ab} or the symplectic form ω_{ab} . Thus, traces are an inherent feature of representations of $O(N)$ and $Sp(N)$, as these groups are by definition the isometry groups of the standard symmetric or symplectic form, respectively. The projectors on representations of $O(N)$ or $Sp(N)$ can be constructed as an elements of the Brauer algebra [217], an algebra generated by diagrams that act on tensors by permuting and contracting their indices. In particular, permutation diagrams form a subset of all Brauer diagrams. To give an example, the diagram


(2.1.8)

permutes the third and fourth indices and contracts the first and second indices of a fourth order tensor. As in the matrix example, in order to obtain irreducible representations of $O(N)$ and $Sp(N)$ it is important to remove the traces. For this purpose the authors of [218] built a universal traceless projector that can then be combined with suitable (anti-)symmetrizers to obtain the desired projector on the representation R .

In the end we have proven an analogous statement to the theorem around Eq. (2.1.7). Tensor models with symmetry given by the $O(N)$ tensor representation R are dual to corresponding tensor models with $Sp(N)$ symmetry, given by the dual representation R' (obtained by exchanging symmetrization and antisymmetrization), in the sense that the amplitudes of graphs in their perturbative expansions are mapped into each other after a change of N to $-N$. The $Sp(N)$ tensor models are fermionic if D is odd. After understanding the representation theoretic aspects, and refining the graphical representation, the proof proceeds similarly to the case with no permutation symmetry of the tensor indices.

For illustration purposes, consider the representation of $O(N)$ on totally symmetric and traceless tensors of order D . The tensor model with this symmetry group is, upon replacement of N by $-N$,

dual to the model with $Sp(N)$ symmetry and totally antisymmetric and traceless tensors, which are fermionic if D is odd.

2.2 Zero-dimensional $O(N)$ model: constructive expansions and transseries

The topic of Chapter 6 is the summation of the perturbative series. Perturbation theory can allow for very precise calculations of physical observables and has been central to the development of QFT in general. But the perturbative series poses a great challenge: in most cases it is only an asymptotic series with zero radius of convergence; and non-analytic terms, e.g. $e^{-1/g}$, which typically arise as instanton effects, are absent because their Taylor expansion at $g = 0$ is identically zero. To incorporate such contributions while retaining, for practical reasons, perturbative methods one employs a more general form of asymptotic expansions known as transseries, which can be understood as a sum of perturbative and nonperturbative sectors—schematically

$$F(g) = \sum_{n \geq 0} a_n g^n + \sum_j e^{\frac{c_j}{g}} g^{\gamma_j} \sum_{n \geq 0} b_{j,n} g^n. \quad (2.2.1)$$

The theory of Borel summation (see Section 1.4) is the standard method to deal with asymptotic series, and in many cases of interest it can be used to reconstruct some information about the non-perturbative sector based on the perturbative one. For example, nonperturbative effects manifest themselves as singularities of the Borel sums. In general, such relations between the perturbative and nonperturbative sectors are known as resurgence. This topic was first explored in the context of ordinary differential equations by Écalle in [219], and later applied to quantum mechanics (see, e.g., [220]), matrix models, large N gauge theories and topological strings (see the reviews [189, 221–223] and references therein).

Zero-dimensional QFT models are useful toy models to study transseries expansions. The complications arising from the computation and renormalization of Feynman diagrams are absent, yet the perturbative series is divergent because of the factorial growth of the number of Feynman graphs. These models are hence purely combinatorial in nature. Concretely, we consider a zero-dimensional $O(N)$ model with quartic interaction. Denoting $\phi = (\phi_a)_{a=1, \dots, N}$ a vector in \mathbb{R}^N , and $\phi^2 = \sum_{a=1}^N \phi_a \phi_a$, the partition function of the model is

$$Z(g, N) = \int_{-\infty}^{+\infty} \left(\prod_{a=1}^N \frac{d\phi_a}{\sqrt{2\pi}} \right) e^{-S[\phi]}, \quad S[\phi] = \frac{1}{2} \phi^2 + \frac{g}{4!} (\phi^2)^2. \quad (2.2.2)$$

The logarithm of the partition function, $W(g, N) = \ln Z(g, N)$, is the free energy. The action in Eq. (2.2.2) has critical points, for $\phi^2 \in \{0, -6/g\}$. The nonzero critical points are the instantons of this model. The action at the instantons is $-3/(2g)$.

The aim of this research work is to analyze $Z(g, N)$ and $W(g, N)$ using techniques from constructive field theory, and not only to compute the respective transseries expansions of these quantities. We focus on techniques that, in principle, can be generalized to higher-dimensional field theory. The main results include employing the Hubbard–Stratonovich intermediate field representation to develop a small N expansion, applying the Loop Vertex Expansion (LVE) to establish analyticity and Borel summability results for the free energy in N and g , and investigating the resurgence properties based on the LVE.

The LVE is a tool developed in the context of constructive field theory (see [196] and [202, 224] for more details). It combines the BKAR forest formula—discussed in Section 1.5 in the introduction—with a Hubbard-Stratonovich intermediate field representation and a replica trick.

Before summarizing the main results, let us introduce some notation. The (convergent) small N expansions of $Z(g, N)$ and $W(g, N)$ write:

$$Z(g, N) = \sum_{n \geq 0} \frac{1}{n!} \left(-\frac{N}{2} \right)^n Z_n(g), \quad \text{and} \quad W(g, N) = \sum_{n \geq 1} \frac{1}{n!} \left(-\frac{N}{2} \right)^n W_n(g). \quad (2.2.3)$$

We write $g = |g|e^{i\varphi}$ and note that φ will often be continued past $\pm\pi$, which corresponds to the next sheets of the Riemann surface of the coupling. Moreover, we define the following sets: $\mathbb{C}_\pi \equiv \mathbb{C} \setminus \mathbb{R}_-$, the complex plane without the negative real axis, and the extended Riemann sheet $\mathbb{C}_{3\pi/2} \equiv \{g = |g|e^{i\varphi} \mid \varphi \in (-3\pi/2, 3\pi/2)\}$.

In Chapter 6, the most important results are listed in the form of several propositions. Here, we summarize their main points:

- **Proposition 1** establishes analyticity and Borel summability of $Z(g, N)$ in \mathbb{C}_π and analytically continues $Z(g, N)$ on a Riemann surface. The transseries expansion of $Z(g, N)$ is calculated. Interestingly, the asymptotic series of the perturbative and nonperturbative sectors are related by substituting $N \leftrightarrow (2 - N)$ and $g \leftrightarrow -g$. The prefactor of the nonperturbative sector is related to the action at instantons.
- **Proposition 2** demonstrates the convergence of the small N series of $Z(g, N)$. The coefficients $Z_n(g)$ are analytic and Borel summable in \mathbb{C}_π and can be analytically continued to the extended Riemann sheet $\mathbb{C}_{3\pi/2}$. The transseries expansion of $Z_n(g)$ is calculated.
- **Propositions 3 and 4** use the LVE to prove analyticity and Borel summability of the free energy $W(g, N)$ and its small N series coefficients $W_n(g)$ in a subset of \mathbb{C}_π . Both functions are analytically continued to a subdomain of the extended Riemann sheet $\mathbb{C}_{3\pi/2}$.
- **Proposition 5** calculates the transseries expansion of $W(g, N)$ and $W_n(g)$.
- **Proposition 6** derives a nonlinear differential equation for $W(g, N)$ and a recursive tower of differential equations for $W_n(g)$. Similar differential equations for $Z(g, N)$ and $Z_n(g)$ are part of Propositions 1 and 2.

For more details and proofs, we refer to the respective chapter. Fig. 2.2 illustrates the fact that $Z(g, N)$, as a function of g , lives on a nontrivial Riemann surface.

The remainder of this section contains additional remarks that will add some technical details and give an impression of the strategies used in the proofs. An important technical tool that is used throughout Chapter 6 is the intermediate field representation. By introducing in Eq. (2.2.2) for $Z(g, N)$ an intermediate field $\sigma \in \mathbb{R}$ via a Hubbard-Stratonovich transformation, the ϕ dependent part becomes Gaussian and can be integrated for $g > 0$. Afterwards, the partition function takes the form

$$Z(g, N) = \int_{-\infty}^{+\infty} \frac{d\sigma}{\sqrt{2\pi}} e^{-\frac{1}{2}\sigma^2} \frac{1}{\left(1 - i\sqrt{\frac{g}{3}}\sigma\right)^{N/2}}, \quad (2.2.4)$$

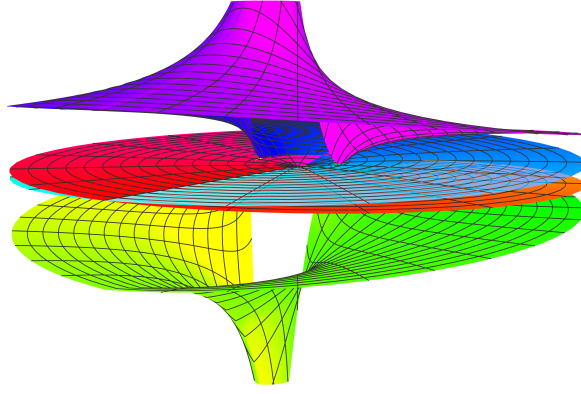


Figure 2.2. Rendering of $Z(g, N = 1)$ that illustrates well the multivaluedness of that function with four Riemann sheets. The vertical direction shows the imaginary part. The principal sheet is displayed in red.

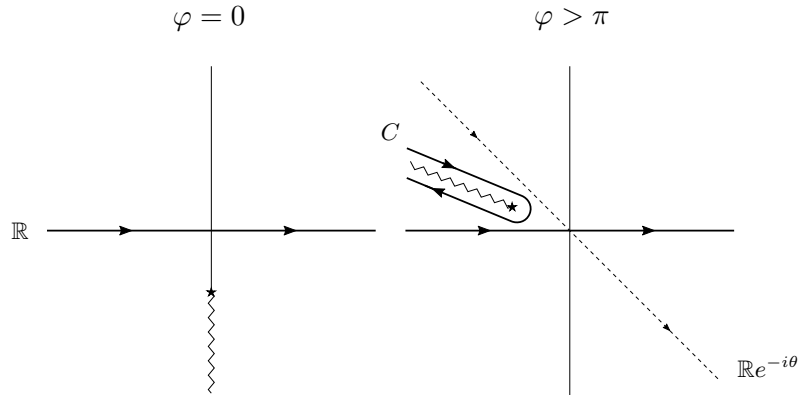


Figure 2.3. As φ increases, the branch cut moves clockwise in the complex σ -plane. When g crosses the negative real axis the tilted contour is equivalent to a Hankel contour C plus the original contour along the real line. Based on Fig. 1 of [4].

which shows that $Z(g, N)$ can be analytically continued in both N and g . It is one of the great strengths of the intermediate field representation of the $O(N)$ vector model that N is an explicit parameter in the integral. On a technical level, there is one observation that underlies most of the stated results: as φ increases, the branch cut in the integral representation of Eq. (2.2.4) moves past the integration contour and the integral picks up an additional contribution—a Hankel contour around the branch cut. This is illustrated in Fig. 2.3. Notably, the contribution from the Hankel contour is proportional to the exponential of minus the instanton action.

The intermediate field representation of Eq. (2.2.4) allows us to write the coefficient functions $Z_n(g)$ of the small N series of $Z(g, N)$ in Eq. (2.2.3) as

$$Z_n(g) = \int_{-\infty}^{+\infty} \frac{d\sigma}{\sqrt{2\pi}} e^{-\frac{1}{2}\sigma^2} \left(\ln(1 - i\sqrt{\frac{g}{3}}\sigma) \right)^n. \quad (2.2.5)$$

The functions $Z_n(g)$ can be treated as moments (n-point correlation functions) of the random vari-

able $\ln(1 - i\sqrt{g/3}\sigma)$. The coefficient functions $W_n(g)$ of the small N series of $W(g, N)$ are the respective cumulants (connected correlations) of this random variable. Both sets of functions are thus related by the Möbius inversion formula, which in this case becomes the moments–cumulants formula. Although the functions $Z_n(g)$ and $W_n(g)$ are related as analytic functions in g , this only translates into a formal relation between $Z(g, N)$ and $W(g, N)$ because the convergence of the series defining $Z(g, N)$ does not imply the convergence of the series defining $W(g, N)$. However, the Möbius inversion turned out to be the most direct way to obtain the transseries expansion of $W(g, N)$. To study the analytic properties of the free energy, the LVE gives an integral equation for the $W_n(g)$ as sums over trees with n vertices. This enables the proof of Propositions 3 and 4 of Chapter 6. We refer the reader to that chapter for the explicit formulas.

The transseries of $W(g, N)$ has the schematic form

$$W(g, N) = \sum_{p \geq 0} e^{\frac{3}{2g}p} \eta^p \left(\frac{g}{3}\right)^{\frac{1-N}{2}p} \sum_{l \geq 0} \left(-\frac{2g}{3}\right)^l a_{p,l}, \quad (2.2.6)$$

with $a_{p,l}$ some explicit and g -independent coefficients. The term $p = 0$ corresponds to the perturbative sector, while terms with $p \geq 1$ represent contributions from p instantons. The transseries parameter η acts as a switch: it equals zero on the principal sheet of the Riemann surface (truncating the sum to just the perturbative sector), and equals one when $|\varphi| > \pi$.²⁷ The transseries of $W_n(g)$ is similar, but the sum over p truncates at $p = n$, such that only up to n instantons contribute. Moreover, this transseries also includes powers of $\ln(g)$. The transseries of $W(g, N)$ agrees with the series obtained by formally taking the logarithm of the transseries expansion of $Z(g, N)$. The added value of our discussion is that we have replaced a formal manipulation on series with a rigorous manipulation on analytic functions.

2.3 Four-dimensional asymptotically free tensor field theory

The last research article of this thesis, reproduced in Chapter 7, studies the $O(N)^3$ tensor field theory in four Euclidean dimensions, in the large N limit, and numerically solves the Schwinger–Dyson equation for the full propagator. The solution of this equation also determines the renormalization flow of the tetrahedral coupling, which is crucial for the model to be asymptotically free (as first observed in [103]). The main results can be summarized as follows:

- Quantum fluctuations generate strong correlations in the infrared and significantly modify the propagator. This effect can be captured by a running coupling (defined below) that grows strong in the infrared and whose flow is driven solely by the wave function renormalization.
- The running coupling remains finite for a wide range of parameters, provided the renormalized mass is above a threshold m^* .
- Approaching the threshold mass m^* from above, the running coupling grows nonlinearly and diverges at a finite infrared energy scale μ^* .

We compare our results with a perturbative RG study carried out in [5].

²⁷ This behavior is related to the so-called Stokes phenomenon.

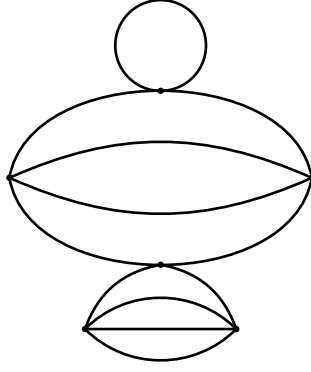


Figure 2.4. A vacuum graph of the type that dominate in the large N limit. The leading order graphs are built from iterative melon and tadpole insertions.

The model has already been defined in Eq. (1.3.40) and discussed in the context of the 2PI effective action in Section 1.3.3, which is the methodological foundation of this work. For convenience, we review the definition of the model again and highlight some important properties. The fundamental fields $\varphi_{\mathbf{a}}$, with $\mathbf{a} = (a^1, a^2, a^3) \in \{1, \dots, N\}^3$, are scalars under spacetime rotations and translations, and transform as real three-index tensors in the trifundamental representation of $O(N)^3$. The model is defined by the action

$$S[\varphi] = \int d^4x \left[\frac{1}{2} \varphi_{\mathbf{a}}(x) (-\Delta + m^2) \varphi_{\mathbf{a}}(x) + \frac{1}{4} \left(g_1 \hat{P}_{\mathbf{ab};\mathbf{cd}}^{(1)} + g_2 \hat{P}_{\mathbf{ab};\mathbf{cd}}^{(2)} + ig \hat{\delta}_{\mathbf{abcd}}^t \right) \varphi_{\mathbf{a}}(x) \varphi_{\mathbf{b}}(x) \varphi_{\mathbf{c}}(x) \varphi_{\mathbf{d}}(x) \right], \quad (2.3.1)$$

which is invariant under the global $O(N)^3$ symmetry. The three interaction terms in the action correspond to the three $O(N)^3$ -invariant contraction patterns: pillow, double-trace and tetrahedron (see Fig. 1.4 in the introduction). The couplings g_1 and g_2 and their associated index contraction operators $\hat{P}^{(1)}$ and $\hat{P}^{(2)}$ are linear combinations of the pillow and double-trace couplings and contraction operators

$$\begin{aligned} \hat{\delta}_{\mathbf{ab};\mathbf{cd}}^p &= \frac{1}{3N^2} \sum_{i=1}^3 \delta_{a^i c^i} \delta_{b^i d^i} \prod_{j \neq i} \delta_{a^j b^j} \delta_{c^j d^j}, & \hat{P}^{(1)} &= 3(\hat{\delta}^p - \hat{\delta}^d), \\ \hat{\delta}_{\mathbf{ab};\mathbf{cd}}^d &= N^{-3} \prod_{i=1}^3 \delta_{a^i b^i} \prod_{j=1}^3 \delta_{c^j d^j}, & \hat{P}^{(2)} &= \hat{\delta}^d, \\ \hat{\delta}_{\mathbf{abcd}}^t &= N^{-3/2} \delta_{a^1 b^1} \delta_{c^1 d^1} \delta_{a^2 c^2} \delta_{b^2 d^2} \delta_{a^3 d^3} \delta_{b^3 c^3}, & g_1 &= \frac{g_p}{3}, \\ & & g_2 &= g_p + g_d. \end{aligned} \quad (2.3.2)$$

They fulfill $\hat{P}_{\mathbf{ab};\mathbf{cd}}^{(1)} \hat{P}_{\mathbf{cd};\mathbf{ef}}^{(2)} = 0$. Crucially, the tetrahedral coupling ig is purely imaginary, which not only makes the Euclidean path integral bounded (provided $g_1, g_2 > 0$), but also leads to asymptotic freedom in the ultraviolet regime [103]. This will be discussed further in Section 8.3.

In the large N limit, the dominant diagrams are built by iteratively inserting melon diagrams containing the tetrahedral coupling and tadpoles with the g_1 or g_2 coupling (see Fig. 2.4 and [96]).

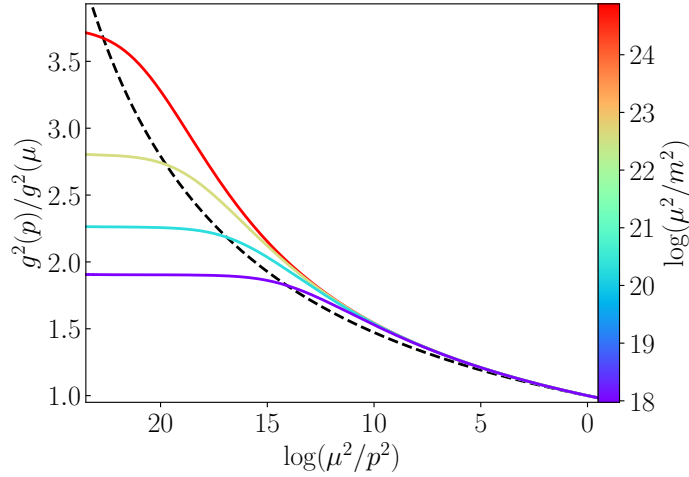


Figure 2.5. Flow of the squared running tetrahedral coupling $g^2(p)$ with momentum p for various renormalized masses m^2 (color scale), with $g(\mu) = 20$ at the renormalization scale μ . The two-loop perturbative running is mass independent and represented as dashed. By means of Eq. (2.3.6) the diagram equally shows $Z^{-2}(p)$. This is Fig. 1 in [5].

Both types of insertions are two-point insertions, and can be resummed using the 2PI formalism, as first applied to tensor models in [99, 119]. In particular only the square of the tetrahedral coupling appears in the large N limit and leads to several sign changes. This yields a self-consistent and closed equation—the Schwinger–Dyson equation—such that the full (resummed) propagator $G_{\text{ab}} = G\delta_{\text{ab}}$ is determined in momentum space by

$$G^{-1}(p) = p^2 + m^2 + g_2 \int \frac{d^4 q}{(2\pi)^4} G(q) + g^2 \int \frac{d^4 q}{(2\pi)^4} \frac{d^4 k}{(2\pi)^4} G(q)G(k)G(p+q+k), \quad (2.3.3)$$

which has the diagrammatic representation

$$\text{---} \text{---} \text{---}^{-1} = \text{---} \text{---}^{-1} + g_2 \text{---} \text{---} \text{---} + g^2 \text{---} \text{---} \text{---} \text{---} \text{---}, \quad (2.3.4)$$

where edges with a filled bivalent vertex represent G , to distinguish them from the (inverse) classical propagator in the first term on the right hand side.

Note that this equation is formally obeyed by the non-renormalized (bare) propagator and still requires regularization and renormalization, as the integrals are ultraviolet divergent. In this summary, for the sake of simplicity, the bare equations are used to display the structure of the model; the renormalization procedure and renormalized equations are detailed in Chapter 7. Effectively, the renormalized equations include subtractions at a momentum scale μ (the renormalization scale). See also [161, 162] for a general discussion of renormalizability in the 2PI formalism.

A second consequence of the tensor large N limit is that no Feynman diagram can give a direct correction to the tetrahedral coupling; it only receives quantum corrections via rescaling through the wave function renormalization.

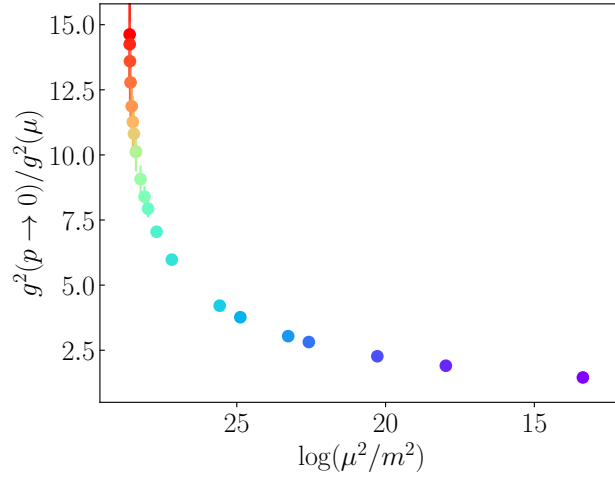


Figure 2.6. Limiting value of the squared running tetrahedral coupling in the infrared for varying renormalized mass. This is Fig. 3 in [5].

We extract the wave function renormalization²⁸ from the nontrivial momentum dependence of the full (renormalized) propagator by

$$Z(p) = \frac{G^{-1}(p) - G^{-1}(0)}{p^2}, \quad (2.3.5)$$

and define the running tetrahedral coupling as

$$g(p) = \frac{g(\mu)}{Z^2(p)}. \quad (2.3.6)$$

The renormalization conditions fix $Z(\mu) = 1$ and the coupling to a given value $g(\mu)$ at the renormalization scale. We solve the renormalized Schwinger–Dyson equation for the renormalized propagator numerically by iteration (details are provided at the end of Chapter 7).

Fig. 2.5 shows the numerical results for the (nonperturbative) running coupling and compares them with the two-loop perturbative prediction. At large momenta, the curves align, which is consistent with asymptotic freedom. At intermediate scales, the nonperturbative running coupling grows faster than the perturbative one. Depending on the renormalized mass, the flow eventually stops deep in the infrared and the coupling reaches a maximum value in the limit $p \rightarrow 0$. However, as shown in Fig. 2.6, this infrared limit of the coupling depends nonlinearly on the renormalized mass. Remarkably, there seems to exist a threshold mass m^* , such that for $m \searrow m^*$ the running coupling diverges in the infrared at a finite scale μ^* .

The work reproduced in Chapter 7 briefly explores the case of a purely real tetrahedral coupling. In this case, the running coupling decreases toward the infrared, and even solutions with zero renormalized mass can be obtained. However, the theory with real tetrahedral coupling is not asymptotically free, so a finite ultraviolet cutoff must be maintained.

²⁸ This momentum dependent function is called a dressing function in the literature on functional methods for renormalization. It is an analog of the wave function renormalization constant known, e.g., in renormalized perturbation theory. The latter is renormalization scale dependent and in the perturbative regime this scale dependence and the momentum dependence of the former function determine each other.

Duality of orthogonal and symplectic random tensor models

Authors: Răzvan Gurău and Hannes Keppler

Published in *Ann. Inst. Henri Poincaré Comb. Phys. Interact.* **12** (2025) 2, 319–362.

Published online first October 2023. DOI: 10.4171/AIHPD/177.

Licensed under CC BY 4.0. Reproduced with permission. Hyperlink colors removed.

Also available as e-print: arXiv 2207.01993 [math-ph].

The original idea was conceived by R. Gurău and further developed by both authors. H. Keppler performed all calculations and produced all figures. The article was originally written by H. Keppler. R. Gurău contributed with corrections and suggestions and supervised the project.

Duality of orthogonal and symplectic random tensor models

Razvan Gurau and Hannes Keppler

Abstract. The groups $O(N)$ and $Sp(N)$ are related by an analytic continuation to negative values of N , $O(-N) \simeq Sp(N)$. This duality has been studied for vector models, $SO(N)$ and $Sp(N)$ gauge theories, as well as some random matrix ensembles. We extend this duality to real random tensor models of arbitrary order D with no symmetry under permutation of the indices and with quartic interactions. The N to $-N$ duality is shown to hold graph by graph to all orders in perturbation theory for the partition function, the free energy and the connected two-point function.

1. Introduction and conclusion

Dualities are non-trivial relations between seemingly different models and therefore of great use in physics and mathematics. It has been known for some time [41] that, for even N , $SO(N)$ and $Sp(N)$ gauge theories are related by changing N to $-N$ and that one can make sense of the relation $SO(-N) \simeq Sp(N)$ for the representations of the respective groups [14]. This duality has furthermore been shown to hold between orthogonal and symplectic matrix ensembles [43]. (These correspond to the $O(N) \otimes O(N)$ and $Sp(N) \otimes Sp(N)$ matrix models of Section 3.)

The N to $-N$ duality inspired in part the conjectured holographic duality between Vasiliev's higher spin gravity [50] in four-dimensional de Sitter space and the three-dimensional Euclidean $Sp(N)$ vector model with anticommuting scalars [2]. This dS/CFT correspondence is in turn based on the conjectured Giombi–Klebanov–Polyakov–Yin duality [22, 35] relating the three-dimensional $O(N)$ vector model in the large N limit to Vasiliev gravity in four-dimensional anti-de Sitter space. In this context, $N \sim (\Lambda G_N)^{-1}$ so that the sign change of the cosmological constant Λ (holding G_N fixed) is accompanied by a change $N \rightarrow -N$.

The perturbative expansion of random matrix models is a sum over *ribbon graphs* representing topological surfaces. The weight of each graph is fixed by the Feynman rules and the perturbative series can be organized [48] as a topological expan-

2020 *Mathematics Subject Classification.* Primary 81T32; Secondary 57M15.

Keywords. Tensor models, random tensors, symplectic group, matrix models, ribbon graphs.

sion in $1/N$. Random matrices yield a theory of random two-dimensional topological surfaces relevant for the study of conformal field theories (CFTs) coupled to two-dimensional Liouville gravity [6, 16, 17, 34, 37] and two-dimensional Jackiw–Teitelboim gravity [33, 45, 47]. They have applications as combinatorial generating functions to several counting problems [4, 49, 53] and to the intersection theory on the moduli space of Riemann surfaces [38, 44, 51].

Random matrices generalize to random tensor models [1, 27, 28, 30] of higher order¹ D which are probability measures of the type

$$d\mu[T] = e^{-S[T]} \prod_{(a_1, \dots, a_D)} \frac{dT^{a_1 \dots a_D}}{\sqrt{2\pi}},$$

where the action $S[T]$ is build out of invariants under some symmetry transformation. These models can also be viewed as 0-dimensional quantum field theories. The Feynman graphs of such models can be interpreted as higher-dimensional cellular complexes and the perturbative series can be reorganized as a series in $1/N$ [3, 5, 9, 10, 12, 25] which is not topological for $D \geq 3$. Zero-dimensional random tensors yield a framework for the study random topological spaces; in one-dimension tensor models provide an alternative to the Sachdev–Ye–Kitaev model without quenched disorder [52]; in higher dimensions, they lead to tensor field theories and a new class of large N *melonic* conformal field theories [8, 20, 21, 31, 36].

Main result. In this paper, we deal with tensors with D indices (i.e., of order D) with no symmetry under their permutations. The position of an index is called its color c , with $c = 1, 2, \dots, D$. The tensors transform in the tensor product of D fundamental representations of $O(N)$ and/or $Sp(N)$, i.e., each tensor index is transformed by a different $O(N)$ or $Sp(N)$ matrix. The tensor components are real Grassmann valued (anticommuting, odd) if the number of $Sp(N)$ factors is odd and real bosonic (commuting, even) if this number is even.² We assign a parity to the tensor indices: $|c| = 0$ or $|c| = 1$ if the index transforms under $O(N_c)$ or $Sp(N_c)$, respectively. We consider actions consisting in invariants up to quartic order (see Section 2 for more details).

¹In the physics literature, one often uses “rank” instead of order, but this may lead to confusion with the many notions of tensor rank in abstract algebra.

²The tensors are even multilinear maps on $\mathbb{R}^{m|n}$, the real graded supervector space with m even and n odd directions. This is natural because the orthosymplectic super Lie group $OSp(m, n)$ contains both $O(m)$ and $Sp(n)$ and acts on $\mathbb{R}^{m|n}$. This will be our guideline in constructing the models of interest.

Definition 1.1. The real quartic graded tensor model, where “graded” refers to symmetry under

$$\mathbf{O}_1(N_1) \otimes \mathbf{O}_2(N_2) \otimes \cdots \otimes \mathbf{O}_D(N_D), \quad \mathbf{O}_c(N_c) = \begin{cases} \mathbf{O}(N_c), & |c| = 0, \\ \mathbf{Sp}(N_c), & |c| = 1 \end{cases}$$

is defined by the measure

$$d\mu[T] \simeq e^{-S[T]} \prod_{a_1, \dots, a_D} dT^{a_1 \dots a_D},$$

$$S[T] = \frac{1}{2} \left(T^{a_1 \dots a_D} T^{b_1 \dots b_D} \prod_{c=1}^D g_{a_c b_c}^c \right) + \sum_{q \in \mathcal{Q}} \frac{\lambda_q}{4} I^q(T),$$

where $g_{a_c b_c}^c$ is the Kronecker delta $\delta_{a_c b_c}$ for $|c| = 0$ or the canonical symplectic form $\omega_{a_c b_c}$ for $|c| = 1$ and the sum over \mathcal{Q} runs over all the independent quartic trace invariants $I^q(T)$.

The partition function Z and the connected two-point function G_2 of the model are defined by

$$Z(\lambda) = \int d\mu[T] \quad \text{and} \quad G_2(\lambda) = \frac{1}{Z} \int d\mu[T] T^{a_1 \dots a_D} T^{b_1 \dots b_D} \prod_{c=1}^D g_{a_c b_c}^c$$

and can be evaluated in a perturbative expansion. Our main theorem is the following.

Theorem 1.2. *The perturbative series of the free energy $\ln Z$ and of the connected two-point function G_2 can be expressed as formal sums over connected, colored multi-ribbon graphs*

$$\ln Z(\lambda) = \sum_{\substack{[\mathbb{G}] \text{ connected, rooted,} \\ \text{at least one } E_q > 0}} \frac{1}{2^{C(\mathbb{G} - \mathcal{E}^\varrho) + 1} \sum_{q \in \mathcal{Q}} E_q} \mathcal{A}(\mathbb{G}),$$

$$G_2(\lambda) = \sum_{[\mathbb{G}] \text{ connected, rooted}} \frac{1}{2^{C(\mathbb{G} - \mathcal{E}^\varrho) - 1}} \mathcal{A}(\mathbb{G})$$

with amplitude

$$\mathcal{A}(\mathbb{G}) = 2^{E^\varrho(\mathbb{G})} \prod_{q \in \mathcal{Q}} (-\lambda_q)^{E_q(\mathbb{G})} \prod_{c=1}^D ((-1)^{|c|} N_c)^{F_c(\mathbb{G})}, \quad (1.1)$$

where E_q , E^ϱ , F_c , $C(\mathbb{G} - \mathcal{E}^\varrho)$ are some combinatorial numbers associated to the multi-ribbon graph \mathbb{G} (see Section 4.2 for the relevant definitions).

Proof. The theorem follows from equations (4.3), (4.5) and (4.6). ■

The crucial remark is that all the factors N_c come in the form $(-1)^{|c|} N_c$, hence each term is mapped into itself by exchanging $O(N_c) \leftrightarrow \mathrm{Sp}(N_c)$ and $N_c \leftrightarrow -N_c$.

Conclusion and outlook. We list some comments on, and possible generalizations of, our result:

- In order to prove our main theorem, we will use in this paper an intermediate field representation adapted to quartic interactions. It should however be possible to extend this result to more general interactions [40].
- While more general models with $\mathrm{OSp}(m, n)$ symmetry could be considered, the construction of super tensor actions is complicated because of the abundance of sign factors [46].
- For $D = 2$ (matrices), the contributions of ribbon graphs and their duals cancel exactly in the fermionic case (see Remark 3.1). It would be interesting to understand similar cancellations in the graded tensor models. This should be related to Poincaré duality between lower-dimensional colored subgraphs.
- One should explore the implications of the $N \rightarrow -N$ duality for tensor field theories. The sign changes may generate new renormalization group fixed points, and the duality may not hold for all the physical properties [39]. Quantum mechanical models of order three tensors with $\mathrm{Sp}(N)$ symmetry have been studied in [11, 24].

Outline of the paper. This paper is organized as follows. In Section 2, the quartic graded tensor model is defined, the relation between directed edge colored graphs and quartic trace invariants is explained, and we collect some definitions and notations on ribbon graphs. Section 3 deals in detail with the order 2 (matrix) case. Section 4 continues with the general case of arbitrary order D tensors. Appendix A contains the calculation of the sign of each ribbon graph amplitude and Appendix B gives details on the calculation of the symmetry factors of the Feynman graphs.

2. Definitions

In this section, we define the models we will be studying. We also give some standard definitions about ribbon graphs and combinatorial maps.

2.1. The real quartic graded tensor models

The orthosymplectic super Lie group $\mathrm{OSp}(m, n)$ is the isometry group of the canonical graded-symmetric bilinear form on the supervector space $\mathbb{R}^{m|n}$,

$$\eta: \mathbb{R}^{m|n} \times \mathbb{R}^{m|n} \rightarrow \Lambda_\infty, \quad (\eta_{ij}) = \left(\begin{array}{c|c} \delta & 0 \\ \hline 0 & \omega \end{array} \right),$$

where Λ_∞ is the Grassmann algebra generated by an infinite number of anticommuting generators. The space $\mathbb{R}^{m|n}$ is a free module over Λ_∞ with m even (commuting) and n odd (anticommuting) basis vectors. Note that non-singularity of η demands that n is an even integer. For later comparison, m is also taken to be even.

Since we are only interested in $O(N)$ and $Sp(N)$, and not the whole $O\text{Sp}(m, n)$, we restrict to supervector spaces that are either purely odd or purely even, and thus have either $O(N)$ or $Sp(N)$ as their isometry group. This information can be encoded as a parity of the index color $|c| \in \{0, 1\}$, with $|c| = 0$ corresponding to orthogonal, and $|c| = 1$ to symplectic symmetry. The tensor components are commuting bosonic or anticommuting Grassmannian, depending on whether the number of indices with $|c| = 1$ is even or odd. Suitable invariants are defined to construct the actions of the models.

Vector spaces. Let $\mathcal{H}_c = \mathbb{R}^{N_c|0}$ for $|c| = 0$, $\mathcal{H}_c = \mathbb{R}^{0|N_c}$ for $|c| = 1$, respectively, be a real supervector space of dimension N_c , that is, either purely even or purely odd and is endowed with a non-degenerate graded symmetric inner product $g^c: \mathcal{H}_c \times \mathcal{H}_c \rightarrow \Lambda_\infty$,

$$g^c(u, v) = (-1)^{|c|} g^c(v, u) \quad \forall u, v \in \mathcal{H}_c, \quad g^c(\cdot, v) = 0 \Leftrightarrow v = 0.$$

In the standard basis g^c agrees with the standard symmetric or symplectic form, that is, $g_{a_c b_c}^c = \delta_{a_c b_c}$ for $|c| = 0$, $g_{a_c b_c}^c = \omega_{a_c b_c}$ for $|c| = 1$, respectively. We denote by $(g^c)^{a_c b_c}$ the matrix element of the inverse $(g^c)^{-1}$. The isometry group preserving g^c is either $O(N_c)$ in the $|c| = 0$ case or $Sp(N_c)$ in the $|c| = 1$ case, denoted collectively by $\mathbf{O}_c(N_c) := \{O_c \mid g_{a_c b_c}^c = O_{a_c}^{a'_c} O_{b_c}^{b'_c} g_{a'_c b'_c}^c = (O g^c O^\top)_{a_c b_c}\}$.

Tensors. Tensors are *even* elements of the tensor product space $T \in \bigotimes_{c=1}^D \mathcal{H}_c$. Choosing a basis $\{[\psi^c]_{a_c}\}_{a_c=1, \dots, N_c}$ in each \mathcal{H}_c and denoting by $\{[\psi_c^\vee]^{a_c}\}_{a_c=1, \dots, N_c}$ the dual basis, the components of a tensor are

$$T^{a_1 \dots a_D} \equiv T([\psi_1^\vee]^{a_1}, \dots, [\psi_D^\vee]^{a_D}),$$

$$T = \sum_{a_c=1, \dots, N_c \forall c} T^{a_1 \dots a_D} [\psi^1]_{a_1} \otimes \dots \otimes [\psi^D]_{a_D}.$$

A generic tensor has no symmetry properties under permutation of its indices a^1, \dots, a^D , hence the indices have a well-defined position c called their *color*. The set of colors is denoted by $\mathcal{D} = \{1, \dots, D\}$. We sometimes call the colors with $|c| = 0$ even and the ones with $|c| = 1$ odd. As the tensors are taken to be even elements of the tensor product space, the tensor components are bosonic (even) if the number of colors with $|c| = 1$ (i.e., odd colors) is even and fermionic (odd) otherwise: the Grassmann number $T^{a_1 \dots a_D}$ has the same parity as $\sum_{c \in \mathcal{D}} |c|$.

The tensors transform in the tensor product representation of several orthogonal and symplectic groups according to the type of the individual \mathcal{H}_c 's:

$$T^{a_1 \dots a_D} \rightarrow (O_1)^{a_1}_{b_1} \dots (O_D)^{a_D}_{b_D} T^{b_1 \dots b_D}, \quad O_1 \otimes \dots \otimes O_D \in \bigotimes_{c \in \mathcal{D}} \mathcal{O}_c(N_c).$$

A tensor can be viewed as a multilinear map $T: \bigotimes_{c \in \mathcal{C}} \mathcal{H}_c^\vee \rightarrow \bigotimes_{c \in \mathcal{D} \setminus \mathcal{C}} \mathcal{H}_c$ for any subset of colors $\mathcal{C} \subset \mathcal{D}$. As the inner product, g^c induces an isomorphism between \mathcal{H}_c and its dual, denoting by $a_{\mathcal{C}} = (a_c, c \in \mathcal{C})$, the matrix elements of this linear map in the tensor product basis are $T^{a_{\mathcal{D} \setminus \mathcal{C}} a_{\mathcal{C}}} \equiv T^{a_1 \dots a_D}$.

Edge colored graphs. Invariant polynomials in the tensor components can be constructed by contracting the indices of color c with the inner product g^c . The unique quadratic invariant is

$$g^{\otimes \mathcal{D}}(T, T) := T^{a_{\mathcal{D}}} T^{b_{\mathcal{D}}} \prod_{c \in \mathcal{D}} g^c_{a_c b_c}.$$

General *trace invariants* are polynomials in the $T^{a_{\mathcal{D}}}$'s build by contracting pairs of indices of the same color. These invariants form an algebraic complete set for all invariant polynomials and admit a straightforward graphical representation as *edge colored graphs*.

Definition 2.1 (Edge colored graphs [28]). A closed edge D -colored graph is a graph $\mathcal{B} = (\mathcal{V}(\mathcal{B}), \mathcal{E}(\mathcal{B}))$ with vertex set $\mathcal{V}(\mathcal{B})$ and edge set $\mathcal{E}(\mathcal{B})$ such that

- The edge set is partitioned into D disjoint subsets $\mathcal{E}(\mathcal{B}) = \bigsqcup_{c=1}^D \mathcal{E}^c(\mathcal{B})$, where $\mathcal{E}^c(\mathcal{B}) \ni e^c = (v, w)$, $v, w \in \mathcal{V}(\mathcal{B})$, is the subset of edges of color c .
- All vertices are D -valent with all the edges incident to a vertex having distinct colors.

In order to incorporate the odd colors appropriately, one needs to consider *directed graphs*, that is, graphs with an additional arrow for every edge (see Figure 1 for an example). Two graphs which are identical up to reorienting one edge of an odd color represent the same invariant up to a global “ $-$ ” sign. We will fix the global sign in the case of quartic invariants below.

Quartic invariants. Quartic invariants are represented by D -colored graphs with four vertices (see Figure 1) and directed edges. Due to the sign ambiguity induced by reversing the edges corresponding to the odd colors, we need to give a prescription to fix the global sign of an invariant. Every directed quartic D -colored graph can be canonically oriented as follows (see again Figure 1):

- The color 1 edges give a pairing of the vertices. We denote by a^1 and b^1 the source vertices of the oriented edges 1 and a^2 and b^2 their targets.

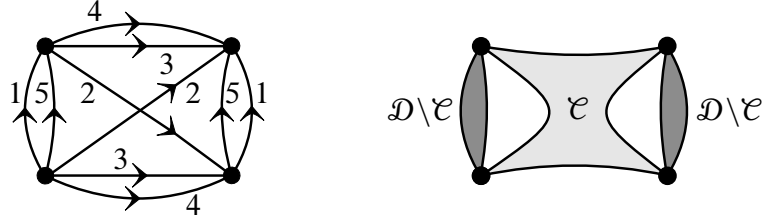


Figure 1. *Left:* Quartic 5-colored graph. *Right:* Schematic representation of a general quartic invariant.

- We orient all the edges that connect (a^1, a^2) (resp. (b^1, b^2)) parallel to the edges 1. We denote their colors by $c \in \mathcal{D} \setminus \mathcal{C}$.
- All the edges of colors $c \in \mathcal{C}$ connect the a pair with the b pair. We orient all of them from the a pair to the b pair. These edges fall into two classes:
 - either they connect a^1 with b^1 and a^2 with b^2 in which case we say they run in the *parallel* channel,
 - or they connect a^1 with b^2 and a^2 with b^1 in which case we say they run in the *cross* channel.

A canonically oriented graph is indexed by a subset of colors $\mathcal{C} \subset \mathcal{D}$, $1 \notin \mathcal{C}$ and permutations of two elements $\pi^c \in \mathfrak{S}_2 = \{\text{id}, (12)\}$, $c \in \mathcal{C}$. The associated invariant is

$$\begin{aligned}
 I(T) &= \sum_{a_{\mathcal{D}}^1, a_{\mathcal{D}}^2, b_{\mathcal{D}}^1, b_{\mathcal{D}}^2} \left(T^{a_{\mathcal{D}}^1} T^{a_{\mathcal{D}}^2} \prod_{c \in \mathcal{D} \setminus \mathcal{C}} g_{a_{\mathcal{D}}^1 a_{\mathcal{D}}^2}^c \right) \left(T^{b_{\mathcal{D}}^1} T^{b_{\mathcal{D}}^2} \prod_{c \in \mathcal{D} \setminus \mathcal{C}} g_{b_{\mathcal{D}}^1 b_{\mathcal{D}}^2}^c \right) \\
 &\quad \times \left(\prod_{c \in \mathcal{C}} (-\text{sgn}(\pi^c))^{|c|} g_{a_{\mathcal{C}}^1 b_{\mathcal{C}}^{\pi^c(1)}}^c g_{a_{\mathcal{C}}^2 b_{\mathcal{C}}^{\pi^c(2)}}^c \right) \\
 &= \sum_{a_{\mathcal{C}}^1, a_{\mathcal{C}}^2, b_{\mathcal{C}}^1, b_{\mathcal{C}}^2} (g^{\otimes \mathcal{D} \setminus \mathcal{C}}(T, T))^{a_{\mathcal{C}}^1 a_{\mathcal{C}}^2} K_{a_{\mathcal{C}}^1 a_{\mathcal{C}}^2, b_{\mathcal{C}}^1 b_{\mathcal{C}}^2} (g^{\otimes \mathcal{D} \setminus \mathcal{C}}(T, T))^{b_{\mathcal{C}}^1 b_{\mathcal{C}}^2}, \quad (2.1)
 \end{aligned}$$

where we introduced the shorthand notation K for the contractions of the indices transmitted between the pairs. Note that this is invariant by exchanging the b vertices and that $(-\text{sgn}(\pi^c))^{|c|}$ is the signature of the permutation $(a^1 a^2)(b^1 b^2)$ to $(a^1 b^{\pi(1)})(a^2 b^{\pi(2)})$ for the odd colors.

Lemma 2.2. *There are $\frac{1+3^{D-1}}{2}$ different quartic trace invariants (see Figure 2 for the $D = 3$ case).*

Proof. There is only one invariant corresponding to $\mathcal{C} = \emptyset$. If \mathcal{C} has q elements, there are 2^q choices for the channels and an overall $\frac{1}{2}$ for the relabeling of the b vertices. Thus the total number of invariants is

$$1 + \frac{1}{2} \sum_{q=1}^{D-1} \binom{D}{q} 2^q = \frac{3^{D-1} + 1}{2}. \quad \blacksquare$$

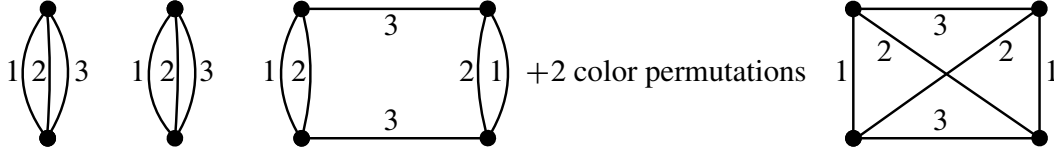


Figure 2. The 5 quartic invariants at order 3 known as double trace, pillow and tetrahedron.

Denote the set of distinct quartic D -colored graphs and the associate trace invariants by $\mathcal{Q} \ni q$ and $I^q(T)$, respectively.

Definition 2.3 (Real quartic graded tensor model). The *real quartic “graded” tensor model* is the measure

$$d\mu[T] = e^{-S[T]} [dT],$$

$$[dT] = \prod_{a_D} dT^{a_1 \dots a_D} \cdot \begin{cases} \frac{1}{(2\pi)^{\prod_c N_c/2}}, & \sum_{c=1}^D |c| = 0 \pmod{2}, \\ 1, & \sum_{c=1}^D |c| = 1 \pmod{2} \end{cases}$$

with

$$S[T] = \frac{1}{2} g^{\otimes D}(T, T) + \sum_{q \in \mathcal{Q}} \frac{\lambda_q}{4} I^q(T),$$

where the normalization is such that

$$\int d\mu[T] = 1 \quad \text{for } \lambda_q = 0 \quad \forall q \in \mathcal{Q}.$$

Convergence issues. Throughout this paper, we treat the measures $d\mu[T]$ as perturbed Gaussian measures. As such we do not concern ourselves with the convergence of the various tensor and matrix integrals. The integrals are always convergent if T is fermionic. If T is bosonic, the integrals converge if $|c| = 0$ for all c , but not necessarily in the other cases. As we treat the Gaussian integrals as generating functions of graphs, we will not worry about such issues.

2.2. Ribbon graphs and combinatorial maps

As ribbon graphs [19, 23] and combinatorial maps play a significant role in the derivation of our results, we review here some of their properties.

Ribbon graphs, see Figure 3 for some examples, are cellularly embedded graphs on topological surfaces, and thus can be viewed as 2-cell-complexes. Due to the embedding, each vertex carries an orientation and the order of edges around a vertex is fixed. A vertex can be re-embedded with the opposite orientation: this amounts to reversing the order of the incident edges and giving them a twist, see Figure 4.

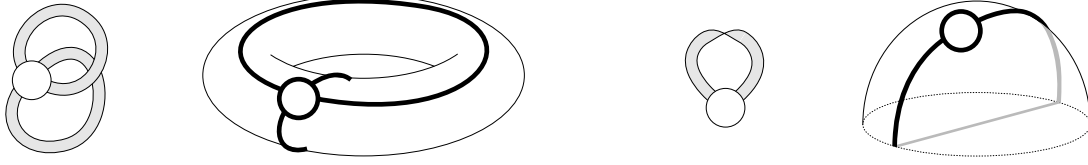


Figure 3. Ribbon graphs, which we denote by \mathcal{G}_{T^2} and $\mathcal{G}_{\mathbb{RP}^2}$, and their cellular embeddings. The rightmost surface is the hemisphere representation of the real projective plane where opposite points along the equator are identified.



Figure 4. Re-embedding a vertex: the order of halfedges is reversed and they gain additional twists. This is an equivalence relation of ribbon graphs.

Definition 2.4 (Ribbon graph [19]). A *ribbon graph* $\mathcal{G} = (\mathcal{V}(\mathcal{G}), \mathcal{E}(\mathcal{G}))$ is a (possibly non-orientable) surface with boundary, represented as the union of two sets of topological discs, a set of *vertices* $\mathcal{V}(\mathcal{G})$, and a set of *edges* $\mathcal{E}(\mathcal{G})$ such that

- (1) The vertices and edges intersect in disjoint line segments.
- (2) Each such line segment lies on the boundary of precisely one vertex and precisely one edge.
- (3) Every edge contains exactly two such line segments.

The boundary components of \mathcal{G} are called *faces*. The two disjoint boundary segments of an edge that are not connected to a vertex (i.e., the two sides of the edge) are called *strands*. We denote the set of faces of \mathcal{G} by $\mathcal{F}(\mathcal{G})$. A ribbon graph becomes a two-dimensional CW complex by sewing two-dimensional patches along its faces.

The numbers of vertices, edges and faces of \mathcal{G} are denoted by $V(\mathcal{G})$, $E(\mathcal{G})$ and $F(\mathcal{G})$, respectively.

Several remarks are in order:

- The strands of an edge can run parallel, in which case the edge is called *untwisted*, or cross, in which case the edge is called *twisted*.
- If $V(\mathcal{G}) = 1$, the graph is called a *rosette graph*. A rosette graph with only one face is called a *superrosette graph*.
- A *self-loop* in \mathcal{G} is an edge $e = \{h_v, h'_v\} \in \mathcal{E}(\mathcal{G})$ connected to just one vertex $v \in \mathcal{V}(\mathcal{G})$. A *simple self-loop* is a self-loop such that its halfedges are direct neighbors in the cyclic ordering around v , thus v has a corner of the form (h_v, h'_v) . If e is (un-)twisted, the simple self-loop is called likewise.

- We denote the ribbon graph consisting in only one vertex with no edge by \mathcal{G}_\circ . By definition, this graph has one face. We denote the ribbon graph with one vertex and one twisted self-loop edge by $\mathcal{G}_{\mathbb{RP}^2}$ and the ribbon graph with one vertex, two untwisted self-loop edges but no simple self-loop by \mathcal{G}_{T^2} .³ The last two graphs are depicted in Figure 3. As a topological surface with boundary $\mathcal{G}_{\mathbb{RP}^2}$ is homeomorphic to a Möbius strip.

Every ribbon graph has a dual ribbon graph with the same number of edges, but with the roles of the vertices and the faces interchanged.

Definition 2.5 (Dual ribbon graph [19]). Let \mathcal{G} be a ribbon graph. The *dual* ribbon graph \mathcal{G}^* is obtained by sewing discs along the faces of \mathcal{G} and deleting the original vertex discs of \mathcal{G} . The new discs make up the dual vertex set $\mathcal{V}(\mathcal{G}^*)$, and the new boundary components created by the deletion are the faces of \mathcal{G}^* . See Figure 5 for an illustration.

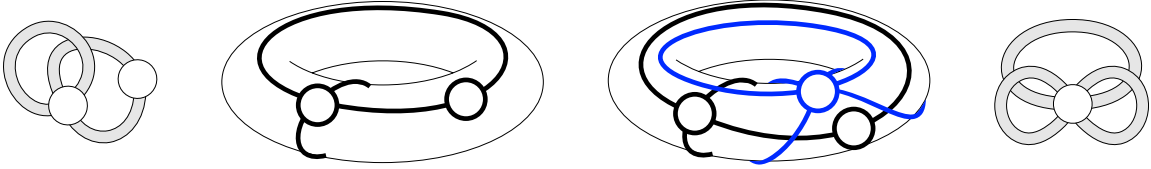


Figure 5. The dual graphs.

Besides ribbon graphs, we will encounter combinatorial maps below.

Definition 2.6 (Combinatorial map). A *combinatorial map* $\mathcal{M} = (\mathcal{S}, \pi, \alpha)$ is a finite set \mathcal{S} of halfedges (or darts) of even cardinality, together with a couple of permutations (π, α) on \mathcal{S} , where α is an involution with no fixed points (a “pairing” of halfedges).

The map \mathcal{M} is called connected if the group freely generated by π and α acts transitively on \mathcal{S} . The dual of \mathcal{M} is the combinatorial map $\mathcal{M}^* = (\mathcal{S}, \alpha \circ \pi, \alpha)$.

Combinatorial maps can be represented as graphs embedded in orientable surfaces. The cycles of π represent vertices with a cyclic order of their halfedges (chosen to be counter-clockwise), and α encodes pairings of halfedges into edges. The faces of a combinatorial map are the cycles of the permutation $\alpha \circ \pi$. In the dual combinatorial map, the role of vertices and faces is reversed.

The definition of combinatorial maps and ribbon graphs can be extended to include a second kind of edges.

³As their names suggest, these graphs can be cellularly embedded into \mathbb{RP}^2 or T^2 , respectively.

Definition 2.7 (Combinatorial map with ϱ -edges). *A combinatorial map with ϱ -edges*

$$\mathcal{M}^\varrho = (\mathcal{S} \sqcup \mathcal{S}^\varrho, \pi, \alpha, \alpha^\varrho)$$

is a finite set $\bar{\mathcal{S}} = \mathcal{S} \sqcup \mathcal{S}^\varrho$ that is the disjoint union of two sets of halfedges, both of even cardinality, together with a triple of permutations $(\pi, \alpha, \alpha^\varrho)$ on $\bar{\mathcal{S}}$. Here α and α^ϱ are fixed-point free involutions on \mathcal{S} and \mathcal{S}^ϱ , respectively, and extended to the whole of $\bar{\mathcal{S}}$ by setting $\alpha(h) = h \ \forall h \in \mathcal{S}^\varrho$ and analogous for α^ϱ .

The cycles of α^ϱ are pairs of halfedges in \mathcal{S}^ϱ which we will call ϱ -edges. The combinatorial map \mathcal{M}^ϱ is connected if the group freely generated by π , α and α^ϱ acts transitively on $\bar{\mathcal{S}}$. The cycles of π are the vertices and the cycles of $\pi \circ \alpha$ are the faces of \mathcal{M}^ϱ . The dual map is defined by changing the role of vertices and faces but not touching the ϱ -edges $\mathcal{M}^{\varrho*} = (\mathcal{S} \sqcup \mathcal{S}^\varrho, \alpha \circ \pi, \alpha, \alpha^\varrho)$.

Deleting all the ϱ -edges, one obtains an ordinary combinatorial map.

Ribbon graphs can be obtained from combinatorial maps by replacing their edges by twisted or untwisted ribbon edges. The same holds true for combinatorial maps with ϱ -edges and *ribbon graphs with ϱ -edges*.

Definition 2.8 (Ribbon graph with ϱ -edges). *A ribbon graph with ϱ -edges*

$$\mathcal{G}^\varrho = (\mathcal{V}, \mathcal{E}, \mathcal{E}^\varrho)$$

is a ribbon graph $\mathcal{G} = (\mathcal{V}, \mathcal{E})$, together with a set of line segments \mathcal{E}^ϱ , called ϱ -edges, such that their endpoints are connected to the corners of the ribbon graph. The ribbon graph \mathcal{G}^ϱ is called connected if it is connected as a topological space. The notions of faces, corners and edges of \mathcal{G}^ϱ refer to the ones of the ribbon graph $\mathcal{G} = \mathcal{G}^\varrho - \mathcal{E}^\varrho$, which is obtained by deleting the ϱ -edges.⁴

This dual of a ribbon graph with ϱ -edges is obtained by performing the partial dual [13, 18, 19] with respect to the ribbon edges. This is the dual of the underlying ribbon graph obtained by ignoring the ϱ -edges, where we keep track of the corners to which the ϱ -edges are hooked.

3. Matrix models

We first deal with the case of matrices (order $D = 2$ tensors) in Definition 2.3. In particular,

$$M^{a_1 a_2} M^{b_1 b_2} = (-1)^{|1|+|2|} M^{b_1 b_2} M^{a_1 a_2},$$

⁴Ribbon graphs with ϱ -edges are embedded in nodal surfaces, that is, Riemann surfaces glued at marked points. The ribbon graphs encode closed topological surfaces and by identifying points that are connected by a ϱ -edge, a gluing prescription is given.

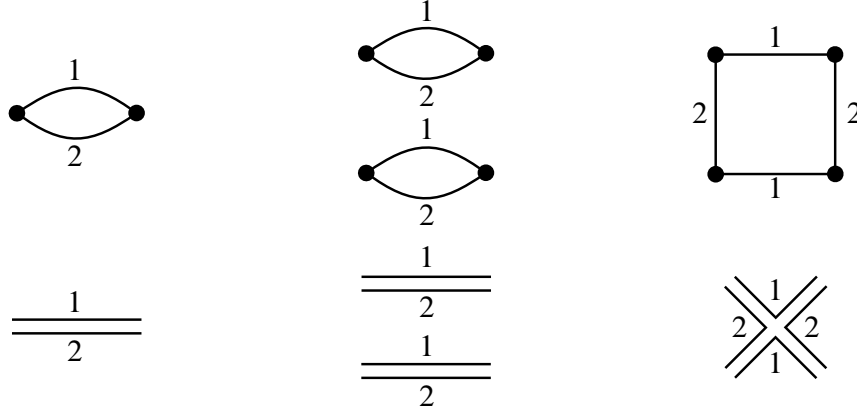


Figure 6. Graphical representation of the matrix model invariants up to quartic order.

i.e., the models with mixed symmetry are fermionic. We show that, for each ribbon graph in the perturbative expansion of the free energy and the two-point function of the model, changing one (or both) of the symmetry group factors in the $O(N_1) \otimes O(N_2)$ -model from $O(N)$ to $Sp(N)$ amounts to changing the sign accompanying the corresponding N factor.

Complex random matrix models in the intermediate field representation have been studied in [32]. The sign changes between the $O(N_1) \otimes O(N_2)$ - and the $Sp(N_1) \otimes Sp(N_2)$ -models have also been studied in [43] by different methods.

Denoting by the superscript \top the transpose, the action of the real quartic graded matrix model is written as⁵

$$\begin{aligned}
 S[M] &= \frac{1}{2} M^{a_1 a_2} g_{a_1 b_1}^1 g_{a_2 b_2}^2 M^{b_1 b_2} + \frac{\kappa}{4} (M^{a_1 a_2} g_{a_1 b_1}^1 g_{a_2 b_2}^2 M^{b_1 b_2})^2 \\
 &\quad + \frac{\lambda}{4} (-1)^{|2|} (M^{a_1^1 a_2^1} g_{a_1^1 a_1^1}^1 M^{a_2^1 a_2^1} g_{a_2^1 b_2^1}^2 g_{a_2^1 b_2^1}^2 (M^{b_1^1 b_2^1} g_{b_1^1 b_1^1}^1 M^{b_2^1 b_2^1})) \\
 &= \frac{1}{2} \text{Tr}[M g^2 M^\top (g^1)^\top] + \frac{\kappa}{4} (\text{Tr}[M g^2 M^\top (g^1)^\top])^2 \\
 &\quad + \frac{\lambda}{4} (-1)^{|1|} \text{Tr}[(M g^2 M^\top g^1)^2],
 \end{aligned} \tag{3.1}$$

where we note that the trace is $\text{Tr}[A] = A_a^a = A^{ab} g_{ba}$. This action is invariant under the transformation $M \rightarrow O_1 X O_2^\top$ with $O_1 \in \mathbf{O}_1(N_1)$, $O_2 \in \mathbf{O}_2(N_2)$. The three terms in (3.1) can be represented by 2-colored graphs or alternatively ribbon graphs, as depicted in Figure 6.

Whereas all terms in the action of the $O(N_1) \otimes O(N_2)$ -model are positive for $\kappa, \lambda \in \mathbb{R}_+$, in the $Sp(N_1) \otimes Sp(N_2)$ -model, this is only true for the κ term: the quadratic and the λ terms are in general indefinite.

⁵In the pure $Sp(N)$ case with $g^1 = g^2 = \omega$, the convergence of (3.1) is not clear, since the quadratic part has negative modes.

3.1. Intermediate field representation

The intermediate field (Hubbard–Stratonovich) representation is obtained by introducing an auxiliary field per quartic interaction and integrating out the original field. To be precise, we use that

$$\begin{aligned} & \exp\left\{-\frac{\kappa}{4}(\text{Tr}[Mg^2M^\top(g^1)^\top])^2 - \frac{\lambda}{4}(-1)^{|1|}\text{Tr}[Mg^2M^\top g^1 Mg^2M^\top g^1]\right\} \\ &= \left[e^{\frac{1}{2}(\frac{\partial}{\partial\sigma} P \frac{\partial}{\partial\sigma})} e^{\frac{1}{2}\frac{\partial}{\partial\varrho}\frac{\partial}{\partial\varrho}} \exp\left\{-\iota\sqrt{\frac{\kappa}{2}}\text{Tr}[Mg^2M^\top(g^1)^\top]\varrho \right. \right. \\ & \quad \left. \left. - \iota\sqrt{\frac{\lambda}{2}}\text{Tr}[Mg^2M^\top(g^1\sigma g^1)^\top]\right\}\right]_{\varrho,\sigma=0}, \end{aligned} \quad (3.2)$$

where ϱ is a real commuting (bosonic) scalar field and $\sigma = (-1)^{|1|}\sigma^\top$ is a (bosonic) real graded-symmetric matrix, and we introduce the shorthand notation:

$$\left(\frac{\partial}{\partial\sigma} P \frac{\partial}{\partial\sigma}\right) := \frac{\partial}{\partial\sigma^{ab}} P^{ab,dc} \frac{\partial}{\partial\sigma^{cd}}, \quad P^{ab,dc} = \frac{1}{2}(g_1^{ad}g_1^{bc} + (-1)^{|1|}g_1^{ac}g_1^{bd})$$

with P the (anti-)symmetric projector, taking into account the symmetry of the σ field. Note that $g^1 Mg^2 M^\top g^1$ has the same graded symmetry as σ .

Equation (3.2) is just a Gaussian integral over the intermediate fields ϱ and σ . We favor here the notation of the Gaussian integral as a differential operator (see, for instance, [7]) for two reasons. First, the Gaussian integral is formal in some cases (that is, the covariance is not necessarily positively defined). Second, in this form the perturbative expansion of the Gaussian integral is straightforward. In order to prove (3.2), we expand the exponentials and commute the sum and the derivatives:

$$\begin{aligned} & \left[e^{\frac{1}{2}(\frac{\partial}{\partial\sigma} P \frac{\partial}{\partial\sigma})} e^{\frac{1}{2}\frac{\partial}{\partial\varrho}\frac{\partial}{\partial\varrho}} \sum_{n,p=0}^{\infty} \frac{(-\frac{\kappa}{2})^n (-\frac{\lambda}{2})^p}{(2n)!(2p)!} \right. \\ & \quad \left. \times (\text{Tr}[Mg^2M^\top(g^1)^\top]\varrho)^{2n} (\text{Tr}[Mg^2M^\top(g^1\sigma g^1)^\top])^{2p} \right]_{\varrho,\sigma=0} \\ &= \left[\sum_{n,p=0}^{\infty} \frac{(-\frac{\kappa}{2})^n (-\frac{\lambda}{2})^p}{2^n n! 2^p p! (2n)!(2p)!} \left(\frac{\partial}{\partial\varrho} \frac{\partial}{\partial\varrho}\right)^n (\text{Tr}[Mg^2M^\top(g^1)^\top]\varrho)^{2n} \right. \\ & \quad \left. \times \left(\frac{\partial}{\partial\sigma} P \frac{\partial}{\partial\sigma}\right)^p (\text{Tr}[Mg^2M^\top(g^1\sigma g^1)^\top])^{2p} \right]_{\varrho,\sigma=0} \\ &= \left[\sum_{n,p=0}^{\infty} \frac{(-\frac{\kappa}{4})^n (-\frac{\lambda}{4})^p}{n! p!} (\text{Tr}[Mg^2M^\top(g^1)^\top])^{2n} \right. \\ & \quad \left. \times ((-1)^{|1|}\text{Tr}[Mg^2M^\top g^1 Mg^2M^\top g^1])^p \right]_{\varrho,\sigma=0}, \end{aligned}$$

where we used

$$\begin{aligned} [g^1 M g^2 M^\top g^1]_{ab} g^{ad} g^{bc} [g^1 M g^2 M^\top g^1]_{cd} \\ = (-1)^{|1|} \text{Tr}[g^1 M g^2 M^\top g^1 M g^2 M^\top g^1]. \end{aligned}$$

The partition function now reads

$$\begin{aligned} Z(\kappa, \lambda) = \int [dM] e^{-\frac{1}{2} \text{Tr}[M g^2 M^\top (g^1)^\top]} \left[e^{\frac{1}{2} (\frac{\partial}{\partial \sigma} P \frac{\partial}{\partial \sigma})} e^{\frac{1}{2} \frac{\partial}{\partial \varrho} \frac{\partial}{\partial \varrho}} \right. \\ \left. \times e^{-\iota \sqrt{\frac{\kappa}{2}} \text{Tr}[M g^2 M^\top (g^1)^\top]} e^{-\iota \sqrt{\frac{\lambda}{2}} \text{Tr}[M g^2 M^\top (g^1 \sigma g^1)^\top]} \right]_{\varrho, \sigma=0}, \end{aligned}$$

and all the terms containing M can be collected in a quadratic form using

$$\text{Tr}(M A M^\top B^\top) = M(B \otimes A)M.$$

The exponent can be written as $-\frac{1}{2} M(R^{-1} \otimes g^2)M$ with the *resolvent operator* R :

$$[R^{-1}(\kappa, \lambda)]^a_b = (1 + \iota \sqrt{2\kappa\varrho})\delta^a_b + \iota \sqrt{2\lambda}(\sigma g^1)^a_b.$$

As the resolvent and its inverse are operators, we write them with a covariant and a contravariant index. These indices are lowered with g^1 and raised with $(g^1)^{-1}$.

Commuting the integral and derivative operators, the integral M is Gaussian and can be performed leading to the *intermediate field representation*:

$$Z(\kappa, \lambda) = \left[e^{\frac{1}{2} (\frac{\partial}{\partial \sigma} P \frac{\partial}{\partial \sigma})} e^{\frac{1}{2} \frac{\partial}{\partial \varrho} \frac{\partial}{\partial \varrho}} e^{(-1)^{|1|+|2|} \frac{N_2}{2} \text{Tr} \ln R(\kappa, \lambda)} \right]_{\varrho, \sigma=0}. \quad (3.3)$$

Now N_2 is an explicit parameter in the integral, while N_1 is hidden in the remaining traces. The sign $(-1)^{|1|+|2|}$ tracks the bosonic/fermionic character of the original matrix. The sign $(-1)^{|1|}$ tracks the symmetry of the intermediate matrix field σ (which agrees with that of g^1). Both indices of σ have color 1 which reflects the fact that σ transforms in the (anti-)symmetric tensor representation of $\mathbf{O}_1(N_1)$, that is, $\sigma \rightarrow O_1 \sigma O_1^\top$ for $O_1 \in \mathbf{O}_1(N_1)$. This is to be contrasted with the field M which transforms in the tensor product of the fundamental representations of $\mathbf{O}_1(N_1)$ and $\mathbf{O}_2(N_2)$.

3.2. Perturbative expansion

The perturbative expansion of Z is obtained by Taylor expanding the interaction:

$$Z(\kappa, \lambda) = \left[e^{\frac{1}{2} (\frac{\partial}{\partial \sigma} P \frac{\partial}{\partial \sigma})} e^{\frac{1}{2} \frac{\partial}{\partial \varrho} \frac{\partial}{\partial \varrho}} \sum_{V=0}^{\infty} \frac{1}{V!} \left(\frac{(-1)^{|1|+|2|} N_2}{2} \text{Tr} \ln R(\kappa, \lambda; \varrho, \sigma) \right)^V \right]_{\varrho, \sigma=0},$$

and commuting the Gaussian integration with the sum. Note that R denotes the resolvent operator, hence it naturally has a covariant and a contravariant index. Taking into account that

$$\begin{aligned}\ln R &= - \sum_{p \geq 1} \frac{(-1)^{p+1}}{p} (\imath \sqrt{2\kappa} \varrho + \imath \sqrt{2\lambda} \sigma g^1)^p, \\ R &= \sum_{p \geq 0} (-1)^p (\imath \sqrt{2\kappa} \varrho + \imath \sqrt{2\lambda} \sigma g^1)^p,\end{aligned}$$

the derivatives of the resolvent and its logarithm are

$$\begin{aligned}\frac{\partial}{\partial \sigma^{ab}} \text{Tr} \ln R &= -\imath \sqrt{2\lambda} P_{ab,cd} R^{dc}, \\ \frac{\partial}{\partial \sigma^{ab}} R^{cd} &= -\imath \sqrt{2\lambda} P_{ab,ef} R^{ce} R^{fd}, \\ \frac{\partial}{\partial \varrho} \text{Tr} \ln R &= -\imath \sqrt{2\kappa} \text{Tr}[R], \\ \frac{\partial}{\partial \varrho} R^{ab} &= -\imath \sqrt{2\kappa} R^{ac} g_{cd}^1 R^{db} = -\imath \sqrt{2\kappa} (R^2)^{ab},\end{aligned}$$

where R^2 denotes the square of the operator R .

Each term in the perturbative series can be represented as a ribbon graph with ϱ -edges (see Section 2.2) as depicted in Figure 7:

- We represent each $\text{Tr} \ln R$ as a disc with boundary oriented counter-clockwise.
- The derivatives with respect to σ create ribbon halfedges representing the free indices of R . The first derivative acting on a vertex creates a halfedge and an R associated to the *corner* (region between two consecutive halfedges) of the vertex. Subsequent derivatives split the existing corners creating new R 's. The indices ab of the resolvent R^{ab} are associated to the ends of the corner: a for the source and b for the target in the sense of the arrow.
- The ribbon halfedges are connected into ribbon edges corresponding to the projectors P inside the $\frac{\partial}{\partial \sigma^{ab}} P^{ab,dc} \frac{\partial}{\partial \sigma^{cd}}$ operators. The edges have an orientation represented by arrows on the strands bounding an edge: corresponding to $P^{ab,dc}$, we orient the strands from (ab) to (dc) . Note that

$$\begin{aligned}(\partial_{\sigma^{ab}} R^{pq}) P^{ab,dc} (\partial_{\sigma^{cd}} R^{ef}) \\ &= (-2\lambda) (R^{pa'} R^{b'q}) P_{ab,a'b'} P^{ab,dc} P_{cd,c'd'} (R^{ec'} R^{d'f}) \\ &= (-\lambda) (R^{pa'} R^{b'q}) 2 P_{a'b'}^{dc} P_{cd,c'd'} (R^{ec'} R^{d'f}) \\ &= (-\lambda) (R^{pa'} R^{b'q}) 2 P_{a'b',d'c'} (R^{ec'} R^{d'f}).\end{aligned}$$

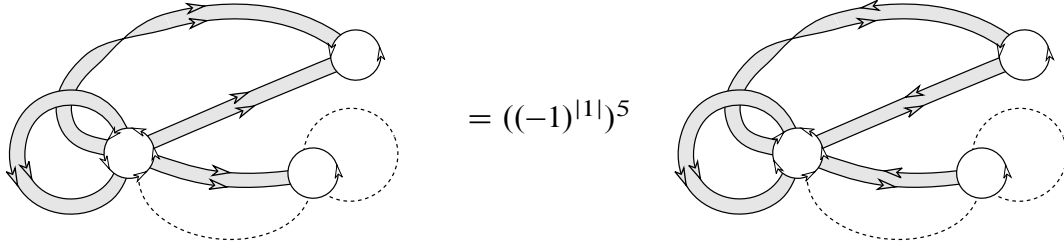


Figure 7. *Left:* A ribbon graph with q -edges in the priori orientation: corners counter-clockwise and strands parallel. *Right:* Coherent orientation of arrows along every face. Five arrows had to be reoriented.

The projector generates two terms. The first one $g_{a'd'}^1 g_{b'c'}^1$ corresponds to an edge with parallel strands. The second one $(-1)^{|1|} g_{a'c'}^1 g_{b'd'}^1$ corresponds to a twisted edge.

- A derivative with respect to q splits corner of a vertex also, but connects these two halves by g^1 . We represent this by a new type of halfedge, called q -halfedge. The q -halfedges are connected into q -edges corresponding to the $\frac{\partial}{\partial q} \frac{\partial}{\partial q}$ operators. We represent these edges as dashed lines.

In the end, all intermediate fields are set to zero thus the resolvents are set to the identity $R = 1$. A corner that has been split by q -halfedges behaves like a single ordinary corner of a ribbon graph: for this reason corner will always refer to the region between two ribbon halfedges only.

Ignoring the twisting of the edges, a ribbon graph is a combinatorial map with q -edges \mathcal{M}^q . We denote by h_v the ribbon-halfedges of the vertex v , each of which comes equipped with a pair of indices (b_{h_v}, a_{h_v}) : b is the target of an arrow and a the source of another one. If h_v and h'_v are two neighboring ribbon-halfedges with $h_v < h'_v$ in the cyclic order around v , the corner between them is denoted by (h_v, h'_v) . A ribbon-edge connecting two vertices $v, w \in \mathcal{M}^q$ is denoted by its halfedges $e = \{h_v, h_w\}$. Furthermore, we denote by $V(\mathcal{M}^q)$, $E(\mathcal{M}^q)$ and $E^q(\mathcal{M}^q)$ the numbers of vertices, ribbon-edges and q -edges of \mathcal{M}^q and by $\deg v$ and $\deg^q v$ the number of ribbon- and q -halfedges at v . The perturbative series can be written as a sum over labeled combinatorial maps with q -edges:

$$\begin{aligned}
 Z(\lambda) = & \sum_{\mathcal{M}^q} \frac{1}{V(\mathcal{M}^q)! 2^{V(\mathcal{M}^q)}} \left(\prod_{v \in \mathcal{M}^q} \frac{1}{\deg v! \deg^q v!} \right) \\
 & \times ((-1)^{|1|+|2|} N_2)^{V(\mathcal{M}^q)} (-\lambda)^{E(\mathcal{M}^q)} (-2\kappa)^{E^q(\mathcal{M}^q)} \\
 & \times \left(\prod_{v \in \mathcal{M}^q} \prod_{\substack{(h_v, h'_v) \\ \text{corner of } v}} g_{a_{h_v} b_{h'_v}}^1 \right) \left(\prod_{\substack{e = \{h_v, h_w\} \\ \text{ribbon-edge}}} 2P^{b_{h_v} a_{h_v}, a_{h_w} b_{h_w}} \right).
 \end{aligned}$$

We expand the two terms in each edge projector to sum over ribbon graphs with (twisted) edges and ϱ -edge. This is because the amplitude depends on the twisting: every face (closed strand) of the ribbon graph contributes a factor of N_1 because along a face an even number of g^1 's concatenate into a trace. However, it might be necessary to transpose several g^1 's in order to get this trace: we represent these transpositions by reversing the corresponding arrows along the edge strands and the corners of the ribbon graph, see Figure 7. Overall we get (we explain the notation below)

$$\begin{aligned}
 Z(\lambda) &= \sum_{\mathcal{M}^\varrho} \frac{1}{V(\mathcal{M}^\varrho)! 2^{V(\mathcal{M}^\varrho)}} \left(\prod_{v \in \mathcal{M}^\varrho} \frac{1}{\deg v! \deg^\varrho v!} \right) \\
 &\quad \times ((-1)^{|1|+|2|} N_2)^{V(\mathcal{M}^\varrho)} (-\lambda)^{E(\mathcal{M}^\varrho)} (-2\kappa)^{E^\varrho(\mathcal{M}^\varrho)} \\
 &\quad \times \sum_{[\mathcal{G}^\varrho] \in \text{Orb}_{\mathfrak{T}}(\mathcal{M}^\varrho)} |\text{Stab}_{\mathfrak{T}}(\mathcal{G}^\varrho)| (N_1)^{F(\mathcal{G}^\varrho)} ((-1)^{|1|})^{\#\text{transpositions} + \#\text{twists}} \\
 &= \sum_{\mathcal{M}^\varrho} \frac{|\text{Stab}_{\mathfrak{T}}(\mathcal{M}^\varrho)|}{V(\mathcal{M}^\varrho)! 2^{V(\mathcal{M}^\varrho)}} \left(\prod_{v \in \mathcal{M}^\varrho} \frac{1}{\deg v! \deg^\varrho v!} \right) \sum_{[\mathcal{G}^\varrho] \in \text{Orb}_{\mathfrak{T}}(\mathcal{M}^\varrho)} \mathcal{A}(\mathcal{G}^\varrho) \quad (3.4)
 \end{aligned}$$

with the amplitude $\mathcal{A}(\mathcal{G}^\varrho)$ of the ribbon graph. Some notation has been introduced in this equation. Because every ribbon-edge can be twisted or not, there are naively 2^E ribbon graphs, associated to \mathcal{M}^ϱ . But ribbon graphs are in fact equivalence classes, emphasized by $[\mathcal{G}^\varrho]$. Two graphs are equivalent if one can be obtained from the other by successively reversing the order of halfedges of a subset of its vertices and—for each vertex separately—twisting all ribbon-edges connected to these vertices (edges with two twists are again untwisted). As proven in Appendix B, this degeneracy is counted by the cardinal of the stabilizer $|\text{Stab}_{\mathfrak{T}}(\mathcal{G}^\varrho)|$ of the action of a finite group⁶ \mathfrak{T} whose elements twist a subset of the ribbon-edges of \mathcal{G}^ϱ (\mathfrak{T} acts trivially on the ϱ -edges). In the last step leading to (3.4), we used the fact that, as \mathfrak{T} is abelian,

$$\text{Stab}_{\mathfrak{T}}(\mathcal{G}) = \text{Stab}_{\mathfrak{T}}(\mathcal{M})$$

for any $\mathcal{G} \in \text{Orb}_{\mathfrak{T}}(\mathcal{M})$, where $\text{Orb}_{\mathfrak{T}}(\mathcal{M})$ is the orbit of the combinatorial map \mathcal{M} under the action of \mathfrak{T} .

For example, the amplitude of the ribbon graph in Figure 7 is

$$\begin{aligned}
 &\underbrace{((-1)^{|1|+|2|} N_2)^3}_{\text{vertices}} \underbrace{(-\lambda)^4}_{\text{edges}} \underbrace{(-2\kappa)^2}_{\varrho\text{-edges}} \underbrace{((-1)^{|1|})}_{\text{twists}} \underbrace{(N_1)}_{\text{faces}} \underbrace{((-1)^{|1|})^5}_{\substack{\text{arrow} \\ \text{reorientations}}} \\
 &= (-\lambda)^4 (-2\kappa)^2 ((-1)^{|1|} N_1) ((-1)^{|2|} N_2)^3.
 \end{aligned}$$

⁶The group \mathfrak{T} is a subgroup of the so called ribbon group, introduced in [18], which also includes the operation of taking the partial dual of a ribbon graph with respect to a subset of its edges.

Amplitudes. The amplitude $\mathcal{A}(\mathcal{G}^\varrho)$ can be further computed.

In Proposition A.1, we prove that any ribbon graph can be deformed into a connected sum of

- a graph without twisted edges embeddable into a closed orientable surface Σ_g of genus g ;
- either no, one or two graphs with a single twisted edge, embeddable into the projective plane \mathbb{RP}^2 .

This is the ribbon graph equivalent of the classification theorem of closed two-dimensional surfaces. The crucial observation is that one can track the power of -1 in the amplitude under these deformations. In Theorem A.11, we show that for a ribbon graph with twists and which requires transpositions in order to coherently orient the faces:

$$(-1)^{V(\mathcal{G})} \left(\prod_{e \in \mathcal{E}(\mathcal{G})} (-1)^{\tau(e)} \right) \left(\prod_{f \in \mathcal{F}(\mathcal{G})} (-1)^{t(f)} \right) = (-1)^{F(\mathcal{G})},$$

where $\tau(e) = 0$ if the edge e is untwisted (straight) and $\tau(e) = 1$ if the edge is twisted; $t(f)$ is the number of reorientations of arrows required to coherently orient the face f .

The graph \mathcal{G}^ϱ can be seen as the union of two ribbon graphs:

- One ribbon graph has color 2 and is trivial. It consisting in all the vertices of \mathcal{G}^ϱ , each bounded by one face and has no edges. The graph has no twists (as it has no edges) and all its faces are coherently oriented.
- The second one is the graph of color 1. It has twisted edges, and some transpositions are needed in order to coherently orient its faces.

Then the amplitude of a graph in (3.4) can be written as

$$\mathcal{A}(\mathcal{G}^\varrho) = (-2\kappa)^{E^\varrho(\mathcal{G}^\varrho)} (-\lambda)^{E(\mathcal{G}^\varrho)} ((-1)^{|1|} N_1)^{F(\mathcal{G}^\varrho)} ((-1)^{|2|} N_2)^{V(\mathcal{G}^\varrho)},$$

proving equation (1.1) in Theorem 1.2 for $D = 2$.

Combinatorial weights. The combinatorial weights in equation (3.4) simplify by gathering the labeled graphs corresponding to the same unlabeled ribbon graph with ϱ -edges:

$$Z(\kappa, \lambda) = \sum_{[\mathcal{G}^\varrho]} \mathcal{W}(\mathcal{G}^\varrho) \mathcal{A}(\mathcal{G}^\varrho),$$

where the (positive) weights $\mathcal{W}(\mathcal{G}^\varrho)$ include all the combinatorial factors coming from partially resumming (3.4) to a sum over equivalence classes.

Remark 3.1 (Dual graphs). The amplitudes of a ribbon graph and its dual are related by

$$\begin{aligned}\mathcal{A}(\mathcal{G}^*) &= (-\lambda)^{E(\mathcal{G}^*)} ((-1)^{|1|} N_1)^{F(\mathcal{G}^*)} ((-1)^{|2|} N_2)^{V(\mathcal{G}^*)} \\ &= (-\lambda)^{E(\mathcal{G})} ((-1)^{|2|} N_2)^{F(\mathcal{G})} ((-1)^{|1|} N_1)^{V(\mathcal{G})}.\end{aligned}$$

We will see below that $\mathcal{W}(\mathcal{G}^\varrho) = \mathcal{W}(\mathcal{G}^{\varrho*})$. In particular, for the mixed $O(N) \otimes \text{Sp}(N)$ -models, we get $\mathcal{A}(\mathcal{G}^{\varrho*}) = (-1)^{V(\mathcal{G}^\varrho) + F(\mathcal{G}^\varrho)} \mathcal{A}(\mathcal{G}^\varrho)$, hence the contributions of a graph and its dual cancel if $V(\mathcal{G}^\varrho) + F(\mathcal{G}^\varrho)$ is odd.

A heuristic argument why $\mathcal{W}(\mathcal{G}^\varrho) = \mathcal{W}(\mathcal{G}^{\varrho*})$ goes as follows. We split the quartic interactions using an intermediate field σ_1 with indices of color 1 coupling to M via $\propto M((g^1 \sigma_1 g^1) \otimes g^2) M$. But one can choose the intermediate field to have indices of color 2 and coupling $\propto M(g^1 \otimes (g^2 \sigma_2 g^2)) M$. The vertices now contribute factors of N_1 and the faces N_2 . For any graph, contracting the intermediate field σ_1 and introducing σ_2 in the orthogonal channel passes to the dual graph.

As the combinatorics is insensitive to the symmetry, we focus on the $O(N_1) \otimes O(N_2)$ -model. The connected two-point function of this model

$$G_2(\kappa, \lambda) = Z^{-1}(\kappa, \lambda) \int d\mu[M] \text{Tr}[M \delta M^\top \delta],$$

obeys a Dyson–Schwinger equation (DSE). Using

$$\begin{aligned}0 &= Z^{-1}(\kappa, \lambda) \int [dM] \\ &\times \frac{\partial}{\partial M^{a_1 a_2}} \left(M^{a_1 a_2} e^{-\frac{1}{2} \text{Tr}[M \delta M^\top \delta]} - \frac{\kappa}{4} (\text{Tr}[M \delta M^\top \delta])^2 - \frac{\lambda}{4} \text{Tr}[(M \delta M^\top \delta)^2] \right),\end{aligned}$$

we conclude that

$$G_2(\kappa, \lambda) = N_1 N_2 + (4\kappa \partial_\kappa + 4\lambda \partial_\lambda) \ln Z(\kappa, \lambda). \quad (3.5)$$

The free energy $\ln Z$ expands in connected graphs. The derivative operator $2\kappa \partial_\kappa + 2\lambda \partial_\lambda$ generates a rooting of the graph, that we get a sum over graphs with a marked ϱ - or ribbon-halfedge. Rooted graphs are simpler to count. In Proposition B.1, we show that the perturbative series of G_2 can be written as

$$G_2(\kappa, \lambda) = \sum_{[\mathcal{G}^\varrho] \text{ connected, rooted}} \frac{1}{2^{C(\mathcal{G}^\varrho - \mathcal{E}^\varrho) - 1}} \mathcal{A}(\mathcal{G}^\varrho), \quad (3.6)$$

where $\mathcal{G}^\varrho - \mathcal{E}^\varrho$ is the graph obtained from \mathcal{G}^ϱ by deleting all the ϱ -edges and $C(\mathcal{G}^\varrho - \mathcal{E}^\varrho)$ denotes the number of its connected components. Note that even if \mathcal{G}^ϱ is connected as a ribbon graph with ϱ -edges, the graph $\mathcal{G}^\varrho - \mathcal{E}^\varrho$ may be disconnected.

It is well known that rooting trivializes the symmetry factors in ordinary combinatorial maps. What is non-trivial is that it also simplifies the factor $2^{-V} |\text{Stab}_{\mathfrak{T}}(\mathcal{M}^{\varrho})|$ in (3.4) to $2^{-(C(\mathcal{G}^{\varrho}) - \mathcal{E}^{\varrho}) - 1}$. The combinatorial weight in (3.6) is manifestly invariant under duality. Rooted ribbon graphs can be embedded into two-dimensional surfaces with one boundary component corresponding to the rooted face.

The Dyson–Schwinger equation for the connected two-point function can be integrated in the sense of formal power series to yield the perturbative expansion of the free energy:

$$\ln Z(\kappa, \lambda) = \sum_{\substack{[\mathcal{G}^{\varrho}] \text{ connected, rooted,} \\ E \text{ or } E^{\varrho} > 0}} \frac{1}{2^{C(\mathcal{G}^{\varrho}) - \mathcal{E}^{\varrho}} + 1} (E + E^{\varrho}) \mathcal{A}(\mathcal{G}^{\varrho}),$$

where E and E^{ϱ} denote the number of ribbon edges and ϱ -edges in \mathcal{G}^{ϱ} , respectively. The integration does not spoil the symmetry under duality because the powers of the coupling constants in the amplitude only depend on the number of edges. Finally, the partition function Z can then be obtained by exponentiating $\ln Z$.

4. Tensor models

The case $D \geq 3$ is treated similarly to the case $D = 2$. However, as the number of available quartic invariants grows exponentially with D (recall Lemma 2.2), the number of intermediate fields grows also. Moreover, the intermediate fields are matrices with different dimensions. At most one of the N_c factors can be rendered explicit as a parameter in the integral, and one must rely on graphical methods to track the other N_c 's.

In $D \geq 3$ the perturbative expansion is an expansion in *colored multi-ribbon graphs* which can be understood intuitively as stacked ribbon graphs. The N_c to $-N_c$ duality holds graph by graph because only the combination $(-1)^{|c|} N_c$ appears in the amplitude of a graph.

If one aims to study tensor (or matrix) models with a sensible large N limit, one needs to rescale the coupling constants with powers of N . Care has to be taken if one wants to preserve the manifest N to $-N$ duality: this can sometimes require a flip of the sign of some of the coupling constants.

4.1. Intermediate field representation

Complex random tensor models in the intermediate field representation were, for example, studied in [15, 26]. We introduce an intermediate field per quartic interaction. For a subset of the colors \mathcal{C} , we denote by $\Sigma^{\mathcal{C}}$ the set of $N^{|\mathcal{C}|} \times N^{|\mathcal{C}|}$ matrices

(where $|\mathcal{C}|$ denotes the cardinality of \mathcal{C}) taken to be symmetric if the sum of the parities of the indices in \mathcal{C} is even and anti-symmetric if it is odd:

$$\begin{aligned} \Sigma^{\mathcal{C}} &= \begin{cases} \text{Sym}^2(\bigotimes_{c \in \mathcal{C}} \mathcal{H}_c), & \sum_{c \in \mathcal{C}} |c| = 0 \pmod{2}, \\ \Lambda^2(\bigotimes_{c \in \mathcal{C}} \mathcal{H}_c), & \sum_{c \in \mathcal{C}} |c| = 1 \pmod{2}, \end{cases} \\ \sigma^{a_{\mathcal{C}}^1 a_{\mathcal{C}}^2} &= (-1)^{\sum_{c \in \mathcal{C}} |c|} \sigma^{a_{\mathcal{C}}^2 a_{\mathcal{C}}^1} \quad \forall \sigma \in \Sigma^{\mathcal{C}}, \end{aligned}$$

where we recall that $a_{\mathcal{C}}$ denotes a multi-index ($a_c \mid c \in \mathcal{C}$). Note that σ is always commuting (bosonic) because $\bigotimes_{c \in \mathcal{C}} \mathcal{H}_c$ is either purely odd or even. For $\mathcal{C} = \emptyset$, set $\sigma \in \Lambda_{\infty}^0$ the commuting scalars. Since σ are (anti-)symmetric under exchange of their two multi-indices, it is useful to introduce the (anti-)symmetric projector

$$\begin{aligned} P_{\mathcal{C}}: \Sigma^{\mathcal{C}} &\rightarrow \Sigma^{\mathcal{C}}, \\ (P_{\mathcal{C}})^{a_{\mathcal{C}}^1 a_{\mathcal{C}}^2}_{, b_{\mathcal{C}}^1 b_{\mathcal{C}}^2} &:= \frac{1}{2} \left(\prod_{c \in \mathcal{C}} \delta_{b_c^1}^{a_c^1} \delta_{b_c^2}^{a_c^2} + (-1)^{\sum_{c \in \mathcal{C}} |c|} \prod_{c \in \mathcal{C}} \delta_{b_c^2}^{a_c^1} \delta_{b_c^1}^{a_c^2} \right), \end{aligned}$$

and $P_{\mathcal{C}}$ is the identity for $\mathcal{C} = \emptyset$. The projector is such that

$$\begin{aligned} (P_{\mathcal{C}})^{a_{\mathcal{C}}^1 a_{\mathcal{C}}^2}_{, b_{\mathcal{C}}^1 b_{\mathcal{C}}^2} &= (-1)^{\sum_{c \in \mathcal{C}} |c|} (P_{\mathcal{C}})^{a_{\mathcal{C}}^2 a_{\mathcal{C}}^1}_{, b_{\mathcal{C}}^1 b_{\mathcal{C}}^2} = (-1)^{\sum_{c \in \mathcal{C}} |c|} (P_{\mathcal{C}})^{a_{\mathcal{C}}^1 a_{\mathcal{C}}^2}_{, b_{\mathcal{C}}^2 b_{\mathcal{C}}^1}, \\ \frac{\partial \sigma^{a_{\mathcal{C}}^1 a_{\mathcal{C}}^2}}{\partial \sigma^{b_{\mathcal{C}}^1 b_{\mathcal{C}}^2}} &= (P_{\mathcal{C}})^{a_{\mathcal{C}}^1 a_{\mathcal{C}}^2}_{, b_{\mathcal{C}}^1 b_{\mathcal{C}}^2}. \end{aligned}$$

Lemma 4.1 (Hubbard–Stratonovich transformation). *Every quartic tensor invariant $I(T)$ in equation (2.1)*

$$\begin{aligned} I(T) &= \sum_{a_{\mathcal{D}}^1, a_{\mathcal{D}}^2, b_{\mathcal{D}}^1, b_{\mathcal{D}}^2} \left(T^{a_{\mathcal{D}}^1} T^{a_{\mathcal{D}}^2} \prod_{c \in \mathcal{D} \setminus \mathcal{C}} g_{a_c^1 a_c^2}^c \right) \left(T^{b_{\mathcal{D}}^1} T^{b_{\mathcal{D}}^2} \prod_{c \in \mathcal{D} \setminus \mathcal{C}} g_{b_c^1 b_c^2}^c \right) \\ &\quad \times \left(\prod_{c \in \mathcal{C}} (-\text{sgn}(\pi^c))^{|c|} g_{a_c^1 b_c^{\pi^c(1)}}^c g_{a_c^2 b_c^{\pi^c(2)}}^c \right) \\ &= \sum_{a_{\mathcal{C}}^1, a_{\mathcal{C}}^2, b_{\mathcal{C}}^1, b_{\mathcal{C}}^2} (g^{\otimes \mathcal{D} \setminus \mathcal{C}}(T, T))^{a_{\mathcal{C}}^1 a_{\mathcal{C}}^2} K_{a_{\mathcal{C}}^1 a_{\mathcal{C}}^2, b_{\mathcal{C}}^1 b_{\mathcal{C}}^2} (g^{\otimes \mathcal{D} \setminus \mathcal{C}}(T, T))^{b_{\mathcal{C}}^1 b_{\mathcal{C}}^2}, \end{aligned}$$

with π^c fixed permutations of two elements, can (formally) be expressed as a Gaussian integral

$$e^{-\frac{\lambda}{4} I(T)} = \left[e^{\frac{1}{2} \left(\frac{\partial}{\partial \sigma}, P_{\mathcal{C}} K \frac{\partial}{\partial \sigma} \right)} e^{-\iota \sqrt{\frac{\lambda}{2}} (\sigma, g^{\otimes \mathcal{D} \setminus \mathcal{C}}(T, T))} \right]_{\sigma=0}$$

with

$$(P_{\mathcal{C}} K)^{a_{\mathcal{C}}^1 a_{\mathcal{C}}^2, b_{\mathcal{C}}^1 b_{\mathcal{C}}^2} = (P_{\mathcal{C}})^{a_{\mathcal{C}}^1 a_{\mathcal{C}}^2}_{, c_{\mathcal{C}}^1 c_{\mathcal{C}}^2} K_{c_{\mathcal{C}}^1 c_{\mathcal{C}}^2, b_{\mathcal{C}}^1 b_{\mathcal{C}}^2}$$

and

$$(A, B) = g^{a_1 a_2} g^{b_1 b_2} A_{a_1 b_1} B_{a_2 b_2},$$

the standard pairing between a vector space and its dual.

Proof. The indices of color c of the kernel K are connected as

$$K_{a_{\mathcal{C}}^1 a_{\mathcal{C}}^2, b_{\mathcal{C}}^1 b_{\mathcal{C}}^2} \sim \begin{cases} (-1)^{|c|} g_{a_{\mathcal{C}}^1 b_{\mathcal{C}}^1}^c g_{a_{\mathcal{C}}^2 b_{\mathcal{C}}^2}^c, & \pi^c = (1)(2), \\ g_{a_{\mathcal{C}}^1 b_{\mathcal{C}}^2}^c g_{a_{\mathcal{C}}^2 b_{\mathcal{C}}^1}^c, & \pi^c = (12), \end{cases}$$

hence, as an operator, $K^2 = 1$ and $P_{\mathcal{C}} K = K P_{\mathcal{C}}$. Taking into account that

$$\begin{aligned} g_{b_{\mathcal{C}}^1 b_{\mathcal{C}}^2}^c &= (-1)^{|c|} g_{b_{\mathcal{C}}^2 b_{\mathcal{C}}^1}^c, & K_{a_{\mathcal{C}}^1 a_{\mathcal{C}}^2, b_{\mathcal{C}}^1 b_{\mathcal{C}}^2}^{a_{\mathcal{C}}^1 a_{\mathcal{C}}^2} &= K_{a_{\mathcal{C}}^2 a_{\mathcal{C}}^1, b_{\mathcal{C}}^2 b_{\mathcal{C}}^1}^{a_{\mathcal{C}}^2 a_{\mathcal{C}}^1}, \\ T^{b_{\mathcal{D}}^1} T^{b_{\mathcal{D}}^2} &= (-1)^{\sum_{c \in \mathcal{D}} |c|} T^{b_{\mathcal{D}}^2} T^{b_{\mathcal{D}}^1}, \end{aligned}$$

we have

$$\begin{aligned} & K_{a_{\mathcal{C}}^1 a_{\mathcal{C}}^2, b_{\mathcal{C}}^1 b_{\mathcal{C}}^2}^{a_{\mathcal{C}}^1 a_{\mathcal{C}}^2} \left(T^{b_{\mathcal{D}}^1} T^{b_{\mathcal{D}}^2} \prod_{c \in \mathcal{D} \setminus \mathcal{C}} g_{b_{\mathcal{C}}^1 b_{\mathcal{C}}^2}^c \right) \\ &= (-1)^{\sum_{c \in \mathcal{C}} |c|} K_{a_{\mathcal{C}}^2 a_{\mathcal{C}}^1, b_{\mathcal{C}}^2 b_{\mathcal{C}}^1}^{a_{\mathcal{C}}^2 a_{\mathcal{C}}^1} \left(T^{b_{\mathcal{D}}^2} T^{b_{\mathcal{D}}^1} \prod_{c \in \mathcal{D} \setminus \mathcal{C}} g_{b_{\mathcal{C}}^2 b_{\mathcal{C}}^1}^c \right), \end{aligned}$$

that is, $P_{\mathcal{C}} K g^{\otimes \mathcal{D} \setminus \mathcal{C}}(T, T) = K g^{\otimes \mathcal{D} \setminus \mathcal{C}}(T, T)$, hence $K g^{\otimes \mathcal{D} \setminus \mathcal{C}}(T, T)$ is a matrix with the same symmetry type as σ . It follows that

$$(g^{\otimes \mathcal{D} \setminus \mathcal{C}}(T, T), (P_{\mathcal{C}} K P_{\mathcal{C}}) g^{\otimes \mathcal{D} \setminus \mathcal{C}}(T, T)) = (g^{\otimes \mathcal{D} \setminus \mathcal{C}}(T, T), K g^{\otimes \mathcal{D} \setminus \mathcal{C}}(T, T)),$$

hence expanding the exponentials and commuting the sum and the derivative operator we get

$$\begin{aligned} & \left[\sum_{n=0}^{\infty} \frac{(-\frac{\lambda}{4})^n}{n!(2n)!} \left(\frac{\partial}{\partial \sigma}, P_{\mathcal{C}} K \frac{\partial}{\partial \sigma} \right)^n (\sigma, g^{\otimes \mathcal{D} \setminus \mathcal{C}}(T, T))^{2n} \right]_{\sigma=0} = \left[\sum_{n=0}^{\infty} \frac{(-\frac{\lambda}{4})^n}{n!} \right. \\ & \quad \times \left((g^{\otimes \mathcal{D} \setminus \mathcal{C}}(T, T) P_{\mathcal{C}})_{a_{\mathcal{C}}^1 a_{\mathcal{C}}^2} (P_{\mathcal{C}} K)_{a_{\mathcal{C}}^1 a_{\mathcal{C}}^2, b_{\mathcal{C}}^1 b_{\mathcal{C}}^2} (P_{\mathcal{C}} g^{\otimes \mathcal{D} \setminus \mathcal{C}}(T, T))_{b_{\mathcal{C}}^1 b_{\mathcal{C}}^2} \right)^n \left. \right]_{\sigma=0} \\ &= \sum_{n=0}^{\infty} \frac{1}{n!} \left(-\frac{\lambda}{4} I(T) \right)^n. \quad \blacksquare \end{aligned}$$

When dealing with several quartic invariants, we will label them q and the corresponding subset of colors \mathcal{C}_q . In order to simplify the notation, we sometimes drop this subscript. Using the intermediate fields, the partition function of the graded quadratic tensor model of Definition 2.3 becomes

$$\begin{aligned} Z(\lambda) &= \int \mu[T] = \int [dT] e^{-\frac{1}{2} g^{\otimes \mathcal{D}}(T, T)} \\ &\quad \times \left[e^{\sum_{q \in \mathcal{Q}} \frac{1}{2} \left(\frac{\partial}{\partial \sigma_q}, P_{\mathcal{C}_q} K_q \frac{\partial}{\partial \sigma_q} \right)} \cdot e^{-\sum_q \iota \sqrt{\frac{\lambda_q}{2}} (\sigma_q, g^{\otimes \mathcal{D} \setminus \mathcal{C}_q}(T, T))} \right]_{\sigma_q=0}, \end{aligned}$$

where we denoted the coupling constants generically by λ . We denote by $1^{\otimes \mathcal{C}}$ the identity operator acting on $\bigotimes_{c \in \mathcal{C}} \mathcal{H}_c$. We define the operator acting on $\bigotimes_{c=1}^D \mathcal{H}_c$

$$A(\lambda) = \sum_{q \in \mathcal{Q}} \iota \sqrt{2\lambda_q} 1^{\otimes \mathcal{D} \setminus \mathcal{C}_q} \otimes \sigma_q,$$

$$A^{a_1^{\mathcal{D}}}_{a_2^{\mathcal{D}}} = \sum_{q \in \mathcal{Q}} \iota \sqrt{2\lambda_q} \left(\prod_{c \in \mathcal{D} \setminus \mathcal{C}_q} \delta^{a_c^1}_{a_c^2} \right) (\sigma_q)^{a_{\mathcal{C}_q}^2}_{a_{\mathcal{C}_q}^1},$$

and perform the Gaussian integral over T to obtain the partition function in the *intermediate field representation*:

$$Z(\lambda) = \left[e^{\sum_{q \in \mathcal{Q}} \frac{1}{2} \left(\frac{\partial}{\partial \sigma_q}, P_{\mathcal{C}_q} K_q \frac{\partial}{\partial \sigma_q} \right)} e^{-\frac{(-1)^{\sum_{c \in \mathcal{D}} |c|}}{2} \text{Tr} \ln(1^{\otimes \mathcal{D}} + A(\lambda))} \right]_{\sigma_q=0}. \quad (4.1)$$

This is the generalization of equation (3.3) to $D > 3$. The *resolvent operator* for tensors is $R = (1^{\otimes \mathcal{D}} + A(\lambda))^{-1}$. The field ϱ we encountered in $D = 2$ corresponds to the unique disconnected quartic invariant $\mathcal{C}_q = \emptyset$. For now, we keep all factors N_c in the trace: the trace over the color 1 space can be performed explicitly because $1 \notin \mathcal{C}_q$ for all $q \in \mathcal{Q}$. In strict generalization of the matrix cases, the sign $(-1)^{\sum_{c \in \mathcal{D}} |c|}$ accounts for fermionic/bosonic nature of the tensor field T . Each intermediate field σ_q has its own symmetry captured by the sign $(-1)^{\sum_{c \in \mathcal{C}_q} |c|}$. The effect of the Hubbard–Stratonovich transformation on the Feynman diagrams is depicted schematically in Figure 8.

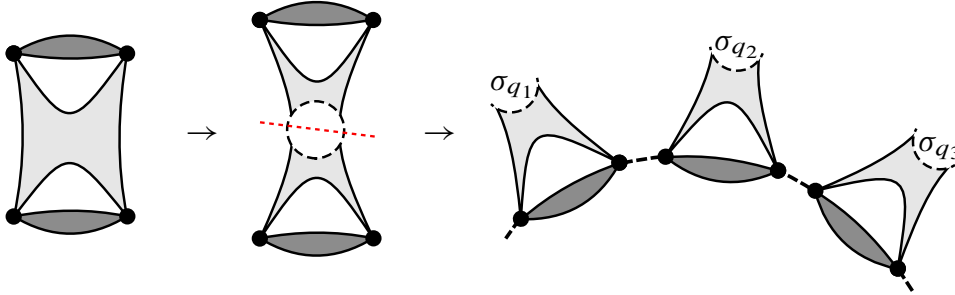


Figure 8. The Hubbard–Stratonovich transformation.

4.2. Perturbative expansion

Because of the tensor products, the Feynman graphs of the perturbative expansion of (4.1) are D -colored *multi-ribbon graphs*. Intuitively, they can be understood as D stacked ribbon graphs. Ribbon graphs are obtained from combinatorial maps by replacing their edges by ribbon edges which can then be twisted or not. Similarly, D -colored multi-ribbon graphs are obtained from *edge multicolored combinatorial maps*. These, in turn, are combinatorial maps with edges labeled by subsets of colors $\mathcal{C} \subset \mathcal{D}$.

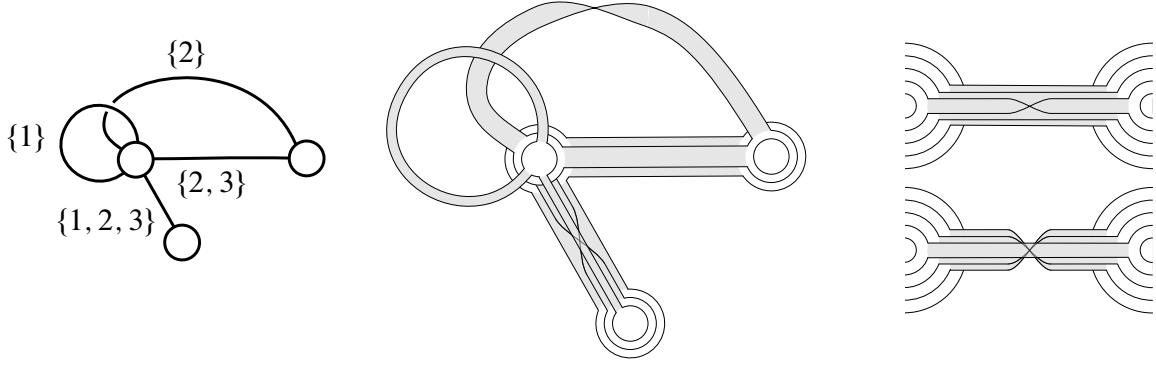


Figure 9. *Left:* Edge multicolored combinatorial map with $D = 3$. Each edge carries a subset of colors. *Center:* A multi-ribbon graph obtained from this multicolored combinatorial map. *Right:* Multi-ribbon edge corresponding to the quartic invariant of Figure 1 in its untwisted (*top*) and twisted (*down*) state.

Definition 4.2 (Edge multicolored combinatorial map [28]). An *edge multicolored combinatorial map* \mathcal{M} , depicted in Figure 9 on the left, is composed of

- a finite set \mathcal{S} that is the disjoint union of sets $\mathcal{S}^{\mathcal{C}}$ of halfedges of the colors $\mathcal{C} \in \mathcal{D}$, all of even cardinality $\mathcal{S} = \bigsqcup_{\mathcal{C} \in \mathcal{D}} \mathcal{S}^{\mathcal{C}}$;
- a permutation π on \mathcal{S} ;
- for every $\mathcal{C} \in \mathcal{D}$ an involution $\alpha^{\mathcal{C}}$ on $\mathcal{S}^{\mathcal{C}}$ with no fixed points. The involution $\alpha^{\mathcal{C}}$ can be extended to the whole of \mathcal{S} by setting $\alpha^{\mathcal{C}}(h) = h \ \forall h \in \mathcal{S} \setminus \mathcal{S}^{\mathcal{C}}$.

The set of cycles of π is the set of vertices of the map $\mathcal{V}(\mathcal{M})$. The set of cycles of $\alpha^{\mathcal{C}}$ is the set of edges of colors \mathcal{C} , $\mathcal{E}_{\mathcal{C}}(\mathcal{M})$, and $\mathcal{E}(\mathcal{M}) = \bigcup_{\mathcal{C} \in \mathcal{D}} \mathcal{E}_{\mathcal{C}}(\mathcal{M})$ is the set of all the edges of the map. The cardinalities of these sets are denoted by $V(\mathcal{M})$, $E_{\mathcal{C}}(\mathcal{M})$, $E(\mathcal{M})$, respectively.

An edge multicolored combinatorial map is connected if and only if the group freely generated by π and the $\alpha^{\mathcal{C}}$ acts transitively on \mathcal{S} .

The following definition of multi-ribbon graphs is a generalization of signed rotation systems [19] which are equivalent to ribbon graphs.

Definition 4.3 (D -colored multi-ribbon graph). A D -colored multi-ribbon graph \mathbb{G} , depicted in Figure 9 in the center, is an edge multicolored combinatorial map \mathcal{M} equipped with binary variables $|\mathcal{C}|$ taking values 0 or 1 on each edge with colors \mathcal{C} (for each edge, we have either a 0 or a 1 for each of its colors):

$$\text{for } e \in \mathcal{E}_{\mathcal{C}}(\mathcal{M}), \quad e \mapsto \tau(e) = \{\tau^c(e) \in \{0, 1\} \mid c \in \mathcal{C}\}.$$

These edges are called (twisted) multi-ribbon edges. Twisting a multi-ribbon edge e amounts to flipping all the variables $\tau(e)$, that is, $\tau^c(e) \rightarrow \tau^c(e) + 1 \pmod{2}$.

Two D -colored multi-ribbon graphs are equivalent if they differ by reversing the order of halfedges around a vertex and simultaneously twisting every incident multi-ribbon edge (self-loops are twisted twice) at a finite number of vertices.

The following graphical representation is depicted in Figure 9. The vertices of a multi-ribbon graph are represented by D concentric discs with colors ordered from the innermost to the outermost circle. A multi-ribbon edge $e \in \mathcal{E}_{\mathcal{C}}(\mathcal{M})$ connects the discs with colors in \mathcal{C} of its end vertices by ribbon edges. Only discs of the same color can be connected and the ribbons carry the color of the discs they are connecting. A 0/1 value of $\tau^c(e)$ indicates that the ribbon with the color c of the edge e is un-/twisted. The whole multi-ribbon edge is called untwisted if the ribbon of biggest color in \mathcal{C} is untwisted. The q -edges encountered in Section 3 are the edges with colors $\mathcal{C} = \emptyset$. They can be represented as dashed.

The *faces* of color c of \mathbb{G} are the closed circuits obtained by going along the sides of the ribbon edges and along the discs of the vertices of color c . The set of faces of color c of \mathbb{G} is denoted $\mathcal{F}_c(\mathbb{G})$ and its cardinality is denoted $F_c(\mathbb{G})$. The restriction of \mathbb{G} to a single color \mathbb{G}_c is obtained by deleting all the discs and ribbon with other colors. The graph \mathbb{G}_c is an ordinary ribbon graph, possibly disconnected. Observe that $F_c(\mathbb{G})$ is also the number of faces of the ribbon graph \mathbb{G}_c .

The perturbative expansion of (4.1) is obtained by Taylor expanding and commuting the sum and the Gaussian integral:

$$Z(\lambda) = \sum_{V=1}^{\infty} \frac{(-1)^V \sum_{c=1}^D |c|}{V! 2^V} \left[e^{\sum_{q \in \mathcal{Q}} \frac{1}{2} \left(\frac{\partial}{\partial \sigma_q} \cdot P_{\mathcal{C}_q} K_q \frac{\partial}{\partial \sigma_q} \right)} (-\text{Tr} \ln(1^{\otimes \mathcal{D}} + A))^V \right]_{\sigma_q=0},$$

where we suppressed the argument of A . Each $\text{Tr} \ln(1^{\otimes \mathcal{D}} + A)^{-1}$ represents a multi-ribbon vertex. The derivatives

$$\begin{aligned} \frac{\partial}{\partial \sigma_q} (1^{\otimes \mathcal{D}} + A)^{-1} &= (1^{\otimes \mathcal{D}} + A)^{-1} \left(-\frac{\partial A}{\partial \sigma_q} \right) (1^{\otimes \mathcal{D}} + A)^{-1}, \\ \frac{\partial}{\partial \sigma_q} \text{Tr} \ln(1^{\otimes \mathcal{D}} + A)^{-1} &= \text{Tr} \left[(1^{\otimes \mathcal{D}} + A)^{-1} \left(-\frac{\partial A}{\partial \sigma_q} \right) \right], \\ \frac{\partial A}{\partial \sigma_q} &= \iota \sqrt{2\lambda_q} 1^{\otimes \mathcal{D} \setminus \mathcal{C}_q} \otimes P_{\mathcal{C}_q} \end{aligned}$$

create multi-ribbon halfedges which, because of the projector, are joined in a twisted or untwisted way. The possible types of multi-ribbon edges depend on the quartic invariants $q \in \mathcal{Q}$: for brevity the multi-ribbon edges associated to the quartic invariant q are called q -edges. The trace induces a cyclic ordering around the vertex which by convention we take to be counter-clockwise. Following an index of color c , it goes around the vertex until it encounters a multi-ribbon halfedge with $c \in \mathcal{C}_q$. As in the matrix case, the order of indices is important if $|c| = 1$. This is accounted for by

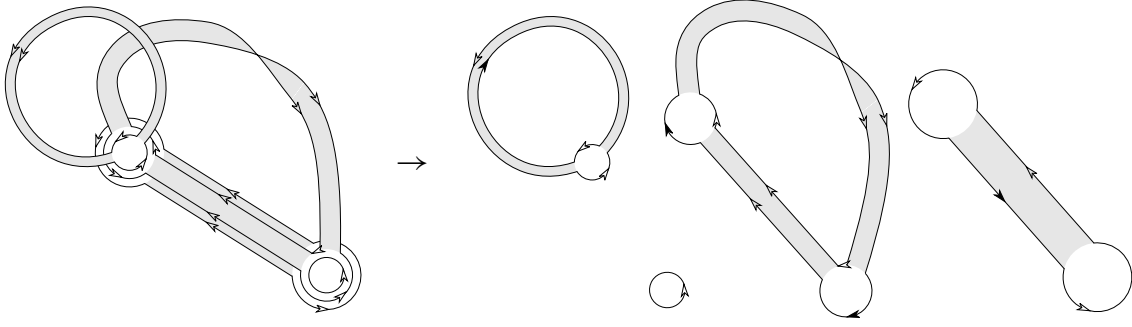


Figure 10. *Left:* A 3-colored multi-ribbon graph. The arrows indicate the order of indices of the $g_{a_c b_c}^c$. In the a priori orientation, arrows point counter-clockwise around vertices and parallel along edges. *Right:* Ribbon graphs obtained by restricting to a single color. The black arrows had to be flipped to arrive at a coherent orientation along each face. Compare to Figure 7.

orienting the strands of a vertex in a counter-clockwise manner (Figure 10). Denoting $R = (1^{\otimes \mathcal{D}} + A)^{-1}$, the contribution of an edge can be written as

$$(-1)^{\sqrt{2\lambda_q}} R_{.b^1} R_{a^1}. (P_{\mathcal{C}_q} K_q)^{b^1 a^1, b^2 a^2} R_{.b^2} R_{a^2.},$$

and upon setting $\sigma_q = 0$ all the resolvents reduce to the identity operator.

We denote by \mathcal{M} the edge multicolored maps and by $\deg^q v$ the number of edges of type q incident to the vertex v . As in the matrix case, the edges with $\mathcal{C} = \emptyset$ are special. We call them ϱ -edges and denote sometimes the number of such edges $E^\varrho(\mathcal{M})$. However, note that the ϱ -edges are also counted as a particular case q -edges for $q \in Q$.

The halfedges incident at a vertex have colors \mathcal{C}_q , and we denote them $h_v^{\mathcal{C}_q}$, $f_v^{\mathcal{C}_{q'}}$ and so on. Each halfedge is composed of $|\mathcal{C}_q|$ ribbon halfedges, one for each color in \mathcal{C}_q . The corners⁷ of the map \mathcal{M} are the pieces of vertices comprised between two consecutive halfedges, and we denote them by $(h_v^{\mathcal{C}_q}, f_v^{\mathcal{C}_{q'}})$, with the successor $f_v^{\mathcal{C}_{q'}}$ of $h_v^{\mathcal{C}_q}$ when turning around v . The partition function becomes

$$\begin{aligned} Z(\lambda) = & \sum_{\mathcal{M}} \frac{1}{V(\mathcal{M})! 2^{V(\mathcal{M})}} \left(\prod_{v \in \mathcal{M}} \frac{1}{\prod_q \deg^q v!} \right) ((-1)^{\sum_{c \in \mathcal{D}} |c|})^{V(\mathcal{M})} 2^{E^\varrho(\mathcal{M})} \\ & \times \prod_{q \in Q} (-\lambda_q)^{E_q(\mathcal{M})} \prod_{v \in \mathcal{V}(\mathcal{M})} \left(\prod_{(h_v^{\mathcal{C}_q}, f_v^{\mathcal{C}_{q'}}) \text{ corner of } v} \prod_{c \in \mathcal{D}} g_{h_v^{\mathcal{C}_q}^c(b_c) f_v^{\mathcal{C}_{q'}}^c} \right) \\ & \times \prod_{e = \{h_v^{\mathcal{C}_q}, h_w^{\mathcal{C}_q}\} \in \mathcal{E}(\mathcal{M})} \left((2P_{\mathcal{C}_q} K_q)^{(b_{\mathcal{C}_q})_{h_v^{\mathcal{C}_q}}^{\mathcal{C}_q} (a_{\mathcal{C}_q})_{h_v^{\mathcal{C}_q}}^{\mathcal{C}_q}, (b_{\mathcal{C}_q})_{h_w^{\mathcal{C}_q}}^{\mathcal{C}_q} (a_{\mathcal{C}_q})_{h_w^{\mathcal{C}_q}}^{\mathcal{C}_q}} \right) \\ & \times \prod_{c \notin C_q} (g^c)^{(b_c)_{h_v^{\mathcal{C}_q}}^{\mathcal{C}_q} (a_c)_{h_v^{\mathcal{C}_q}}^{\mathcal{C}_q}} (g^c)^{(b_c)_{h_w^{\mathcal{C}_q}}^{\mathcal{C}_q} (a_c)_{h_w^{\mathcal{C}_q}}^{\mathcal{C}_q}} \end{aligned}$$

⁷We exclude the ϱ halfedges when identifying the corners.

with the convention such that if $\mathcal{C}_q = \emptyset$, then there is no corner and the edge $(2P_{\mathcal{C}_q}K_q)$ equals 1.

An index of color c is insensitive to the halfedges with colors different from c : an index follows a face and closes in a trace when the face closes. As in the matrix case, we obtain either straight edges or twisted ones coming from the two terms in $P_{\mathcal{C}_q}$. In turn, the edges contract on K_p kernels that send the color c either in a parallel channel or in a cross one. Overall, the ribbon of color c of the edge $(2P_{\mathcal{C}_q}K_q)$ can either be straight, which we denote $\tau^c(e) = 0$, or twisted, which we denote $\tau^c(e) = 1$. Let us track the indices of color c coming from a term in $P_{\mathcal{C}_q}$ and one possible K_q , for instance,

$$(2P_{\mathcal{C}_q}K_q) \sim \delta^{b_c^1}_i \delta^{a_c^1}_j (-1)^{|c|} g^{i b_c^2} g^{j a_c^2} = (-1)^{|c|} g^{b_c^1 b_c^2} g^{a_c^1 a_c^2}.$$

As this term contracts the indices b together and the indices a together, it corresponds to a ribbon of color c which is twisted. Proceeding similarly for all the edges and recalling that some g 's need to be transposed in order to orient coherently the faces, we conclude that

$$\begin{aligned} Z(\lambda) &= \sum_{\mathcal{M}} \frac{|\text{Stab}_{\mathfrak{T}}(\mathcal{M})|}{V(\mathcal{M})! 2^{V(\mathcal{M})}} \left(\prod_{v \in \mathcal{M}} \frac{1}{\prod_q \deg^q v!} \right) \sum_{[\mathbb{G}] \in \text{Orb}_{\mathfrak{T}}(\mathcal{M})} \mathcal{A}(\mathbb{G}), \\ \mathcal{A}(\mathbb{G}) &= ((-1)^{\sum_{c \in \mathcal{D}} |c|} V(\mathbb{G}) 2^{E^\theta(\mathbb{G})} \prod_{q \in \mathcal{Q}} (-\lambda_q)^{E_q(\mathbb{G})}) \\ &\quad \times \left(\prod_{C_q \neq \emptyset} \prod_{e \in \mathcal{E}_{\mathcal{C}_q}(\mathbb{G})} (-1)^{\sum_{c \in \mathcal{C}_q} \tau^c(e) |c|} \right) \prod_c \prod_{f \in \mathcal{F}_c(\mathbb{G})} (-1)^{t(f) |c|} N_c, \end{aligned} \quad (4.2)$$

where $t(f)$ denotes the number of transpositions needed to orient the face f coherently.

Amplitudes. Up to the overall coupling constants, the amplitude of a graph factors over the ribbon graphs \mathbb{G}_c

$$\begin{aligned} \mathcal{A}(\mathbb{G}) &= 2^{E^\theta(\mathbb{G})} \prod_{q \in \mathcal{Q}} (-\lambda_q)^{E_q(\mathbb{G})} \prod_{c \in \mathcal{D}} \left[(-1)^{V(\mathbb{G}_c) |c|} \left(\prod_{e \in \mathcal{E}(\mathbb{G}_c)} (-1)^{\tau^c(e) |c|} \right) \right. \\ &\quad \left. \times \left(\prod_{f \in \mathcal{F}_c(\mathbb{G})} (-1)^{t(f) |c|} N_c \right) \right], \end{aligned}$$

and using Theorem A.11, this is

$$\mathcal{A}(\mathbb{G}) = 2^{E^\theta(\mathbb{G})} \prod_{q \in \mathcal{Q}} (-\lambda_q)^{E_q(\mathbb{G})} \prod_{c=1}^D ((-1)^{|c|} N_c)^{F_c(\mathbb{G})}, \quad (4.3)$$

and thus obeys the $N_c \rightarrow -N_c$ duality. The ϱ -edges associated to the unique disconnected invariant $\mathcal{C}_q = \emptyset$ do not have a twisted or untwisted state and bring a relative factor of two compared to the other multi-ribbon edges.

The two-point function. The connected two-point function of the tensor model

$$G_2(\lambda) := Z^{-1}(\lambda) \int d\mu[T] T^{a\mathcal{D}} T^{b\mathcal{D}} g_{a_1 b_1}^1 \cdots g_{a_D b_D}^D$$

can be expressed as a perturbative series over rooted multi-ribbon graphs. As in the matrix case, rooting drastically simplifies the combinatorial factors. The DSE for G_2 follows from

$$0 = \int dT \frac{\partial}{\partial T^{a\mathcal{D}}} (T^{a\mathcal{D}} e^{-S[T]}) \Rightarrow G_2(\lambda) = \prod_{c \in \mathcal{D}} N_c + \sum_{q \in \mathcal{Q}} 4\lambda_q \partial_{\lambda_q} \ln Z. \quad (4.4)$$

Graphically, the derivatives select an edge of a multi-ribbon graph and because every edge has two halfedges, $\sum_{q \in \mathcal{Q}} 2\lambda_q \partial_{\lambda_q}$ generates a sum over all possible rootings. Rooted unlabeled multi-ribbon graphs are equivalence classes of labeled multi-ribbon graphs that differ only by relabeling of their halfedges, but keeping the root halfedge fixed. The calculation of $|\text{Stab}_{\mathfrak{T}}(\mathbb{G})|$ is a straightforward generalization of the ordinary ribbon graph case, and in Proposition B.1 we show that

$$G_2(\lambda) = \sum_{[\mathbb{G}] \text{ connected, rooted}} \frac{1}{2^{C(\mathbb{G} - \mathcal{E}^\varrho) - 1}} \mathcal{A}(\mathbb{G}), \quad (4.5)$$

where $C(\mathbb{G} - \mathcal{E}^\varrho)$ counts the number of connected components of the multi-ribbon graph obtained after deletion of the ϱ -edges. The free energy $\ln Z(\lambda)$ can be obtained by integrating the DSE,

$$\ln Z(\lambda) = \sum_{\substack{[\mathbb{G}] \text{ connected, rooted,} \\ \text{at least one } E_q > 0}} \frac{1}{2^{C(\mathbb{G} - \mathcal{E}^\varrho) + 1} \sum_{q \in \mathcal{Q}} E_q(\mathbb{G})} \mathcal{A}(\mathbb{G}). \quad (4.6)$$

Rescaled theories. Models which admit a good $1/N$ expansion involve couplings rescaled by various powers of N . In order to maintain the N to $-N$ duality of the amplitudes, one needs sometimes to flip the sign of the couplings. For instance, for $D = 2$, in order to get a sensible large N limit, one needs to rescale the coupling by a factor N . If one rescales $\lambda \rightarrow \lambda/N$ in the $O(N) \otimes O(N)$ -model and $\lambda \rightarrow -\lambda/N$ in the $\text{Sp}(N) \otimes \text{Sp}(N)$ -model, the amplitudes graphs differ by $(-1)^{\chi(\mathcal{E})}$.⁸ The equality is reestablished if one sends at the same time $\lambda \rightarrow -\lambda$.

⁸This was also found in [43].

A. Classification of ribbon graphs

A.1. Canonical form

We prove in this subsection that a ribbon graph can be brought into a canonical form obtained by first separating the oriented and unoriented parts of the graph (Proposition A.1) and then simplifying the oriented part (Proposition A.3).

Proposition A.1. *Every connected ribbon graph \mathcal{G} is homeomorphic as a topological surface (two-dimensional CW complex) to a ribbon graph \mathcal{G}' such that*

- \mathcal{G}' has only one vertex;
- \mathcal{G}' has either none, or one or two twisted simple self-loops;
- all the remaining edges of \mathcal{G}' are untwisted.

Equivalently,

$$\mathcal{G} \cong \mathcal{G}' \cong \begin{cases} \mathcal{G}_{\Sigma_g}, & \text{orientable with } k = 2g, \\ \mathcal{G}_{\Sigma_g} \vee \mathcal{G}_{\mathbb{RP}^2}, & \text{unorientable with } k = 2g + 1, \\ \mathcal{G}_{\Sigma_g} \vee \mathcal{G}_{\mathbb{RP}^2} \vee \mathcal{G}_{\mathbb{RP}^2}, & \text{unorientable with } k = 2g + 2, \end{cases}$$

where \mathcal{G}_{Σ_g} a ribbon subgraph of \mathcal{G}' containing only untwisted edges and is cellularly embedded into a closed orientable surface Σ_g with orientable genus g (we reserve the notation g for the orientable genus) and k is the non-orientable genus of \mathcal{G}' .

Proposition A.1 is illustrated in Figure 11.

In order to state our second proposition, we need the notion of *clean nice crossing*.

Definition A.2 (Nice crossing and clean nice crossing). Let $e = \{e_1, e_2\}$ and $f = \{f_1, f_2\}$ be two untwisted self-loop edges connected to the same vertex v of a ribbon graph. Assume $f_1 < f_2$ and $e_1 < e_2$ in the cyclic order around v .

- The pair (e, f) is a *nice crossing* [29] if and only if e_2 is the successor of f_1 .
- A nice crossing (e, f) is called *clean nice crossing* if there is no other halfedge h of v distinct from e_2, f_1 satisfying $e_1 < h < f_2$, i.e., along v the halfedges are encountered in the order $\dots e_1 f_1 e_2 f_2 \dots$.

Proposition A.3. *Every ribbon graph \mathcal{G} composed of only untwisted edges is homeomorphic as a topological surface (two-dimensional CW complex) to a ribbon graph \mathcal{G}' with one vertex, one face and $2g$ edges forming g clean nice crossings, where g is the orientable genus of \mathcal{G} . Equivalently,*

$$\mathcal{G} \simeq \mathcal{G}' \cong \mathcal{G}_\circ \bigvee_g \mathcal{G}_{T^2} \quad \text{with } \chi = 2 - 2g.$$

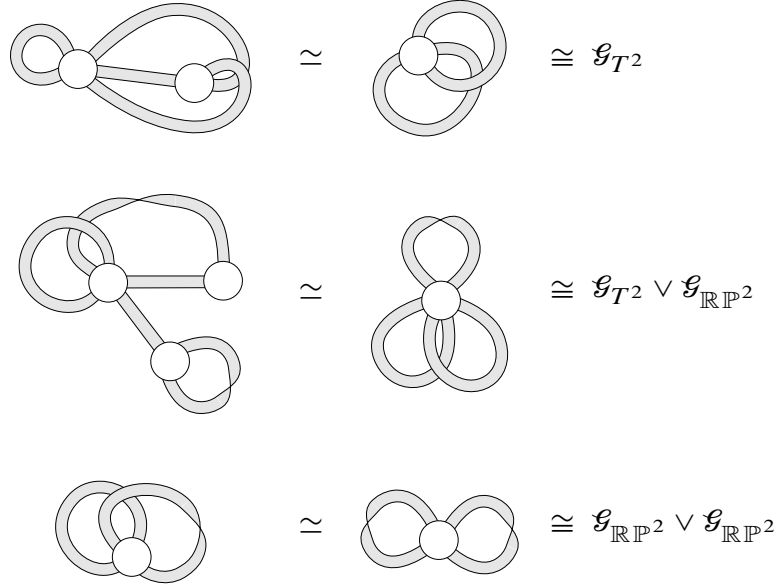


Figure 11. Illustration of Proposition A.1. In the first line the orientable part was further simplified using Proposition A.3. We call the right-hand side the canonical form.

Note that Proposition A.3 can be applied to \mathcal{G}_{Σ_g} in Proposition A.1, yielding

$$\mathcal{G} \simeq \mathcal{G}_o \bigvee_g \mathcal{G}_{T^2} \bigvee_{0, 1 \text{ or } 2} \mathcal{G}_{\mathbb{RP}^2}.$$

We call the right-hand side of this equation the *canonical form* of \mathcal{G} , see Figure 11. This is the ribbon graph version of classification theorem of closed surfaces, stating that every such surface is homeomorphic to the connected sum of a sphere, some number of tori, and either no, one or two real projective planes.

Contraction and sliding of edges. We introduce two homeomorphisms of ribbon graphs, viewed as a topological surface with boundary. Similar moves are known in the literature [23, 42].

Definition A.4 (Contraction of an edge, see Figure 12). Let \mathcal{G} be a ribbon graph and $e \in \mathcal{E}(\mathcal{G})$ an edge connecting two distinct vertices $v, w \in \mathcal{V}(\mathcal{G})$ of coordination p and q . Remember that v, w and e are all topological discs.

If e is untwisted, we define \mathcal{G}/e to be the ribbon graph obtained from \mathcal{G} by replacing v, w and e by the single vertex $u = v \cup e \cup w$ (which is again a topological disc) of coordination $p + q - 2$ such that in the cyclic ordering around this vertex the halfedges of v proceed the halfedges of w . The ribbon graph \mathcal{G}/e has one vertex and one edge fewer than \mathcal{G} , but the same number of faces.

If e is twisted, we first push the twist along the graph by reembedding the vertex w such that e is untwisted and proceed as before.

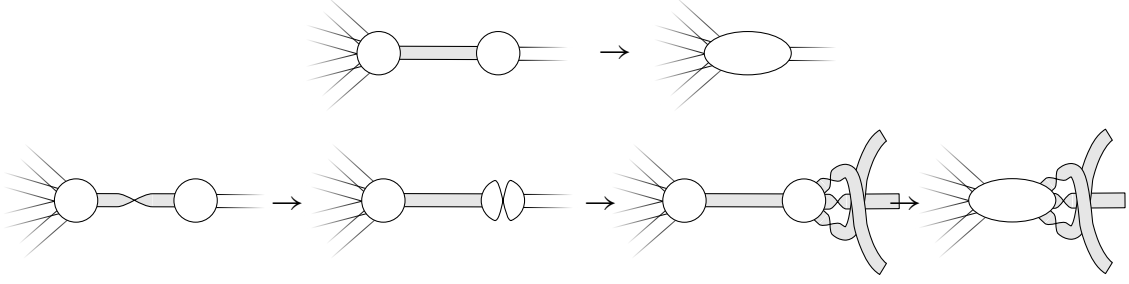


Figure 12. Contraction of an untwisted (*first line*) and twisted (*second line*) edge in a ribbon graph.

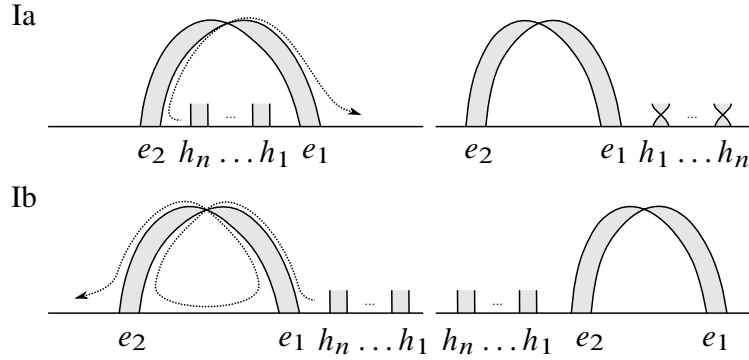


Figure 13. Sliding of edges Ia and Ib. The horizontal line is the vertex with ordering from right to left.

The contraction preserves the Euler characteristic and the orientability, and is thus a homeomorphism of surfaces.

A spanning tree of \mathcal{G} , that is, a connected acyclic subgraph $\mathcal{T} \subset \mathcal{G}$, has $E(\mathcal{T}) = V(\mathcal{G}) - 1$ edges. One can contract all the edges in a spanning tree and decrease the numbers of vertices and edges of \mathcal{G} to

$$V(\mathcal{G}) \rightarrow V(\mathcal{G}) - (V(\mathcal{G}) - 1) = 1 \quad \text{and} \quad E(\mathcal{G}) \rightarrow E(\mathcal{G}) - (V(\mathcal{G}) - 1).$$

The resulting graph is a rosette graph homeomorphic to \mathcal{G} .

Definition A.5 (Sliding of edges Ia, see Figure 13). Let $e = \{e_1, e_2\}$ be a twisted self-loop edge on the vertex v of a ribbon graph. In the cyclic ordering of halfedges around v , let $e_1 < e_2$ and denote by $e_1 < h_1 < h_2 < \dots < h_n < e_2$ all the halfedges of v that are between e_1 and e_2 .

Sliding of the halfedges h_1, \dots, h_n out of the twisted edge e is defined as

- (1) Reordering the halfedges to $h_n < \dots < h_2 < h_1 < e_1 < e_2$.
- (2) Adding a twist (recall that two twists on the same edge cancel) to all the edges to which h_1, \dots, h_n belong.

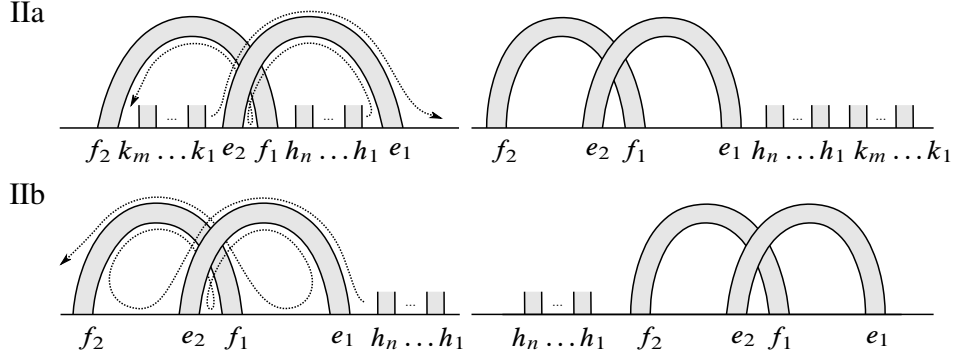


Figure 14. Sliding of edges IIa and IIb.

Note that the order of the h_i 's has been reversed. Also, note that and after the sliding, e is a simple twisted self-loop.

Definition A.6 (Sliding of edges Ib, see Figure 13). Let $e = \{e_1, e_2\}$ be a simple twisted self-loop on the vertex v of a ribbon graph. In the cyclic ordering of halfedges around v , let $e < 1 < e_2 < h_1 < h_2 < \dots < h_n$ with h_i a collection of consecutive halfedges preceding e_1 on v . As e is a simple self-loop, there is no halfedge between e_1 and e_2 .

Sliding of the halfedges h_1, \dots, h_n past the twisted edge e is defined as

- (1) Reordering the halfedges to $e_1 < e_2 < h_1 < h_2 < \dots < h_n$.

Note that the relative order of the h_i 's has not changed, no additional twists were introduced and e remains a simple twisted self-loop.

Both sliding operation (Ia) and (Ib) preserve the number of faces, do not change the numbers of vertices and edges and do not alter the orientability. Thus these operations are homeomorphisms of two-dimensional surfaces.

Definition A.7 (Sliding of edges IIa, see Figure 14). Let $(e = \{e_1, e_2\}, f = \{f_1, f_2\})$ be a nice crossing at the vertex v of a ribbon graph. In the cyclic ordering of halfedges around v , let us denote by

$$e_1 < h_1 < \dots < h_n < f_1 < e_2 < k_1 < \dots < k_m < f_2$$

the halfedges located between e_1 and f_2 .

Sliding of the halfedges $h_1, \dots, h_n, k_1, \dots, k_m$ out of the nice crossing (e, f) is defined as

- (1) Reordering the halfedges to $k_1 < \dots < k_m < h_1 < \dots < h_n < e_1 < f_1 < e_2 < f_2$.

Note that the order of the set of h_i 's and k_j 's was interchanged, but the relative order in each set remained unchanged. After sliding, (e, f) is a clean nice crossing.

Definition A.8 (Sliding of edges IIb, see Figure 14). Let $(e = \{e_1, e_2\}, f = \{f_1, f_2\})$ be a clean nice crossing at the vertex v of a ribbon graph. In the cyclic ordering of halfedges around v , let us denote by

$$h_1 < \dots < h_n < e_1 < f_1 < e_2 < f_2$$

a collection of consecutive halfedges preceding e_1 on v .

Sliding of the halfedges h_1, \dots, h_n past the clean nice crossing (e, f) is defined as

- (1) Reordering the halfedges to $e_1 < f_1 < e_2 < f_2 < h_1 < \dots < h_n$.

Note that the relative order of the h_i 's is unchanged; (e, f) remains a clean nice crossing.

Like the sliding along twisted edges, the sliding along a nice crossing (IIa, IIb) is a homeomorphism of two-dimensional surfaces.

Proof of Proposition A.1. Let \mathcal{G} be a connected ribbon graph.

First. Contract a spanning tree $\mathcal{T} \subset \mathcal{G}$. This decreases the number of edges and vertices by $V(\mathcal{G}) - 1$ and the resulting ribbon graph \mathcal{G}/\mathcal{T} is a rosette graph, that is, a graph with only one vertex.

Second. If \mathcal{G}/\mathcal{T} does not contain any twisted edges, then it can be embedded into an orientable surface Σ_g of genus g .

Otherwise, use sliding out of twisted self-loop edges (Ia) to create simple twisted self-loops. This operation may create new twists in the halfedges. Once a twisted self-loop is created, use the slide (Ib) to move it “to the right” on the vertex.

Proceed until all the twisted edges of the rosette graph belong to simple twisted self-loops. The resulting graph is a connected sum of an orientable graph \mathcal{O} containing only untwisted edges and p copies of $\mathcal{G}_{\mathbb{RP}^2}$, i.e., ribbon graphs with only one simple twisted loop:

$$\mathcal{O} \vee \underbrace{\mathcal{G}_{\mathbb{RP}^2} \vee \dots \vee \mathcal{G}_{\mathbb{RP}^2}}_{p\text{-times}}.$$

Third. By sliding as depicted in Figure 15, three neighboring simple twisted self-loops can be reduced to one simple twisted self-loop and a clean nice crossing:

$$\mathcal{G}_{\mathbb{RP}^2} \vee \mathcal{G}_{\mathbb{RP}^2} \vee \mathcal{G}_{\mathbb{RP}^2} \cong \mathcal{G}_{\mathbb{RP}^2} \vee \mathcal{G}_{T^2},$$

hence it is possible to reduce the number of simple twisted self-loops (and twisted edges in total) to zero, one or two. Slide (Ib) the clean nice crossings to the left of the twisted self-loops.

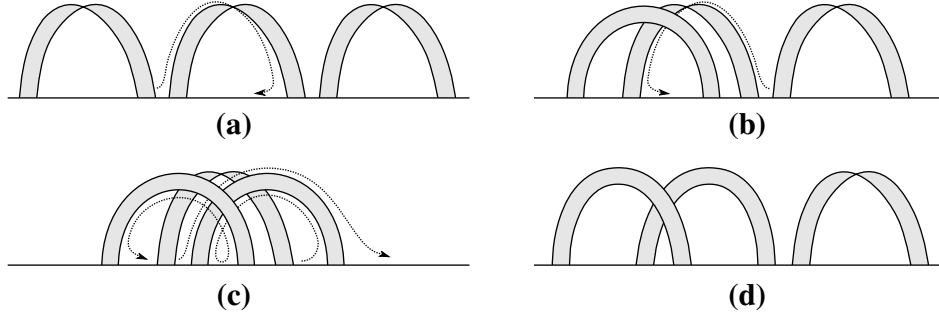


Figure 15. Deforming three neighboring simple twisted self-loops into a graph with only one twisted edge. (a) and (b): By inverting (Ia), slide a halfedge of the left and right twisted simple loop into the central one. This creates a nice crossing. (c): Use (IIa) to slide the central twisted loop out of the nice crossing. (d): The result has only a single simple twisted loop.

Finally. One arrives at a graph \mathcal{G}' of the form

$$\mathcal{G}' \cong \begin{cases} \mathcal{G}_{\Sigma_g}, & \text{orientable with } k = 2g, \\ \mathcal{G}_{\Sigma_g} \vee \mathcal{G}_{\mathbb{RP}^2}, & \text{unorientable with } k = 2g + 1, \\ \mathcal{G}_{\Sigma_g} \vee \mathcal{G}_{\mathbb{RP}^2} \vee \mathcal{G}_{\mathbb{RP}^2}, & \text{unorientable with } k = 2g + 2 \end{cases}$$

with $\chi(\mathcal{G}) = \chi(\mathcal{G}') = 2 - k$. ■

Proof of Proposition A.3. Let \mathcal{G} be a connected ribbon graph with only untwisted edges. Such a graph can be embedded into an orientable surface.

First. Contract a spanning tree $\mathcal{T}_1 \subset \mathcal{G}$ to arrive at a rosette graph $\mathcal{G}/\mathcal{T}_1$.

Second. Contract a spanning tree in the dual graph $\mathcal{T}_2 \subset (\mathcal{G}/\mathcal{T}_1)^*$. This corresponds to deleting edges in \mathcal{G} in a way that preserves the Euler characteristic, the orientability and the connectivity.

This reduces the number of faces and edges by $F(\mathcal{G}) - 1$ and gives a superrosette graph \mathcal{R} , that is, a graph with one vertex, one face and only untwisted edges. A superrosette always contains at least one nice crossing.

Third. Choose a nice crossing (e, f) in \mathcal{R} and slide (IIa) all the halfedges encompassed by the nice crossing out of (e, f) . The result has the structure

$$\mathcal{R} \cong \mathcal{R}/(e, f) \vee \mathcal{G}_{T^2},$$

where $\mathcal{R}/(e, f)$ is again a superrosette graph with genus decreased by one. Iterating one arrives at

$$\mathcal{R} \cong \mathcal{G}_o \vee \underbrace{\mathcal{G}_{T^2} \vee \cdots \vee \mathcal{G}_{T^2}}_{g\text{-times}}.$$
■

A.2. Sign of a ribbon graph

Let \mathcal{G} be a connected ribbon graph. An *a priori arrow orientation*⁹ of a \mathcal{G} (which has nothing to do with the orientability of the embedding surface) is defined by the following:

- (1) counter-clockwise pointing arrows at the corners of each vertex;
- (2) parallel pointing arrows on the strands of each edge.

We denote $\tau(e) = 0$ if the edge e is untwisted (straight) and $\tau(e) = 1$ if the edge e is twisted. Furthermore, we denote by $t(f)$ the number of reorientations of arrows required to coherently orient the face f with all the arrows pointing in the same direction along its boundary. The *sign* of \mathcal{G} is defined as

$$\text{sgn}(\mathcal{G}) = (-1)^{V(\mathcal{G})} \left(\prod_{e \in \mathcal{E}(\mathcal{G})} (-1)^{\tau(e)} \right) \left(\prod_{f \in \mathcal{F}(\mathcal{G})} (-1)^{t(f)} \right).$$

This is well defined. In order to determine the sign of \mathcal{G} , one needs to determine the number of arrow flips that are necessary to go from an a priori orientation of \mathcal{G} to an orientation where all arrows point coherently along the faces of \mathcal{G} (such an orientation will be called *coherent*). Since every face consists of as many corners as edge strands, the total number of arrows along a face is even and switching between two coherent orientations requires an even number of arrow flips. Also, as any two a priori orientations differ by an even number of arrow flips (pairs of arrows along the edge strands), switching between a priori orientations at fixed coherent orientation does not change the sign of the graph.

Lemma A.9. *The sign of a graph is*

- *invariant under reembedding of the vertices;*
- *invariant under contraction of a tree edge.*

Proof. Consider an a priori arrow orientation of \mathcal{G} . Re-embedding a vertex of degree d brings d new twists, but one needs to reverse d vertex corners in order to orient the re-embedded vertex counter-clockwise.

Consider now a tree edge e connecting two vertices v and w in a graph with a priori orientation (which by the first item we can assume to be untwisted). A flip of an arrow coherently orients the disc $u = v \cup e \cup w$, but this is canceled by the fact that under contraction the number of vertices of the graph goes down by 1. ■

Lemma A.10. *The sign of a graph is invariant under the sliding moves.*

Proof. We consider a graph \mathcal{G} having a twisted self-loop as in Figure 16 (a).

⁹This is the arrow orientation encountered in Section 4.

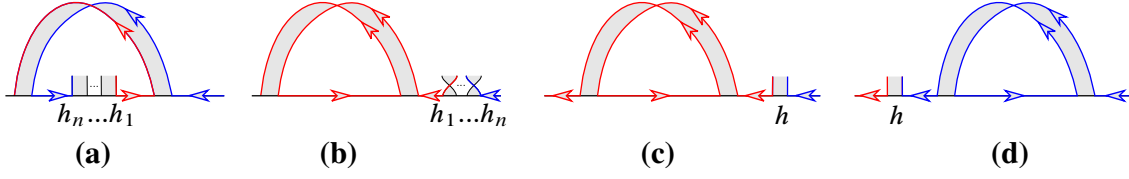


Figure 16. Sliding I at a twisted self-loop in a coherently oriented graph. The red and blue corners and strands belong to the red and blue face, respectively. The number of reversed arrows and additional twists is always even.

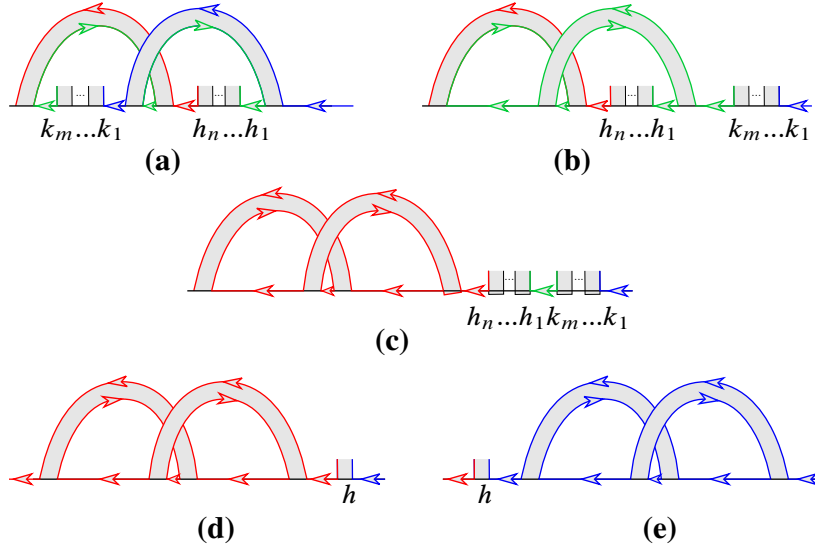


Figure 17. Sliding II at a nice crossing in a coherently oriented graph. No arrows are reversed, nor are halfedges twisted.

We denote by \mathcal{G}' the graph obtained from \mathcal{G} by the sliding Ia. All else being equal, in order to pass from an a priori orientation of \mathcal{G} to the coherent orientation depicted in Figure 16(a) two corner arrows had to be reversed, while for \mathcal{G}' only one. However, \mathcal{G}' has one twist more than \mathcal{G} . As the graphs are otherwise identical, they have the same sign. For Ib sliding, there is no extra twist, but both graphs need only one local arrow reorientation.

We now consider a graph \mathcal{G} having a nice crossing as in Figure 17(a) and denote by \mathcal{G}' the graph obtained from \mathcal{G} after sliding. In all the cases, the same number of arrow flips is needed in order to pass locally from an a priori to the coherent orientations depicted. As \mathcal{G} and \mathcal{G}' are identical elsewhere, they have the same sign. ■

Theorem A.11 (Sign of a ribbon graph). *For any connected ribbon graph \mathcal{G} , we have*

$$\text{sgn}(\mathcal{G}) = (-1)^{V(\mathcal{G})} \left(\prod_{e \in \mathcal{E}(\mathcal{G})} (-1)^{\tau(e)} \right) \left(\prod_{f \in \mathcal{F}(\mathcal{G})} (-1)^{t(f)} \right) = (-1)^{F(\mathcal{G})},$$

where $F(\mathcal{G})$ is the number of faces of \mathcal{G} .

Proof. From Lemmas A.9 and A.10, the sign of a graph is invariant under the reduction moves used in Proposition A.1. It follows that, not only

$$\mathcal{G} \cong \mathcal{G}' \cong \begin{cases} \mathcal{G}_{\Sigma_g}, & \text{orientable with } k = 2g, \\ \mathcal{G}_{\Sigma_g} \vee \mathcal{G}_{\mathbb{RP}^2}, & \text{unorientable with } k = 2g + 1, \\ \mathcal{G}_{\Sigma_g} \vee \mathcal{G}_{\mathbb{RP}^2} \vee \mathcal{G}_{\mathbb{RP}^2}, & \text{unorientable with } k = 2g + 2, \end{cases}$$

but also $\text{sgn}(\mathcal{G}) = \text{sgn}(\mathcal{G}')$. The sign of \mathcal{G}' is easy to compute using the following:

- \mathcal{G}' has one vertex;
- each simple twisted self-loop brings a (-1) for the twist and another (-1) in order to change from an a priori arrow orientation to a coherent one;
- the number of untwisted edges of \mathcal{G}' is the number of edges of \mathcal{G}_{Σ_g} , that is, $E(\mathcal{G}_{\Sigma_g})$. Exactly one arrow for each such edge needs to be flipped in order to pass from an a priori to a coherent arrow orientation of \mathcal{G}' .

Therefore, $\text{sgn}(\mathcal{G}') = (-1)^{1+E(\mathcal{G}_{\Sigma_g})}$. The theorem follows by observing that the Euler relation for \mathcal{G}_{Σ_g} reads $1 - E(\mathcal{G}_{\Sigma_g}) + F(\mathcal{G}_{\Sigma_g}) = 2 - 2g(\mathcal{G}_{\Sigma_g})$, hence $F(\mathcal{G}_{\Sigma_g}) = 1 + E(\mathcal{G}_{\Sigma_g}) \bmod 2$, and the number of faces is invariant under contraction and sliding $F(\mathcal{G}_{\Sigma_g}) = F(\mathcal{G}') = F(\mathcal{G})$. ■

B. Symmetry factors

The aim of this section is to prove the following proposition.

Proposition B.1. *The perturbative series of the two-point function*

$$G_2(\lambda) := Z^{-1}(\lambda) \int d\mu[T] T^{a\mathcal{D}} T^{b\mathcal{D}} g_{a_1 b_1}^1 \cdots g_{a_D b_D}^D$$

can be written as the sum

$$G_2(\kappa, \lambda) = \sum_{[\mathcal{G}^\varrho] \text{ connected, rooted}} \frac{1}{2^{C(\mathcal{G}^\varrho - \mathcal{E}^\varrho) - 1}} \mathcal{A}(\mathcal{G}^\varrho).$$

Before proving this proposition, we discuss some useful facts. The symmetry factor of a ribbon graph in the perturbative series (3.4) of $Z(\lambda)$ is obtained as

- a factor $\frac{1}{2^{V n_{\text{IVP}}}}$, where n_{IVP} is the number of permutations of vertex labels, that give the same labeled map;
- a factor $\frac{1}{\deg v! \deg^\varrho v!}$ for every vertex;
- a factor counting the number of ways to connect labeled halfedges to form the same combinatorial map \mathcal{M}^ϱ underlying \mathcal{G}^ϱ , taking into account the different ways to label the halfedges;

- a factor $|\text{Stab}_{\mathfrak{T}}|$ and the number of combinatorial maps such that \mathcal{G}^{ϱ} is contained in their orbits under \mathfrak{T} .

For example, the weight of the ribbon graph in Figure 7 is

$$\frac{1}{2^3 \cdot 1} \frac{|\text{Stab}_{\mathfrak{T}}|}{2^2} \frac{\text{labeling and connecting halfedges}}{2 \cdot 5! \cdot 3!} = \frac{1}{2}.$$

$2^V n_{\text{IVP}} \quad \prod_v \deg v! \deg^{\varrho} v!$

Stabilizer of rooted ribbon graphs with respect to \mathfrak{T} . Rooting simplifies the calculation of $|\text{Stab}_{\mathfrak{T}}(\mathcal{M})|$. The finite group \mathfrak{T} that twists the ribbon edges is defined on graphs with a fixed but arbitrary labeling of their edges. The rooting can be used to induce such a labeling: Fix a spanning tree and enumerate all edges as they are encountered on a counter-clockwise walk following the unique face of the tree, starting at the root.

We first focus on ordinary combinatorial maps and ribbon graphs. The results can be generalized to graphs with ϱ -edges, by considering the ordinary ribbon graph that is obtained by deleting the ϱ -edges.

Lemma B.2. *Let \mathcal{G} be a rooted, connected ribbon graph. We denote by V_1 and V_2 the numbers of non-root vertices of degree one and two, respectively. Then*

$$|\text{Stab}_{\mathfrak{T}}(\mathcal{G})| = 2^{V_1 + V_2}.$$

Proof. The orientation of the root vertex is held fixed. If a non-root vertex has degree one, twisting the edge incident to it does not change the ribbon graph—the twist is “reducible”. If a non-root vertex has degree two, twisting both incident edges again does not change the ribbon graph. If both halfedges of a degree two vertex belong to the same edge, it is necessarily the root vertex, since \mathcal{G} is assumed to be connected. This is depicted in Figure 18. ■

It follows that

$$\sum_{\substack{\mathcal{M} \\ \text{connected,} \\ \text{rooted}}} \frac{|\text{Stab}_{\mathfrak{T}}(\mathcal{M})|}{2^V} \sum_{[\mathcal{G}] \in \text{Orb}_{\mathfrak{T}}(\mathcal{M})} \mathcal{A}(\mathcal{G}) = \sum_{\substack{\mathcal{M} \\ \text{connected,} \\ \text{rooted}}} \frac{1}{2^{V_{\geq 3}}} \sum_{[\mathcal{G}] \in \text{Orb}_{\mathfrak{T}}(\mathcal{M})} \mathcal{A}(\mathcal{G}), \quad (\text{B.1})$$

where $V_{\geq 3}$ denotes the number of non-root vertices of degree ≥ 3 . In order to reshuffle this expression into a sum over rooted ribbon graphs, we recall that two ribbon graphs are equivalent if one can be obtained from the other by vertex re-embeddings. This implies that if two combinatorial maps \mathcal{M}_1 and \mathcal{M}_2 differ only by reversing the order of halfedges around some of their vertices, then $\text{Orb}_{\mathfrak{T}}(\mathcal{M}_1) = \text{Orb}_{\mathfrak{T}}(\mathcal{M}_2)$. Reversing the order of halfedges at a vertex of degree lower than three is trivial, hence for rooted



Figure 18. Reducible twists at vertices of degree one and two.

ribbon graphs the multiplicity is $2^{V_{\geq 3}}$. As a result, the perturbative series of the two-point function G_2 (3.5) for $\kappa = 0$ is

$$G_2(0, \lambda) = \sum_{[\mathcal{G}] \text{ connected, rooted}} \mathcal{A}(\mathcal{G}).$$

When taking the ϱ -edges into account, we recall that \mathfrak{T} acts trivially on them. Thus, it is sufficient to consider the ribbon graph $\mathcal{G} = \mathcal{G}^\varrho - \mathcal{E}^\varrho$ obtained by deleting all the ϱ -edges of \mathcal{G}^ϱ . However, when calculating $|\text{Stab}_{\mathfrak{T}}(\mathcal{G}^\varrho)|$ a subtlety arises: $\mathcal{G} = \mathcal{G}^\varrho - \mathcal{E}^\varrho$ is not necessarily connected. The ϱ -edges can be used to induce a rooting at every connected component $\mathcal{G}_c \subset \mathcal{G}$: Consider the connected components as effective vertices in a graph with only ϱ -edges; pick a spanning tree in that graph; from every \mathcal{G}_c there is a unique path in the tree to the original root; let the halfedge of \mathcal{G}_c , belonging to that path, be another root. The stabilizer $\text{Stab}_{\mathfrak{T}}(\mathcal{G})$ factors over the \mathcal{G}_c and using Lemma B.2 for each rooted connected component, one obtains

$$|\text{Stab}_{\mathfrak{T}}(\mathcal{G})| = \prod_{\mathcal{G}_c \subset \mathcal{G}} 2^{V_1(\mathcal{G}_c) + V_2(\mathcal{G}_c)}.$$

One has to partially resume the double sum over combinatorial maps and ribbon graphs with ϱ -edges analogous to (B.1) into a sum over rooted ribbon graphs with ϱ -edges. The multiplicity of a ribbon graph with multiple rooted connected components is $\prod_{\mathcal{G}_c \subset \mathcal{G}} 2^{V_{\geq 3}(\mathcal{G}_c)}$ and one arrives at

$$\prod_{\mathcal{G}_c \subset \mathcal{G}} 2^{V(\mathcal{G}_c) - 1} = 2^{V(\mathcal{G}) - C(\mathcal{G})},$$

where C denotes the number of connected components: the -1 in the exponent appears because V_1 , V_2 and $V_{\geq 3}$ count only non-root vertices, hence sum up to $V(\mathcal{G}_c) - 1$ in each connected component.

Proof of Proposition B.1. The discussion above goes through mutatis mutandis for multi-ribbon graphs. Combining (4.2) with (4.4), the perturbative series of the two-point function can be written as

$$G_2(\lambda) = \sum_{\substack{\mathcal{M} \\ \text{connected, rooted}}} \frac{|\text{Stab}_{\mathfrak{T}}(\mathcal{M})|}{V(\mathcal{M})! 2^{V(\mathcal{M}) - 1}} \left(\prod_{v \in \mathcal{M}} \frac{1}{\prod_q \deg^q v!} \right) \sum_{[\mathbb{G}] \in \text{Orb}_{\mathfrak{T}}(\mathcal{M})} \mathcal{A}(\mathbb{G})$$

with \mathcal{M} and edge multicolored combinatorial map. All objects in the above expression are fully labeled. Rooting prevents non-trivial symmetry factors, thus it is sufficient to count the ways to assign labels to a multi-ribbon graph:

- (1) Pick a spanning tree.
- (2) There are $V!$ ways to label the vertices.
- (3) At the root vertex v_0 , the root breaks the cyclicity of halfedges, thus there are $\prod_q \deg^q v_0!$ ways to label the different types of multi-ribbon halfedges.
- (4) At each non-root vertex one halfedge is part of the unique path in the tree towards the root.

This again breaks cyclicity and there are $\prod_q \deg^q v!$ ways to label the halfedges. The amplitudes do not depend on the labeling, thus, in terms of unlabeled but rooted objects,

$$G_2(\lambda) = \sum_{\substack{\mathcal{M} \text{ connected,} \\ \text{rooted,} \\ \text{unlabeled}}} \frac{|\text{Stab}_{\mathfrak{T}}(\mathcal{M})|}{2^{V(\mathcal{M})-1}} \sum_{[\mathbb{G}] \in \text{Orb}_{\mathfrak{T}}(\mathcal{M})} \mathcal{A}(\mathbb{G}) = \sum_{\substack{[\mathbb{G}] \\ \text{connected,} \\ \text{rooted}}} \frac{1}{2^{C(\mathbb{G}-\mathcal{E}^e)-1}} \mathcal{A}(\mathbb{G}),$$

where $C(\mathbb{G} - \mathcal{E}^e)$ counts the number of connected components of the multi-ribbon graph after deletion of the e -edges. ■

For example, G_2 up to quadratic order in the coupling constants for $D = 2$ is

$$\begin{aligned} G_2(\kappa, \lambda) = & N_1 N_2 - \lambda(N_1 N_2 + N_1^2 N_2 + N_1 N_2^2) \\ & + \lambda^2((2+2+1)N_1 N_2 + (4+1)N_1^2 N_2 + (4+1)N_1 N_2^2 \\ & + (4+1)N_1^2 N_2^2 + 2N_1 N_2^3 + 2N_1^3 N_2) - 2\kappa\left(N_1 N_2 + \frac{1}{2}N_1^2 N_2^2\right) \\ & + 4\kappa^2\left((1+2)N_1 N_2 + \frac{1}{2}(4+1)N_1^2 N_2^2 + \frac{2}{4}N_1^3 N_2^3\right) \\ & + 2\kappa\lambda\left((4+2)N_1 N_2 + (4+2)N_1^2 N_2 + (4+2)N_1 N_2^2\right) \\ & + \frac{4}{2}N_1^2 N_2^2 + \frac{4}{2}N_1^3 N_2^2 + \frac{4}{2}N_1^2 N_2^3 + \dots \end{aligned}$$

Take, for example, the last three graphs. After deleting the ϱ -edges, each graph splits into two connected components, this gives a factor $\frac{1}{2}$ and in addition there are 4 distinct ways of rooting these graphs.

Acknowledgments. The authors would like to thank Dario Benedetti for comments and discussions at the early stages of this project.

Funding. This work was supported by the European Research Council (ERC) under the European Union’s Horizon 2020 research and innovation program (grant agreement No 818066) and by the Deutsche Forschungsgemeinschaft (DFG, German Research Foundation) under Germany’s Excellence Strategy EXC-2181/1 – 390900948 (the Heidelberg STRUCTURES Cluster of Excellence).

References

- [1] J. Ambjørn, B. Durhuus, and T. Jónsson, Three-dimensional simplicial quantum gravity and generalized matrix models. *Modern Phys. Lett. A* **6** (1991), no. 12, 1133–1146
Zbl 1020.83537 MR 1115607
- [2] D. Anninos, T. Hartman, and A. Strominger, Higher spin realization of the DS/CFT correspondence. *Classical Quantum Gravity* **34** (2017), no. 1, article no. 015009
Zbl 1354.83043 MR 3596141
- [3] D. Benedetti, S. Carrozza, R. Gurau, and M. Kolanowski, The $1/N$ expansion of the symmetric traceless and the antisymmetric tensor models in rank three. *Comm. Math. Phys.* **371** (2019), no. 1, 55–97 Zbl 1425.81071 MR 4015340
- [4] D. Bessis, C. Itzykson, and J. B. Zuber, Quantum field theory techniques in graphical enumeration. *Adv. in Appl. Math.* **1** (1980), no. 2, 109–157 Zbl 0453.05035 MR 603127
- [5] V. Bonzom, R. Gurau, and V. Rivasseau, Random tensor models in the large N limit: Uncoloring the colored tensor models. *Phys. Rev. D* **85** (2012), no. 2, article no. 084037
- [6] E. Brézin and V. A. Kazakov, Exactly solvable field theories of closed strings. *Phys. Lett. B* **236** (1990), no. 2, 144–150 MR 1040213
- [7] D. C. Brydges, Lectures on the renormalisation group. In *Statistical mechanics*, pp. 7–93, IAS/Park City Math. Ser. 16, American Mathematical Society, Providence, RI, 2009
Zbl 1186.82033 MR 2523458
- [8] K. Bulycheva, I. R. Klebanov, A. Milekhin, and G. Tarnopolsky, Spectra of operators in large N tensor models. *Phys. Rev. D* **97** (2018), no. 2, article no. 026016 MR 3877831
- [9] S. Carrozza, Large N limit of irreducible tensor models: $O(N)$ rank-3 tensors with mixed permutation symmetry. *J. High Energy Phys.* **2018** (2018), no. 6, article no. 039
Zbl 1395.81155 MR 3850828
- [10] S. Carrozza and S. Harribey, Melonic large N limit of 5-index irreducible random tensors. *Comm. Math. Phys.* **390** (2022), no. 3, 1219–1270 Zbl 1487.81125 MR 4389081

- [11] S. Carrozza and V. Pozsgay, SYK-like tensor quantum mechanics with $\mathrm{Sp}(N)$ symmetry. *Nuclear Phys. B* **941** (2019), 28–52 Zbl 1415.81131 MR 3916553
- [12] S. Carrozza and A. Tanasă, $O(N)$ random tensor models. *Lett. Math. Phys.* **106** (2016), no. 11, 1531–1559 Zbl 1362.83010 MR 3555413
- [13] S. Chmutov, Generalized duality for graphs on surfaces and the signed Bollobás–Riordan polynomial. *J. Combin. Theory Ser. B* **99** (2009), no. 3, 617–638 Zbl 1172.05015 MR 2507944
- [14] P. Cvitanović and A. D. Kennedy, Spinors in negative dimensions. *Phys. Scripta* **26** (1982), no. 1, 5–14 Zbl 1063.22500 MR 669170
- [15] T. Delepouve, R. Gurau, and V. Rivasseau, Universality and Borel summability of arbitrary quartic tensor models. *Ann. Inst. Henri Poincaré Probab. Stat.* **52** (2016), no. 2, 821–848 Zbl 1341.81045 MR 3498011
- [16] P. Di Francesco, P. Ginsparg, and J. Zinn-Justin, 2D gravity and random matrices. *Phys. Rep.* **254** (1995), no. 1–2, 1–133 MR 1320471
- [17] M. R. Douglas and S. H. Shenker, Strings in less than one dimension. *Nuclear Phys. B* **335** (1990), no. 3, 635–654 MR 1059822
- [18] J. A. Ellis-Monaghan and I. Moffatt, Twisted duality for embedded graphs. *Trans. Amer. Math. Soc.* **364** (2012), no. 3, 1529–1569 Zbl 1238.05067 MR 2869185
- [19] J. A. Ellis-Monaghan and I. Moffatt, *Graphs on surfaces: Dualities, polynomials, and knots*. SpringerBriefs Math., Springer, New York, 2013 Zbl 1283.57001 MR 3086663
- [20] S. Giombi, I. R. Klebanov, F. Popov, S. Prakash, and G. Tarnopolsky, Prismatic large N models for bosonic tensors. *Phys. Rev. D* **98** (2018), no. 10, article no. 105005 MR 3954724
- [21] S. Giombi, I. R. Klebanov, and G. Tarnopolsky, Bosonic tensor models at large N and small ε . *Phys. Rev. D* **96** (2017), no. 10, article no. 106014 MR 3867822
- [22] S. Giombi and X. Yin, Higher spin gauge theory and holography: the three-point functions. *J. High Energy Phys.* **2010** (2010), no. 9, article no. 115 Zbl 1291.83107 MR 2776932
- [23] J. L. Gross and T. W. Tucker, *Topological graph theory*. Wiley-Intersci. Ser. Discrete Math. Optim., John Wiley & Sons, Inc., New York, 1987 Zbl 0621.05013 MR 898434
- [24] S. S. Gubser, M. Heydeman, C. Jepsen, S. Parikh, I. Saberi, B. Stoica, and B. Trundy, Melonic theories over diverse number systems. *Phys. Rev. D* **98** (2018), no. 12, article no. 126007 MR 3974315
- [25] R. Gurau, The complete $1/N$ expansion of colored tensor models in arbitrary dimension. *Ann. Henri Poincaré* **13** (2012), no. 3, 399–423 Zbl 1245.81118 MR 2909101
- [26] R. Gurau, The $1/N$ expansion of tensor models beyond perturbation theory. *Comm. Math. Phys.* **330** (2014), no. 3, 973–1019 Zbl 1297.81126 MR 3227505
- [27] R. Gurau, Invitation to random tensors. *SIGMA Symmetry Integrability Geom. Methods Appl.* **12** (2016), article no. 094 Zbl 1346.83030 MR 3550395
- [28] R. Gurau, *Random tensors*. Oxford University Press, Oxford, 2017 Zbl 1371.81007 MR 3616422
- [29] R. Gurau and V. Rivasseau, Parametric representation of noncommutative field theory. *Comm. Math. Phys.* **272** (2007), no. 3, 811–835 Zbl 1156.81465 MR 2304476

- [30] R. Gurau and J. P. Ryan, Colored tensor models – a review. *SIGMA Symmetry Integrability Geom. Methods Appl.* **8** (2012), article no. 020 Zbl 1242.05094 MR 2942819
- [31] R. G. Gurau, Notes on tensor models and tensor field theories. *Ann. Inst. Henri Poincaré D* **9** (2022), no. 1, 159–218 Zbl 07509420 MR 4408001
- [32] R. G. Gurau and T. Krajewski, Analyticity results for the cumulants in a random matrix model. *Ann. Inst. Henri Poincaré D* **2** (2015), no. 2, 169–228 Zbl 1353.60009 MR 3354330
- [33] C. V. Johnson, The microstate physics of JT gravity and supergravity. 2022, arXiv:2201.11942
- [34] V. A. Kazakov, Ising model on a dynamical planar random lattice: Exact solution. *Phys. Lett. A* **119** (1986), no. 3, 140–144 MR 871244
- [35] I. R. Klebanov and A. M. Polyakov, AdS dual of the critical $O(N)$ vector model. *Phys. Lett. B* **550** (2002), no. 3–4, 213–219 Zbl 1001.81057 MR 1948547
- [36] I. R. Klebanov, F. Popov, and G. Tarnopolsky, TASI lectures on large N tensor models. *Proc. of Sci.* **305** (2018), article no. PoS(TASI2017)004
- [37] V. G. Knizhnik, A. M. Polyakov, and A. B. Zamolodchikov, Fractal structure of 2D-quantum gravity. *Modern Phys. Lett. A* **3** (1988), no. 8, 819–826 MR 947880
- [38] M. Kontsevich, Intersection theory on the moduli space of curves and the matrix Airy function. *Comm. Math. Phys.* **147** (1992), no. 1, 1–23 Zbl 0756.35081 MR 1171758
- [39] A. LeClair and M. Neubert, Semi-Lorentz invariance, unitarity, and critical exponents of symplectic fermion models. *J. High Energy Phys.* **2007** (2007), no. 10, article no. 027 MR 2357951
- [40] L. Lionni and V. Rivasseau, Intermediate field representation for positive matrix and tensor interactions. *Ann. Henri Poincaré* **20** (2019), no. 10, 3265–3311 Zbl 1425.81074 MR 4009682
- [41] R. L. Mkrтчian, The equivalence of $Sp(2N)$ and $SO(-2N)$ gauge theories. *Phys. Lett. B* **105** (1981), no. 2–3, 174–176
- [42] I. Moffatt and E. Mphako-Banda, Handle slides for delta-matroids. *European J. Combin.* **59** (2017), 23–33 Zbl 1348.05109 MR 3546900
- [43] M. Mulase and A. Waldron, Duality of orthogonal and symplectic matrix integrals and quaternionic Feynman graphs. *Comm. Math. Phys.* **240** (2003), no. 3, 553–586 Zbl 1033.81062 MR 2005857
- [44] R. C. Penner, Perturbative series and the moduli space of Riemann surfaces. *J. Differential Geom.* **27** (1988), no. 1, 35–53 Zbl 0608.30046 MR 918455
- [45] P. Saad, S. H. Shenker, and D. Stanford, JT gravity as a matrix integral. 2019, arXiv:1903.11115
- [46] N. Sasakura, Super tensor models, super fuzzy spaces and super n -ary transformations. *Internat. J. Modern Phys. A* **26** (2011), no. 24, 4203–4216 Zbl 1247.83058
- [47] D. Stanford and E. Witten, JT gravity and the ensembles of random matrix theory. *Adv. Theor. Math. Phys.* **24** (2020), no. 6, 1475–1680 Zbl 07433590 MR 4285616
- [48] G. 't Hooft, A planar diagram theory for strong interactions. *Nuclear Phys. B* **72** (1974), no. 3, 461–473

- [49] A. Tanasă, *Combinatorial physics: Combinatorics, quantum field theory, and quantum gravity models*. Oxford University Press, Oxford, 2021 Zbl 1480.81004 MR 4516827
- [50] M. A. Vasiliev, Consistent equations for interacting gauge fields of all spins in $3 + 1$ dimensions. *Phys. Lett. B* **243** (1990), no. 4, 378–382 Zbl 1332.81084 MR 1062824
- [51] E. Witten, Two-dimensional gravity and intersection theory on moduli space. In *Surveys in differential geometry (Cambridge, MA, 1990)*, pp. 243–310, Lehigh University, Bethlehem, PA, 1991 Zbl 0757.53049 MR 1144529
- [52] E. Witten, An SYK-like model without disorder. *J. Phys. A* **52** (2019), no. 47, article no. 474002 Zbl 1509.81564 MR 4028950
- [53] P. Zinn-Justin, The general $O(n)$ quartic matrix model and its application to counting tangles and links. *Comm. Math. Phys.* **238** (2003), no. 1–2, 287–304 Zbl 1033.57004 MR 1990878

Communicated by Adrian Tanasă

Received 13 July 2022; revised 13 January 2023.

Razvan Gurau

Institut für Theoretische Physik, Heidelberg University, Philosophenweg 19,
69120 Heidelberg, Germany; Centre de Physique Théorique (CPHT), Ecole Polytechnique,
Route de Saclay, 91128 Palaiseau, France; Perimeter Institute for Theoretical Physics,
31 Caroline St. N, Waterloo, ON N2L 2Y5, Canada; gurau@thphys.uni-heidelberg.de

Hannes Keppler

Institut für Theoretische Physik, Heidelberg University, Philosophenweg 19,
69120 Heidelberg, Germany; keppler@thphys.uni-heidelberg.de

Duality of orthogonal and symplectic random tensor models: general invariants

Authors: Hannes Keppler and Thomas Muller

Published in *Lett. Math. Phys.* **113** (2023) 4, article no. 83. DOI: 10.1007/s11005-023-01706-7.

Licensed under CC BY 4.0. Reproduced with permission. Hyperlink colors removed.

Also available as e-print: arXiv 2304.03625 [hep-th].

Both authors contributed equally to the project and the manuscript. H. Keppler produced all figures.



Duality of orthogonal and symplectic random tensor models: general invariants

Hannes Keppler¹ · Thomas Muller²

Received: 26 April 2023 / Revised: 26 April 2023 / Accepted: 27 June 2023 /
Published online: 12 July 2023
© The Author(s) 2023

Abstract

In Gurau and Keppler 2022 (arxiv:2207.01993), a relation between orthogonal and symplectic tensor models with quartic interactions was proven. In this paper, we provide an alternative proof that extends to polynomial interactions of arbitrary order. We consider tensor models of order D with no symmetry under permutation of the indices that transform in the tensor product of D fundamental representations of $O(N)$ and $Sp(N)$. We explicitly show that the models obey the N to $-N$ duality graph by graph in perturbation theory.

Keywords Tensor model · Symplectic group · Negative dimensions · Edge-colored graphs

Mathematics Subject Classification 81T32

Contents

1 Introduction	2
2 Setup of the models	4
3 Perturbative expansions in terms of colored graphs	9
4 Conclusion and outlook	13
References	14

✉ Hannes Keppler
keppler@thphys.uni-heidelberg.de

Thomas Muller
thomas.muller.1@u-bordeaux.fr

¹ Institut für Theoretische Physik, Heidelberg University, Philosophenweg 19, 69120 Heidelberg, Germany

² Université de Bordeaux, LaBRI CNRS UMR 5800, Talence, France

1 Introduction

Random tensor models [1–6], introduced as a generalization of random matrix models, are probability measures of the type:

$$d\mu[T] = e^{-S[T]} \prod_{(a_1, \dots, a_D)} \frac{dT^{a_1 \dots a_D}}{\sqrt{2\pi}}, \quad (1.1)$$

where the action $S[T]$ is build out of invariants under some symmetry transformation. These models are analog to zero-dimensional quantum field theory and their perturbative expansion can be reorganized as a series in $1/N$ [7–14]. As their Feynman graphs are dual to higher-dimensional triangulations, random tensors provide a framework for the study of random topological spaces; in one dimension tensor models provide an alternative to the Sachdev–Ye–Kitaev model without quenched disorder [15, 16]; in higher dimensions they lead to tensor field theories and a new class of large N *melonic* conformal field theories [17–21].

In this paper, we study tensor models with symplectic and/or orthogonal symmetry. Several incarnations of the relation between the orthogonal and symplectic group for negative dimensions have been studied in the literature: On the one hand, in the context of representation theory, one can make sense of the relation $SO(-N) \simeq Sp(N)$ [22–25]. On the other hand, for even N , $SO(N)$ and $Sp(N)$ gauge theories are known to be related by changing N to $-N$ [26]. A vector model with symplectic fermions in three space-time dimensions has been studied in [27] and an example of $SO(N)$ and $Sp(N)$ gauge theories with matter fields and Yukawa interactions can be found in [28]. This duality has furthermore been shown to hold between orthogonal and symplectic matrix ensembles (the $\beta = 1, 4$ ensembles) [29].

The orthogonal/symplectic duality has already been studied for tensor models by one of the authors in [30]. There, a graded colored tensor model (reviewed in Def. 1) was introduced. It was then shown that the partition function and connected two point correlation function of this model was invariant when replacing $N_c \leftrightarrow -N_c$ and at the same time changing the symmetry $O(N_c) \leftrightarrow Sp(N_c)$. However, the analysis in [30] made use of an intermediate field/Hubbard–Stratonovich transformation. This method allows to work with bosonic fields only, but is only applicable to the case of quartic interactions. Working directly in the usual colored graph representation of tensor models, we generalize results of [30] to interactions of arbitrary order and proceed in a more direct way.

Main result. We consider tensors of order D with no symmetry under permutation of their indices and call the position of an index its color c , with $c = 1, 2, \dots, D$. The tensors transform in the tensor product of D fundamental representations of $O(N)$ and/or $Sp(N)$, i.e., each tensor index is transformed by a different $O(N)$ or $Sp(N)$ matrix. The tensor components are real fermionic (anticommuting, odd) if the number of $Sp(N)$ factors is odd and real bosonic (commuting, even) if this number is even. It is convenient to assign a parity to the tensor indices: $|c| = 0$ or $|c| = 1$ if the index transforms under $O(N_c)$ or $Sp(N_c)$, respectively. In this paper, we generalize the results of [30] by allowing arbitrary polynomial interactions.

Definition 1 The real graded tensor model obeys the symmetry:

$$\mathbf{O}_1(N_1) \otimes \mathbf{O}_2(N_2) \otimes \cdots \otimes \mathbf{O}_D(N_D), \quad \mathbf{O}_c(N_c) = \begin{cases} O(N_c), & |c| = 0 \\ Sp(N_c), & |c| = 1 \end{cases}, \quad (1.2)$$

(therefore the name “graded”) is defined by the measure:

$$d\mu[T] \simeq e^{-S[T]} \prod_{a_1, \dots, a_D} dT^{a_1 \dots a_D},$$

$$S[T] = \frac{1}{2} \left(T^{a_1 \dots a_D} T^{b_1 \dots b_D} \prod_{c=1}^D g_{a_c b_c}^c \right) + \sum_{\substack{\mathcal{B} \text{ connected,} \\ |V(\mathcal{B})| > 2}} \frac{\lambda_{\mathcal{B}}}{|V(\mathcal{B})|} I_{\mathcal{B}}(T), \quad (1.3)$$

where $g_{a_c b_c}^c$ is the Kronecker $\delta_{a_c b_c}$ for $|c| = 0$ or the canonical symplectic form $\omega_{a_c b_c}$ for $|c| = 1$ and the sum runs over independent connected trace invariants $I_{\mathcal{B}}(T)$ of order higher than two, indexed by undirected colored graphs \mathcal{B} (see Sect. 2 for more details).

The partition function Z and the expectation value of an invariant $\langle I_{\mathcal{B}}(T) \rangle$ are defined by:

$$Z(\{\lambda\}) = \int d\mu[T], \quad \text{and} \quad \langle I_{\mathcal{B}}(T) \rangle(\{\lambda\}) = \frac{1}{Z} \int d\mu[T] I_{\mathcal{B}}(T), \quad (1.4)$$

and can be evaluated in a perturbative expansion. Our main theorem is the following:

Theorem 2 *The perturbative series of the partition function Z and expectation values of invariants $\langle I_{\mathcal{B}}(T) \rangle$ can be expressed as a formal sum over $(D+1)$ -colored undirected graphs \mathcal{G} . Each summand, corresponding to a specific graph \mathcal{G} , writes as a product:*

$$K(\{\lambda\}, \mathcal{G}) \cdot \prod_{c \in \mathcal{D}} ((-1)^{|c|} N_c)^{F_{c/0}(\mathcal{G})}, \quad (1.5)$$

of a term K , encoding the dependence on the coupling constants $\lambda_{\mathcal{B}}$ and some combinatorial numbers associated to \mathcal{G} , and a term depending on N_1, N_2, \dots, N_D (see Sect. 2 for the relevant definitions and Sect. 3 for the precise form of the series).

Proof The theorem follows from Proposition 8 and Cor. 9. \square

The essential remark is that all the factors N_c come in the form $(-1)^{|c|} N_c$; hence, each term is mapped into itself by exchanging $O(N_c) \leftrightarrow Sp(N_c)$ and $N_c \leftrightarrow -N_c$. Because graphically each N_c is associated to a face of colors $c/0$ (cycle of edges of alternating colors c and 0), this result can be seen as a generalization of the usual minus sign in quantum field theory for each fermionic loop. But one should keep in mind, that the full tensor is not necessary fermionic (its components are not necessarily anticommuting Grassmann numbers).

2 Setup of the models

In this section, we define the model. First, we specify the space of tensors we are interested in. Second, we give a description of the possible tensor invariants in terms of directed edge colored graphs, and third, we specify the model and its invariance properties.

The tensors A generic tensor $T^{a_1 \dots a_D}$ has no symmetry properties under permutation of its indices; hence, the indices have a well-defined position c , called their *color*. The set of colors is denoted $\mathcal{D} = \{1, \dots, D\}$. We assign a parity to each color and sometimes call the colors with $|c| = 0$ even and the ones with $|c| = 1$ odd. The tensor components shall be bosonic (even) if the number of colors with $|c| = 1$ (i.e. odd colors) is even and fermionic (odd) otherwise: the Grassmann number $T^{a_1 \dots a_D}$ has the same parity as $\sum_{c \in \mathcal{D}} |c|$.

Let $H_c = \mathbb{R}^{N_c|0}$ for $|c| = 0$, respectively $H_c = \mathbb{R}^{0|N_c}$ for $|c| = 1$ be a real supervector space of dimension N_c that is either purely even or purely odd. Each H_c is endowed with a non-degenerate *graded symmetric* inner product g^c :

$$g^c(u, v) = (-1)^{|c|} g^c(v, u), \quad \forall u, v \in H_c. \quad (2.1)$$

In a standard basis, g^c agrees with the standard symmetric or symplectic form, that is $g_{a_c b_c}^c = \delta_{a_c b_c}$ for $|c| = 0$, respectively $g_{a_c b_c}^c = \omega_{a_c b_c}$ for $|c| = 1$. As usual, we write $g^{c, a_c b_c}$ for the components of $(g^c)^{-1}$. The isometry group preserving g^c is either $O(N_c)$ in the $|c| = 0$ case or $Sp(N_c)$ in the $|c| = 1$ case, denoted collectively by $\mathcal{O}_c(N_c) := \{O_c \mid g_{a_c b_c}^c = O_{a_c}^{a'_c} O_{b_c}^{b'_c} g_{a'_c b'_c}^c = (O^c g^c O^T)_{a_c b_c}\}$.

The tensors are elements of

$$H_1 \otimes H_2 \otimes \dots \otimes H_D, \quad (2.2)$$

and transform in the tensor product representation of several orthogonal and symplectic groups according to the type of the individual H_c 's:

$$T^{a_1 \dots a_D} \rightarrow (O_1)^{a_1}_{b_1} \dots (O_D)^{a_D}_{b_D} T^{b_1 \dots b_D}, \quad O_1 \otimes \dots \otimes O_D \in \bigotimes_{c \in \mathcal{D}} \mathcal{O}_c(N_c). \quad (2.3)$$

Directed edge colored graphs and invariants Invariant polynomials in the tensor components are constructed by contracting the indices of color c with the inner product g^c . The unique quadratic invariant is:

$$g^{\otimes D}(T, T) = T^{a_{\mathcal{D}}} T^{b_{\mathcal{D}}} \prod_{c \in \mathcal{D}} g_{a_c b_c}^c. \quad (2.4)$$

General *trace invariants* are polynomials in the $T^{a_{\mathcal{D}}}$'s build by contracting pairs of indices of the same color. These invariants admit a graphical representation as *directed edge colored graphs*. The graphical representatives of tensor invariants are often called *bubbles* [2, 5].

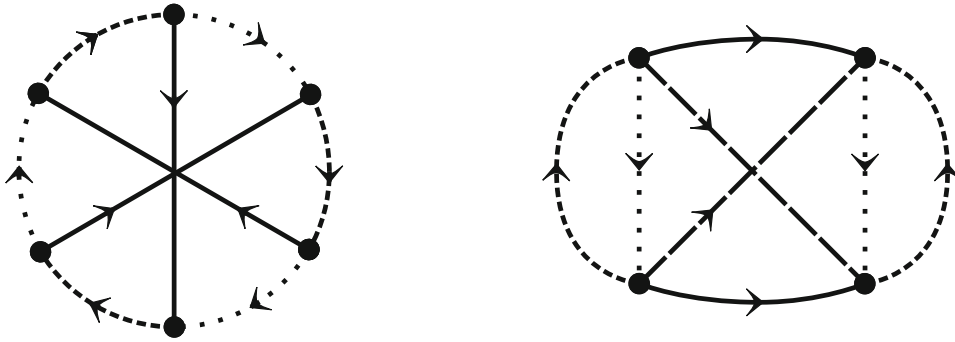


Fig. 1 Examples of colored directed graphs: a 3-colored sextic graph on the left (the wheel) and a 4-colored quartic one on the right. The different colors are represented by different line styles

Definition 3 (Directed edge colored graphs) A closed directed edge D -colored graph (directed colored graph for short) is a directed graph $\vec{\mathcal{B}} = (V(\vec{\mathcal{B}}), \vec{E}(\vec{\mathcal{B}}))$ with vertex set $V(\vec{\mathcal{B}})$ and edge set $\vec{E}(\vec{\mathcal{B}})$ such that:

- The edge set is partitioned into D disjoint subsets $\vec{E}(\vec{\mathcal{B}}) = \bigsqcup_{c=1}^D \vec{E}^c(\vec{\mathcal{B}})$, where we denote the subset of edges of color c by $\vec{E}^c(\vec{\mathcal{B}}) \ni e^c = (v, w)$, with $v, w \in V(\vec{\mathcal{B}})$.
- Each set $\vec{E}^c(\vec{\mathcal{B}})$ is a directed pairing of the vertices.

As a consequence all vertices are D -valent with all the edges incident to a vertex having distinct colors, and $V(\vec{\mathcal{B}})$ is of even cardinality. We denote by $F_{c/c'}(\vec{\mathcal{B}})$ the number of faces of colors $c \neq c'$, that is cycles made of alternating edges of these two distinct colors. Per default, we will consider directed graphs $\vec{\mathcal{B}}$ and view undirected graphs as equivalence classes $\mathcal{B} = [\vec{\mathcal{B}}]$ of their directed versions. All graphs have labeled vertices. Some examples are depicted in Figs. 1, 2.

Due to the signs introduced by the reversing the edges of odd colors (remember that this corresponds to transposing the antisymmetric matrix ω), several invariants differ only by a minus sign. This ambiguity can be fixed by using a sign fixing prescription generalizing the one given in [30].

The invariant of order $2k$ defined by the directed colored graph $\vec{\mathcal{B}}$ with vertices $V(\vec{\mathcal{B}}) = \{1, 2, \dots, 2k\}$, will be denoted by $I_{\vec{\mathcal{B}}}(T)$, and is given by the following expression:

$$\begin{aligned} I_{\vec{\mathcal{B}}}(T) &= \sum_{a_{\mathcal{D}}^1, a_{\mathcal{D}}^2, \dots, a_{\mathcal{D}}^{2k}} \left(\prod_{(i,j) \in \vec{P}_{ref,2k}} T^{a_{\mathcal{D}}^i} T^{a_{\mathcal{D}}^j} \right) \prod_{c \in \mathcal{D}} \left(\epsilon(\vec{P}_{ref,2k}, \vec{E}^c(\vec{\mathcal{B}}))^{|c|} \prod_{(i,j) \in \vec{E}^c(\vec{\mathcal{B}})} g_{a_c^i a_c^j}^c \right) \\ &= \sum_{a_{\mathcal{D}}^1, a_{\mathcal{D}}^2, \dots, a_{\mathcal{D}}^{2k}} \left(\prod_{(i,j) \in \vec{P}_{ref,2k}} T^{a_{\mathcal{D}}^i} T^{a_{\mathcal{D}}^j} \right) \left(\prod_{c \in \mathcal{D}} \epsilon(\vec{P}_{ref,2k}, \vec{E}^c(\vec{\mathcal{B}}))^{|c|} K_{\vec{\mathcal{B}}, a_c^1, \dots, a_c^{2k}}^c \right), \end{aligned} \quad (2.5)$$

here $\vec{P}_{ref,2k}$ is an arbitrary but fixed reference pairing on the set of vertices, chosen to be $\vec{P}_{ref,2k} = \{(1, 2), \dots, (2k-1, 2k)\}$, and the sign of the pairings $\epsilon(\vec{P}_{ref,2k}, \vec{E}^c(\vec{\mathcal{B}}))^{|c|}$ was introduced to fix the sign ambiguity. As an example, consider the pillow interaction

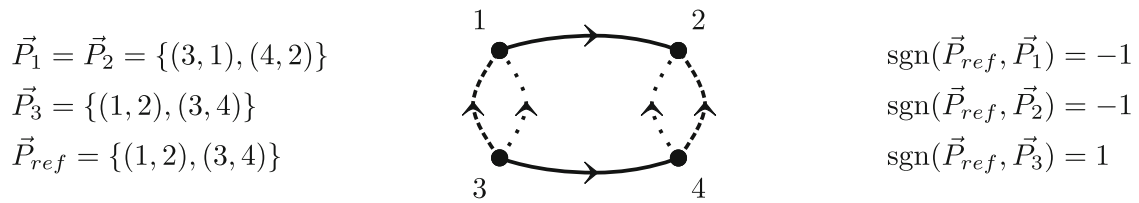


Fig. 2 A colored directed graph (the pillow $\vec{\mathcal{P}}$) defined by three pairings. The edges of colors one, two and three are represented by dashed, dotted and solid lines, respectively. The associated invariant is given in (2.6)

(Fig. 2) defined by the graph $\vec{\mathcal{P}}$. The corresponding tensor invariant is:

$$I_{\vec{\mathcal{P}}} = (-1)^{|1|+|2|} \sum_{a,b,c,d} \left(T^{a_1 a_2 a_3} T^{b_1 b_2 b_3} \right) \left(T^{c_1 c_2 c_3} T^{d_1 d_2 d_3} \right) g_{c_1 a_1}^1 g_{d_1 b_1}^1 g_{c_2 a_2}^2 g_{d_2 b_2}^2 g_{a_3 b_3}^3 g_{c_3 d_3}^2. \quad (2.6)$$

Before reviewing the definition and properties of ϵ , which will play a central role, let us comment about how the sign ambiguity shall be understood:

- Because the tensors may anticommute, for writing down the expression for the invariant, it is necessary to fix an order. This is done by the reference pairing $\vec{P}_{ref, 2k}$.
- If two directed colored graphs $\vec{\mathcal{A}}$ and $\vec{\mathcal{B}}$ differ only by redirecting some of their edges, the corresponding trace invariants are the same, up to transposing some $(g^c)^T = (-1)^{|c|} g^c$ which could lead to a sign difference between $I_{\vec{\mathcal{A}}}(T)$ and $I_{\vec{\mathcal{B}}}(T)$. In order to restrict to independent invariants, we consider such directed graphs to be in the same *equivalence class* $[\vec{\mathcal{A}}] = [\vec{\mathcal{B}}]$, i.e., they describe the same *undirected* colored graph.
- The sign prescription ensures that $I_{\vec{\mathcal{B}}}(T)$ is a *class function*:

$$I_{\vec{\mathcal{A}}}(T) = I_{\vec{\mathcal{B}}}(T) \quad \text{if } \mathcal{A} = \mathcal{B}, \quad (2.7)$$

and thus any representative of $[\vec{\mathcal{B}}]$ can be used to write down the invariant.

Because of the last point, from now on, we will label the invariants by undirected graphs \mathcal{B} , and it is understood that for (2.5) an arbitrary directed representative $\vec{\mathcal{B}} \in [\vec{\mathcal{B}}] \equiv \mathcal{B}$ has been chosen.

A trace invariant is called *connected*, if the corresponding colored graph is so. Note that any product of two invariants can be written as a single disconnected invariant such that:

$$I_{\mathcal{A}}(T) I_{\mathcal{B}}(T) = I_{\mathcal{A} \sqcup \mathcal{B}}(T), \quad (2.8)$$

and a new reference pairing is given by the disjoint union of the original reference pairings (2.12).

Sign of oriented pairings

Consider two oriented pairings \vec{P}_1 and \vec{P}_2 on the same set of $2k$ elements:

$$\begin{aligned}\vec{P}_1 &= \{(i_1, i_2), \dots, (i_{2k-1}, i_{2k})\}, \\ \vec{P}_2 &= \{(j_1, j_2), \dots, (j_{2k-1}, j_{2k})\}.\end{aligned}\quad (2.9)$$

The sign $\epsilon(\vec{P}_1, \vec{P}_2)$ of the two pairings with respect to each another is defined as the sign of the permutation that takes $i_1 \dots i_{2k}$ into $j_1 \dots j_{2k}$. The properties of this sign are:

1. The sign is symmetric under permutation of its arguments:

$$\epsilon(\vec{P}_1, \vec{P}_2) = \epsilon(\vec{P}_2, \vec{P}_1). \quad (2.10)$$

2. For three pairings $\vec{P}_1, \vec{P}_2, \vec{P}_3$ on the same set, one has:

$$\epsilon(\vec{P}_1, \vec{P}_2) = \epsilon(\vec{P}_1, \vec{P}_3)\epsilon(\vec{P}_2, \vec{P}_3). \quad (2.11)$$

3. For two pairings \vec{P}_1, \vec{P}_2 on a first set S_1 of $2k$ elements and two pairings \vec{P}_3, \vec{P}_4 on a second set S_2 of $2p$ elements, the product $\epsilon(\vec{P}_1, \vec{P}_2)\epsilon(\vec{P}_3, \vec{P}_4)$ can be written as the sign of the disjoint union of pairings $\vec{P}_1 \sqcup \vec{P}_3$ and $\vec{P}_2 \sqcup \vec{P}_4$ (on the set $S_1 \sqcup S_2$):

$$\epsilon(\vec{P}_1, \vec{P}_2)\epsilon(\vec{P}_3, \vec{P}_4) = \epsilon(\vec{P}_1 \sqcup \vec{P}_3, \vec{P}_2 \sqcup \vec{P}_4). \quad (2.12)$$

The sign of two pairings has a nice graphical interpretation that will be of great use.

Lemma 4 *Depicting the $2k$ elements of a set S as vertices, the two pairings \vec{P}_c and $\vec{P}_{c'}$ on this set can be represented by colored (one color— c or c' —for each pairing), oriented edges connecting the vertices. Define a face of colors c/c' as an alternating cycle of edges of color c and c' . A face is called even (resp. odd), if an even (odd) number of its edges point in the same directions around its cycles.¹ Denoting $F_{c/c', \text{even}}$ resp. $F_{c/c', \text{odd}}$ the number of even and odd faces of colors c/c' , the sign $\epsilon(\vec{P}_c, \vec{P}_{c'})$ can be expressed as:*

$$\epsilon(\vec{P}_c, \vec{P}_{c'}) = (-1)^{F_{c/c', \text{even}}}. \quad (2.13)$$

See Fig. 3 for an illustration.

Proof Denoting $\vec{P}_c = \{(i_1, i_2), \dots, (i_{2k-1}, i_{2k})\}$ and $\vec{P}_{c'} = \{(j_1, j_2), \dots, (j_{2k-1}, j_{2k})\}$, by definition, $\epsilon(\vec{P}_c, \vec{P}_{c'})$ is the sign of the permutation $\sigma = \begin{pmatrix} i_1 & i_2 & \dots & i_{2k-1} & i_{2k} \\ j_1 & j_2 & \dots & j_{2k-1} & j_{2k} \end{pmatrix}$. One can define a second permutation ρ , whose cycles coincide with the faces of $\vec{P}_c \sqcup \vec{P}_{c'}$ (neglecting for a moment the orientation of the edges). The permutation ρ is defined by:

- $\rho(i)$ is the successor of the vertex i that is reached by going clockwise around the face of colors c/c' to which i belongs.

¹ Note that a face of colors c/c' always has an even number of edges, and hence this notion is well defined.

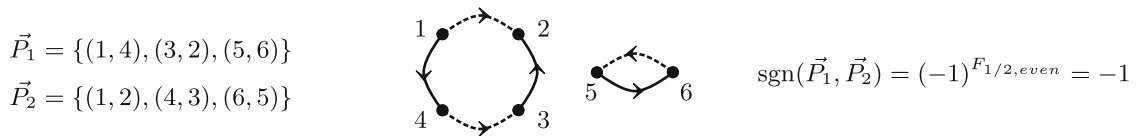


Fig. 3 Illustration of Lemma 4. \vec{P}_1 is represented with solid and \vec{P}_2 with dashed edges. The face on the left is odd and the face on the right is even

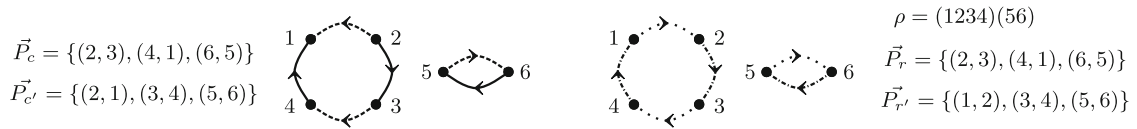


Fig. 4 Illustration of the Proof of Lemma 4. The faces of colors r/r' coincide with the cycles of ρ , and with the faces of colors c/c' , up to the orientation of their edges. \vec{P}_c solid line, $\vec{P}_{c'}$ dashed, \vec{P}_r dash-dotted, $\vec{P}_{r'}$ dotted

- Writing $\rho = \begin{pmatrix} l_1 & l_2 & \dots & l_{2k-1} & l_{2k} \\ m_1 & m_2 & \dots & m_{2k-1} & m_{2k} \end{pmatrix}$, one can think of ρ as consisting of two directed pairings $\vec{P}_r = \{(l_1, l_2), \dots, (l_{2k-1}, l_{2k})\}$ and $\vec{P}_{r'} = \{(m_1, m_2), \dots, (m_{2k-1}, m_{2k})\}$ that differ from \vec{P}_c and $\vec{P}_{c'}$ only by the direction of their edges.

Since all the faces are of even length, the sign of the permutation ρ is given by $\text{sgn}(\rho) = (-1)^{F_{c/c'}}$. The crucial point is that ρ is chosen such that it differs from σ by an odd number of transpositions for each odd face, i.e., $\text{sgn}(\sigma) = (-1)^{F_{c/c', \text{odd}}} \text{sgn}(\rho) = (-1)^{F_{c/c', \text{even}}}$. See Fig. 4 for an illustration. \square

For a review on the connection of directed pairings and their sign with pfaffians and fermionic Gaußian integrals, we refer the interested reader to the Appendix of [31].

Graded colored tensor model As discussed above, the set of independent trace invariants is indexed by equivalence classes of directed colored graphs $\mathcal{B} = [\vec{\mathcal{B}}]$. Being class functions, any representative $\vec{\mathcal{B}} \in \mathcal{B}$ can be used to define $I_{\vec{\mathcal{B}}}(T)$.

Definition 5 (Real Graded Tensor Model) The *real graded tensor model* is the measure²:

$$\begin{aligned}
 d\mu[T] &= e^{-S[T]} [dT], \quad [dT] = \prod_{a \in \mathcal{D}} dT^{a_1 \dots a_D} \cdot \begin{cases} \frac{1}{(2\pi)^{\prod_c N_c/2}}, & \sum_{c=1}^D |c| = 0 \pmod{2} \\ 1, & \sum_{c=1}^D |c| = 1 \pmod{2} \end{cases}, \\
 \text{with } S[T] &= \frac{1}{2} g^{\otimes D}(T, T) + \sum_{\substack{\mathcal{B} \text{ connected,} \\ |V(\mathcal{B})| > 2}} \frac{\lambda_{\mathcal{B}}}{|V(\mathcal{B})|} I_{\vec{\mathcal{B}}}(T),
 \end{aligned} \tag{2.14}$$

where the normalization is such that $\int d\mu[T] = 1$ for $\lambda_{\mathcal{B}} = 0 \forall \mathcal{B}$.

² We treat the measures $d\mu[T]$ as a perturbed Gaußian measures. As such we do not concern ourselves with the convergence of the various tensor and matrix integrals. As we treat the Gaußian integrals as generating functions of graphs, we will not address such issues.

3 Perturbative expansions in terms of colored graphs

In this section, we compute the expectation value of invariants and show that these obey the $N \rightarrow -N$ duality graph by graph in the perturbative expansion. On a technical level, most statements are generalizations of the known results for colored random tensor models, as summarized, e.g., in [2, 5]. Let us recall the commutation relation of the tensor component:

$$T_{a_{\mathcal{D}}} T_{b_{\mathcal{D}}} = (-1)^{\sum_{c \in \mathcal{D}} |c|} T_{a_{\mathcal{D}}} T_{b_{\mathcal{D}}} , \quad (3.1)$$

and introduce the following short hand notations:

$$\begin{aligned} \delta_{b_{\mathcal{D}}}^{a_{\mathcal{D}}} &= \prod_{i=1}^D \delta_{b_i}^{a_i} , \quad g_{a_{\mathcal{D}} b_{\mathcal{D}}} = \prod_{c \in \mathcal{D}} g_{a_c b_c} , \quad g^{a_{\mathcal{D}} b_{\mathcal{D}}} = \prod_{c \in \mathcal{D}} g^{c, a_c b_c} , \\ \text{and } (\partial_T, \partial_T) &= \sum_{a_{\mathcal{D}}, b_{\mathcal{D}}} \frac{\partial}{\partial T^{a_{\mathcal{D}}}} g^{a_{\mathcal{D}} b_{\mathcal{D}}} \frac{\partial}{\partial T^{b_{\mathcal{D}}}} . \end{aligned} \quad (3.2)$$

We first compute the expectation values with respect to the Gaussian measure that is obtained by setting all coupling constants $\lambda_{\mathcal{B}}$ to zero. This is Wick's theorem for the Gaussian expectation value $\langle \dots \rangle_0$ of $2k$ anticommuting variables.

Lemma 6 *The Gaussian expectation value of an even number of tensors:*

$$\langle T^{a_{\mathcal{D}}^1} \dots T^{a_{\mathcal{D}}^{2k}} \rangle_0 = \int [dT] e^{-\frac{1}{2} g^{\otimes D}(T, T)} T^{a_{\mathcal{D}}^1} \dots T^{a_{\mathcal{D}}^{2k}} , \quad (3.3)$$

can be computed as a sum over the set \mathcal{P}_{2k} of (undirected) pairings of $2k$ elements:

$$\langle T^{a_{\mathcal{D}}^1} \dots T^{a_{\mathcal{D}}^{2k}} \rangle_0 = \sum_{P \in \mathcal{P}_{2k}} \epsilon(\vec{P}_{ref, 2k}, \vec{P})^{\sum_{c \in \mathcal{D}} |c|} \left(\prod_{(i, j) \in \vec{P}} g^{a_{\mathcal{D}}^i a_{\mathcal{D}}^j} \right) , \quad (3.4)$$

where \vec{P} is an (arbitrarily chosen) directed version of P . Each summand is independent of that choice, because the sign $\epsilon(\vec{P}_{ref, 2k}, \vec{P})$ is odd under reordering of pairs, while $g^{a_{\mathcal{D}}^i a_{\mathcal{D}}^j}$ is antisymmetric in the relevant cases. The odd moments vanish and the sign is trivial for commuting (bosonic) tensor components.

Proof This classical statement is proved using the derivative representation of normalized Gaussian measures:

$$\begin{aligned}
 \langle T^{a_1^1} \dots T^{a_{2k}^{2k}} \rangle_0 &= \left[e^{\frac{1}{2}(\partial_T, \partial_T)} T^{a_1^1} \dots T^{a_{2k}^{2k}} \right]_{T^{a_i^i}=0, \forall i} \\
 &= \left[\sum_{n \geq 0} \frac{1}{n! 2^n} ((\partial_T, \partial_T))^n T^{a_1^1} \dots T^{a_{2k}^{2k}} \right]_{T=0} \\
 &= \left[\sum_{n \geq 0} \frac{1}{n! 2^n} ((\partial_T, \partial_T))^{n-1} \sum_{b_{\mathcal{D}}, c_{\mathcal{D}}} \frac{\partial}{\partial T^{b_{\mathcal{D}}}} g^{b_{\mathcal{D}} c_{\mathcal{D}}} \right. \\
 &\quad \times \sum_{r=1}^{2k} (-1)^r \sum_{c \in \mathcal{D}} |c| \delta_{c_{\mathcal{D}}}^{a_r^r} T^{a_1^1} \dots \widehat{T^{a_r^r}} \dots T^{a_{2k}^{2k}} \left. \right]_{T=0}.
 \end{aligned} \tag{3.5}$$

Iterating this procedure, the derivatives will create (directed) pairings \vec{P} of the $2k$ tensors, and pick up minus signs if they have to anticommute with an odd number of tensors. The total sign, generated in this way, is just the sign of \vec{P} relative to the reference pairing $\vec{P}_{ref, 2k} = \{(1, 2), (2, 3), \dots, (2k-1, 2k)\}$.

$$\sum_{\vec{P} \in \vec{\mathcal{P}}_{2k}} \frac{1}{2^k} \epsilon(\vec{P}_{ref, 2k}, \vec{P})^{\sum_{c \in \mathcal{D}} |c|} \left(\prod_{(i, j) \in \vec{P}} g^{a_i^i a_j^j} \right), \tag{3.6}$$

where $\vec{\mathcal{P}}_{2k}$ is the set of directed pairings of $2k$ elements. Because the sign $\epsilon(\vec{P}_{ref, 2k}, \vec{P})$ is odd under reordering of pairs, while $g^{a_i^i a_j^j} = (-1)^{\sum_{c \in \mathcal{D}} |c|} g^{a_j^j a_i^i}$, each summand does not depend on the order of the pairs in \vec{P} . If P is an (undirected) pairing of $2k$ elements, there are 2^k directed pairings \vec{P} associated to it. Taking this multiplicity into account, the statement follows. \square

Proposition 7 *The Gaussian expectation of an invariant of order $2k$, specified by a D -colored directed graph $\vec{\mathcal{B}}$:*

$$\langle I_{\vec{\mathcal{B}}}(T) \rangle_0 = \int [dT] e^{-\frac{1}{2} g^{\otimes D}(T, T)} I_{\vec{\mathcal{B}}}(T), \tag{3.7}$$

can be computed as a sum over $(D+1)$ -colored undirected graphs $\mathcal{G} = [\vec{\mathcal{G}}]$ (Feynman graphs) having edges of an additional color 0, such that $\mathcal{B} \subset \mathcal{G}$ is the maximal D -colored subgraph of colors $c \in \mathcal{D}$:

$$\langle I_{\vec{\mathcal{B}}}(T) \rangle_0 = \sum_{\substack{\mathcal{G}, \mathcal{B} \subset \mathcal{G} \\ |V(\mathcal{G})|=2k}} \prod_{c \in \mathcal{D}} ((-1)^{|c|} N_c)^{F_{c/0}(\mathcal{G})}. \tag{3.8}$$

The power of N_c is given by the number of faces of \mathcal{G} , of alternating colors c and 0.

Since the invariants are class functions, the result does only depend on undirected graphs.

Proof Using Lemma 6, one has:

$$\begin{aligned} \langle I_{\vec{\mathcal{B}}}(T) \rangle_0 &= \sum_{\{a_{\mathcal{D}}\}} \left\langle \prod_{(i,j) \in \vec{P}_{ref,2k}} T^{a_{\mathcal{D}}^i} T^{a_{\mathcal{D}}^j} \right\rangle_0 \prod_{c \in \mathcal{D}} \left(\epsilon(\vec{P}_{ref,2k}, \vec{E}^c(\vec{\mathcal{B}}))^{|c|} \prod_{(i,j) \in \vec{E}^c(\vec{\mathcal{B}})} g_{a_i a_j}^c \right) \\ &= \sum_{\{a_{\mathcal{D}}\}} \sum_{P \in \mathcal{P}_{2k}} \epsilon(\vec{P}_{ref,2k}, \vec{P})^{\sum_{c \in \mathcal{D}} |c|} \left(\prod_{(i,j) \in \vec{P}} g_{a_i a_j}^{a_{\mathcal{D}}^i a_{\mathcal{D}}^j} \right) \prod_{c \in \mathcal{D}} \\ &\quad \times \left(\epsilon(\vec{P}_{ref,2k}, \vec{E}^c(\vec{\mathcal{B}}))^{|c|} \prod_{(i,j) \in \vec{E}^c(\vec{\mathcal{B}})} g_{a_i a_j}^c \right). \end{aligned} \quad (3.9)$$

Now, using Property (2.11) of the sign of two pairings to eliminate the dependence on reference $\vec{P}_{ref,2k}$ and reorganizing the products according to color leads to:

$$\sum_{\{a_{\mathcal{D}}\}} \sum_{P \in \mathcal{P}_{2k}} \prod_{c \in \mathcal{D}} \left(\epsilon(\vec{P}, \vec{E}^c(\vec{\mathcal{B}}))^{|c|} \left(\prod_{(i,j) \in \vec{P}} g_{a_i a_j}^{c, a_i^c a_j^c} \right) \left(\prod_{(i,j) \in \vec{E}^c(\vec{\mathcal{B}})} g_{a_i a_j}^c \right) \right). \quad (3.10)$$

By adding edges of a new color 0 to $\vec{\mathcal{B}}$, according to the pairing \vec{P} , a $(D+1)$ directed colored graph $\vec{\mathcal{G}}$ is obtained. Along the faces of colors $c/0$, g^c and $(g^c)^{-1}$ alternate and since all indices are summed, each such face contributes a factor N_c . Note, however, that since $g_{a_c b_c}^c g_{b_c d_c}^{d_c} = (-1)^{|c|} \delta_{a_c}^{d_c}$, a face picks up an additional sign if an odd number of edges are pointing in the same direction around the face (such a face was called odd). With this and the expression of $\epsilon(\vec{P}, \vec{E}^c(\vec{\mathcal{B}}))$ in terms of the number of even faces of colors $c/0$ (Lemma 4) we obtain:

$$\sum_{\{a_{\mathcal{D}}\}} \sum_{\substack{\mathcal{G}, \mathcal{B} \subset \mathcal{G} \\ |V(\mathcal{G})|=2k}} \prod_{c \in \mathcal{D}} \left(((-1)^{F_{c/0, \text{even}}(\vec{\mathcal{G}})})^{|c|} ((-1)^{F_{c/0, \text{odd}}(\vec{\mathcal{G}})})^{|c|} (N_c)^{F_{c/0}(\vec{\mathcal{G}})} \right), \quad (3.11)$$

and since the sum of the number of even and odd face of colors $c/0$ is equal to the total number of such faces in $\vec{\mathcal{G}}$ (equivalent to the ones in \mathcal{G}), this concludes the proof. Note, however, that the result does not depend on the particular choices of directed graph. This is true at each intermediate step because the symmetry properties of $\epsilon(\cdot, \cdot)^{|c|}$ always agree with the graded symmetry of g^c . \square

At this point, we have all the ingredients for the perturbative evaluation of the partition function.

Proposition 8 *The partition function $Z(\{\lambda\})$ of the graded colored tensor model (Def. 5) can be evaluated by a formal power series in the coupling constants that is indexed by $(D+1)$ -colored undirected graphs \mathcal{G} . Let us denote the D -colored maximally*

connected subgraphs of colors $c \in \mathcal{D}$, called bubbles, by $\mathcal{B} \subset \mathcal{G}$. The sum runs only over graphs \mathcal{G} without bubbles having exactly two vertices:

$$Z(\{\lambda_{\mathcal{B}}\}) = \sum_{\substack{\mathcal{G} \\ |V(\mathcal{B})| \neq 2 \ \forall \mathcal{B} \subset \mathcal{G}}} \frac{1}{n_b(\mathcal{G})!} \left(\prod_{\mathcal{B} \subset \mathcal{G}} \frac{\lambda_{\mathcal{B}}}{|V(\mathcal{B})|} \right) \left(\prod_{c \in \mathcal{D}} ((-1)^{|c|} N_c)^{F_{c/0}(\mathcal{G})} \right), \quad (3.12)$$

and $n_b(\mathcal{G})$ denotes the total number of bubbles in \mathcal{G} .

Proof We expand the interaction part to find:

$$Z = \int [dT] e^{-\frac{1}{2} g^{\otimes}(T, T)} \sum_{\{p_{\mathcal{B}} \geq 0\}} \prod_{\mathcal{B}} \frac{1}{p_{\mathcal{B}}!} \left(\frac{\lambda_{\mathcal{B}}}{|V(\mathcal{B})|} I_{\mathcal{B}}(T) \right)^{p_{\mathcal{B}}}, \quad (3.13)$$

where we associate to each undirected D -colored graph \mathcal{B} a multiplicity $p_{\mathcal{B}} \geq 0$, and sum over these. Commuting the sum and the Gaußian integral, we obtain the perturbative series:

$$\sum_{\{p_{\mathcal{B}} \geq 0\}} \left(\prod_{\mathcal{B}} \frac{1}{p_{\mathcal{B}}!} \left(\frac{\lambda_{\mathcal{B}}}{|V(\mathcal{B})|} \right)^{p_{\mathcal{B}}} \right) \langle \prod_{\mathcal{B}} (I_{\mathcal{B}}(T))^{p_{\mathcal{B}}} \rangle_0. \quad (3.14)$$

As any product of invariants can be seen as a single disconnected invariant (2.8), Proposition 7 can be directly applied, and one obtains a sum over $(D+1)$ -colored undirected graphs \mathcal{G} with the only condition, that they do not have bubbles $\mathcal{B} \subset \mathcal{G}$ with exactly two vertices. Whenever the graph \mathcal{G} contains a bubble \mathcal{B} this contributes a factor $\lambda_{\mathcal{B}}$:

$$\sum_{\substack{\mathcal{G} \\ |V(\mathcal{B})| \neq 2 \ \forall \mathcal{B} \subset \mathcal{G}}} \frac{1}{n_b(\mathcal{G})!} \left(\prod_{\mathcal{B} \subset \mathcal{G}} \frac{\lambda_{\mathcal{B}}}{|V(\mathcal{B})|} \right) \left(\prod_{c \in \mathcal{D}} ((-1)^{|c|} N_c)^{F_{c/0}(\mathcal{G})} \right), \quad (3.15)$$

here $n_b(\mathcal{G})$ is the total number of bubbles in \mathcal{G} . \square

Corollary 9 *The expectation value of trace invariants is computed as derivatives of the logarithm of the partition function:*

$$\begin{aligned} \text{for } |V(\mathcal{B})| = 2 : \quad \langle g^{\otimes D}(T, T) \rangle &= \left(\prod_{c \in \mathcal{D}} (-1)^{|c|} N_c \right) \\ &+ \left(\sum_{\substack{\mathcal{B} \text{ connected,} \\ |V(\mathcal{B})| > 2}} \lambda_{\mathcal{B}} |V(\mathcal{B})| \frac{\partial}{\partial \lambda_{\mathcal{B}}} \right) \ln Z(\{\lambda\}), \quad (3.16) \\ \text{for } |V(\mathcal{B})| > 2 : \quad \langle I_{\mathcal{B}}(T) \rangle &= -|V(\mathcal{B})| \frac{\partial}{\partial \lambda_{\mathcal{B}}} \ln Z(\{\lambda\}). \end{aligned}$$

The expectation value can be computed explicitly as a formal sum, analogous to $Z(\{\lambda\})$. The derivative acts on one $\lambda_{\mathcal{B}}$ in the product and marks the corresponding bubble $[\mathcal{B}] \subset [\mathcal{G}]$:

$$\begin{aligned} & \text{for } |V(\mathcal{B})| > 2 : \quad \langle I_{\vec{\mathcal{B}}}(T) \rangle \\ &= \sum_{\substack{\mathcal{G} \text{ connected,} \\ \vec{\mathcal{B}} \subset \mathcal{G} \text{ marked,} \\ |V(\mathcal{B}')| \neq 2 \ \forall \mathcal{B}' \subset \mathcal{G}}} \frac{1}{n_b(\mathcal{G})!} \left(\prod_{\substack{\mathcal{B}' \subset \mathcal{G} \\ \mathcal{B}' \neq \mathcal{B}}} \frac{\lambda_{\mathcal{B}'}}{|V(\mathcal{B}')|} \right) \left(\prod_{c \in \mathcal{D}} ((-1)^{|c|} N_c)^{F_{c/0}(\mathcal{G})} \right). \quad (3.17) \end{aligned}$$

Proof The statements for $|V(\mathcal{B})| > 2$ follow from Definition 5, (1.4), Proposition 8 and the usual fact, that the logarithm restricts to a sum over connected graphs. For $|V(\mathcal{B})| = 2$ consider the following Schwinger–Dyson equation:

$$\begin{aligned} 0 &= \frac{(-1)^{\sum_c |c|}}{Z} \int [dT] \sum_{a_{\mathcal{D}}} \frac{\partial}{\partial T^{a_{\mathcal{D}}}} \left(T^{a_{\mathcal{D}}} e^{-S[T]} \right) \\ &= \left(\prod_{c \in \mathcal{D}} (-1)^{|c|} N_c \right) - \langle g^{\otimes D}(T, T) \rangle - \sum_{\substack{\mathcal{B} \text{ conn.} \\ |V(\mathcal{B})| > 2}} \lambda_{\mathcal{B}} \langle I_{\vec{\mathcal{B}}}(T) \rangle, \quad (3.18) \end{aligned}$$

and use the result for $\langle I_{\vec{\mathcal{B}}}(T) \rangle$. The first term in the second line can be interpreted as a ring-graph without any vertex but D colored edges. \square

4 Conclusion and outlook

In this paper, we showed the N to $-N$ duality between colored tensor models with orthogonal and symplectic symmetry. We showed that the amplitude of any graph \mathcal{G} comes with a factor $\prod_{c \in \mathcal{C}} ((-1)^{|c|} N_c)^{F_{c/0}(\mathcal{G})}$, where $|c|$ is a grading assigned to the color c controlling its symmetry properties ($|c| = 0$ for $O(N_c)$ and $|c| = 1$ for $Sp(N_c)$), and $F_{c/0}(\mathcal{G})$ is the number of faces of color c in \mathcal{G} . As a consequence, the amplitude of any graph is invariant under simultaneously changing $O(N_c) \leftrightarrow Sp(N_c)$ and $N_c \leftrightarrow -N_c$ for any color c . Our analysis relies heavily on the properties of the sign of oriented pairings. This sign ensures that the invariants are specified by undirected graphs and do not depend on the arbitrarily chosen orientation of edges. Then, by carefully keeping track of the signs coming from the bosonic or fermionic nature, as well as reorientations of edges in directed graphs, we obtain the desired expressions for the graph amplitudes.

A natural follow-up of this project is to consider tensors with symmetry properties under permutation of their indices. The work of [22–25] suggests that similar models could be constructed for arbitrary (also mixed) tensor representations of the orthogonal and symmetric group. For example, we suspect a relation between a tensor model with tensors of order D transforming in the totally symmetric representation of $O(N)$

(similar to [11, 12, 32]) and a model build on the totally antisymmetric representation of $Sp(N)$. For odd D , the symplectic model should again be fermionic. Moreover, one should also explore the implications of the $N \rightarrow -N$ duality for tensor field theories. The sign change may generate new renormalization group fixed points. Finally, more general models with $OSp(m, n)$ symmetry could be considered. In this case, one would interchange n and m .

Acknowledgements We thank Razvan Gurau, Thomas Krajewski and Adrian Tanasa for comments and discussions. The authors gratefully acknowledge support of the Institut Henri Poincaré (UAR 839 CNRS-Sorbonne Université), and LabEx CARMIN (ANR-10-LABX-59-01), where some of this work has been carried out. H. K. has been supported by the Deutsche Forschungsgemeinschaft (DFG, German Research Foundation) under Germany's Excellence Strategy EXC-2181/1 -390900948 (the Heidelberg STRUCTURES Cluster of Excellence). T. M. has been partially supported by the ANR-20-CE48-0018 "3DMaps" grant.

Funding Open Access funding enabled and organized by Projekt DEAL.

Data availability No datasets were generated or analyzed during the current study.

Declarations

Conflict of interest On behalf of all authors, the corresponding author states that there is no conflict of interest.

Open Access This article is licensed under a Creative Commons Attribution 4.0 International License, which permits use, sharing, adaptation, distribution and reproduction in any medium or format, as long as you give appropriate credit to the original author(s) and the source, provide a link to the Creative Commons licence, and indicate if changes were made. The images or other third party material in this article are included in the article's Creative Commons licence, unless indicated otherwise in a credit line to the material. If material is not included in the article's Creative Commons licence and your intended use is not permitted by statutory regulation or exceeds the permitted use, you will need to obtain permission directly from the copyright holder. To view a copy of this licence, visit <http://creativecommons.org/licenses/by/4.0/>.

References

1. Ambjørn, J., Durhuus, B., Jonsson, T.: Three-dimensional simplicial quantum gravity and generalized matrix models. *Mod. Phys. Lett. A* **6**, 1133 (1991). <https://doi.org/10.1142/S0217732391001184>
2. Gurau, R.: *Random Tensors*, 1st edn. Oxford University Press, Oxford (2017)
3. Gurau, R.: Invitation to random tensors. *SIGMA* **12**, 94 (2016). <https://doi.org/10.3842/SIGMA.2016.094>. [arxiv:1609.06439]
4. Gurau, R., Ryan, J.P.: Colored tensor models - a review. *SIGMA* **8**, 20 (2012). <https://doi.org/10.3842/SIGMA.2012.020>. [arxiv:1109.4812]
5. Tanasa, A.: *Combinatorial Physics*. Oxford University Press, Oxford (2021)
6. Gurau, R.: *Notes on Tensor Models and Tensor Field Theories* (2019)
7. Gurau, R.: The complete $1/N$ expansion of colored tensor models in arbitrary dimension. *Ann. Henri Poincaré* **13**, 399 (2012). <https://doi.org/10.1007/s00023-011-0118-z>. [arxiv:1102.5759]
8. Bonzom, V., Gurau, R., Rivasseau, V.: Random tensor models in the large N limit: uncoloring the colored tensor models. *Phys. Rev. D* **85**, 084037 (2012). <https://doi.org/10.1103/PhysRevD.85.084037>. arxiv:1202.3637
9. Carrozza, S., Tanasa, A.: $O(N)$ random tensor models. *Lett. Math. Phys.* **106**, 1531 (2016). <https://doi.org/10.1007/s11005-016-0879-x>. arxiv:1512.06718

10. Benedetti, D., Carrozza, S., Gurau, R., Kolanowski, M.: The $1/N$ expansion of the symmetric traceless and the antisymmetric tensor models in rank three. *Commun. Math. Phys.* **371**, 55 (2019). <https://doi.org/10.1007/s00220-019-03551-z>. arxiv:1712.00249
11. Carrozza, S.: Large N limit of irreducible tensor models: $O(N)$ rank-3 tensors with mixed permutation symmetry. *JHEP* **06**, 39 (2018). [https://doi.org/10.1007/JHEP06\(2018\)039](https://doi.org/10.1007/JHEP06(2018)039). arxiv:1803.02496
12. Carrozza, S., Harribey, S.: Melonic large N limit of 5-index irreducible random tensors. *Commun. Math. Phys.* **390**, 1219 (2022). <https://doi.org/10.1007/s00220-021-04299-1>. arxiv:2104.03665
13. Dartois, S., Rivasseau, V., Tanasa, A.: The $1/N$ expansion of multi-orientable random tensor models. *Annales Henri Poincaré* **15**, 965 (2013). <https://doi.org/10.1007/s00023-013-0262-8>
14. Krajewski, T., Muller, T., Tanasa, A.: Double scaling limit of the prismatic tensor model. *J. Phys. A Math. Theor.* **56**, 235401 (2023)
15. Witten, E.: An SYK-like model without disorder. *J. Phys. A* **52**, 474002 (2019). <https://doi.org/10.1088/1751-8121/ab3752>. [arxiv:1610.09758]
16. Klebanov, I.R., Tarnopolsky, G.: Uncolored random tensors, melon diagrams, and the Sachdev-Ye-Kitaev models. *Phys. Rev. D* **95**, 046004 (2017). <https://doi.org/10.1103/PhysRevD.95.046004>. arxiv:1611.08915
17. Giombi, S., Klebanov, I.R., Tarnopolsky, G.: Bosonic tensor models at large N and small ϵ . *Phys. Rev. D* **96**, 106014 (2017). <https://doi.org/10.1103/PhysRevD.96.106014>. arxiv:1707.03866
18. Bulycheva, K., Klebanov, I.R., Milekhin, A., Tarnopolsky, G.: Spectra of operators in large N tensor models. *Phys. Rev. D* **97**, 026016 (2018). <https://doi.org/10.1103/PhysRevD.97.026016>. arxiv:1707.09347
19. Giombi, S., Klebanov, I.R., Popov, F., Prakash, S., Tarnopolsky, G.: Prismatic large N models for bosonic tensors. *Phys. Rev. D* **98**, 105005 (2018). <https://doi.org/10.1103/PhysRevD.98.105005>. arxiv:1808.04344
20. Klebanov, I.R., Popov, F., Tarnopolsky, G.: TASI lectures on large N tensor models, PoS **TASI2017** (2018) 004 <https://doi.org/10.22323/1.305.0004> arxiv:1808.09434
21. Gurau, R.: Notes on tensor models and tensor field theories, 1907.03531
22. King, R.C.: Modification rules and products of irreducible representations of the unitary, orthogonal, and symplectic groups. *J. Math. Phys.* **12**, 1588 (1971). <https://doi.org/10.1063/1.1665778>
23. Cvitanović, P., Kennedy, A.D.: Spinors in negative dimensions. *Phys. Scr.* **26**, 5 (1982). <https://doi.org/10.1088/0031-8949/26/1/001>
24. Mkrtchyan, R.L., Veselov, A.P.: On duality and negative dimensions in the theory of Lie groups and symmetric spaces. *J. Math. Phys.* **52**, 083514 (2011). <https://doi.org/10.1063/1.3625954>
25. Cvitanović, P.: *Group Theory*. Princeton University Press, Princeton (2008)
26. Mkrtchian, R.L.: The equivalence of $Sp(2N)$ and $SO(-2N)$ gauge theories. *Phys. Lett. B* **105**, 174 (1981). [https://doi.org/10.1016/0370-2693\(81\)91015-7](https://doi.org/10.1016/0370-2693(81)91015-7)
27. LeClair, A., Neubert, M.: Semi-lorentz invariance, unitarity, and critical exponents of symplectic fermion models. *JHEP* (2007). <https://doi.org/10.1088/1126-6708/2007/10/027>. arxiv:0705.4657
28. Bond, A.D., Litim, D.F., Steudtner, T.: Asymptotic safety with majorana fermions and new large N equivalences. *Phys. Rev. D* (2020). <https://doi.org/10.1103/PhysRevD.101.045006>. arxiv:1911.11168
29. Mulase, M., Waldron, A.: Duality of orthogonal and symplectic matrix integrals and quaternionic feynman graphs. *Commun. Math. Phys.* **240**, 553 (2003). <https://doi.org/10.1007/s00220-003-0918-1>. arxiv:math-ph/0206011
30. Gurau, R., Keppeler, H.: Duality of orthogonal and symplectic random tensor models. *AIHPD* (2022). <https://doi.org/10.48550/ARXIV.2207.01993>
31. Caracciolo, S., Sokal, A.D., Sportiello, A.: Algebraic/combinatorial proofs of Cayley-type identities for derivatives of determinants and pfaffians. *Adv. Appl. Math.* **50**, 474 (2013). <https://doi.org/10.1016/j.aam.2012.12.001>. [arxiv:1105.6270]
32. Carrozza, S., Pozsgay, V.: SYK-like tensor quantum mechanics with $sp(n)$ symmetry. *Nucl. Phys.* (2019). <https://doi.org/10.1016/j.nuclphysb.2019.02.012>. arxiv:1809.07753

Duality of $O(N)$ and $Sp(N)$ random tensor models: tensors with symmetries

Authors: Hannes Keppler, Thomas Krajewski, Thomas Muller and
Adrian Tanasa





Published in *J. Phys. A: Math. Theor.* **56** (2023) 49, 495206. DOI: 10.1088/1751-8121/ad0af4.

© 2023 IOP Publishing. Reproduced with permission. All rights reserved. The article version in this thesis is the accepted manuscript with hyperlink colors removed.

Also available as e-print: arXiv 2307.01527 [math-ph].

The original idea was the result of various discussions between the four co-authors. H. Keppler and T. Muller were entirely responsible for the development and understanding of the technical result, as well as for the calculations. H. Keppler and T. Muller also contributed predominantly to the manuscript. H. Keppler produced Figures 1 and 3 and all Brauer diagrams. T. Krajewski and A. Tanasa supervised the project and provided various hints.

Duality of $O(N)$ and $Sp(N)$ random tensor models: tensors with symmetries

H. Keppler ¹, T. Krajewski ², T. Muller ³, and A. Tanasa ^{3,4,5}

¹*Heidelberg University, Institut für Theoretische Physik, Philosophenweg 19, 69120 Heidelberg, Germany, EU*

²*Aix Marseille Univ, Université de Toulon, CNRS, CPT, Marseille, France, EU*

³*Université de Bordeaux, LaBRI CNRS UMR 5800, Talence, France, EU*

⁴*DFT, H. Hulubei Nat. Inst. Phys. Nucl. Engineering, Magurele, Magurele, Romania, EU*

⁵*Université Sorbonne Paris Nord, LIPN, CNRS UMR 7030, Villetaneuse, France, EU*

Abstract

In a recent series of papers, a duality between orthogonal and symplectic random tensor models has been proven, first for quartic models and then for models with interactions of arbitrary order. However, the tensor models considered so far in the literature had no symmetry under permutation of the indices. In this paper, we generalize these results for tensors models with interactions of arbitrary order which further have non-trivial symmetry under the permutation of the indices. Totally symmetric and anti-symmetric tensors are thus treated as a particular case of our result.

Contents

1. Introduction	2
2. Prerequisite	3
2.1. Irreducible representations of the orthogonal and symplectic group	3
2.2. Sign of directed pairings	8
2.3. Pairings, the Brauer algebra, propagators and projectors	9
3. The graded tensor model	10
4. Proof of the main result	12
5. Illustration: totally symmetric and antisymmetric tensor models	17
5.1. $O(N)$ tensor models	17
5.2. $Sp(N)$ tensor models	17
A. Projector of tensors with irreducible symmetry	18
References	22

1. Introduction

Random tensor models (see the recent books [1, 2] or the reviews [3–7]) are 0–dimensional quantum field theoretical generalisations of the celebrated matrix models [8]. Within this framework, they can be seen as probability measures on tensor spaces; this is the point of view we take in this paper.

Tensor models have thus been used as tools to generate discrete random geometries in more than two dimensions. Moreover, they have been further used to construct models similar to the holographic Sachdev-Ye-Kitaev model but without quenched disorder [9, 10], and new (*melon*) Conformal Field Theories [11–16].

Many of the original rigorous results on tensor models relied on the presence of a very large symmetry group (usual several distinct copies of $U(N)$ or $O(N)$) that forbids the tensor to have any symmetry under permutation of their indices [17–25]. Later on, tensor models with tensors living on some non-trivial (mostly $O(N)$) representation were studied systematically [21–23, 26–28].

In [29, 30] the authors studied tensor models with symplectic symmetry $Sp(N)$ in which case the tensor components sometimes are anticommuting (fermionic/odd Grassmann) variables.

Relations between the representations of $O(N)$ and $Sp(N)$ have a long history. King [31] showed that the dimensions of irreducible representations of both groups agree, when exchanging symmetrization and antisymmetrization (transposed Young tableau) and replacing N by $-N$. So called negative dimension theorems, or N to $-N$ dualities, relating the orthogonal and symplectic group via the formal relation $SO(-N) \simeq Sp(N)$ are well known [32–37] for matrix and vector models. Several incarnations of this relation can be found in the literature: for even N , $SO(N)$ and $Sp(N)$ gauge theories are known to be related by changing N to $-N$ [38]; a vector model with symplectic fermions in three space-time dimensions has been studied in [39] and an example of $SO(N)$ and $Sp(N)$ gauge theories with matter fields and Yukawa interactions can be found in [40]; a duality between orthogonal and symplectic matrix ensembles (the $\beta = 1, 4$ ensembles) has been shown in [41]. From a supergeometric or supersymmetric point of view such relations can be seen to arise naturally [42]. Let us also mention A. Abdesselam’s result of section 4 of [43], where he linked Penrose-like spin network calculations with antisymmetrisers to Clebsch-Gordan-like calculations with symmetrisers.

As a natural followup of these matrix model results, we show in this paper how the N to $-N$ symmetry arises in the tensor model case for tensors with interactions of arbitrary order, which further have non-trivial symmetry under the permutation of their indices. This result is a generalization of similar results obtained in simpler settings: for quartic interactions this was proven in [29] and for tensor models with interactions of arbitrary order this was done in [30]. However, let us emphasize that, unlike the results of this paper, both the results of [29] and [30] were obtained for tensor models that had no symmetry under the permutation of indices.

More precisely, the main result of this paper is the following. We consider tensors of order D that transform in some tensor representation R of $O(N)$ or $Sp(N)$. This implies that the tensors may obey some non-trivial symmetry under permutation of their indices. In order to treat models with orthogonal and symplectic symmetry simultaneously, we introduce a grading parameter $\mathfrak{b} \in \{0, 1\}$, such that $\mathfrak{b} = 0$ corresponds to the $O(N)$ symmetric model and $\mathfrak{b} = 1$ to the $Sp(N)$ symmetric one. The tensor components are real fermionic (anticommuting, odd) if $\mathfrak{b} = 1$ and D is odd, and real bosonic (commuting, even) otherwise.

Definition 1. *The real graded tensor model with symmetry R is defined by the measure*

$$d\mu[T] \simeq e^{-S[T]} \prod_{a_1, \dots, a_D} dT^{a_1 \dots a_D},$$

$$S[T] = T^{a_D} C_{a_D b_D}^{-1} T^{b_D} + \sum_{\substack{\mathcal{S} \text{ connected,} \\ |V(\mathcal{S})| > 2}} \frac{\lambda_{\mathcal{S}}}{|V(\mathcal{S})|/D} I_{\mathcal{S}}(T), \quad (1.1)$$

where $g_{a_c b_c}^{\mathfrak{b}}$ is the Kronecker $\delta_{a_c b_c}$ for $\mathfrak{b} = 0$ or the canonical symplectic form $\omega_{a_c b_c}$ for $\mathfrak{b} = 1$ and the sum runs over independent connected invariants $I_{\mathcal{S}}(T)$ of order higher than two, indexed by undirected stranded graphs \mathcal{S} (see section 3 for more details).

The partition function Z and the expectation value of an invariant $\langle I_{\mathcal{S}}(T) \rangle$ are defined by:

$$Z(\{\lambda\}) = \int d\mu[T], \quad \text{and} \quad \langle I_{\mathcal{S}}(T) \rangle(\{\lambda\}) = \frac{1}{Z} \int d\mu[T] I_{\mathcal{S}}(T), \quad (1.2)$$

and can be evaluated in perturbation theory. The main theorem of this paper is:

Theorem 2. *The perturbative series of the partition function Z and expectation values of invariants $\langle I_{\mathcal{S}}(T) \rangle$ can be expressed as a formal sum over 2-colored stranded graphs \mathcal{G} . Each summand, corresponding to a specific graph \mathcal{G} (called the amplitude of that graph), writes as a product:*

$$K(\{\lambda\}, \mathcal{G}) \cdot \left((-1)^{\mathfrak{b}} N \right)^{F(\mathcal{G})}, \quad (1.3)$$

of a term depending on N and a term K , encoding both the dependence on the coupling constants $\lambda_{\mathcal{S}}$ and some combinatorial factors associated to \mathcal{G} (see section 3 for the relevant definitions).

The main result of this paper follows as a direct consequence of the theorem above:

Corollary 3. *Tensor models of the form in definition 1 with symmetry given by the $O(N)$ tensor representation R are dual to corresponding tensor models with $Sp(N)$ symmetry given by the representation with transposed Young diagrams R' (exchanging symmetrization and antisymmetrization) in the sense that the amplitudes of graphs in their perturbative expansions are mapped into each other after a change of N to $-N$.*

Proof. This follows from Theorem 2. The replacement $\mathfrak{b} \rightarrow \mathfrak{b} + 1 \pmod{2}$ and $N \rightarrow -N$ leaves the amplitude (1.3) unchanged, and, as will be noted in section 2.1, the shift $\mathfrak{b} \rightarrow \mathfrak{b} + 1 \pmod{2}$ exchanges symmetrization and antisymmetrization in the tensor representation R . This has the effect of transposing all Young diagrams $\lambda \rightarrow \lambda'$, and leads to the tensor representation R' . \square

The paper is organized as follows. In section 2 we recall several results on representation theory of the orthogonal and symplectic group. Focusing on the Brauer algebra, that plays a similar role as the algebra of the symmetric group for representations of $GL(N)$. At the end of this section we give a dictionary between notions used in the physics/tensor model and representation theory literature. In section 3 we define the tensor models of interest for this paper and give their diagrammatic representation in terms of stranded graphs. In section 4 we give the proof of our main result, and in section 5 we use, as an explicit example, the totally symmetric and antisymmetric tensor representations to illustrate the duality between $O(N)$ and $Sp(N)$ tensor models proved in the previous section.

2. Prerequisite

2.1. Irreducible representations of the orthogonal and symplectic group

In this section we review some definitions and results of the theory of irreducible representations of the general linear group $GL(N)$ and its connection to representations of the symmetric group \mathfrak{S}_D and Young diagrams. We further review irreducible representations of the groups $O(N)$ and $Sp(N)$, preserving some non-degenerate bilinear form and their connections to the Brauer algebra.

Let $V = \mathbb{R}^N$. Both $GL(N)$ and \mathfrak{S}_D act on the tensor product space $V^{\otimes F}$. Irreducible representations of $GL(N)$ can be obtained as the image of certain elements of the group algebra $\mathbb{C}\mathfrak{S}_D$ (Young

symmetrizers). Analogously, irreducible representations of $O(N)$ or $Sp(N)$ can be obtained using projectors, defined by elements of the Brauer algebra B_D .

Our exposition is based on [44] and, when concerning the Brauer algebra, on [45]. We further refer the interested reader to [46, 47] or to the books [48] or [36].

Young tableaux. For general combinatorial references on Young tableaux, we refer to chapter XIV of the handbook [49]. To a partition $\lambda = (\lambda_1, \lambda_2, \dots, \lambda_k)$ of $D \in \mathbb{N}$, denoted as $\lambda \vdash D$, i.e. a sequence of non increasing integers with $|\lambda| = \sum_{i=1}^k \lambda_i = D$, we associate a *Young diagram*

$$\lambda = \begin{array}{c} \lambda_1 \\ \lambda_2 \\ \lambda_3 \\ \lambda_4 \\ \lambda_5 \end{array} \begin{array}{|c|c|c|} \hline & & \\ \hline & & \\ \hline & & \\ \hline & & \\ \hline & & \\ \hline \end{array} \quad (2.1)$$

with λ_i boxes in the i th row. Note that we are using here the English notation for Young diagrams and tableaux. The dual diagram λ' is obtained by interchanging rows and columns in the Young diagram. Let us recall that Young diagrams can be used to define projectors onto irreducible representations of the symmetric group \mathfrak{S}_D .

Given a Young diagram, a *Young tableau* is a numbering of the boxes by the integers $1, 2, \dots, D$. The canonical Young tableau is obtained by numbering the boxes consecutively:

$$\begin{array}{|c|c|c|} \hline 1 & 2 & 3 \\ \hline 4 & 5 & 6 \\ \hline 7 & 8 & \\ \hline 9 & & \\ \hline 10 & & \\ \hline \end{array} . \quad (2.2)$$

Define the sets of row and column permutations:

$$\begin{aligned} P_\lambda &= \{g \in \mathfrak{S}_D \mid g \text{ preserves each row}\} , \\ Q_\lambda &= \{g \in \mathfrak{S}_D \mid g \text{ preserves each column}\} . \end{aligned} \quad (2.3)$$

Next, one introduces two elements of the group algebra $\mathbb{C}\mathfrak{S}_D$:

$$a_\lambda = \sum_{g \in P_\lambda} g , \quad b_\lambda = \sum_{g \in Q_\lambda} \text{sgn}(g)g . \quad (2.4)$$

Noting that $\mathbb{C}\mathfrak{S}_D$ acts on $V^{\otimes D}$ by permuting factors, a_λ acts as a symmetrizer and b_λ as an antisymmetrizer on the tensors. Finally, the *Young symmetrizer* is defined as:

$$c_\lambda = a_\lambda \cdot b_\lambda . \quad (2.5)$$

Consider as an example $\lambda = \square\square\square$ or $\begin{smallmatrix} \square & \square \\ \square \end{smallmatrix}$. The image of the action of c_λ on $V^{\otimes 3}$ is $\text{Sym}^3 V$ or $\wedge^3 V$, the spaces of totally symmetric or antisymmetric tensors, respectively.

The permutation group \mathfrak{S}_D acts on tensors in $V^{\otimes D}$ by permutation of the indices, with V a vector space of dimension N . Then all the previous projectors give rise to representations, which are in general reducible. The dimension of a representation indexed by the Young diagram λ reads:

$$\dim(\pi_{\lambda, N}) = \prod_{(i,j) \in \lambda} \frac{N - i + j}{h_{ij}} , \quad (2.6)$$

with i (resp. j) the row (resp. column) label of the box and h_{ij} the hook length of the box (i, j) , i.e.

$$h_{i,j} = \#\{(k, l) \in \lambda \text{ with } k = i, l \geq j \text{ or } l = j, k \geq i\}. \quad (2.7)$$

Then, it is worthwhile to notice that this is a polynomial in N obeying the relation:

$$\dim(\pi_{\lambda, -N}) = (-1)^{|\lambda|} \dim(\pi_{\lambda', N}), \quad (2.8)$$

with $|\lambda|$ the number of boxes in λ and λ' the dual diagram. Therefore, trading N for $-N$ involves exchanging rows and columns, or equivalently, symmetrization and antisymmetrization. For example:

$$\dim\left(\begin{array}{|c|c|} \hline \square & \square \\ \hline \square & \square \\ \hline \end{array}, N\right) = \frac{N(N-1)(N-2)(N+1)}{4 \cdot 2 \cdot 1 \cdot 1} \stackrel{\text{dual}}{\leftrightarrow} \dim\left(\begin{array}{|c|c|} \hline \square & \square \\ \hline \square & \square \\ \hline \end{array}, -N\right) = \frac{N(N-1)(N+1)(N+2)}{4 \cdot 2 \cdot 1 \cdot 1}. \quad (2.9)$$

These encode representations of the symmetric group. For our purposes it turns out to be helpful to identify irreducible representations of the groups $O(N)$ and $Sp(N)$ inside the previous ones, as we shall do in the following.

Representations. Let us recall that a representation of the group $GL(N)$ on $V^{\otimes D}$ is semisimple and decomposes into a direct sum of irreducible representations that are determined by irreducible representations of \mathfrak{S}_D , and thus indexed by Young diagrams. For simplicity, we focus on N much larger than D ($N \geq 2D$). Note that for small N not all Young diagrams give irreducible representations.

An analogous construction holds for the groups $O(N)$ and $Sp(N)$ that preserve a non-degenerate (skew-)symmetric bilinear form. The main difference lies in the ability to form traces by contacting two factors of $V^{\otimes D}$ with the bilinear form. To allow for these contractions, the group algebra $\mathbb{C}\mathfrak{S}_D$ is replaced by the Brauer algebra B_D [46]. As subgroups $O(N), Sp(N) \subset GL(N)$, irreducible representations of $GL(N)$ are still representations of $O(N)$ and $Sp(N)$, but not necessarily irreducible. However, irreducible $O(N)$ or $Sp(N)$ representations can be obtained by traceless projections of irreducible representations of $GL(N)$. In [45], a universal traceless projector $\mathfrak{P}_D \in B_D$ was constructed, such that irreducible $O(N)$ or $Sp(N)$ representations can be obtained by first subtracting traces by applying \mathfrak{P}_D , and second applying a projector (e.g. Young symmetrizer) to an irreducible $GL(N)$ representation. Note that, in particular, both operations commute.

Brauer algebra. Let us now exhibit the Brauer algebra $B_D(z)$, for $D \in \mathbb{N}$, $z \in \mathbb{C}$.

For $D \in \mathbb{N}$, draw two horizontal rows of vertices labelled $1, 2, \dots, D$. *Brauer diagrams* are represented by pairings of these $2D$ vertices. If every vertex in the top row is connected to a vertex in the bottom row, these elements represent permutation diagrams. Thus, \mathfrak{S}_D is a subset of the diagrams and $\mathbb{C}\mathfrak{S}_D$ a subset of the algebra. For example:

$$\sigma = \begin{array}{c} \begin{array}{cccc} 1 & 2 & 3 & 4 \\ \bullet & \bullet & \bullet & \bullet \end{array} \\ \diagdown \quad \diagup \quad \diagdown \quad \diagup \\ \begin{array}{cccc} \bullet & \bullet & \bullet & \bullet \\ 1 & 2 & 3 & 4 \end{array} \end{array}, \quad \tau = \begin{array}{c} \begin{array}{cccc} 1 & 2 & 3 & 4 \\ \bullet & \bullet & \bullet & \bullet \end{array} \\ \diagdown \quad \diagup \quad \diagdown \quad \diagup \\ \begin{array}{cccc} \bullet & \bullet & \bullet & \bullet \\ 1 & 2 & 3 & 4 \end{array} \end{array}. \quad (2.10)$$

For simplicity, from now on we omit the labels on our diagrams. Since Brauer diagrams are more general than permutation diagrams, the set of Brauer diagrams includes elements such as

$$\beta = \begin{array}{c} \begin{array}{cccc} \bullet & \bullet & \bullet & \bullet \end{array} \\ \text{---} \quad \text{---} \quad \text{---} \quad \text{---} \\ \begin{array}{cccc} \bullet & \bullet & \bullet & \bullet \end{array} \end{array}, \quad v = \begin{array}{c} \begin{array}{cccc} \bullet & \bullet & \bullet & \bullet \end{array} \\ \text{---} \quad \text{---} \quad \text{---} \quad \text{---} \\ \begin{array}{cccc} \bullet & \bullet & \bullet & \bullet \end{array} \end{array}, \quad (2.11)$$

having arcs connecting vertices of the same row. The product of two Brauer diagrams $\sigma\tau$ is defined by placing σ below τ and “straightening” the lines:

$$\sigma\tau = \text{[diagram]} = \text{[straightened diagram]} . \quad (2.12)$$

For permutation diagrams, this is equivalent to the product of the permutations. Whenever loops appear, they get deleted to obtain again a Brauer diagram.

The Brauer algebra $B_D(z)$ is the free \mathbb{C} -algebra on the set of Brauer diagrams together with the above product and the additional rule stating that when $l \geq 0$ loops appear in the product of two Brauer diagrams, the resulting diagram gets multiplied by a factor z^l .

$$\beta v = \text{[diagram with loop]} = z \text{[diagram without loop]} . \quad (2.13)$$

Note that one has: $\mathbb{C}\mathfrak{S}_D \subset B_D(z)$ (diagrams with zero arcs).

A set of generators of $B_D(z)$ is given by σ_i and β_i ($i = 1, 2, \dots, D-1$):

$$\sigma_i = \text{[diagram with crossing at i, i+1]}, \quad \beta_i = \text{[diagram with arc at i, i+1]} . \quad (2.14)$$

Furthermore, we introduce the following elements for $i < j$:

$$\sigma_{ij} = \text{[diagram with crossing at i, j]}, \quad \beta_{ij} = \text{[diagram with arc at i, j]} . \quad (2.15)$$

Action on $V^{\otimes D}$. If V is a real N -dimensional vector space with non-degenerate bilinear form g , that can be the standard symmetric or symplectic form, one considers integer values of $z = (-1)^{\mathfrak{b}}N$, $N \in \mathbb{N}$ ($\mathfrak{b} = 0$ in the symmetric, and $\mathfrak{b} = 1$ in the symplectic case). The Brauer algebra $B_D((-1)^{\mathfrak{b}}N)$ acts naturally on tensors of order D that we represent by their components

$$T = T^{a_1 a_2 \dots a_D} e_{a_1} \otimes e_{a_2} \otimes \dots \otimes e_{a_D} , \quad (2.16)$$

where $\{e_a\}_{a=1,2,\dots,N}$ is a standard basis with respect to the bilinear form g on V . An element $\beta \in B_D((-1)^{\mathfrak{b}}N)$, corresponding to a single Brauer diagram, acts as follows on $T^{b_1 b_2 \dots b_D}$:

1. Place the indices $b_1 b_2 \dots b_D$ in the top row of the Brauer diagram.
2. Permute them according to the lines that connect the bottom to the top row.
3. Contract them with g if they are connected by an arc in the top row.
4. Add a factor $g^{a_i a_j}$ for each arc in the bottom row.
5. Multiply the result by $(\eta(\beta))^{\mathfrak{b}}$, where $\eta(\beta) = (-1)^m$ where m is the minimal number of crossings in β .¹

Crucially, because of the last point, in applications to $Sp(N)$, $B_D(-N)$ acts in a signed representation. More explicit, we can associate to β a linear map in $\text{End}(V^{\otimes D})$, whose components write

$$(\beta)_{b_1 b_2 \dots b_D}^{a_1 a_2 \dots a_D} = \eta(\beta)^{\mathfrak{b}} \prod_{\substack{(i,j) \\ i \text{ in the bottom row} \\ \text{connected to } j \text{ in the top row}}} \delta_{b_j}^{a_i} \prod_{\substack{(k,l) \\ k \text{ connected to } l \\ \text{by an arc in the bottom row}}} g^{a_k a_l} \prod_{\substack{(m,p) \\ m \text{ connected to } p \\ \text{by an arc in the top row}}} g_{b_m b_p} , \quad (2.17)$$

and it acts on the tensor components as:

$$\beta \cdot T^{a_1 a_2 \dots a_D} = \sum_{b_1, b_2, \dots, b_D} (\beta)_{b_1 b_2 \dots b_D}^{a_1 a_2 \dots a_D} T^{b_1 b_2 \dots b_D} . \quad (2.18)$$

For example, one has:

$$\sigma_{ij} \cdot T^{a_1 \dots a_i \dots a_j \dots a_D} = T^{a_1 \dots a_j \dots a_i \dots a_D} , \quad (2.19)$$

$$\beta_{ij} \cdot T^{a_1 \dots a_i \dots a_j \dots a_D} = g^{a_i a_j} g_{b_i b_j} T^{a_1 \dots b_i \dots b_j \dots a_D} , \quad (2.20)$$

$$v \cdot T^{a_1 a_2 a_3 a_4} = g^{a_1 a_3} g_{b_1 b_2} T^{b_1 b_2 a_4 a_2} . \quad (2.21)$$

The action is extended to arbitrary elements of the Brauer algebra by linearity. One can also raise the indices of the linear map using the bilinear form such that:

$$\begin{aligned} (\beta)^{a_1 a_2 \dots a_D, b_1 \dots b_D} &= (\beta)_{c_1 c_2 \dots c_D}^{a_1 a_2 \dots a_D} g^{c_1 b_1} \dots g^{c_D b_D} \\ &= \eta(\beta)^{\mathfrak{b}} \prod_{\substack{(i,j) \\ i \text{ in the bottom row} \\ \text{connected to } j \text{ in the top row}}} g^{a_i b_j} \prod_{\substack{(k,l) \\ k \text{ connected to } l \\ \text{by an arc in the bottom row}}} g^{a_k a_l} \prod_{\substack{(m,p) \\ m \text{ connected to } p \\ \text{by an arc in the top row}}} g^{b_m b_p} . \end{aligned} \quad (2.22)$$

Note that because of the sign $\eta(\beta)$ in the definition of the action on $V^{\otimes D}$, the interchange of symmetrization and antisymmetrization when going from $O(N)$ representations to $Sp(N)$ representations is already built in. This can be seen by the fact that in the case where σ is a permutation, the sign $\eta(\sigma)$ corresponds to $\text{sgn}(\sigma)$. The components of the linear map associated to a_λ and b_λ (see (2.4)) are:

$$\begin{aligned} (a_\lambda)_{b_1 \dots b_D}^{a_1 \dots a_D} &= \sum_{\sigma \in P_\lambda} \text{sgn}(\sigma)^{\mathfrak{b}} \prod_{\substack{(i,j) \\ j=\sigma(i)}} \delta_{b_j}^{a_i} , \\ (b_\lambda)_{b_1 \dots b_D}^{a_1 \dots a_D} &= \sum_{\tau \in Q_\lambda} \text{sgn}(\tau)^{\mathfrak{b}+1} \prod_{\substack{(i,j) \\ j=\tau(i)}} \delta_{b_j}^{a_i} . \end{aligned} \quad (2.23)$$

In conclusion, in the $O(N)$ case ($\mathfrak{b} = 0$), a_λ acts as a symmetrizer and b_λ as an antisymmetrizer whereas the roles are reversed in the $Sp(N)$ case ($\mathfrak{b} = 1$). The product $c_\lambda = a_\lambda \cdot b_\lambda$ thus corresponds to the Young symmetrizer associated to a tableau λ when $\mathfrak{b} = 0$ and to the symmetrizer associated to the dual tableau λ' , obtained by permuting the rows and columns of λ , when $\mathfrak{b} = 1$.

Traceless projector. In order to implement the projection onto irreducible representations of $O(N)$ or $Sp(N)$, the authors of [45] build a universal traceless projector, which we introduce here, for the sake of completeness. The main building block of this projector is:

$$A_D = \sum_{1 \leq i < j \leq D} \beta_{ij} \in B_D((-1)^{\mathfrak{b}} N) . \quad (2.24)$$

Let us now list some important properties of A_D :

¹This sign can be expressed as the sign of oriented pairings in subsection 2.3.

- It commutes with all elements of $\mathbb{C}\mathfrak{S}_D \subset B_D(N)$. Thus, in particular, it commutes with Young symmetrizers.
- The action of A_D on $V^{\otimes D}$ is diagonalizable.
- The kernel $\ker A_D \subset V^{\otimes D}$ is exactly the space of traceless tensors.
- Its non-zero eigenvalues are in $(-1)^b \mathbb{N}$.

The proof of these statements can be found in [45], and the universal traceless projector is given by:

$$\mathfrak{P}_D = \sum_{\alpha \text{ non-zero eigenvalue of } A_D} \left(1 - \frac{1}{\alpha} A_D\right). \quad (2.25)$$

Explicit formulas for the non-zero eigenvalues α are also given in [45].

2.2. Sign of directed pairings

In this subsection, we define the sign given by two oriented pairings and give some of its properties.

Consider two oriented pairings \vec{M}_1 and \vec{M}_2 on a set of $2D$ elements, suppose these two pairings are given by:

$$\begin{aligned} \vec{M}_1 &= \{(i_1, i_2), \dots, (i_{2D-1}, i_{2D})\}, \\ \vec{M}_2 &= \{(j_1, j_2), \dots, (j_{2D-1}, j_{2D})\}. \end{aligned} \quad (2.26)$$

The sign $\epsilon(\vec{M}_1, \vec{M}_2)$ of the two pairings is defined as the sign of the permutation $\sigma = \begin{pmatrix} i_1 & i_2 & \dots & i_{2D-1} & i_{2D} \\ j_1 & j_2 & \dots & j_{2D-1} & j_{2D} \end{pmatrix}$:

$$\epsilon(\vec{M}_1, \vec{M}_2) = \text{sgn} \left(\begin{pmatrix} i_1 & i_2 & \dots & i_{2D-1} & i_{2D} \\ j_1 & j_2 & \dots & j_{2D-1} & j_{2D} \end{pmatrix} \right) \quad (2.27)$$

We give here a list of some of the properties of the sign $\epsilon(\vec{M}_1, \vec{M}_2)$:

1. It is symmetric under permutation of its arguments:

$$\epsilon(\vec{M}_1, \vec{M}_2) = \epsilon(\vec{M}_2, \vec{M}_1). \quad (2.28)$$

2. For three pairings $\vec{M}_1, \vec{M}_2, \vec{M}_3$ on the same set, one has:

$$\epsilon(\vec{M}_1, \vec{M}_2) = \epsilon(\vec{M}_1, \vec{M}_3) \epsilon(\vec{M}_2, \vec{M}_3). \quad (2.29)$$

3. For two pairings \vec{M}_1, \vec{M}_2 on a first set \mathcal{S}_1 of $2D$ elements and two pairings \vec{M}_3, \vec{M}_4 on a second set \mathcal{S}_2 of $2p$ elements, one has:

$$\epsilon(\vec{M}_1, \vec{M}_2) \epsilon(\vec{M}_3, \vec{M}_4) = \epsilon(\vec{M}_1 \sqcup \vec{M}_3, \vec{M}_2 \sqcup \vec{M}_4). \quad (2.30)$$

4. Consider a set of elements \mathcal{S}_v and two pairings \vec{M}_1 and \vec{M}_2 on this set. Depict each elements of \mathcal{S}_v as a node and each pair in \vec{M}_1 and \vec{M}_2 as an oriented edge pointing from the first element to the second, of color 1 for the pairs in \vec{M}_1 and color 2 for the ones in \vec{M}_2 . The sign $\epsilon(\vec{M}_1, \vec{M}_2)$ can be written as:

$$\epsilon(\vec{M}_1, \vec{M}_2) = (-1)^{F_{1/2, \text{even}}}. \quad (2.31)$$

In the equation above, $F_{1/2, \text{even}}$ is the number of even faces of color 1 and 2 of the graphical representation described above. An even, resp. odd, face of color 1 and 2 is defined as a closed cycle of alternating colors 1 and 2 where an even, resp. odd, number of edges point in one direction around the cycle. Because each face consists of an even number of edges, this notion is well defined.

In the sequel, the sign ϵ plays a crucial role in the proof of our main theorem. Let us first link this quantity to the Brauer algebra and connect them to tensor models.

2.3. Pairings, the Brauer algebra, propagators and projectors

In this subsection we exhibit the connection between the notions of subsections 2.1 and 2.2, and propagators in the random tensor models we study in this paper.

The relation between Brauer diagrams and pairings is straightforward, as each Brauer diagram is a pairing of $2D$ vertices. Moreover, the sign $\eta(\beta)$ that appears in the description of the action of $B_D((-1)^b N)$ on $V^{\otimes D}$, can be expressed as the sign of two directed pairings by the following construction:

1. Label the vertices in the Brauer diagram $1, 2, \dots, D$ in the top row and $D+1, D+2, \dots, 2D$ in the bottom row.
2. Let $\vec{\beta}$ be the directed pairing induced by β , where edges are oriented from top to bottom, left to right in the top row and right to left in the bottom row.
3. Let $\vec{M}_{ref} = \{(1, D+1), (2, D+2), \dots, (D, 2D)\}$ be the reference pairing, that pair top to bottom vertices.
4. One then has: $\eta(\beta) = \epsilon(\vec{\beta}, \vec{M}_{ref})$.

This follows from the use of (2.31). Moreover, $\beta^{a_1 \dots a_D, a_{D+1} \dots a_{2D}}$ admits a compact form in term of the oriented pairing $\vec{\beta}$:

$$(\beta)^{a_1 a_2 \dots a_D, a_{D+1} \dots a_{2D}} = \epsilon(\vec{\beta}, \vec{M}_{ref})^b \prod_{(i,j) \in \vec{\beta}} g^{a_i a_j}. \quad (2.32)$$

In a random tensor model, with tensors of order D , living in a representation $R \subset V^{\otimes D}$ of the group $O(N)$ or $Sp(N)$, a propagator is a $O(N)$ - or $Sp(N)$ -linear map $C \in \text{End}(R)$. As the Brauer algebra is isomorphic (for N large enough) to this space of $O(N)$ - or $Sp(N)$ -linear maps, each propagator is also an element of $B_D((-1)^b N)$.

As a consequence of Schur's lemma, if the representation R is irreducible, C is proportional to the identity on R , and if R is reducible and decomposes into a direct sum of distinct irreducible representations R_i ($R = \bigoplus_{i=1}^k R_i$), then C decomposes as well into a direct sum of maps P_i , each proportional to the identity on R_i .

Denoting by $P_R \in \text{End}(V^{\otimes D})$ the orthogonal projector on R , i.e. $\text{im}(P_R) = R$. The propagator can be trivially extended to the whole space $V^{\otimes D}$ by $C \circ P_R$. Thus, reformulating the implications of Schur's Lemma: If R is irreducible the propagator is proportional to the projector on R , and if R decomposes into distinct irreducible representations as above, the propagator is a linear combination of the projectors on the R_i .

When studying tensor models from a quantum field theoretical perspective, one is interested in the calculation of expectation values of the form:

$$\langle f(T) \rangle = \frac{\left[e^{\partial_T C \partial_T} e^{-V(T)} f(T) \right]_{T=0}}{\left[e^{\partial_T C \partial_T} e^{-V(T)} \right]_{T=0}}, \quad (2.33)$$

where $V(T)$ and $f(T)$ are invariant under the group action, and $\partial_T C \partial_T$ is a short hand notation for the Laplacian-like second order differential operator:

$$\partial_T C \partial_T := \sum_{a_1^1, \dots, a_D^1, a_1^2, \dots, a_D^2=1}^N \frac{\partial}{\partial T^{a_1^1 \dots a_D^1}} C^{a_1^1 \dots a_D^1, a_1^2 \dots a_D^2} \frac{\partial}{\partial T^{a_1^2 \dots a_D^2}}. \quad (2.34)$$

Note that indices are raised and lowered by the non-degenerate bilinear form, as usual. In the above formulation, the tensors are elements of R , i.e. have some non-trivial symmetry. But one can as well consider every tensor $T \in R$ to arise from the projection of a tensor $\tilde{T} \in V^{\otimes D}$ without symmetry under permutation of its indices. Thus, if we supplement the derivative operator with the appropriate projector, only modes obeying the symmetry (tensors in R) propagate and T can be replaced by \tilde{T} :

$$\langle f(T) \rangle = \frac{\left[e^{\partial_{\tilde{T}}(CP_R)\partial_{\tilde{T}} e^{-V(\tilde{T})}} f(\tilde{T}) \right]_{\tilde{T}=0}}{\left[e^{\partial_{\tilde{T}}(CP_R)\partial_{\tilde{T}} e^{-V(\tilde{T})}} \right]_{\tilde{T}=0}}, \quad (2.35)$$

with the convention $\partial_{\tilde{T}}\tilde{T} = id_{V^{\otimes D}}$.

3. The graded tensor model

Let $T^{a_1 \dots a_D}$ be the components of a generic random tensor with D indices (an order D tensor). Each index of the tensor ranges from 1 to N , the tensor has thus N^D independent components. As already mentioned above, we introduce a parameter \mathfrak{b} , equal to 0 or 1, that defines the symmetry properties of the tensor. If $\mathfrak{b} = 0$, resp. $\mathfrak{b} = 1$, the tensor transforms in some representation R of order D of the orthogonal group $O(N)$, resp. symplectic group $Sp(N)$. Using Einstein summation convention the group action writes:

$$T^{a_1 \dots a_D} \rightarrow T'^{a_1 \dots a_D} = (O_{\mathfrak{b}})^{a_1}_{b_1} (O_{\mathfrak{b}})^{a_2}_{b_2} \dots (O_{\mathfrak{b}})^{a_D}_{b_D} T^{b_1 \dots b_D}, \quad O_{\mathfrak{b}} \in \begin{cases} O(N) & , \mathfrak{b} = 0 \\ Sp(N) & , \mathfrak{b} = 1 \end{cases}. \quad (3.1)$$

Moreover, the indices of the tensor are contracted using a graded symmetric form $g^{\mathfrak{b}}$ such that $g^{\mathfrak{b}}_{ab} = (-1)^{\mathfrak{b}} g^{\mathfrak{b}}_{ba}$. One has:

$$g^{\mathfrak{b}}_{ab} = \begin{cases} \delta_{ab} & , \mathfrak{b} = 0 \\ \omega_{ab} & , \mathfrak{b} = 1 \end{cases}, \quad \text{with} \quad \delta = \left(\begin{array}{c|c} \mathbb{1}_{N/2} & 0 \\ \hline 0 & \mathbb{1}_{N/2} \end{array} \right) \quad \text{and} \quad \omega = \left(\begin{array}{c|c} 0 & \mathbb{1}_{N/2} \\ \hline -\mathbb{1}_{N/2} & 0 \end{array} \right). \quad (3.2)$$

Thus, the tensor components are fermionic (odd graßmannian) if $\mathfrak{b} = 1$ and D odd, and bosonic otherwise (the parity of the tensor components is $\mathfrak{b}D \bmod 2$).

Invariants and directed stranded graphs. By contracting indices with $g^{\mathfrak{b}}$ one can build invariant polynomials in the tensor components. Unlike the graded colored tensor models studied previously in [29, 30], two indices at different positions can now be contracted. Therefore, the invariants do not admit a graphical representation in term of directed edge colored graphs but they do admit one in terms of directed stranded graphs such that:

- each tensor is represented by a set of D nodes labeled by its indices.
- each contraction of indices is represented by a strand connecting the corresponding nodes.

Definition 4 (Stranded Graph). *We encode a directed stranded graph $\vec{\mathcal{S}}$ with D strands by a set of nodes $V(\vec{\mathcal{S}})$ with $|V(\vec{\mathcal{S}})|$ elements, that comes in groups of D , and a set of edges, called strands, $\vec{E}(\vec{\mathcal{S}})$, such that $\vec{E}(\vec{\mathcal{S}})$ is a directed pairing of $V(\vec{\mathcal{S}})$. One often refers to the D nodes as vertices. If two such vertices are directly connected by D strands one often refers to this collection of D strands as edge.*

We also denote the undirected version of a directed stranded graph by \mathcal{S} . Two examples are drawn in figure 1.

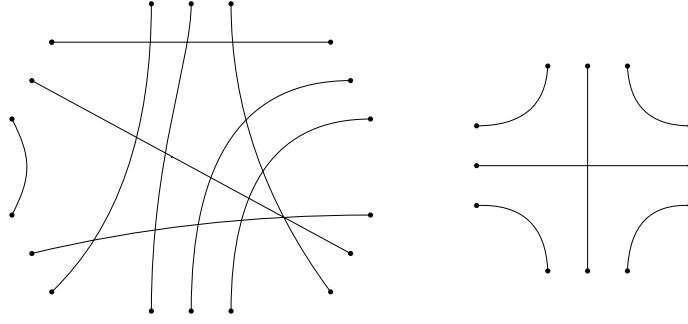


Figure 1. Two stranded graphs for $D = 3$.

As a shorthand notation we write $a_{\mathcal{D}} = (a_1, a_2, \dots, a_D)$ for the sequence of D indices. To each directed stranded graph $\vec{\mathcal{S}}$ is then associated an invariant whose expression reads:

$$I_{\vec{\mathcal{S}}}(T) = \left(\prod_{(i,j) \in \vec{M}_{ref}} T^{a_{\mathcal{D}}^i} T^{a_{\mathcal{D}}^j} \right) \epsilon(\vec{M}_{ref}^D, \vec{E}(\vec{\mathcal{S}}))^b \prod_{(k,l) \in \vec{E}(\vec{\mathcal{S}})} g_{kl}^b. \quad (3.3)$$

In the equation above, \vec{M}_{ref} is an arbitrary reference pairing of $2p = |V(\vec{\mathcal{S}})|/D$ tensors. The pairing \vec{M}_{ref}^D is a directed pairing of the indices of the tensors given by the disjoint union of D copies of \vec{M}_{ref} . An illustration is given in figure 4. The term $\epsilon(\vec{M}_{ref}^D, \vec{E}(\vec{\mathcal{S}}))^b$ is the sign of the pairing \vec{M}_{ref}^D with respect to $\vec{E}(\vec{\mathcal{S}})$; this sign is defined in (2.27).

Introducing the sign of the pairings in the expression of an invariant fixes the ambiguity induced by the graded symmetry of g^b . Two invariants associated to two directed versions of the same stranded graph \mathcal{S} are in fact equal. This means that $I_{\vec{\mathcal{S}}}(T)$ is a class function and we can choose a single representative of \mathcal{S} in the action of our model. More comments on this can be found in [30]. As a consequence, we drop the arrow in the notation if we refer to the undirected version of the graph and if the quantity does not depend on the chosen orientation of the graph.

As one may contract indices of different positions together, there are several possible quadratic invariants. We group them into a quadratic term of the form $T^{a_{\mathcal{D}}} C_{a_{\mathcal{D}} b_{\mathcal{D}}}^{-1} T^{b_{\mathcal{D}}}$. The propagator of the model is given by

$$C^{a_{\mathcal{D}} b_{\mathcal{D}}} = \sum_{M \in \mathbf{M}\{a_{\mathcal{D}} b_{\mathcal{D}}\}} \gamma_M \epsilon(\vec{M}, \vec{M}_{ref,C})^b \prod_{(i,j) \in \vec{M}} g_b^{ij}, \quad \gamma_M \in \mathbb{R}, \quad (3.4)$$

where $g_b^{a_1 b_1}$ denotes the components of the inverse of g^b such that $g_{ac}^b g_b^{cd} = \delta_a^d$. Moreover, $\mathbf{M}\{a_{\mathcal{D}} b_{\mathcal{D}}\}$ is the set of non oriented pairing on the set of $2D$ indices $a_{\mathcal{D}} \cup b_{\mathcal{D}}$ and \vec{M} is a chosen oriented version of M . The pairing $\vec{M}_{ref,C}$ is a reference pairing of the indices given by:

$$\vec{M}_{ref,C} = \{(a_1, b_1), \dots, (a_D, b_D)\}. \quad (3.5)$$

This corresponds to the case where each index of the first tensor propagates to the index at the same position in the second tensor (see figure 2).

Let us emphasize that the product $\mathbf{C} \mathbf{P}_R$ in (2.35) is a particular case of the general propagator (3.4), when $\mathbf{C} = \mathbb{1}$ and \mathbf{P}_R is the projector on the irreducible representation R of $O(N)$ or $Sp(N)$. This is explained in detail in Appendix A.

As noted in subsection 2.3, $C^{a_{\mathcal{D}} b_{\mathcal{D}}}$ is an element of the Brauer algebra $B_D((-1)^b N)$. Each pairing M in the sum represents a Brauer diagram and the factors γ_M are the coefficients in the linear combination. The reference pairing $\vec{M}_{ref,C}$ coincides with \vec{M}_{ref} from subsection 2.2. Note that Brauer diagrams are conventionally read from top to bottom, whereas propagators are usually drawn from left to right.

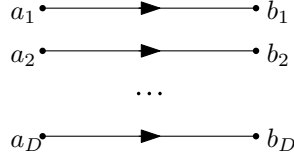


Figure 2. Graphical representation of $\vec{M}_{ref,C}$

Definition 5 (Graded Tensor Model with Symmetry). *We define the graded tensor model with symmetry R by the measure:*

$$d\mu[T] = e^{-S[T]} [dT], \quad [dT] = \zeta \prod_{a_D} dT^{a_1 \dots a_D},$$

$$\text{with } S[T] = T^{a_D} C_{a_D b_D}^{-1} T^{b_D} + \sum_{\substack{\mathcal{S} \text{ connected,} \\ |V(\mathcal{S})|/D > 2}} \frac{\lambda_{\mathcal{S}}}{|V(\mathcal{S})|/D} I_{\mathcal{S}}(T), \quad (3.6)$$

and normalization ζ such that $\int d\mu[T] = 1$ for $\lambda_{\mathcal{S}} = 0 \ \forall \lambda_{\mathcal{S}}$. All tensors are elements of the $O(N)$ (for $\mathfrak{b} = 0$), resp. $Sp(N)$ (for $\mathfrak{b} = 1$), representation R .

In the definition above, the constant $\lambda_{\mathcal{S}}$ is the coupling constant of the invariant associated to \mathcal{S} . The partition function of this models writes:

$$Z = \int d\mu[T] = \left[e^{\partial_T C \partial_T} e^{\sum \frac{\lambda_{\mathcal{S}}}{|V(\mathcal{S})|/D} I_{\mathcal{S}}(T)} \right]_{T=0}, \quad (3.7)$$

where the derivative representation [1, 50, 51] of the Gaussian integral is used and $\partial_T C \partial_T$ is a short-hand notation for:

$$\partial_T C \partial_T := \frac{\partial}{\partial T^{a_D^1}} C^{a_D^1 a_D^2} \frac{\partial}{\partial T^{a_D^2}}. \quad (3.8)$$

When making use of the derivative representation, as discussed in section 2.3, we can take the tensors to have no symmetries under permutations of their indices, but instead incorporate an appropriate projector on the space R in the definition of the propagator.

4. Proof of the main result

In this section, we prove the main theorem of our paper. We show that the partition function of the graded tensor model is invariant under the change of parameters $\mathfrak{b} \rightarrow \mathfrak{b} + 1 \pmod{2}$ and $N \rightarrow -N$. By choosing the propagator according to a given symmetry specified by the $O(N)$ or $Sp(N)$ representation R this implies the stated duality. The appropriate choice of the propagator as an element of the respective Brauer algebra was discussed in section 2.2. From a mathematical point of view, the choice is implemented by fixing the pairings \vec{M} and constants γ_M in (3.4) accordingly.

Let us first recall the commutation relation of the tensor components: $T^{a_D} T^{b_D} = (-1)^{\mathfrak{b}D} T^{b_D} T^{a_D}$. The Gaussian (free) expectation value $\langle T^{a_D^1} \dots T^{a_D^{2p}} \rangle_0$ of $2p$ tensors whose order is encoded by \vec{M}_{ref} is defined as:

$$\langle T^{a_D^1} \dots T^{a_D^{2p}} \rangle_0 = \left[e^{\partial_T C \partial_T} T^{a_D^1} \dots T^{a_D^{2p}} \right]_{T=0}. \quad (4.1)$$

For our model, Wick's theorem expresses this expectation as a sum over pairings of $2p$ elements:

$$\langle T^{a_D^1} \dots T^{a_D^{2p}} \rangle_0 = \sum_{M_0 \in \mathbf{M}_{2p}} \epsilon(\vec{M}_{ref}, \vec{M}_0)^{\mathfrak{b}D} \left(\prod_{(i,j) \in \vec{M}_0} C^{a_D^i a_D^j} \right). \quad (4.2)$$

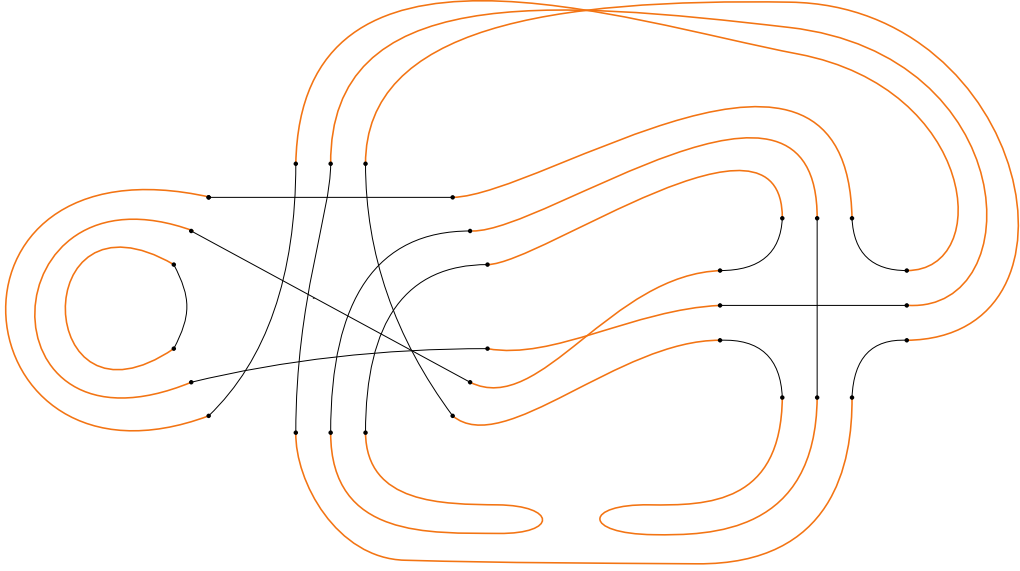


Figure 3. A 2-colored stranded graph for $D = 3$, obtained by connecting the two stranded graphs in figure 1 by propagator edges (elongated Brauer diagrams). The color 0 is represented by orange and color 1 by black lines.

The sign $\epsilon(\vec{M}_{ref,2p}, \vec{M}_0)^{bD}$ in (4.2) takes into account the type (bosonic/fermionic) of the tensor components. The directed pairing \vec{M}_0 is an arbitrary oriented version of M_0 , but notice that the term $\epsilon(\vec{M}_{ref,2p}, \vec{M}_0)^{bD} \left(\prod_{(i,j) \in \vec{M}_0} C^{a_D^i a_D^j} \right)$ is invariant under reorientation of pairs in \vec{M}_0 .

The Gaußian (free) expectation of an invariant $I_S(T)$ of order $2p$ specified by a stranded graph \mathcal{S} is defined as:

$$\langle I_S(T) \rangle_0 = \left[e^{\partial_T C \partial_T} I_S(T) \right]_{T=0} . \quad (4.3)$$

This expectation value can be computed by pairing the $2p$ groups of D vertices in \mathcal{S} by propagators (3.4). We represent this pairing by edges of a new color 0, each consists again of D strands.

The result is a sum over 2-colored stranded graphs \mathcal{G} , such that $\mathcal{S} \subset \mathcal{G}$ is the maximal subgraph of color 1 (see Fig. 3 for an example of such a graph).

Lemma 6. *The Gaussian expectation (4.3) writes:*

$$\langle I_S(T) \rangle_0 = \sum_{\substack{\mathcal{G}, \mathcal{S} \subset \mathcal{G} \\ |V(\mathcal{G})| = 2pD}} \gamma_{\mathcal{G}} \left((-1)^{bN} \right)^{F(\mathcal{G})} , \quad (4.4)$$

where the power of N is given by the number of faces of \mathcal{G} . Moreover, the factor $\gamma_{\mathcal{G}}$ is a product of weights associated to the edges of color 0, given by the expression of the propagator in (3.4). It writes:

$$\gamma_{\mathcal{G}} = \prod_{e \in E_0(\mathcal{G})} \gamma_{M^e} , \quad (4.5)$$

with $E_0(\mathcal{G})$ the set of edges of color 0 and M^e the pairing (Brauer diagram) defining the path of the D strands of the color 0 edge e .

Proof. Applying Wick's theorem (4.2) to the formula of an invariant of order $2p$ specified by a directed

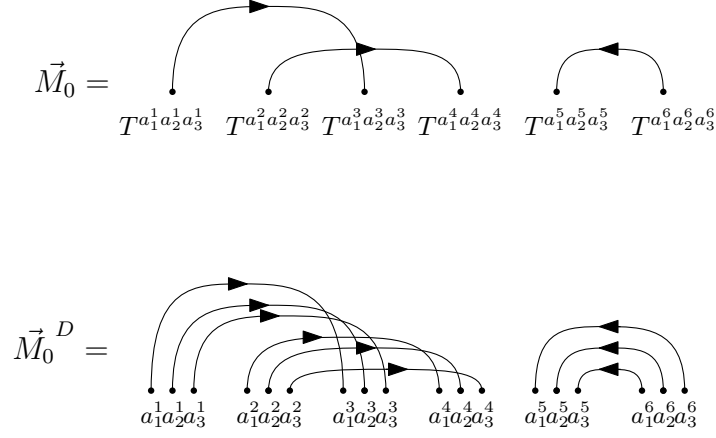


Figure 4. The pairing \vec{M}_0 of tensors is promoted to the pairing \vec{M}_0^D of their indices.

stranded graph $\vec{\mathcal{S}}$ (3.3), leads to the following form of the Gaußian expectation:

$$\begin{aligned}
\langle I_{\mathcal{S}} \rangle_0 &= \left\langle \prod_{(i,j) \in \vec{M}_{ref}} T^{a_{\mathcal{D}}^i} T^{a_{\mathcal{D}}^j} \right\rangle_0 \epsilon(\vec{M}_{ref}^D, \vec{E}(\vec{\mathcal{S}}))^b \left(\prod_{(k,l) \in \vec{E}(\vec{\mathcal{S}})} g_{kl}^b \right) \\
&= \sum_{M_0 \in \mathbf{M}_{2p}} \epsilon(\vec{M}_{ref}^D, \vec{E}(\vec{\mathcal{S}}))^b \epsilon(\vec{M}_{ref}, \vec{M}_0)^{bD} \left(\prod_{(i,j) \in \vec{M}_0} C^{a_{\mathcal{D}}^i a_{\mathcal{D}}^j} \right) \left(\prod_{(k,l) \in \vec{E}(\vec{\mathcal{S}})} g_{kl}^b \right).
\end{aligned} \tag{4.6}$$

First, the dependence on the reference pairing can be eliminated using the properties (2.30) and (2.29) of the sign ϵ such that:

$$\epsilon(\vec{M}_{ref}^D, \vec{E}(\vec{\mathcal{S}}))^b \epsilon(\vec{M}_{ref}, \vec{M}_0)^{bD} = \epsilon(\vec{M}_0^D, \vec{E}(\vec{\mathcal{S}}))^b, \tag{4.7}$$

where \vec{M}_0^D is the oriented pairing given by the disjoint union of D copies of \vec{M}_0 . This pairing can be seen as taking each pairs of tensors in \vec{M}_0 and pairing their indices, respecting their position. An illustration can be found in figure 4.

Second, we rewrite the term $\left(\prod_{(i,j) \in \vec{M}_0} C^{a_{\mathcal{D}}^i a_{\mathcal{D}}^j} \right)$ using (3.4) as:

$$\begin{aligned}
\prod_{(i,j) \in \vec{M}_0} C^{a_{\mathcal{D}}^i a_{\mathcal{D}}^j} &= \prod_{(i,j) \in \vec{M}_0} \left(\sum_{M_{ij} \in \mathbf{M}\{a_{\mathcal{D}}^i a_{\mathcal{D}}^j\}} \gamma_M \epsilon(\vec{M}_{ij}, \vec{M}_{ref,ij,C})^b \prod_{(m,n) \in \vec{M}_{ij}} g_{\mathbf{b}}^{mn} \right) \\
&= \sum_{M_{tot} \in \mathbf{M}_{tot}} \gamma_{M_{tot}} \epsilon(\vec{M}_{tot}, \vec{M}_0^D)^b \left(\prod_{(m,n) \in \vec{M}_{tot}} g_{\mathbf{b}}^{mn} \right),
\end{aligned} \tag{4.8}$$

where $\mathbf{M}\{a_{\mathcal{D}}^i a_{\mathcal{D}}^j\}$ is the set of pairings of elements $a_{\mathcal{D}}^i \cup a_{\mathcal{D}}^j$, and \mathbf{M}_{tot} is the set of pairings given by the disjoint union of all $\mathbf{M}\{a_{\mathcal{D}}^i a_{\mathcal{D}}^j\}$ with $(i,j) \in \vec{M}_0$. A pairing $M_{tot} \in \mathbf{M}_{tot}$ is therefore the disjoint union of p pairings belonging to the sets $\mathbf{M}\{a_{\mathcal{D}}^i a_{\mathcal{D}}^j\}$. An example is shown in figure 5. Denoting these p pairings as $M^1 \dots M^p$, the factor $\gamma_{M_{tot}}$ is equal to:

$$\gamma_{M_{tot}} = \prod_{x=1}^p \gamma_{M^x}. \tag{4.9}$$

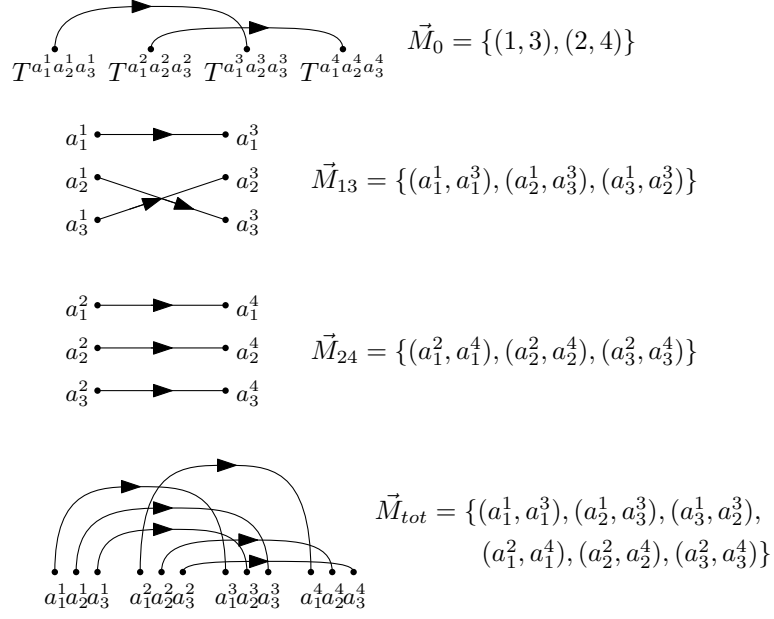


Figure 5. The construction of a pairing \vec{M}_{tot} , from a pairing \vec{M}_0 of four tensors of rank 3, as well as two pairings of indices \vec{M}_{13} and \vec{M}_{24} . In spirit, these describe propagators connecting the different tensors.

We used here the fact that, by construction, the disjoint union of the $M_{ref,ij,C}$ is equal to \vec{M}_0^D . This comes from the fact that both contract the indices of a pair of tensors present in \vec{M}_0 , respecting the position of indices (see figure 6).

Inserting (4.7) and (4.8) in (4.6), we obtain:

$$\langle I_{\vec{S}} \rangle_0 = \sum_{\substack{M_0 \in \mathbf{M}_{2p} \\ M_{tot} \in \mathbf{M}_{tot}}} \gamma_{M_{tot}} \epsilon(\vec{M}_0^D, \vec{E}(\vec{S}))^b \epsilon(\vec{M}_{tot}, \vec{M}_0^D)^b \left(\prod_{(m,n) \in \vec{M}_{tot}} g_b^{mn} \right) \left(\prod_{(k,l) \in \vec{E}(\vec{S})} g_{kl}^b \right), \quad (4.10)$$

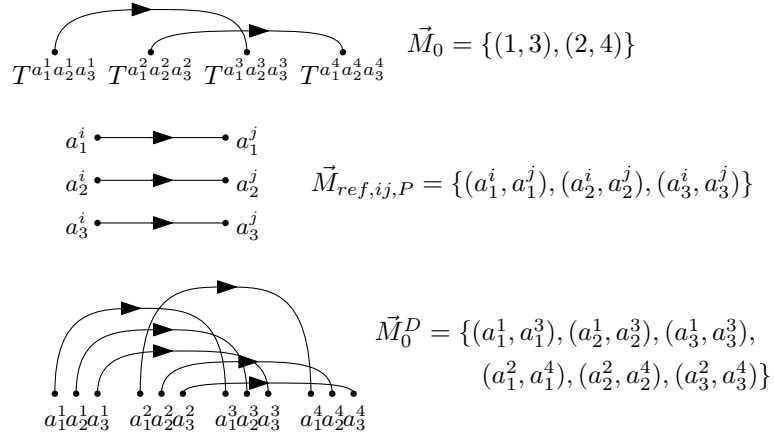


Figure 6. Illustration of the correspondence between \vec{M}_0^D and $\vec{M}_{ref,ij,C}$.

and using property (2.29) this leads to:

$$\langle I_S \rangle_0 = \sum_{\substack{M_0 \in \mathbf{M}_{2p} \\ M_{tot} \in \mathbf{M}_{tot}}} \gamma_{M_{tot}} \epsilon(\vec{M}_{tot}, \vec{E}(\vec{\mathcal{S}}))^b \left(\prod_{(m,n) \in \vec{M}_{tot}} g_b^{mn} \right) \left(\prod_{(k,l) \in \vec{E}(\vec{\mathcal{S}})} g_b^{kl} \right). \quad (4.11)$$

Adding oriented edges of a new color 0 to \mathcal{S} , according to \vec{M}_{tot} , yields a 2-color directed stranded graph $\vec{\mathcal{G}}$. We define a face in \mathcal{G} as a cycle with strands of alternating colors. Along a face, g_b and its inverse alternate and all indices are summed. Therefore, each face contributes a factor N . However, because of the graded symmetry $g_{ac}^b = (-1)^b g_{ca}^b$ a face also picks up a factor $(-1)^b$ if an odd number of strands point in one of the two directions around the face, we characterize such a face to be *odd*, otherwise a face is called *even*. The term $\left(\prod_{(m,n) \in \vec{M}_{tot}} g_b^{mn} \right) \left(\prod_{(k,l) \in \vec{E}(\vec{\mathcal{S}})} g_b^{kl} \right)$ thus contributes:

$$\left(\prod_{(m,n) \in \vec{M}_{tot}} g_b^{mn} \right) \left(\prod_{(k,l) \in \vec{E}(\vec{\mathcal{S}})} g_b^{kl} \right) = (-1)^{b F_{odd}(\vec{\mathcal{G}})} N^{F(\mathcal{G})} \quad (4.12)$$

Using property (2.31) we also rewrite the term $\epsilon(\vec{M}_{tot}, \vec{E}(\vec{\mathcal{S}}))^b$ as:

$$\epsilon(\vec{M}_{tot}, \vec{E}(\vec{\mathcal{S}}))^b = (-1)^{F_{even}(\vec{\mathcal{G}})b}, \quad (4.13)$$

where $F_{even}(\vec{\mathcal{G}})$, resp. $F_{odd}(\vec{\mathcal{G}})$, denotes the number of even, resp. odd, faces of $\vec{\mathcal{G}}$ and $F(\mathcal{G}) = F_{odd}(\vec{\mathcal{G}}) + F_{even}(\vec{\mathcal{G}})$ is the total number of faces of \mathcal{G} , which does not depend on any chosen orientation.

The expectation value $\langle I_S \rangle_0$ can thus be evaluated as a sum over 2-colored stranded graphs \mathcal{G} :

$$\langle I_S \rangle_0 = \sum_{\substack{\mathcal{G}, \mathcal{S} \subset \mathcal{G} \\ |V(\mathcal{G})| = 2pD}} \gamma_{M_{tot}} \left((-1)^b N \right)^{F(\mathcal{G})}. \quad (4.14)$$

This concludes the proof. \square

Each term in (4.4) is invariant under the transformation:

$$\mathbf{b} \rightarrow \mathbf{b} + 1 \text{ and } N \rightarrow -N. \quad (4.15)$$

Thus, this transformation does not affect the Gaußian expectation value of any invariant nor the amplitude of its graphs and is hence a duality of our model.

The invariance of the partition function under the duality follows directly from the above statement, using a perturbative expansion of the interaction part of the action:

$$\begin{aligned} Z &= \left[e^{\partial_T C \partial_T} \sum_{\{p_S \geq 0\}} \prod_S \frac{1}{p_S!} \left(\frac{\lambda_S}{|V(\mathcal{S})|/D} I_S(T) \right)^{p_S} \right]_{T=0} \\ &= \sum_{\{p_S \geq 0\}} \prod_S \frac{1}{p_S!} \left(\frac{\lambda_S}{|V(\mathcal{S})|/D} \right)^{p_S} \left\langle \prod_S I_S(T)^{p_S} \right\rangle_0. \end{aligned} \quad (4.16)$$

Since any product of invariants is a single disconnected invariant, the factor $\left\langle \prod_S I_S(T)^{p_S} \right\rangle_0$ is invariant under the duality (4.15). Hence the partition function of the model is invariant under (4.15).

As usually, expectation values of invariants are calculated by taking derivatives of $\ln Z$ with respect to the couplings λ_S (see, for example, [1, 30]). Diagrammatically, the derivative marks a 1-colored stranded subgraph of type \mathcal{S} and this leads to the conclusion stating that the expectation value of an invariant can be expressed as a formal sum over 2-colored stranded graphs (see again [30]).

5. Illustration: totally symmetric and antisymmetric tensor models

In this section, we exhibit the general duality result proved in the previous section for the particular case of totally symmetric and antisymmetric tensor models.

5.1. $O(N)$ tensor models

The vector space V is, in this case, an ordinary even (bosonic) N -dimensional real vector space and the tensor product space $V^{\otimes D}$ is an even vector space $\forall D \in \mathbb{N}$. As already explained above, the grading parameter now takes the value $\mathfrak{b} = 0$.

To the $GL(N)$ representation of totally symmetric tensors $\text{Sym}^D(V)$ of order D is associated the following Young diagram:

$$\lambda_S = \underbrace{\square \square \cdots \square}_{\text{length } D} . \quad (5.1)$$

The corresponding Young symmetrizer is: $c_S = \sum_{\sigma \in \mathfrak{S}_D} \sigma$. The projector on the $O(N)$ representation of traceless symmetric tensors is (see equation (4.21) and proposition 4.2 in [45]):

$$P_{D,N}^{(\lambda_S)} = \prod_{f=1}^{\lfloor \frac{D}{2} \rfloor} \left(1 - \frac{A_D}{(N + 2(D - f - 1))f} \right) . \quad (5.2)$$

This is a restricted version of the universal traceless projector (2.25) and it removes the trace modes after restriction to symmetrized tensors. As an element of the Brauer algebra $B_D(N)$, a propagator (\mathbf{C} in definition 5) of a symmetric $O(N)$ tensor model is proportional to the projector:

$$P_{D,N}^{(\lambda_S)} \frac{c_S}{D!} . \quad (5.3)$$

The Brauer algebra acts on tensors by permuting and contracting their indices (see again subsection 2.1).

To the $GL(N)$ representation of totally antisymmetric tensors $\Lambda^D(V)$ of order D is associated the Young diagram:

$$\lambda_\Lambda = \left. \begin{array}{c} \square \\ \square \\ \vdots \\ \square \end{array} \right\} \text{length } D . \quad (5.4)$$

The corresponding Young symmetrizer is: $c_\Lambda = \sum_{\sigma \in \mathfrak{S}_D} \text{sgn}(\sigma) \sigma$. A totally antisymmetric $O(N)$ tensor is automatically traceless, i.e. $\Lambda^D(V)$ is already an irreducible $O(N)$ representation. Thus a propagator of an antisymmetric $O(N)$ tensor model, as an element of $B_D(N)$, is proportional to the projector:

$$\frac{c_\Lambda}{D!} , \quad (5.5)$$

that acts by antisymmetrizing all indices.

5.2. $Sp(N)$ tensor models

In this case, the N -dimensional vector space V is an odd (fermionic) real super-vector space and order D tensors are bosonic if D is an even integer and fermionic if D is odd. Therefore the grading parameter now takes the value $\mathfrak{b} = 1$.

The representation of the dual tensor model with $Sp(N)$ symmetry is obtained by transposing the Young diagram: $\lambda'_S = \lambda_\Lambda$. Therefore, the dual model to the symmetric traceless $O(N)$ tensor model is

the antisymmetric traceless $Sp(N)$ tensor model. The projector onto this representation is given by:

$$P_{D,-N}^{(\lambda_\wedge)} = \prod_{f=1}^{\lfloor \frac{D}{2} \rfloor} \left(1 - \frac{A_D}{(-N + 2(D - f - 1))f} \right), \quad (5.6)$$

seen as an element of $B_D(-N)$ that differs from (5.3) by the sign of N . Recall the difference in the action of β when $\mathfrak{b} = 1$ instead of $\mathfrak{b} = 0$: the action of β on tensors differs by a factor $\eta(\beta) = (-1)^m$, where m = minimal number of crossings in β . If β is a permutation, we have $\eta(\beta) = \text{sgn}(\beta)$ and thus, the Young symmetrizer $c_S \in B_D(-N)$ acts by antisymmetrizing the indices of a tensor, whereas $c_S \in B_D(N)$ acts by symmetrization.

The dual model to the antisymmetric $O(N)$ tensor model contains tensors transforming in the symmetric representation of $Sp(N)$. Note that these tensors are also automatically traceless:

$$\omega_{a_i a_j} T^{a_1 \dots a_i \dots a_j \dots a_D} = 0, \quad (5.7)$$

because of the antisymmetry of the symplectic form. Thus, the projector is equal to 5.5, but regarded as an element of $B_D(-N)$, and acts by symmetrizing the tensors. The diagrammatic (Feynman type) expansions of a model and its dual contain exactly the same stranded graphs, but while the amplitude of a stranded graph picks up a factor N for each face in the $O(N)$ models, in the $Sp(N)$ models, each face contributes a factor $-N$. For example, the graph in figure 3 has three faces and thus contributes as N^3 in an $O(N)$ model, but $-N^3$ in an $Sp(N)$ model.

Concluding remarks. In this paper, we proved a duality between tensor models built with irreducible representations of the groups $O(N)$ and $Sp(N)$.

As a natural follow-up of this work, one could consider more general tensor models with $OSp(m, n)$ symmetries where $OSp(m, n)$ is the orthosymplectic super Lie group. The groups $O(N)$ and $Sp(N)$ studied in this paper are subgroups of $OSp(m, n)$ and are obtained when the supervector spaces are restricted to the purely even ($OSp(N, 0)$) or purely odd ($OSp(0, N)$) cases.

Moreover, another potential extensions of our present work is given by the investigation of the implications of the duality studied here for the case of the so-called tensor field theories [52]. This comes from the fact that the change $N \rightarrow -N$ could lead to new renormalization group fixed points.

Integrals over the unitary group $U(N)$, (Haar averages) are ubiquitous in random matrix theory and have e.g. applications to random circuits in quantum computing (see for examples [53]). On the mathematical side, the issue of computing analogous averages over $O(N)$ and $Sp(N)$ was studied in [54]. Thus, an interesting perspective for future work is given by the investigation of potential physical applications (such as potential applications to tensor networks) of $O(N)$ and $Sp(N)$ averages, keeping in mind the duality studied in this paper.

A. Projector of tensors with irreducible symmetry

Let us now consider an irreducible representation of $O(N)$ or $Sp(N)$ given by the Young tableau λ . The projector on this space of tensors is given by the product of the Young symmetrizer c_λ with the traceless projector \mathfrak{P}_D :

$$\begin{aligned} P_R^{a_1 \dots a_D a_{D+1} \dots a_{2D}} &= (c_\lambda \cdot \mathfrak{P}_D)^{a_1 \dots a_D a_{D+1} \dots a_{2D}} \\ &= \sum_{\substack{\alpha \text{ non-zero} \\ \text{eigenvalue of } A_D \\ \sigma \in P_\lambda, \tau \in Q_\lambda}} \left(\text{sgn}(\tau) \sigma \cdot \tau + \frac{-\text{sgn}(\tau)}{\alpha} \sigma \cdot \tau \cdot A_D \right)^{a_1 \dots a_D a_{D+1} \dots a_{2D}} \end{aligned} \quad (A.1)$$

The products of the elements σ , τ and A_D of the Brauer algebra lead to ϕ and χ , which are elements of $B_D((-1)^b N)$. We thus rewrite the terms present in P_R as:

$$\begin{aligned} \sum_{\substack{\alpha \text{ non-zero} \\ \text{eigenvalue of } A_D \\ \sigma \in P_\lambda, \tau \in Q_\lambda}} \text{sgn}(\tau) \sigma \cdot \tau &= \sum_{\phi \in P_\lambda \cdot Q_\lambda} \gamma_\phi \phi, \\ \sum_{\substack{\alpha \text{ non-zero} \\ \text{eigenvalue of } A_D \\ \sigma \in P_\lambda, \tau \in Q_\lambda}} \frac{-\text{sgn}(\tau)}{\alpha} \sigma \cdot \tau \cdot A_D &= \sum_{\chi \in P_\lambda \cdot Q_\lambda \cdot \mathbb{B}} \gamma_\chi \chi, \end{aligned} \quad (\text{A.2})$$

where \mathbb{B} is the set of elements β_{ij} of the Brauer algebra (see (2.15)), and γ_ϕ and resp. γ_χ are factors taking into account the fact that different products of σ and τ may lead to the same ϕ . We use then expression (2.32) to write:

$$P_R^{a_1 \dots a_D a_{D+1} \dots a_{2D}} = \sum_{\vec{\phi} \in \mathbb{M}_\phi} \gamma_\phi \epsilon(\vec{\phi}, \vec{M}_{ref})^b \prod_{(i,j) \in \vec{\phi}} g^{a_i a_j} + \sum_{\vec{\chi} \in \mathbb{M}_\chi} \gamma_\chi \epsilon(\vec{\chi}, \vec{M}_{ref})^b \prod_{(i,j) \in \vec{\chi}} g^{a_i a_j}, \quad (\text{A.3})$$

where the sum over the elements ϕ and χ of $B_D((-1)^b N)$ is replaced by a sum over their associated oriented pairings $\vec{\phi}$ and $\vec{\chi}$.

Thus, the projector P_R is shown to be a particular case of the general projector (3.4).

Acknowledgements. The authors warmly acknowledge Răzvan Gurău for useful discussions at various stages of this research project. T. K., T. M. and A. T. have been partially supported by the ANR-20-CE48-0018 “3DMaps” grant and by the PHC Procope program “Combinatorics of random tensors”. A. T. has been partially supported by the PN 23210101/2023 grant. H. K. has been supported by the Deutsche Forschungsgemeinschaft (DFG, German Research Foundation) under Germany’s Excellence Strategy EXC-2181/1 – 390900948 (the Heidelberg STRUCTURES Cluster of Excellence), and his mobilities were partially supported in the form of PPP France (DAAD). The authors further acknowledge support from the Institut Henri Poincaré (UAR 839 CNRS-Sorbonne Université), and LabEx CARMIN (ANR-10-LABX-59-01), where this project initiated, during the “Quantum gravity, random geometry and holography” trimester.

References

- [1] Gurau R 2017 *Random Tensors* 1st ed (Oxford: Oxford University Press) ISBN 978-0-19-878793-8
- [2] Tanasa A 2021 *Combinatorial physics* 1st ed (Oxford: Oxford University Press) ISBN 978-0-19-289549-3
- [3] Gurau R 2016 *Invitation to Random Tensors SIGMA* **12** 94 (*Preprint* 1609.06439)
- [4] Gurau R and Ryan J P 2012 *Colored Tensor Models - a Review SIGMA* **8** 20 (*Preprint* 1109.4812)
- [5] Tanasa A 2016 *The Multi-Orientable Random Tensor Model, a Review SIGMA* **12** 056 (*Preprint* 1512.02087)
- [6] Tanasa A 2012 *Tensor models, a quantum field theoretical particularization Proc. Rom. Acad. A* **13** 225–234 (*Preprint* 1211.4444)
- [7] Gurau R G 2022 *Notes on tensor models and tensor field theories Ann. Inst. H. Poincaré D: Comb. Phys. Interact.* **9** 159–218 (*Preprint* 1907.03531)

- [8] Di Francesco P, Ginsparg P H and Zinn-Justin J 1995 *2-D Gravity and random matrices Phys. Rept.* **254** 1–133 (*Preprint* [hep-th/9306153](#))
- [9] Witten E 2019 *An SYK-Like Model Without Disorder J. Phys. A* **52** 474002 (*Preprint* [1610.09758](#))
- [10] Klebanov I R and Tarnopolsky G 2017 *Uncolored random tensors, melon diagrams, and the Sachdev-Ye-Kitaev models Phys. Rev. D* **95** 046004 (*Preprint* [1611.08915](#))
- [11] Giombi S, Klebanov I R and Tarnopolsky G 2017 *Bosonic tensor models at large N and small ϵ Phys. Rev. D* **96** 106014 (*Preprint* [1707.03866](#))
- [12] Bulycheva K, Klebanov I R, Milekhin A and Tarnopolsky G 2018 *Spectra of Operators in Large N Tensor Models Phys. Rev. D* **97** 026016 (*Preprint* [1707.09347](#))
- [13] Giombi S, Klebanov I R, Popov F, Prakash S and Tarnopolsky G 2018 *Prismatic Large N Models for Bosonic Tensors Phys. Rev. D* **98** 105005 (*Preprint* [1808.04344](#))
- [14] Klebanov I R, Popov F and Tarnopolsky G 2018 *TASI Lectures on Large N Tensor Models PoS TASI2017* 004 (*Preprint* [1808.09434](#))
- [15] Gurau R 2019 *Notes on Tensor Models and Tensor Field Theories arXiv e-prints* (*Preprint* [1907.03531](#))
- [16] Harribey S 2022 *Renormalization in tensor field theory and the melonic fixed point* Ph.D. thesis Heidelberg U. (*Preprint* [2207.05520](#))
- [17] Gurau R 2012 *The complete $1/N$ expansion of colored tensor models in arbitrary dimension Ann. Henri Poincaré* **13** 399–423 (*Preprint* [1102.5759](#))
- [18] Tanasa A 2012 *Multi-orientable Group Field Theory J. Phys. A* **45** 165401 (*Preprint* [1109.0694](#))
- [19] Bonzom V, Gurau R and Rivasseau V 2012 *Random tensor models in the large N limit: Uncoloring the colored tensor models Phys. Rev. D* **85** 084037 (*Preprint* [1202.3637](#))
- [20] Carrozza S and Tanasa A 2016 *$O(N)$ Random Tensor Models Lett. Math. Phys.* **106** 1531–1559 (*Preprint* [1512.06718](#))
- [21] Benedetti D, Carrozza S, Gurau R and Kolanowski M 2019 *The $1/N$ expansion of the symmetric traceless and the antisymmetric tensor models in rank three Commun. Math. Phys.* **371** 55–97 (*Preprint* [1712.00249](#))
- [22] Carrozza S 2018 *Large N limit of irreducible tensor models: $O(N)$ rank-3 tensors with mixed permutation symmetry JHEP* **06** 39 (*Preprint* [1803.02496](#))
- [23] Carrozza S and Harribey S 2022 *Melonic Large N Limit of 5-Index Irreducible Random Tensors Commun. Math. Phys.* **390** 1219–1270 (*Preprint* [2104.03665](#))
- [24] Dartois S, Rivasseau V and Tanasa A 2013 *The $1/N$ Expansion of Multi-Orientable Random Tensor Models Annales Henri Poincaré* **15** 965–984 URL <https://doi.org/10.1007/s00023-013-0262-8>
- [25] Krajewski T, Muller T and Tanasa A 2023 *Double scaling limit of the prismatic tensor model* (*Preprint* [2301.02093](#))
- [26] Klebanov I R and Tarnopolsky G 2017 *On Large N Limit of Symmetric Traceless Tensor Models JHEP* **10** 037 (*Preprint* [1706.00839](#))

- [27] Gurau R 2018 *The $1/N$ expansion of tensor models with two symmetric tensors* *Commun. Math. Phys.* **360** 985–1007 (*Preprint* 1706.05328)
- [28] Carrozza S and Pozsgay V 2019 *SYK-like tensor quantum mechanics with $Sp(N)$ symmetry* *Nucl. Phys. B* **941** 28–52 (*Preprint* 1809.07753)
- [29] Gurau R and Keppler H 2023 *Duality of Orthogonal and Symplectic Random Tensor Models* *Ann. Inst. Henri Poincaré D : Comb. Phys. Interact.* (*Preprint* 2207.01993)
- [30] Keppler H and Muller T 2023 *Duality of Orthogonal and Symplectic Random Tensor Models: General Invariants* *Lett. Math. Phys.* **113** Paper No. 83, 15 ISSN 0377-9017,1573-0530 (*Preprint* 2304.03625)
- [31] King R C 1971 *The Dimensions of Irreducible Tensor Representations of the Orthogonal and Symplectic Groups* *Can. J. Math.* **23** 176–188
- [32] King R C 1971 *Modification Rules and Products of Irreducible Representations of the Unitary, Orthogonal, and Symplectic Groups* *Journal of Mathematical Physics* **12** 1588–1598
- [33] Cvitanović P and Kennedy A D 1982 *Spinors in Negative Dimensions* *Phys. Scripta* **26** 5
- [34] Parisi G and Sourlas N 1979 *Random Magnetic Fields, Supersymmetry, and Negative Dimensions* *Phys. Rev. Lett.* **43**(11) 744–745 URL <https://link.aps.org/doi/10.1103/PhysRevLett.43.744>
- [35] Ramgoolam S 1994 *Comment on two-dimensional $O(N)$ and $Sp(N)$ Yang-Mills theories as string theories* *Nuclear Physics B* **418** 30–44 ISSN 0550-3213 (*Preprint* 9307085)
- [36] Cvitanović P 2008 *Group Theory* (Princeton, N.J.: Princeton University Press) ISBN 978-0-691-11836-9
- [37] Mkrtchyan R L and Veselov A P 2011 *On duality and negative dimensions in the theory of Lie groups and symmetric spaces* *Journal of Mathematical Physics* **52** 083514
- [38] Mkrtchian R L 1981 *The Equivalence of $Sp(2N)$ and $SO(-2N)$ Gauge Theories* *Phys. Lett. B* **105** 174–176
- [39] LeClair A and Neubert M 2007 *Semi-Lorentz invariance, unitarity, and critical exponents of symplectic fermion models* *JHEP* **10** (*Preprint* 0705.4657)
- [40] Bond A D, Litim D F and Steudtner T 2020 *Asymptotic safety with Majorana fermions and new large N equivalences* *Phys. Rev. D* **101**(4) (*Preprint* 1911.11168)
- [41] Mulase M and Waldron A 2003 *Duality of orthogonal and symplectic matrix integrals and quaternionic Feynman graphs* *Commun. Math. Phys.* **240** 553–586 (*Preprint* math-ph/0206011)
- [42] Dunne G V 1989 *Negative-dimensional groups in quantum physics* *Journal of Physics A: Mathematical and General* **22** 1719
- [43] Abdesselam A 2012 *On the volume conjecture for classical spin networks* *Journal of Knot Theory and Its Ramifications* **12** 1250022 (*Preprint* 0904.1734)
- [44] Fulton W and Harris J 2004 *Representation theory* 9th ed Graduate texts in mathematics (New York, NY: Springer) ISBN 0-387-97495-4
- [45] Bulgakova D V, Goncharov Y O and Helpin T 2022 *Construction of the traceless projection of tensors via the Brauer algebra* *arXiv e-prints* (*Preprint* 2212.14496)

- [46] Brauer R 1937 *On Algebras Which are Connected with the Semisimple Continuous Groups* *Annals of mathematics* **38** 857–872
- [47] Wenzl H 1988 *On the Structure of Brauer’s Centralizer Algebras* *Annals of Mathematics* **128** 173–193 ISSN 0003486X
- [48] Weyl H 1997 *The Classical Groups* 2nd ed Princeton Landmarks in Mathematics and Physics (Princeton, NJ: Princeton Univ. Press) ISBN 0-691-05756-7
- [49] Bóna M (ed) 2015 *Handbook of Enumerative Combinatorics* 1st ed Discrete Mathematics and its Applications (Boca Raton, FL: CRC Press/Chapman and Hall) ISBN 978-1-4822-2085-8
- [50] Brydges D C and Slade G 2015 *A renormalisation group method* *J. Statist. Phys.* **159** 421 (*Preprint* 1403.7244)
- [51] Salmhofer M 1999 *Renormalization* Texts and monographs in physics (Berlin ; Heidelberg [u.a.]: Springer) ISBN 978-3-540-64666-2
- [52] Carrozza S 2014 *Tensorial Methods and Renormalization in Group Field Theories* (Springer International Publishing) ISBN 978-3-319-05866-5
- [53] Horodecki M, Horodecki P and Horodecki R 1999 *General teleportation channel, singlet fraction, and quasidistillation* *Phys. Rev. A* **60**(3) 1888–1898 (*Preprint* quant-ph/9807091)
- [54] Collins B and Śniady P 2006 *Integration with respect to the Haar measure on unitary, orthogonal and symplectic group* *Comm. Math. Phys.* **264** 773–795 ISSN 0010-3616,1432-0916 (*Preprint* math-ph/0402073)

The small- N series in the zero-dimensional $O(N)$ model: constructive expansions and transseries

Authors: Dario Benedetti, Răzvan Gurău, Hannes Keppeler and
Davide Lettera

Published in *Ann. Henri Poincaré* **25** (2024), 5367–5428. DOI: 10.1007/s00023-024-01437-y.
Licensed under CC BY 4.0. Reproduced with permission. Hyperlink colors removed.
Also available as e-print: arXiv 2210.14776 [hep-th].

The original idea was conceived by B. Benedetti and R. Gurău. All authors contributed to establishing the results, finding solution strategies, and calculations. H. Keppeler proved Proposition 5 and contributed substantially to the proof of Proposition 2 and decisively to the proof of Propositions 3 and 4. H. Keppeler produced Figures 1, 4 and 5. All authors contributed with corrections and suggestions to the manuscript and improvements during the review process.



The Small- N Series in the Zero-Dimensional $O(N)$ Model: Constructive Expansions and Transseries

Dario Benedetti, Razvan Gurau, Hannes Keppler  and Davide Lettera

Abstract. We consider the zero-dimensional quartic $O(N)$ vector model and present a complete study of the partition function $Z(g, N)$ and its logarithm, the free energy $W(g, N)$, seen as functions of the coupling g on a Riemann surface. We are, in particular, interested in the study of the transseries expansions of these quantities. The point of this paper is to recover such results using constructive field theory techniques with the aim to use them in the future for a rigorous analysis of resurgence in genuine quantum field theoretical models in higher dimensions. Using constructive field theory techniques, we prove that both $Z(g, N)$ and $W(g, N)$ are Borel summable functions along all the rays in the cut complex plane $\mathbb{C}_\pi = \mathbb{C} \setminus \mathbb{R}_-$. We recover the transseries expansion of $Z(g, N)$ using the intermediate field representation. We furthermore study the small- N expansions of $Z(g, N)$ and $W(g, N)$. For any $g = |g|e^{i\varphi}$ on the sector of the Riemann surface with $|\varphi| < 3\pi/2$, the small- N expansion of $Z(g, N)$ has infinite radius of convergence in N , while the expansion of $W(g, N)$ has a finite radius of convergence in N for g in a subdomain of the same sector. The Taylor coefficients of these expansions, $Z_n(g)$ and $W_n(g)$, exhibit analytic properties similar to $Z(g, N)$ and $W(g, N)$ and have transseries expansions. The transseries expansion of $Z_n(g)$ is readily accessible: much like $Z(g, N)$, for any n , $Z_n(g)$ has a zero- and a one-instanton contribution. The transseries of $W_n(g)$ is obtained using Möbius inversion, and summing these transseries yields the transseries expansion of $W(g, N)$. The transseries of $W_n(g)$ and $W(g, N)$ are markedly different: while $W(g, N)$ displays contributions from arbitrarily many multi-instantons, $W_n(g)$ exhibits contributions of only up to n -instanton sectors.

Contents

1. Introduction	5368
2. Borel Summable Series and Borel Summable Functions	5374
3. The Partition Function $Z(g, N)$	5376
3.1. Analytic Continuation and Transseries	5376
3.2. Convergent Small- N Series of $Z(g, N)$ and Transseries of Its Coefficients $Z_n(g)$	5383
4. The Free Energy $W(g, N)$	5385
4.1. Constructive Expansion	5386
4.2. Transseries Expansion	5390
4.3. Differential Equations	5393
Acknowledgements	5393
A. Asymptotic Expansions	5394
A.1. The ϕ Representation of the Partition Function	5394
B. A Simple Generalization of the Nevanlinna–Sokal Theorem	5397
C. Proofs of Propositions	5398
C.1. Properties of $Z(g, N)$	5399
C.2. Properties of $Z_n(g)$	5407
C.3. The LVE, Analyticity	5411
C.4. Borel Summability of $W_n(g)$ and $W(g, N)$ in \mathbb{C}_π	5414
C.5. Transseries Expansion of $W_n(g)$ and $W(g, N)$	5417
D. The BKAR Formula	5422
D.1. Feynman Graphs and $W(g, N)$	5423
References	5426

1. Introduction

The most famous problem of the perturbative expansion in quantum field theory is the existence of ultraviolet divergences in the amplitudes of Feynman diagrams. This is successfully dealt with using the theory of perturbative renormalization. However, even in one and zero dimensions (quantum mechanics and combinatorial models, respectively), where renormalization is not needed, perturbation theory poses another notorious challenge: in most cases the perturbative series is only an asymptotic series, with zero radius of convergence. Borel resummation is the standard strategy to address this problem, but this comes with its own subtleties. From a practical standpoint, we are often only able to compute just the first few terms in the perturbative expansion. At a more fundamental level, singularities are present in the Borel plane, associated to instantons (and renormalons in higher dimensions). The instanton singularities are not accidental: they stem from the factorial growth of the number

of Feynman diagrams with the perturbation order, which is also the origin of the divergence of the perturbation series.¹

From the resummation point of view, the most inconvenient feature of perturbation theory is that it does not naively capture contributions from non-analytical terms. For example, it is well known that instanton contributions of the type $e^{-1/g}$ ($g > 0$ being the coupling constant) can be present in the evaluation of some quantity of interest, but they are missed in the perturbative series as their Taylor expansion at $g = 0$ vanishes identically.

Such exponentially suppressed terms are the archetypal example of non-perturbative effects, and their evaluation poses an interesting challenge. Aiming to include them, but still relying for practical reasons on perturbative methods, one ends up with a more general form of asymptotic expansion, known as *transseries*, which is roughly speaking a sum of perturbative and nonperturbative sectors, for example:

$$F(g) \simeq \sum_{n \geq 0} a_n g^n + \sum_i e^{\frac{c_i}{g}} g^{\gamma_i} \sum_{n \geq 0} b_{i,n} g^n. \quad (1.1)$$

Over time it became increasingly clear that, in many examples of interest, using the theory of Borel summation for the perturbative sector it is possible to reconstruct some information about the nonperturbative ones. This relation between the perturbative and nonperturbative sectors is known as *resurgence*, and it was originally developed by Écalle in the context of ordinary differential equations [1] (see [2] for a modern review). Ideas coming from resurgence theory were extensively used in quantum field theory: for recent reviews with a quantum field theory scope, see [3–5], and in particular [6], which contains also a comprehensive list of references to applications and other reviews.

Zero-dimensional quantum field theoretical models, which are purely combinatorial models,² are useful toy models for the study of transseries expansions. Most conveniently, they allow one to set aside all the complications arising from the evaluation and renormalization of Feynman diagrams. Moreover, their partition functions and correlations typically satisfy ordinary differential equations, thus fitting naturally in the framework of Écalle's theory of resurgence. The zero-dimensional ϕ^4 , or more generally ϕ^{2k} with $k \geq 2$, models in zero dimensions have been exhaustively studied [6, 10]. From a physics perspective, the current mathematical literature on resurgence deals mainly with such zero-dimensional models.

At the opposite end, the rigorous study of the Borel summability in fully fledged quantum field theory is the object of constructive field theory [11–13]. It should come as no surprise that the generalization of results on resurgence in zero dimensions to the higher-dimensional setting is very much an open topic: while Écalle's theory can serve as good inspiration, as in [3–6], the rigorous study of resurgence in higher-dimensional quantum field theory is much more

¹The renormalon singularities specific to higher dimensions are different. They are located on the positive real axis and stem from the factorial growth of the renormalized amplitude of a family of diagrams consisting in essentially one diagram per perturbation order.

²These are for example of interest in the context of random geometry, see for example [7–9].

involved. First of all, in higher dimensions the partition function (and correlators) does not obey an ordinary differential equation, and one cannot simply invoke Écalle's theory. Moreover, the coefficients of the perturbative series are given by divergent Feynman amplitudes, which need to be renormalized, leading to a running coupling. Incorporating the effects of renormalization in the resurgence analysis is an open question (see, for instance, [14] for an investigation of resurgence in the Callan–Symanzik renormalization group equation). One thing is clear: in order to answer such questions, it is insufficient to simply invoke the current theory of resurgence, and one needs to develop new techniques adapted to the more general context of quantum field theory.

From this perspective, revisiting the resurgence in zero-dimensional models using techniques inspired by constructive field theory can be of great use. Following such route, we consider the zero-dimensional $O(N)$ model with quartic potential.³ Denoting $\phi = (\phi_a)_{a=1,\dots,N} \in \mathbb{R}^N$ a vector in \mathbb{R}^N and $\phi^2 = \sum_{a=1}^N \phi_a \phi_a$ the $O(N)$ invariant, the partition function of the model is⁴:

$$Z(g, N) = \int_{-\infty}^{+\infty} \left(\prod_{a=1}^N \frac{d\phi_a}{\sqrt{2\pi}} \right) e^{-S[\phi]}, \quad S[\phi] = \frac{1}{2}\phi^2 + \frac{g}{4!}(\phi^2)^2. \quad (1.2)$$

The $N = 1$ case has been extensively studied in [6]. One can analytically continue $Z(g, 1)$, regarded as a function of the coupling constant g , to a maximal domain in the complex plane. Subsequently, one discovers that $Z(g, 1)$ displays a branch cut at the real negative axis and that the nonperturbative contributions to $Z(g, 1)$ are captured by its discontinuity at the branch cut. A resurgent transseries is obtained when one considers g as a point on a Riemann surface with a branch point at $g = 0$. From now on we parameterize this Riemann surface as $g = |g|e^{i\varphi}$ and we choose as principal sheet $\varphi \in (-\pi, \pi)$.

An approach to the study of the partition function in Eq. (1.2) in the case $N = 1$ is to use the steepest-descent method [16, 17]. We concisely review this in Appendix A. One notes that on the principal sheet only one Lefschetz thimble contributes. As g sweeps through the principal sheet the thimble is smoothly deformed, but not in the neighborhood of the saddle point: the asymptotic evaluation of the integral is unchanged. When g reaches the negative real axis, there is a discontinuous jump in the relevant thimbles and a pair of thimbles (passing through a pair of conjugated non-trivial saddle points of the action) starts contributing, giving rise to a one-instanton sector in the transseries of $Z(g, 1)$.

³The same model has been considered in a similar context in [15], where the problem of constructing Lefschetz thimbles in the N -dimensional space have been studied. By using the intermediate field formalism, we will bypass such problem here.

⁴Note that we do not use the usual normalization $g/4$ of the interaction in the $O(N)$ model, but stick to $g/4!$ in order to facilitate the comparison with the literature on transseries which deals mostly with the $N = 1$ case for which the normalization $g/4!$ is standard. Also, we do not use the 't Hooft coupling $\lambda = gN$, which is needed for a well defined $1/N$ expansion: in this paper we keep N small.

Another approach to the transseries expansion of $Z(g, 1)$ is to use the theory of ordinary differential equations [6, 10]. It turns out that $Z(g, 1)$ obeys a second-order homogeneous linear ordinary differential equation for which $g = 0$ is an irregular singular point (e.g., [16]), giving another perspective on why the expansion one obtains is only asymptotic.

More interestingly, one can wonder what can be said about the non-perturbative contributions to the free energy, that is, the logarithm of the partition function $W(g, 1) = \ln Z(g, 1)$, or to the connected correlation functions. If we aim to study the free energy, the steepest-descent method does not generalize straightforwardly as we lack a simple integral representation for $W(g, 1)$. One can formally write $Z(g, 1)$ as a transseries and then expand the logarithm in powers of the transseries monomial $e^{\frac{c}{g}}$, thus obtaining a multi-instanton transseries. However, this is very formal, as the transseries is only an asymptotic expansion, and we would like to have a direct way to obtain the asymptotic expansion of $W(g, 1)$. The closest one can get to an integral formula for the free energy is to use the Loop Vertex Expansion (LVE) [18]. This constructive field theory expansion is a combination of the intermediate field representation with the Brydges–Kennedy–Abdesselam–Rivasseau (BKAR) formula and has successfully been used in higher-dimensional quantum field theory [19] to prove Borel summability results and even study the decay of the correlations. (Note, however, that the results of [19] concern a theory with fixed UV and IR cutoffs, bypassing the issue of the renormalization group flow.) However, deriving directly the transseries expansion of $W(g, 1)$ using the steepest-descent method on the LVE proved so far impractical. One can study the transseries expansion of $W(g, 1)$ using again the theory of ordinary differential equations as $W(g, 1)$ obeys a nonlinear ordinary differential equation [6], but this cannot be directly generalized to higher dimensions.

In this paper, we consider a general N and we revisit both the partition function $Z(g, N)$ and the free energy $W(g, N)$ from a different angle. We focus, in particular, on the small- N expansion, which provides a natural interpretation for the LVE. Such expansion could be physically interesting in higher dimensions, where the $N \rightarrow 0$ limit of the model is related to self-avoiding random walks [20], an active area of investigation in modern statistical physics [21]. However, it should be noticed that our results will not be confined to infinitesimal N , as such expansion has a finite radius of convergence (Proposition 2 below).

The aim of our paper is not to “solve the problem” of computing the transseries expansion of $Z(g, N)$ or $W(g, N)$: this can be done almost immediately using known results about special functions and classical results in resurgence theory. Our aim is to analyze these objects using techniques one can then employ in the interesting case of quantum field theory in higher dimensions. The main results of this paper are the use of the Hubbard–Stratonovich intermediate field formulation to introduce a small- N expansion (Sect. 3.2), the application of the LVE to prove analyticity and Borel summability results for the free energy (Sect. 4.1), *in N and g* , and the study of the resurgence properties of the LVE. The results of the present paper provide a proof of

concept for a set of techniques which can be employed in higher dimensions, starting in the quantum mechanical case and then moving on to quantum field theory.

The paper is organized as follows. In Sect. 2, we review the Borel summability of asymptotic series as well as the notion of Borel summable functions, deriving in the process a slight extension of the Nevanlinna–Sokal theorem.

In Sect. 3, we study $Z(g, N)$ in the intermediate field representation. This allows us to quickly prove its Borel summability along all the rays in the cut complex plane $\mathbb{C}_\pi = \mathbb{C} \setminus \mathbb{R}_-$. More importantly, the intermediate field representation provides a new perspective on the origin of the instanton contributions: in this representation, the steepest-descent contour never changes, but when g reaches the negative real axis a singularity traverses it and detaches a Hankel contour around a cut. We insist that this Hankel contour is *not* a steepest-descent contour, but it *does* contribute to the asymptotic evaluation of the integral, because the cut is an obstruction when deforming the contour of integration toward the steepest-descent path. It is precisely the Hankel contour that yields the one-instanton contribution. We then build the analytic continuation of $Z(g, N)$ to the whole Riemann surface, identify a second Stokes line, compute the Stokes data encoding the jumps in the analytic continuation at the Stokes lines and discuss the monodromy of $Z(g, N)$. Next we observe that, because in the intermediate field representation N appears only as a parameter in the action, we can perform a small- N expansion:

$$Z(g, N) = \sum_{n \geq 0} \frac{1}{n!} \left(-\frac{N}{2} \right)^n Z_n(g). \quad (1.3)$$

We thus study $Z_n(g)$ for all integer n , proving its Borel summability in \mathbb{C}_π and computing its transseries expansion in an extended sector of the Riemann surface, with $\arg(g) \in (-3\pi/2, 3\pi/2)$, which we denote $\mathbb{C}_{3\pi/2}$.

In Sect. 4, we proceed to study $W(g, N) = \ln(Z(g, N))$. We first establish its Borel summability along all the rays in \mathbb{C}_π using constructive field theory techniques. We then proceed to the small- N expansion of this object:

$$W(g, N) = \sum_{n \geq 1} \frac{1}{n!} \left(-\frac{N}{2} \right)^n W_n(g), \quad (1.4)$$

and prove that this is an absolutely convergent series in a subdomain of $\mathbb{C}_{3\pi/2}$ and that both $W(g, N)$ and $W_n(g)$ are Borel summable along all the rays in \mathbb{C}_π . Finally, in order to obtain the transseries expansion of $W_n(g)$ and $W(g, N)$ we note that $W_n(g)$ can be written in terms of $Z_n(g)$ using the Möbius inversion formula relating moments and cumulants. Because of the absolute convergence of the small- N series, it makes sense to perform the asymptotic expansion term by term, and thus, we rigorously obtain the transseries for $W(g, N)$ in a subdomain of $\mathbb{C}_{3\pi/2}$. In the Appendices we gather some technical results, and the proofs of our propositions.

Ultimately, we obtain less information on the Stokes data for $W(g, N)$ than for $Z(g, N)$. While for $Z(g, N)$ we are able to maintain analytic control in the whole Riemann surface of g , the constructive field theory techniques we

employ here allow us to keep control over $W(g, N)$ as an analytic function on the Riemann surface only up to $\varphi = \pm 3\pi/2$, that is past the first Stokes line, but not up to the second one. The reason for this is that close to $\varphi = \pm 3\pi/2$ there is an accumulation of Lee–Yang zeros, that is zeros of $Z(g, N)$, which make the explicit analytic continuation of $W(g, N)$ past this sector highly non-trivial. New techniques are needed if one aims to recover the Stokes data for $W(g, N)$ farther on the Riemann surface: an analysis of the differential equation obeyed by $W(g, N)$ similar to the one of [22] could provide an alternative way to access it directly.

One can naturally ask what is the interplay between our results at small N and the large- N nonperturbative effects, first studied for the zero-dimensional $O(N)$ model in [23] (see also [3] for a general review, and [24] for a more recent point view). This is a very interesting question: indeed, the relation between the two expansions is a bit more subtle than the relation between the small coupling and the large coupling expansions for instance. The reason is that, when building the large N series, one needs to use the 't Hooft coupling, which is a rescaling of the coupling constant by a factor of N . This changes the N -dependence of the partition function and free energy, making the relation between small- N and large- N expansions nontrivial. A good news on this front is that the analyticity domains in g becomes uniform in N when recast in terms of the 't Hooft coupling [25]. But there is still quite some work to do in order to connect the transseries analysis at small N with that at large N . However, we stress once more that, while the large- N expansion is asymptotic, the small- N expansion is convergent.

Main results. Our main results are the following:

- In Proposition 1, we study $Z(g, N)$. While most of the results in this proposition are known for $N = 1$, we recover them using the intermediate field representation (which provides a new point of view) and generalize them to arbitrary $N \in \mathbb{R}$. In particular, we uncover an interplay between $Z(g, N)$ and $Z(-g, 2 - N)$ in the transseries expansion of the partition function for general N .
- Proposition 2 deals with the function $Z_n(g)$, notably its Borel summability, transseries, and associated differential equation. To our knowledge, $Z_n(g)$ has not been studied before and all of the results presented here are new.
- Proposition 3 and 4 generalize previous results in the literature [26] on the analyticity and Borel summability of $W(g, 1)$ to $W(g, N)$ and furthermore derive parallel results for $W_n(g)$.
- Proposition 5 contains the transseries expansion of $W_n(g)$, which has not been previously considered in the literature. We also give a closed formula for the transseries expansion of $W(g, N)$.
- Lastly, in Proposition 6, we derive the tower of recursive differential equations obeyed by $W_n(g)$. This serves as an invitation for future studies of the transseries of $W_n(g)$ from an ordinary differential equations perspective.

The natural next step is to explore how this picture is altered in higher dimensions. While this is a wide open question, several lessons can be learned from our present work. First, the small N series for the free energy W obtained via the LVE will very likely be convergent; hence, one should be able to study the resurgence properties of W by first studying such properties for the “cumulants” W_n , which can be done by studying the “moments Z_n ” and using Möbius inversion. Second, for the moments Z_n , the steepest-descent contour in the intermediate σ field representation will be insensitive to the coupling constant; hence, in this representation the Stokes phenomenon will correspond to singularities crossing this fixed contour.

2. Borel Summable Series and Borel Summable Functions

When dealing with asymptotic series, a crucial notion is that of Borel summability. Less known, there exists a notion of Borel summability of *functions*, intimately related to the Borel summability of series. In this section we present a brief review of these notions, which will play a central role in the rest of the paper, as well as a slight generalization of the (optimal) Nevanlinna–Sokal theorem on Borel summability [27]. We will repeatedly use this theorem in this paper.

Notation. We use K as a dustbin notation for irrelevant (real positive) multiplicative constants, and R and ρ for the important (real positive) constants.

Borel summable series. A formal power series $A(z) = \sum_{k=0}^{\infty} a_k z^k$ is called a *Borel summable series along the positive real axis* if the series

$$B(t) = \sum_{k=0}^{\infty} \frac{a_k}{k!} t^k, \quad (2.1)$$

is absolutely convergent in some disk $|t| < \rho$ and $B(t)$ admits an analytic continuation in a strip of width ρ along the positive real axis such that for t in this strip $|B(t)| < K e^{|t|/R}$ for some real positive R . The function $B(t)$ is called the *Borel transform* of $A(z)$, and the *Borel sum* of $A(z)$ is the Laplace transform of its Borel transform:

$$f(z) = \frac{1}{z} \int_0^{\infty} dt e^{-t/z} B(t). \quad (2.2)$$

It is easy to check that the function f is analytic in a disk of diameter R tangent to the imaginary axis at the origin, $\text{Disk}_R = \{z \in \mathbb{C} \mid \text{Re}(1/z) > 1/R\}$.

Clearly, if it exists, the Borel sum of a series is unique. This raises the following question: given a function $h(z)$ whose asymptotic series at zero is the Borel summable series $A(z)$, does the Borel resummation of $A(z)$ reconstruct $h(z)$? That is, is $f(z) = h(z)$? The answer to this question is *no* in general: for instance the function $e^{-1/z}$ is asymptotic (along the positive real axis) at 0 to the Borel summable series $a_k = 0$. It turns out that one can formulate necessary and sufficient conditions for $h(z)$ which ensure that it is indeed the Borel sum of its asymptotic series, as we now recall.

Borel summable functions. A function $f : \mathbb{C} \rightarrow \mathbb{C}$ is called a *Borel summable function along the positive real axis* if it is analytic in a disk Disk_R and has an asymptotic series at 0 (which can have zero radius of convergence),

$$f(z) = \sum_{k=0}^{q-1} a_k z^k + R_q(z) , \quad (2.3)$$

such that the rest term of order q obeys the bound:

$$|R_q(z)| \leq K q! q^\beta \rho^{-q} |z|^q , \quad z \in \text{Disk}_R , \quad (2.4)$$

for some fixed $\beta \in \mathbb{R}_+$. Note that the bound in Eq. (2.4) is slightly weaker than the one in [27]. The positive real axis is selected by the position of the center of Disk_R . We call $\text{Disk}_R = \{z \in \mathbb{C} \mid \text{Re}(1/z) > 1/R\}$ a *Sokal disk*.

These two notions are intimately related: the Borel sums of Borel summable series are Borel summable functions (this is straightforward to prove). Moreover, the asymptotic series of Borel summable functions are Borel summable series.

Theorem 1 (Nevanlinna–Sokal [27], extended). *Let $f : \mathbb{C} \rightarrow \mathbb{C}$ be a Borel summable function, hence analytic and obeying the bound (2.4) with some fixed β . Then:*

- the Borel transform of the asymptotic series of f ,

$$B(t) = \sum_{k=0}^{\infty} \frac{1}{k!} a_k t^k , \quad (2.5)$$

is convergent in a disk of radius ρ in t , and it defines an analytic function in this domain.

- $B(t)$ can be analytically continued to the strip $\{t \in \mathbb{C} \mid \text{dist}(t, \mathbb{R}_+) < \rho\}$ and in this strip it obeys an exponential bound $|B(t)| < K e^{|t|/R}$.
- for all $z \in \text{Disk}_R$ we can reconstruct the function $f(z)$ by the absolutely convergent Laplace transform:

$$f(z) = \frac{1}{z} \int_0^\infty dt e^{-t/z} B(t) . \quad (2.6)$$

Proof. See Appendix B. □

We emphasize that both for series and for functions, Borel summability is directional:

- for series, Borel summability along a direction requires the unimpeded analytic continuation of $B(t)$ in a thin strip centered on that direction.
- for functions, Borel summability along a direction requires analyticity and bound on the Taylor rest terms in a Sokal disk (with 0 on its boundary) centered on that direction.

Clearly, the singularities of the Borel transform $B(t)$ are associated to directions along which the function $f(z)$ ceases to be Borel summable.

3. The Partition Function $Z(g, N)$

In this section, we collect some facts about the asymptotic expansion of the partition function (1.2). Most of them are known, or derivable from the expression of the $Z(g, N)$ in terms of special functions, whose asymptotic expansions are to a large degree known [28]. Nonetheless, we present a “path integral–like” derivation and rather explicit formulae for the coefficients that should be useful, as they are more directly generalizable, in applications to proper field theories.

We study $Z(g, N)$ by means of the Hubbard–Stratonovich intermediate field formulation [29, 30], which is crucial to the Loop Vertex Expansion [18] of the free energy $W(g, N)$ that we will study below. This is based on rewriting the quartic term of the action as a Gaussian integral over an auxiliary variable σ (or field, in higher dimensions):

$$e^{-\frac{g}{4!}(\phi^2)^2} = \int_{-\infty}^{+\infty} [d\sigma] e^{-\frac{1}{2}\sigma^2 + \imath\sqrt{\frac{g}{12}}\sigma\phi^2}, \quad (3.1)$$

where the Gaussian measure over σ is normalized, i.e., $[d\sigma] = d\sigma/\sqrt{2\pi}$ and $\imath = e^{\imath\frac{\pi}{2}}$. Note that σ is a real number, not a vector. With this trick, the integral over ϕ becomes Gaussian and can be performed for $g > 0$, leading to a rewriting of the partition function (1.2) as:

$$Z(g, N) = \int_{-\infty}^{+\infty} [d\sigma] e^{-\frac{1}{2}\sigma^2} \frac{1}{(1 - \imath\sqrt{\frac{g}{3}}\sigma)^{N/2}}. \quad (3.2)$$

Although the original partition function is defined only for integer N and we have assumed that $g > 0$, in the σ representation (3.2) it becomes transparent that $Z(g, N)$ can be analytically continued both in N and in g .

3.1. Analytic Continuation and Transseries

As a matter of notation, we denote $\varphi \equiv \arg(g)$, and, in order to label some sets that will appear repeatedly in the rest of the paper, we define:

$$\mathbb{C}_\psi \equiv \{g \in \mathbb{C}, g = |g|e^{\imath\varphi} : \varphi \in (-\psi, \psi)\}. \quad (3.3)$$

In particular, $\mathbb{C}_\pi = \mathbb{C} \setminus \mathbb{R}_-$ is the cut complex plane. For $\psi > \pi$, the set \mathbb{C}_ψ should be interpreted as a sector of a Riemann sheet, extending the principal sheet \mathbb{C}_π into the next sheets.

Our first aim is to understand the analytic continuation of the partition function in the maximal possible domain of the Riemann surface. For later convenience, we introduce the following function, not to be confused with the partition function $Z(g, N)$:

$$Z^{\mathbb{R}}(g, N) = \int_{-\infty}^{+\infty} [d\sigma] e^{-\frac{1}{2}\sigma^2} \frac{1}{\left(1 - \imath e^{\imath\frac{\varphi}{2}} \sqrt{\frac{|g|}{3}}\sigma\right)^{N/2}}, \quad \forall \varphi \neq (2k+1)\pi, k \in \mathbb{Z}, \quad (3.4)$$

which is an absolutely convergent integral for any $|g|$ and any $\varphi \neq (2k+1)\pi$. We have used a superscript \mathbb{R} to distinguish it from $Z(g, N)$ and to emphasize

that the integral is performed on the real line, irrespective of the value of $\varphi \neq (2k+1)\pi$. Moreover, for $N/2 \notin \mathbb{Z}$, the integrand is computed using the principal branch of the logarithm:

$$\ln \left(1 - e^{i\frac{\pi+\varphi}{2}} \sqrt{\frac{|g|}{3}} \sigma \right) = \frac{1}{2} \ln \left[\left(\cos \frac{\varphi}{2} \right)^2 + \left(\sin \frac{\varphi}{2} + \sqrt{\frac{|g|}{3}} \sigma \right)^2 \right] + i \operatorname{Arg} \left(1 - e^{i\frac{\pi+\varphi}{2}} \sqrt{\frac{|g|}{3}} \sigma \right), \quad (3.5)$$

where the Arg function is the principal branch of the argument, valued in $(-\pi, \pi)$. In particular, a change of variables $\sigma \rightarrow -\sigma$ shows that $Z^{\mathbb{R}}(g, N) = Z^{\mathbb{R}}(e^{2\pi i} g, N)$, which is thus a single-valued function on \mathbb{C}_{π} , with a jump at \mathbb{R}_{-} . The analytic continuation of the partition function $Z(g, N)$ will instead be a multi-valued function on \mathbb{C} , and thus require the introduction of a Riemann surface. We can view $Z^{\mathbb{R}}(g, N)$ as a periodic function on the same Riemann surface, with of course $Z(g, N) = Z^{\mathbb{R}}(g, N)$ for $g \in \mathbb{C}_{\pi}$, and $Z(g, N) \neq Z^{\mathbb{R}}(g, N)$ once one steps out of the principal Riemann sheet.

We collect all the relevant result concerning the partition function in Proposition 1. For now we restrict to N real, but the proposition can be extended to complex N with little effort.⁵ We will drop this assumption later.

Proposition 1 (Properties of $Z(g, N)$). *Let $N \in \mathbb{R}$ be a fixed parameter. The partition function $Z(g, N)$ satisfies the following properties:*

1. *for every $g \in \mathbb{C}_{\pi}$, the integral in Eq. (3.2) is absolutely convergent and bounded from above by*

$$|Z(g, N)| \leq \begin{cases} \left(\cos \frac{\varphi}{2} \right)^{-N/2}, & N \geq 0 \\ 2^{|N|/2} + \frac{2^{3|N|/4}}{\sqrt{\pi}} \frac{|g|^{N/4}}{3^{|N|/4}} \Gamma \left(\frac{|N|+2}{4} \right), & N < 0 \end{cases}; \quad (3.6)$$

hence, $Z(g, N)$ is analytic in \mathbb{C}_{π} .

2. *For $g \in \mathbb{C}_{\pi}$, the partition function is $Z(g, N) = Z^{\mathbb{R}}(g, N)$ and has the perturbative expansion:*

$$Z(g, N) \simeq \sum_{n=0}^{\infty} \frac{\Gamma(2n + N/2)}{2^{2n} n! \Gamma(N/2)} \left(-\frac{2g}{3} \right)^n, \quad (3.7)$$

where \simeq means that the equation has to be interpreted in the sense of asymptotic series, i.e.,

$$\lim_{\substack{g \rightarrow 0 \\ g \in \mathbb{C}_{\pi}}} g^{-n_{\max}} \left| Z(g, N) - \sum_{n=0}^{n_{\max}} \frac{\Gamma(2n + N/2)}{2^{2n} n! \Gamma(N/2)} \left(-\frac{2g}{3} \right)^n \right| = 0, \quad \forall n_{\max} \geq 0. \quad (3.8)$$

3. *The function $Z(g, N)$ is Borel summable along all the directions in \mathbb{C}_{π} .*

⁵For N complex with positive real part, for instance, one uses the inequality $|z^{-N/2}| \leq |\operatorname{Re}(z)|^{-\operatorname{Re}(N)/2} e^{\pi |\operatorname{Im}(N)|/2}$.

4. $Z(g, N)$ can be continued past the cut, on the entire Riemann surface. However, \mathbb{R}_- is a Stokes line, that is, the anticlockwise and clockwise analytic continuations $Z_+(g, N)$ and $Z_-(g, N)$ are not equal and cease to be Borel summable at \mathbb{R}_- . A second Stokes line is found at \mathbb{R}_+ on the second sheet. For $\varphi \notin \pi\mathbb{Z}$, the analytic continuation of the partition function to the whole Riemann surface writes:

$$2k\pi < |\varphi| < (2k+1)\pi :$$

$$\begin{aligned} Z(g, N) &= \omega_{2k} Z(e^{i(2k)\tau\pi} g, N) \\ &+ \eta_{2k} \frac{\sqrt{2\pi}}{\Gamma(N/2)} e^{i\tau\frac{\pi}{2}} e^{\frac{3}{2g}} \left(e^{i(2k+1)\tau\pi} \frac{g}{3} \right)^{\frac{1-N}{2}} Z(e^{i(2k+1)\tau\pi} g, 2-N) \\ &= \omega_{2k} Z^{\mathbb{R}}(g, N) \\ &+ \eta_{2k} \frac{\sqrt{2\pi}}{\Gamma(N/2)} e^{i\tau\frac{\pi}{2}} e^{\frac{3}{2g}} \left(e^{i(2k+1)\tau\pi} \frac{g}{3} \right)^{\frac{1-N}{2}} Z^{\mathbb{R}}(-g, 2-N), \end{aligned}$$

$$(2k+1)\pi < |\varphi| < (2k+2)\pi :$$

$$\begin{aligned} Z(g, N) &= \omega_{2k+1} Z(e^{i(2k+2)\tau\pi} g, N) \\ &+ \eta_{2k+1} \frac{\sqrt{2\pi}}{\Gamma(N/2)} e^{i\tau\frac{\pi}{2}} e^{\frac{3}{2g}} \left(e^{i(2k+1)\tau\pi} \frac{g}{3} \right)^{\frac{1-N}{2}} Z(e^{i(2k+1)\tau\pi} g, 2-N) \\ &= \omega_{2k+1} Z^{\mathbb{R}}(g, N) \\ &+ \eta_{2k+1} \frac{\sqrt{2\pi}}{\Gamma(N/2)} e^{i\tau\frac{\pi}{2}} e^{\frac{3}{2g}} \left(e^{i(2k+1)\tau\pi} \frac{g}{3} \right)^{\frac{1-N}{2}} Z^{\mathbb{R}}(-g, 2-N), \end{aligned} \quad (3.9)$$

where $\tau = -\text{sgn}(\varphi)$ and the Stokes parameters (ω, η) are defined recursively as:

$$\begin{aligned} (\omega_0, \eta_0) &= (1, 0), \quad \begin{cases} \omega_{2k+1} = \omega_{2k} \\ \eta_{2k+1} = \eta_{2k} + \omega_{2k} \end{cases}, \\ \begin{cases} \omega_{2(k+1)} = \omega_{2k+1} + \tilde{\tau} \eta_{2k+1} \\ \eta_{2(k+1)} = e^{i\tau\pi(N-1)} \eta_{2k+1} \end{cases}, \end{aligned} \quad (3.10)$$

with $\tilde{\tau} = e^{i\tau\pi\frac{N+1}{2}} 2 \sin \frac{N\pi}{2}$. The recursion gives:

$$(\omega_{2k}, \eta_{2k}) = \begin{cases} e^{i\tau\pi N \frac{k}{2}} (1, 0) & , k \text{ even} \\ e^{i\tau\pi N \frac{k+1}{2}} (1, -1) & , k \text{ odd} \end{cases}. \quad (3.11)$$

The monodromy group of $Z(g, N)$ is of order 4 if N is odd, and of order 2 if N is even. More generally, we have a monodromy group of finite order if N is a rational number, and an infinite monodromy otherwise.

5. From Properties 2 and 4, we obtain that for g in the sector $k\pi < |\varphi| < (k+1)\pi$ of the Riemann surface the partition function has the following transseries expansion:

$$\begin{aligned} Z(g, N) &\simeq \omega_k \sum_{n=0}^{\infty} \frac{\Gamma(2n+N/2)}{2^{2n} n! \Gamma(N/2)} \left(-\frac{2g}{3} \right)^n + \eta_k e^{i\tau\pi(1-\frac{N}{2})} \sqrt{2\pi} \\ &\times \left(\frac{g}{3} \right)^{\frac{1-N}{2}} e^{\frac{3}{2g}} \sum_{q \geq 0} \frac{1}{2^{2q} q! \Gamma(\frac{N}{2} - 2q)} \left(\frac{2g}{3} \right)^q, \end{aligned} \quad (3.12)$$

where we used:

$$\begin{aligned} & \Gamma(2q+1-N/2)\Gamma(N/2-2q) \\ &= \frac{\pi}{\sin(\pi \frac{N}{2} - 2\pi q)} = \Gamma(1-N/2)\Gamma(N/2). \end{aligned} \quad (3.13)$$

The transseries displays an additional property: the instanton series is obtained from the perturbative one by substituting $N \rightarrow 2-N$ and $g \rightarrow -g$ and vice versa.

6. From Property 5, the discontinuity of the partition function at the negative real axis:

$$\text{disc}_\pi(Z(g, N)) \equiv \lim_{g \rightarrow \mathbb{R}_-} \left(Z_-(g, N) - Z_+(g, N) \right), \quad (3.14)$$

has the following asymptotic expansion:

$$\begin{aligned} \text{disc}_\pi(Z_n(g)) &\simeq \frac{e^{-\frac{3}{2|g|}}}{\sqrt{2\pi}} \sqrt{\frac{|g|}{3}} \sum_{q=0}^{\infty} \sum_{p=0}^n \frac{1}{q!} \left(-\frac{|g|}{6} \right)^q \binom{n}{p} \frac{d^p \Gamma(z)}{dz^p} \Big|_{z=2q+1} \\ &\times \left[\left(\ln \left| \frac{g}{3} \right| - i\pi \right)^{n-p} - \left(\ln \left| \frac{g}{3} \right| + i\pi \right)^{n-p} \right]. \end{aligned} \quad (3.15)$$

where for N even integer the sum truncates at $q = N/4 - 1$, if N is a multiple of 4, and at $q = \lfloor N/4 \rfloor$ otherwise.

7. The partition function obeys an homogenous linear ordinary differential equation:

$$\begin{aligned} & 16g^2 Z''(g, N) + ((8N+24)g + 24) Z'(g, N) \\ & + N(N+2)Z(g, N) = 0, \end{aligned} \quad (3.16)$$

which can be used to reconstruct the resurgent transseries expansion of $Z(g, N)$.

Proof. See Appendix C.1. □

The proof of this proposition is quite technical. The most interesting points come at Property 4. While the full details can be found in Appendix C.1, we discuss here how the Stokes phenomenon arises in the intermediate field representation.

In order to obtain the asymptotic approximation of an integral, we need to deform the integration contour to steepest-descent contours (or Lefschetz thimbles) where the Laplace method can be applied. An integration contour will in principle intersect several steepest-ascent (upwards) paths of several saddle points and it must then be deformed (i.e., relaxed under the gradient flow) to run along the thimbles of these saddle points [6,17]. When varying some parameter continuously, the relevant thimbles can collide and change discontinuously leading to discontinuous changes of the asymptotic regimes at Stokes lines. This is exactly the picture in the ϕ representation of the partition function, which we recall in Appendix A.

In the σ representation the picture is different. Let us go back to Eq. (3.2) expressing $Z(g, N)$ as an integral over the real line. The partition function

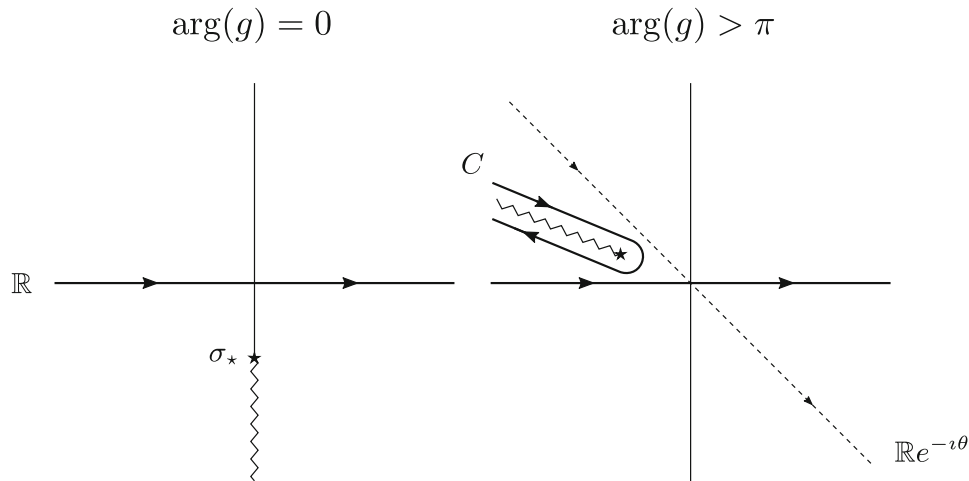


FIGURE 1. As $\arg(g)$ increases, the branch cut moves clockwise in the complex σ -plane. When g crosses the negative real axis, the tilted contour is equivalent to a Hankel contour C plus the original contour along the real line (3.17)

$Z(g, N)$ is analytically continued to the extended Riemann sheet $\mathbb{C}_{3\pi/2}$ by tilting the integration contour to $e^{-i\theta}\sigma$, respectively $e^{i\theta}\sigma$, with $\theta > 0$ for its anticlockwise, respectively clockwise, analytic continuations $Z_+(g, N)$ and $Z_-(g, N)$.

In this representation, the Lefschetz thimble is always the real axis, irrespective of g . In fact, as g goes to zero, the Laplace method instructs us to look for the saddle point of the exponent in the integrand (the function $f(x)$ in Eq. (A.1)), which in this case is a simple quadratic function,⁶ while the subexponential function (the function $a(x)$ in Eq. (A.1)) is irrelevant for the determination of the saddle points. However, what happens is that the integrand has a branch point (or pole for N a positive even integer) and this point crosses the thimble at the Stokes line. This is depicted in Fig. 1.

In detail, as long as $g = |g|e^{i\varphi} \in \mathbb{C}_\pi$, the integral converges because the branch point $\sigma_* = -i\sqrt{3/g}$ with branch cut $\sigma_* \times (1, +\infty)$ lies outside the integration contour. As g approaches \mathbb{R}_- , the branch point hits the contour of integration: for $\varphi \nearrow \pi$ the branch point hits the real axis at $-\sqrt{3/|g|}$. The analytic continuation $Z_+(g, N)$ consists in tilting the contour of integration in σ to avoid the collision with the branch point. However, in order to derive the asymptotic behavior of $Z_+(g, N)$, we need to deform the integration contour back to the thimble, which is always the real axis. Once g passes on the second Riemann sheet ($\varphi > \pi$), when deforming the tilted contour to the real axis we

⁶This is perhaps more clear after rescaling σ by $1/\sqrt{g}$ to cast our integral in the same form as Eq. (A.1).

generate an additional Hankel contour (see Fig. 1):

$$\begin{aligned} Z_{\pm}(g, N)|_{\varphi \begin{smallmatrix} > \pi \\ < -\pi \end{smallmatrix}} &= \int_{e^{\mp i\theta}\mathbb{R}} [d\sigma] \frac{e^{-\frac{1}{2}\sigma^2}}{(1 - i\sqrt{\frac{g}{3}}\sigma)^{N/2}} = Z^{\mathbb{R}}(g, N) + Z_{\pm}^C(g, N) \\ Z^{\mathbb{R}}(g, N) &= \int_{\mathbb{R}} [d\sigma] e^{-\frac{1}{2}\sigma^2} \frac{1}{(1 - i\sqrt{\frac{g}{3}}\sigma)^{N/2}}, \\ Z_{\pm}^C(g, N) &= \int_C [d\sigma] e^{-\frac{1}{2}\sigma^2} \frac{1}{(1 - i\sqrt{\frac{g}{3}}\sigma)^{N/2}}, \end{aligned} \quad (3.17)$$

where the Hankel contour C turns clockwise around the cut $\sigma_{\star} \times (1, +\infty)$, i.e., starting at infinity with argument $\frac{3\pi}{2} - \frac{\varphi}{2}$ and going back with argument $-\frac{\pi}{2} - \frac{\varphi}{2}$ after having encircled the branch point σ_{\star} . We kept a subscript \pm for the contribution of the Hankel contour, because, even though the definition of $Z_{\pm}^C(g, N)$ and C might suggest that it is one single function of g , in fact the integral around the cut is divergent for $|\varphi| < \pi/2$, and therefore, the integrals at $\pi < \varphi < 3\pi/2$ and at $-\pi > \varphi > -3\pi/2$ are *not* the analytic continuation of each other. This fact is reflected in the τ -dependence of the asymptotic expansion in Eq. (3.12).

The appearance of the Hankel contour marks a discontinuity of the contour of integration in σ as a function of the argument of g , which translates into a discontinuity of the asymptotic expansion of $Z(g, N)$, that is, a Stokes phenomenon. We insist that the Hankel contour is *not* a thimble for the integral in Eq. (3.2), but it *contributes* to the asymptotic evaluation of the integral, providing the one-instanton contribution in the transseries of $Z(g, N)$.

In order to go beyond $|\varphi| = 3\pi/2$, one notices that we can analytically continue separately $Z^{\mathbb{R}}(g, N)$ and $Z_{\pm}^C(g, N)$. The first is analytic in the range $|\varphi| \in (\pi, 3\pi)$, where its asymptotic expansion is just the standard perturbative series. The analytic continuation of $Z_{\pm}^C(g, N)$ is not immediate in the Hankel contour representation, which is only convergent for $\pi/2 < |\varphi| < 3\pi/2$, but after resolving the discontinuity at the cut and using again the Hubbard–Stratonovich trick (as detailed in Appendix C.1), it turns out that it can be rewritten as:

$$Z_{\pm}^C(g, N) = e^{i\tau\pi(1-\frac{N}{2})} \left(\frac{g}{3}\right)^{\frac{1-N}{2}} e^{\frac{3}{2g}} \frac{\sqrt{2\pi}}{\Gamma(N/2)} Z(e^{i\tau\pi}g, 2-N). \quad (3.18)$$

with $\tau = -\text{sgn}(\varphi)$. In this form it is manifest that $Z_{\pm}^C(g, N)$ is analytic in g as long as $e^{i\tau\pi}g$ belongs to the principal sheet of the Riemann surface, that is for $\pi < |\varphi| < 2\pi$. We have thus shown that, when going from $|\varphi| < \pi$ to $\pi < |\varphi| < 2\pi$, our analytic continuation of $Z(g, N)$ switches:

$$\begin{aligned} Z(g, N) &\xrightarrow{|\varphi| \nearrow \pi_+} Z^{\mathbb{R}}(g, N) + \frac{\sqrt{2\pi}}{\Gamma(N/2)} e^{i\tau\frac{\pi}{2}} e^{\frac{3}{2g}} \left(e^{i\tau\pi}\frac{g}{3}\right)^{\frac{1-N}{2}} Z^{\mathbb{R}}(-g, 2-N) \\ &= Z(e^{i(2\tau\pi)}g, N) + \frac{\sqrt{2\pi}}{\Gamma(N/2)} e^{i\tau\frac{\pi}{2}} e^{\frac{3}{2g}} \left(e^{i\tau\pi}\frac{g}{3}\right)^{\frac{1-N}{2}} Z(e^{i\tau\pi}g, 2-N), \end{aligned} \quad (3.19)$$

where we explicitly exhibited the argument at which the switching takes place. In the second line above, for $\pi < |\varphi| < 2\pi$, both arguments $e^{i(2\tau\pi)}g$ and $e^{i\tau\pi}g$ belong to the principal sheet of the Riemann surface, where $Z(g, N)$ has already been constructed and proven to be analytic. The first term in Eq. (3.19) is regular up to $|\varphi| = 3\pi$, but the second one has a problem when $e^{i\tau\pi}g$ reaches the negative real axis and retracing our steps we conclude that the analytic continuation switches again:

$$Z(e^{i\tau\pi}g, 2 - N) \xrightarrow{|\varphi| \nearrow 2\pi+} Z(e^{i(3\tau\pi)}g, 2 - N) + \frac{\sqrt{2\pi}}{\Gamma(1 - N/2)} e^{i\tau\frac{\pi}{2}} e^{\frac{3}{2g}e^{i\tau\pi}} \left(e^{i(2\tau\pi)}\frac{g}{3} \right)^{\frac{N-1}{2}} Z(e^{i(2\tau\pi)}g, N), \quad (3.20)$$

where this time the arguments at which Z is evaluated on the right hand side stay in the principal sheet for $2\pi < |\varphi| < 3\pi$. Iterating, one obtains the analytic continuation to the whole Riemann surface.

Remark 1. The differential equation (3.16) can be solved in terms of special functions. For $N = 1$, setting $Z(g, 1) = \sqrt{\frac{3}{2\pi g}} e^{\frac{3}{4g}} f(\frac{3}{4g})$, we find that the equation reduces to a modified Bessel's equation for $f(z)$:

$$z^2 f''(z) + z f'(z) - \left(z^2 + \frac{1}{16} \right) f(z) = 0. \quad (3.21)$$

Its two linearly independent solutions are the modified Bessel functions of the first and second kind of order $1/4$. However, only the second, $K_{1/4}(z)$, decays for $z \rightarrow \infty$; hence, the initial condition $Z(0, 1) = 1$ fixes $f(z) = K_{1/4}(z)$.

Similarly, for general N , we find that setting $Z(g, N) = (\frac{3}{2g})^{N/4} f(\frac{3}{2g})$ the differential equation reduces to Kummer's equation for $f(z)$:

$$z f''(z) + \left(\frac{1}{2} - z \right) f'(z) - \frac{N}{4} f(z) = 0. \quad (3.22)$$

With the addition of the initial condition $Z(0, N) = 1$, we find that the solution is given by the Tricomi confluent hypergeometric function $f(z) = U(N/4, 1/2, z)$, whose transseries expansion can easily be obtained order by order. However, such expressions of the partition function in terms of special functions do not generalize to quantum field theory. Similarly, even the more general resurgence theory for formal solutions of ordinary differential equations will be of limited use in that context, as the partition function of a quantum field theory model does not satisfy an ordinary differential equation. For this reason, while displaying for completeness the relevant ordinary differential equations, in this work we do not make use of them and rather refer to the literature (see references in [6]).

Our result (3.12) provides a useful repackaging of the transseries expansion of the partition function and an alternative derivation that should be more easily generalizable to quantum field theory.

3.2. Convergent Small- N Series of $Z(g, N)$ and Transseries of Its Coefficients $Z_n(g)$

We will now study the discontinuity of $Z(g, N)$ from a different perspective. We expand the integrand of Eq. (3.2) in powers of N and exchange the order of summation and integration:

$$Z(g, N) = \sum_{n \geq 0} \frac{1}{n!} \left(-\frac{N}{2}\right)^n Z_n(g), \quad Z_n(g) = \int_{-\infty}^{+\infty} [d\sigma] e^{-\frac{1}{2}\sigma^2} \left(\ln\left(1 - \imath \sqrt{\frac{g}{3}}\sigma\right)\right)^n. \quad (3.23)$$

Unlike the usual perturbative expansions in g , this is a convergent expansion: from the bound in Property 1 of Proposition 2 below, the Gaussian integral and the sum can be commuted due to Fubini's Theorem. As a function of N , we can regard $Z(g, N)$ as a generating function of “moments”: unlike the usual moments, we are dealing with expectations of powers of the logarithm.

Proposition 2 (Properties of $Z_n(g)$). *The $Z_n(g)$, $n \in \mathbb{N}_{\geq 0}$ satisfy the following properties:*

1. $Z_n(g)$ is analytic in the cut plane \mathbb{C}_π . Indeed, for every $g \in \mathbb{C}_\pi$, the integral (3.23) is absolutely convergent and bounded from above by:

$$|Z_n(g)| \leq K^n \frac{\left(|\ln(\cos \frac{\varepsilon}{2})| + 1\right)^n}{\varepsilon^n} \left(1 + |g|^{\frac{n\varepsilon}{2}} \Gamma\left(\frac{n\varepsilon+1}{2}\right)\right), \quad (3.24)$$

for any $\varepsilon > 0$ and with K some g -independent constant. Using this bound with some fixed $\varepsilon < 2$ shows that, $\forall g \in \mathbb{C}_\pi$ the series in Eq. (3.23) has infinite radius of convergence in N .

2. For $g \in \mathbb{C}_\pi$, $Z_n(g)$ has the perturbative expansion:

$$\begin{aligned} Z_n(g) &\simeq \sum_{m \geq n/2} \left(-\frac{2g}{3}\right)^m \frac{(2m)!}{2^{2m}m!} \sum_{\substack{m_1, \dots, m_{2m-n+1} \geq 0 \\ \sum k m_k = 2m, \sum m_k = n}} \frac{(-1)^n n!}{\prod_k k^{m_k} m_k!} \\ &\equiv Z_n^{\text{pert.}}(g). \end{aligned} \quad (3.25)$$

3. The functions $Z_n(g)$ are Borel summable along all the directions in \mathbb{C}_π .
4. $Z_n(g)$ can be continued past the cut on the extended Riemann sheet $\mathbb{C}_{3\pi/2}$, and the small- N series has infinite radius of convergence in N in this domain. However, \mathbb{R}_- is a Stokes line and the anticlockwise and clockwise analytic continuations $Z_{n+}(g)$ and $Z_{n-}(g)$ are not equal and cease to be Borel summable at \mathbb{R}_- .
5. For $g \in \mathbb{C}_{3\pi/2}$, $Z_n(g)$ has the following transseries expansion:

$$Z_n(g) \simeq Z_n^{\text{pert.}}(g) + \eta e^{\frac{3}{2g}} Z_n^{(\eta)}(g), \quad (3.26)$$

with $Z_n^{\text{pert.}}(g)$ as in Eq. (3.25), and:

$$\begin{aligned} Z_n^{(\eta)}(g) &= \frac{\imath}{\sqrt{2\pi}} \sqrt{\frac{g}{3}} \sum_{q=0}^{\infty} \sum_{p=0}^n \frac{1}{q!} \left(\frac{g}{6}\right)^q \binom{n}{p} \frac{d^p \Gamma(z)}{dz^p} \Big|_{z=2q+1} \\ &\quad \times \left[\left(\ln\left(e^{\imath\tau\pi} \frac{g}{3}\right) - \imath\pi\right)^{n-p} - \left(\ln\left(e^{\imath\tau\pi} \frac{g}{3}\right) + \imath\pi\right)^{n-p} \right], \end{aligned} \quad (3.27)$$

with $\tau = -\text{sgn}(\varphi)$ and η a transseries parameter which is zero on the principal Riemann sheet and one if $|\varphi| > \pi$. Proceeding in parallel to Proposition 1, one can study the full monodromy of $Z_n(g)$.

6. The discontinuity on the negative axis has the following asymptotic expansion:

$$\begin{aligned} \text{disc}_\pi(Z_n(g)) &\simeq \frac{e^{-\frac{3}{2|g|}}}{\sqrt{2\pi}} \sqrt{\frac{|g|}{3}} \sum_{q=0}^{\infty} \sum_{p=0}^n \frac{1}{q!} \left(-\frac{|g|}{6}\right)^q \binom{n}{p} \frac{d^p \Gamma(z)}{dz^p} \Big|_{z=2q+1} \\ &\quad \times \left[\left(\ln \left|\frac{g}{3}\right| - i\pi\right)^{n-p} - \left(\ln \left|\frac{g}{3}\right| + i\pi\right)^{n-p} \right]. \end{aligned} \quad (3.28)$$

Summing over n , the discontinuity of the partition function (3.15) is recovered.

7. The functions $Z_n(g)$ obey a tower of linear, inhomogeneous ordinary differential equations:

$$\begin{aligned} Z_0(g) &= 1, \\ 4g^2 Z_1''(g) + 6(g+1) Z_1'(g) &= 1, \\ 4g^2 Z_n''(g) + 6(g+1) Z_n'(g) &= n(4g Z_{n-1}'(g) + Z_{n-1}(g)) \\ &\quad - n(n-1) Z_{n-2}(g). \end{aligned} \quad (3.29)$$

which can be used to reconstruct the resurgent transseries expansion of $Z_n(g)$.

Proof. See Appendix C.2 □

As with Proposition 1, the most interesting points are Properties 4 and 5. Again the analytic continuations $Z_{n\pm}(g)$ of $Z_n(g)$ to the extended Riemann sheet $\mathbb{C}_{3\pi/2}$ are obtained by tilting the integration contour to $e^{\mp i\theta}\sigma$ with $\theta > 0$. The branch point σ_* of the integrand in Eq. (3.23) crosses the real axis when g reaches \mathbb{R}_- , and deforming the tilted contours back to the real axis detaches Hankel contours around the cut $\sigma_* \times (1, +\infty)$:

$$\begin{aligned} Z_{n\pm}(g) \Big|_{\varphi_{<-\pi}} &= \int_{e^{\mp i\theta}\mathbb{R}} [d\sigma] e^{-\frac{1}{2}\sigma^2} \left(\ln \left(1 - i\sqrt{\frac{g}{3}}\sigma \right) \right)^n = Z_n^{\mathbb{R}}(g) + Z_{n\pm}^C(g) \\ Z_n^{\mathbb{R}}(g) &= \int_{\mathbb{R}} [d\sigma] e^{-\frac{1}{2}\sigma^2} \left(\ln \left(1 - i\sqrt{\frac{g}{3}}\sigma \right) \right)^n, \\ Z_{n\pm}^C(g) &= \int_C [d\sigma] e^{-\frac{1}{2}\sigma^2} \left(\ln \left(1 - i\sqrt{\frac{g}{3}}\sigma \right) \right)^n. \end{aligned} \quad (3.30)$$

The transseries of $Z_n(g)$ is obtained by summing the asymptotic expansions of the two pieces:

$$Z_n^{\mathbb{R}}(g) \simeq Z_n^{\text{pert.}}(g), \quad Z_{n\pm}^C(g) \simeq e^{\frac{3}{2g}} Z_n^{(\eta)}(g) \Big|_{\tau=\mp 1}.$$

Notice that the homogeneous equation in Property 7 in Proposition 2 is the same for all $n \geq 1$, and it admits an exact solution in the form of a

constant plus an imaginary error function:

$$4g^2 Z_1''(g) + 6(g+1)Z_1'(g) = 0 \quad \Rightarrow \quad Z_1(g) = c_1 + c_2 \int_0^{\imath\sqrt{\frac{3}{2g}}} e^{-t^2} dt. \quad (3.31)$$

The asymptotic expansion of the error function reproduces the one-instanton contribution of Eq. (3.26) for $n = 1$. For $n > 1$, instead, this is only part of the instanton contribution, the rest being generated by the recursive structure of the inhomogeneous equations. Similarly, the perturbative expansion comes from the special solution to the inhomogeneous equation, even at $n = 1$, as for those we cannot match exponential terms with the right-hand side. For $n > 1$ the homogeneous equation remains the same, but the inhomogeneous part depends on the solutions to previous equations, and thus, it can also contain exponential terms.

4. The Free Energy $W(g, N)$

We now turn to the free energy $W(g, N) = \ln Z(g, N)$. Our aim is find the equivalent of the results listed in Proposition 1, in the case of $W(g, N)$. Taking the logarithm has drastic effects: the nonperturbative effects encountered in $W(g, N)$ are significantly more complicated than the ones encountered for $Z(g, N)$. One can understand this from the fact that the linear differential equation satisfied by $Z(g, N)$ translates into a nonlinear one for $W(g, N)$, leading to an infinite tower of multi-instanton sectors in the transseries [6]. Here we will follow a different route, based on the small- N expansion.

Much like the partition function $Z(g, N)$, its logarithm $W(g, N)$ can also be expanded in N :

$$W(g, N) = \ln(Z(g, N)) \equiv \sum_{n \geq 1} \frac{1}{n!} \left(-\frac{N}{2}\right)^n W_n(g). \quad (4.1)$$

The coefficients $W_n(g)$ can be computed in terms of $Z_n(g)$. As already mentioned, $Z_n(g)$ are the moments of the random variable $\ln(1 - \imath\sqrt{g/3}\sigma)$; hence, W_n are the cumulants of the same variable and can be computed in terms of $Z_n(g)$ by using the Möbius inversion formula (which in this case becomes the moments-cumulants formula). Let us denote π a partition of the set $\{1, \dots, n\}$, $b \in \pi$ the parts in the partition, $|\pi|$ the number of parts of π and $|b|$ the cardinal of b . Then:

$$Z_n(g) = \sum_{\pi} \prod_{b \in \pi} W_{|b|}(g), \quad W_n(g) = \sum_{\pi} \lambda_{\pi} \prod_{b \in \pi} Z_{|b|}(g), \quad (4.2)$$

where $\lambda_{\pi} = (-1)^{|\pi|-1}(|\pi| - 1)!$ is the Möbius function on the lattice of partitions. Grouping together the partitions having the same number n_i of parts of

size i , this becomes⁷

$$\begin{aligned}
 Z_n(g) &= \sum_{\substack{n_1, \dots, n_n \geq 0 \\ \sum i n_i = n}} \frac{n!}{\prod_i n_i! (i!)^{n_i}} \prod_{i=1}^n W_i(g)^{n_i}, \\
 W_n(g) &= \sum_{k=1}^n (-1)^{k-1} (k-1)! \sum_{\substack{n_1, \dots, n_{n-k+1} \geq 0 \\ \sum i n_i = n, \sum n_i = k}} \frac{n!}{\prod_i n_i! (i!)^{n_i}} \prod_{i=1}^{n-k+1} Z_i(g)^{n_i}.
 \end{aligned} \tag{4.3}$$

Equation (4.3) relates $W_n(g)$ and $Z_n(g)$ as analytic functions of g . However, this translates into a relation between $W(g, N)$ and $Z(g, N)$ which holds only *in the sense of formal power series in N* . Even though $Z(g, N)$ is analytic in some domain, one cannot conclude that $W(g, N)$ is also analytic in the same domain: convergence of the series defining $Z(g, N)$ does not imply convergence of the series defining $W(g, N)$ in Eq. (4.1). This can most readily be seen at the zeros of the partition function, the so-called Lee–Yang zeros, which are singular points for the free energy. In order to study the analyticity properties of $W(g, N)$ one needs to use a completely different set of tools. However, as we will see below, the Möbius inversion has its own uses: it is the most direct way to access the transseries expansion of $W(g, N)$.

4.1. Constructive Expansion

The following Proposition 3 is a slight variation on the Loop Vertex Expansion (LVE) introduced in [18] (see also [26] for more details). It gives an integral representation for $W_n(g)$ in Eq. (4.1) which allows us to prove that $W(g, N)$ is convergent (hence analytic) in a bounded domain on the extended Riemann sheet $\mathbb{C}_{3\pi/2}$, wrapping around the branch point at the origin.

In Proposition 1 we fixed N to be a real parameter. However, Eq. (3.23) writes $Z(g, N)$ as an expansion in N with a nonzero (infinite!) radius of convergence in N , as long as $|\varphi| < 3\pi/2$ (note that the bound in Property 1 of Proposition 2 suffices only for $|\varphi| < \pi$; in order to reach $|\varphi| < 3\pi/2$, one needs to use the improved bound in Eq. (C.42)). We can therefore extend N to a larger domain in the complex plane. As the following proposition shows, something similar applies also to $W(g, N)$, but with a finite radius of convergence.

Notation. Let us denote T_n the set of combinatorial trees with n vertices labeled $1, \dots, n$. There are $\frac{(n-2)!}{\prod_{i=1}^n (d_i-1)!}$ trees over n labeled vertices with coordination d_i at the vertex i and $\sum_i d_i = 2(n-1)$. The total number of trees in T_n is n^{n-2} . Let $\mathcal{T} \in T_n$ be such a tree. We denote $P_{k-l}^{\mathcal{T}}$ the (unique) path in the

⁷This can also be obtained directly from Faà di Bruno's formula:

$$\frac{d^n}{du^n} \ln Z|_{u=0} = \sum_{\substack{n_1, \dots, n_n \geq 0 \\ \sum i n_i = n}} \frac{n!}{\prod_i n_i! (i!)^{n_i}} (n_1 + \dots + n_n - 1)! \frac{(-1)^{n_1 + \dots + n_n - 1}}{Z^{n_1 + \dots + n_n}} \prod_{i \geq 1} [Z^{(i)}]^{n_i} |_{u=0},$$

noticing that for $u = -N/2$, we have $Z^{(i)} = Z_i$.

tree \mathcal{T} connecting the vertices k and l . If we associate to each edge $(k, l) \in \mathcal{T}$ a variable u_{kl} between 0 and 1, we can define the $n \times n$ matrix $w^{\mathcal{T}}$:

$$w_{kl}^{\mathcal{T}} \equiv \begin{cases} 1, & \text{if } k = l \\ \inf_{(i,j) \in P_{k-l}^{\mathcal{T}}} \{u_{ij}\}, & \text{else} \end{cases}. \quad (4.4)$$

The matrix $w^{\mathcal{T}}$ is a positive matrix for any choice of u parameters and is strictly positive outside a set of measure 0 (see Appendix D for more details). Of course the matrix w depends on u , but we suppress this in order to simplify the notation.

Proposition 3 (The LVE, analyticity). *Let N be a fixed complex parameter and let us denote $g = |g|e^{i\varphi}$. The cumulants $W_n(g)$ can be written as:*

$$\begin{aligned} W_1(g) &= Z_1(g) = \int_{-\infty}^{+\infty} [d\sigma] e^{-\frac{1}{2}\sigma^2} \ln \left[1 - i\sqrt{\frac{g}{3}}\sigma \right], \\ W_n(g) &= - \left(\frac{g}{3}\right)^{n-1} \sum_{\mathcal{T} \in T_n} \int_0^1 \prod_{(i,j) \in \mathcal{T}} du_{ij} \int_{-\infty}^{+\infty} \frac{\prod_i [d\sigma_i]}{\sqrt{\det w^{\mathcal{T}}}} e^{-\frac{1}{2} \sum_{i,j} \sigma_i (w^{\mathcal{T}})^{-1}_{ij} \sigma_j} \\ &\quad \times \prod_i \frac{(d_i - 1)!}{(1 - i\sqrt{\frac{g}{3}}\sigma_i)^{d_i}}, \end{aligned} \quad (4.5)$$

where we note that the Gaussian integral over σ is well defined, as $w^{\mathcal{T}}$ is positive, and normalized. Furthermore:

1. The functions $W_n(g), n \geq 2$ are bounded by:

$$|W_n(g)| \leq \frac{(2n-3)!}{(n-1)!} \left| \frac{g}{3(\cos \frac{\varphi}{2})^2} \right|^{n-1}. \quad (4.6)$$

Therefore, they are analytic in the cut plane \mathbb{C}_π .

2. The series

$$W(g, N) = \sum_{n \geq 1} \frac{1}{n!} \left(-\frac{N}{2}\right)^n W_n(g) \quad (4.7)$$

is absolutely convergent in the following cardioid domain:

$$\mathbb{D}_0 = \left\{ g \in \mathbb{C}, g = |g|e^{i\varphi} : |g| < \frac{1}{|N|} \frac{3}{2} (\cos \frac{\varphi}{2})^2 \right\}. \quad (4.8)$$

3. $W_n(g)$ can be analytically continued to a subdomain of the extended Riemann sheet $\mathbb{C}_{3\pi/2}$ by tilting the integration contours to $\sigma \in e^{-i\theta}\mathbb{R}$:

$$\begin{aligned} W_{1\theta}(g) &= e^{-i\theta} \int_{-\infty}^{+\infty} [d\sigma] e^{-\frac{1}{2}e^{-2i\theta}\sigma^2} \ln \left(1 - i\sqrt{\frac{g}{3}}e^{-i\theta}\sigma \right), \\ W_{n\theta}(g) &= - \left(\frac{g}{3}\right)^{n-1} \sum_{\mathcal{T} \in T_n} \int_0^1 \prod_{(i,j) \in \mathcal{T}} du_{ij} \\ &\quad \times \int_{\mathbb{R}} \frac{\prod_i e^{-i\theta} [d\sigma_i]}{\sqrt{\det w^{\mathcal{T}}}} e^{-\frac{1}{2}e^{-2i\theta} \sum_{i,j} \sigma_i (w^{\mathcal{T}})^{-1}_{ij} \sigma_j} \prod_i \frac{(d_i - 1)!}{(1 - i\sqrt{\frac{g}{3}}e^{-i\theta}\sigma_i)^{d_i}}. \end{aligned} \quad (4.9)$$

4. For $n \geq 2$ we have the following bound:

$$|W_{n\theta}(g)| \leq \frac{(2n-3)!}{(n-1)!} \frac{1}{\sqrt{\cos(2\theta)}} \left| \frac{g}{3\sqrt{\cos(2\theta)} \left(\cos \frac{\varphi-2\theta}{2}\right)^2} \right|^{n-1}. \quad (4.10)$$

5. The series

$$W_\theta(g, N) = \sum_{n \geq 1} \frac{1}{n!} \left(-\frac{N}{2}\right)^n W_{n\theta}(g), \quad (4.11)$$

is absolutely convergent in the following domain:

$$\mathbb{D}_\theta = \left\{ g \in \mathbb{C}, g = |g|e^{i\varphi} : |g| < \frac{1}{|N|} \frac{3}{2} \left(\cos \frac{\varphi-2\theta}{2}\right)^2 \sqrt{\cos(2\theta)} \right\}. \quad (4.12)$$

Consequently, $W_n(g)$ and $W(g, N)$ can be analytically extended to the following respective domains:

$$\begin{aligned} W_n(g) : \quad & |2\theta| < \frac{\pi}{2}, \quad |\varphi - 2\theta| < \pi, \\ W(g, N) : \quad & |2\theta| < \frac{\pi}{2}, \quad |\varphi - 2\theta| < \pi, \quad |g| < \frac{1}{|N|} \frac{3}{2} \left(\cos \frac{\varphi-2\theta}{2}\right)^2 \sqrt{\cos(2\theta)}. \end{aligned} \quad (4.13)$$

Pushing $\theta \rightarrow \pm\pi/4$ allows us to write a convergent expansion for all $|\varphi| < \frac{3\pi}{2}$.

Proof See Appendix C.3 □

The main point of the proposition is that by constructive methods we can prove analyticity of $W(g, N)$ in a nontrivial domain. In a first step, without touching the integration contours, we prove that such domain is the cardioid of Eq.(4.8). However, the cardioid does not allow us to reach (and cross) the branch cut. Tilting the integration contours by θ , we are able to extend the original cardioid domain to the larger domain of Eq. (4.12) (see Fig. 2), going beyond the cut on a subdomain of the extended Riemann sheet $\mathbb{C}_{3\pi/2}$. The optimal domain \mathbb{D}_{opt} can be found by maximizing the right-hand side of Eq. (4.12) with respect to θ , at fixed φ , but a simpler and qualitatively similar choice is to take $\theta = \varphi/6$.

Note that the domain of analyticity of $W(g, N)$, Eq. (4.12), depends on N and shrinks to zero for $N \rightarrow \infty$. Results uniform in N can only be established if one keeps the 't Hooft coupling $g_t = gN$ fixed [26]. On the other hand, for any g on the extended Riemann sheet $\mathbb{C}_{3\pi/2}$, the radius of convergence of the LVE in N is nonzero.

Remark 2. It is also worth noticing that the explicit expressions for the partition function in terms of special functions, discussed around Eq. (3.21), provide us with some useful information about the zeros of $Z(g, N)$ (Lee–Yang zeros), and hence about the singularities of $W(g, N)$. For example, in the case $N = 1$, the partition function is expressed in terms of a modified Bessel function of the second kind, whose zeros have been studied in some depth.

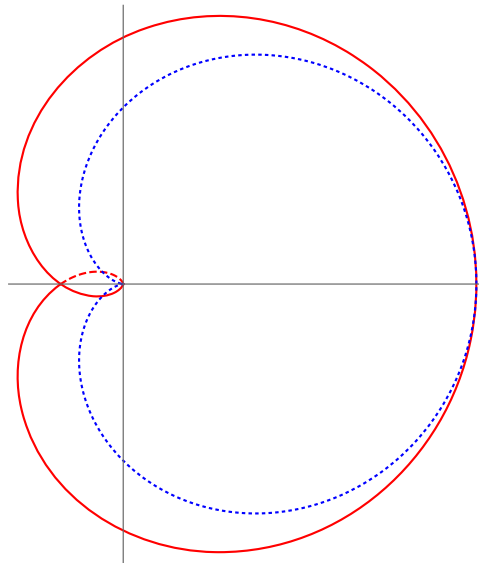


FIGURE 2. The cardioid domain \mathbb{D}_0 of Eq. (4.8) (dotted blue line) and the extended cardioid \mathbb{D}_θ of Eq. (4.12) (red line), for $\theta = \varphi/6$, which is similar to the optimal domain \mathbb{D}_{opt} , in the complex g -plane. The branch cut is on the negative real axis; thus, the portions of \mathbb{D}_θ going beyond it are to be understood as being on different Riemann sheets

In particular, from what is known about $K_\nu(z)$ (e.g., [31]) we deduce that $Z(g, 1) = \sqrt{\frac{3}{2\pi g}} e^{\frac{3}{4g}} K_{1/4}(\frac{3}{4g})$ has no zeros in the principal sheet \mathbb{C}_π , while on each of the two following sheets it has an infinite sequence of zeros approaching the semiaxis at $|\varphi| = 3\pi/2$ from the left, and accumulating toward $g = 0$ (see Fig. 3). Therefore, it should come as no surprise that $W(g, N)$ cannot be analytically continued around the origin beyond $|\varphi| = 3\pi/2$.

Remark 3. Integrating out the u parameters and performing the sum over trees, one should be able to prove that integral expressions (4.9) reproduce the moment-cumulant relation in Eq. (4.3). In particular this would provide an alternative proof that the moment cumulant relation holds in the sense of analytic functions on the Riemann surface. The proof that this indeed happens is involved as the summation over trees requires the use of combinatorial techniques similar to the ones discussed in Appendix D. We postpone this for future work.

In [18] the LVE is used to prove the Borel summability of $W(g, 1)$ along the positive real axis. Building on the techniques introduced in [18], we now generalize this result.

Proposition 4 (Borel summability of $W_n(g)$ and $W(g, N)$ in \mathbb{C}_π). *The cumulants $W_n(g)$ and the free energy $W(g, N)$ at any fixed complex N are Borel summable along all the directions in the cut complex plane \mathbb{C}_π .*

Proof. See Appendix C.4. □

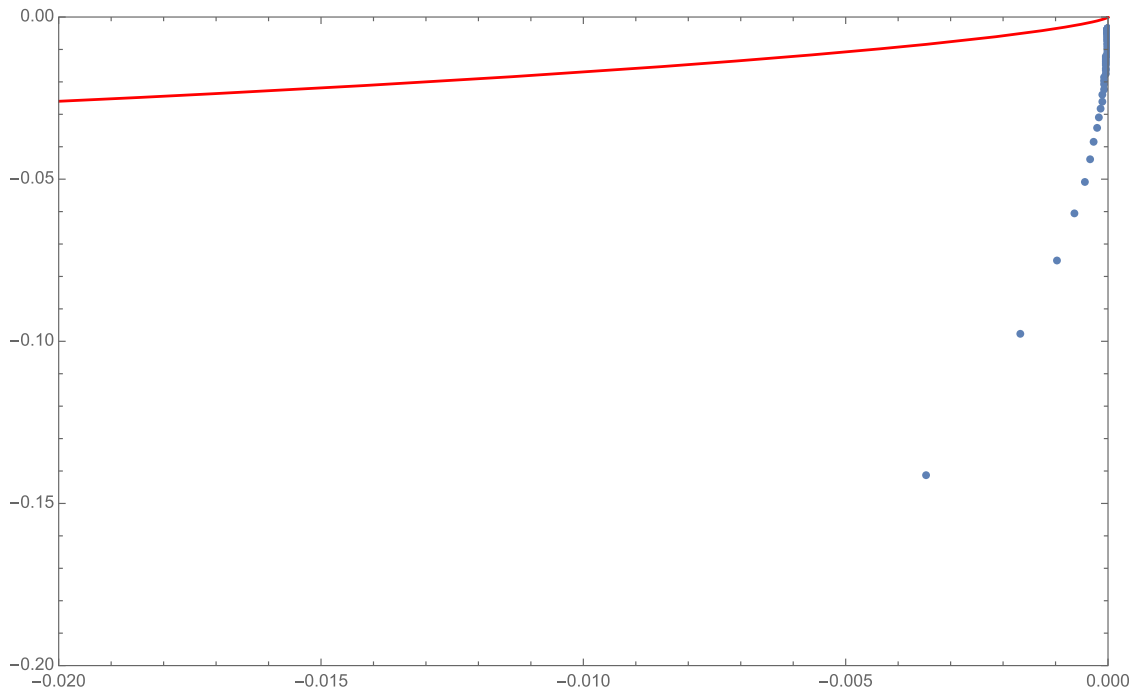


FIGURE 3. Approximate location (see [31]) of the Lee–Yang zeros of $Z(g, 1)$ (blue dots) in the quadrant $\pi < \varphi < 3\pi/2$ of $\mathbb{C}_{3\pi/2}$, together with the boundary of the domain \mathbb{D}_θ (in red)

4.2. Transseries Expansion

It is well known that the (perturbative) asymptotic series of $W(g, N)$ at $g = 0$ is a sum over connected Feynman graphs. The connection between the LVE of $W(g, N)$ presented in Proposition 3 and the Feynman graphs is discussed in Appendix D.1. On the other hand, the power series in each multi-instanton sector of the transseries of $W(g, N)$ has no simple diagrammatic interpretation; they can be constructed from the nonlinear differential equation obeyed by $W(g, N)$, or more formally by expanding the logarithm of the transseries expansion of $Z(g, N)$ in powers of the transseries monomial $\exp\{3/(2g)\}$ (e.g., [6]). The latter is, however, only a meaningful operation in the sense of formal power series.

In this section we take a different route and derive rigorously the transseries expansion of $W(g, N)$ by exploiting the analytical control we have on the small- N expansion. We first notice that, from Propositions 2 and 3, $W_n(g)$ and $Z_n(g)$ are analytic functions on the extended Riemann sheet $\mathbb{C}_{3\pi/2}$. Next, we use Eq. (4.3) to construct $W_n(g)$ as a finite linear combination of finite products of $Z_i(g)$'s. Each such product is in fact a (factored) multidimensional integral; hence, we can apply to it the steepest descent method to obtain its asymptotic expansion. In \mathbb{C}_π , the asymptotic expansion of each factor $Z_i(g)$ is of the perturbative type, Eq. (3.25), and $W_n(g)$ is just a finite linear combination of Cauchy products of such series.

When turning g past the negative real axis, each integration contour in this multidimensional integral must be deformed past a cut and each $Z_{i\pm}(g) =$

$Z_i^{\mathbb{R}}(g) + Z_{i\pm}^C(g)$ (see the discussion below Proposition 2). It follows that $W_i(g)$ is a linear combination of products involving $Z_i^{\mathbb{R}}(g)$'s and $Z_{i\pm}^C(g)$, and this representation holds in the sense of analytic functions on the Riemann surface. In order to obtain the transseries of $W_n(g)$, one needs to build the transseries expansion of each of the terms in the linear combinations. As the multidimensional integrals are factored, this is just the Cauchy product of the transseries $Z_i^{\text{pert.}}(g)$ and $e^{\frac{3}{2g}} Z_i^{(\eta)}(g)$ corresponding to $Z_i^{\mathbb{R}}(g)$ and $Z_{i\pm}^C(g)$, respectively.

The summation over n is more delicate, as it is an infinite series. As we have seen in Proposition 3, the small- N series of $W(g, N)$ converges in the domain \mathbb{D}_0 of Eq. (4.12), thus yielding $W(g, N)$ in terms of $W_n(g)$ as an analytic function on such domain. Therefore, we can apply the steepest-descent method term by term to the small- N series, and hence, the transseries of $W(g, N)$ is rigorously reconstructed by substituting the transseries for $W_n(g)$ in Eq. (4.1).

Unsurprisingly, at the end we recover the formal transseries of $W(g, N)$ which can be obtained by direct substitution of the transseries expansion of $Z(g, N)$, taking formally its logarithm, and then expanding in powers of $Z_i^{(\eta)}(g)$ and $Z_i^{\text{pert.}}(g) - 1$. What we gained in the process is that we replaced a formal manipulation on transseries with a rigorous manipulation on analytic functions.

Proposition 5. *The cumulant $W_n(g)$ and the full free energy $W(g, N)$ have transseries expansions that can be organized into instanton sectors. The instanton counting parameter is denoted by p .*

1. *For $g \in \mathbb{C}_{3\pi/2}$, the cumulant $W_n(g)$ has the transseries expansion:*

$$W_n(g) = \sum_{p=0}^n e^{\frac{3}{2g}p} \left(\eta \sqrt{2\pi} \sqrt{\frac{g}{3}} \right)^p \sum_{l'=0}^{n-p} \left(\ln \left(\frac{g}{3} \right) \right)^{l'} \sum_{l \geq 0} g^l W_{n;l,l'}^{(p)}, \quad (4.14)$$

where \mathbb{R}_- is a Stokes line, $\tau = -\text{sgn}(\varphi)$ and η is a transseries parameter which is zero on the principal Riemann sheet and is one when $|\varphi| > \pi$.

The g -independent coefficient $W_{n;l,l'}^{(p)}$ is given by the following nested sum:

$$\begin{aligned} W_{n;l,l'}^{(p)} = & \sum_{\substack{k=p \\ k+p \geq 1}}^n (-1)^{k-1} (k-1)! \sum_{\substack{n_1, \dots, n_{n-k+1} \geq 0 \\ \sum i n_i = n, \sum n_i = k}} \sum_{\substack{\{0 \leq p_i \leq n_i\} \\ i=1, \dots, n-k+1 \\ \sum p_i = p}} \frac{n!}{\prod_i (n_i - p_i)! p_i! (i!)^{n_i}} \\ & \times \sum_{\substack{\{a_j^i \geq 0\}_{j=1, \dots, n-k+1} \\ \sum_i \sum_j a_j^i = l}} \sum_{\substack{\{0 \leq c_j^i \leq i-1\}_{j=1, \dots, n-k+1} \\ \sum_i \sum_j c_j^i = l'}} \left(\frac{1}{6} \right)^{\sum_{i=1}^{n-k+1} \sum_{j=1}^{p_i} a_j^i} \left(-\frac{2}{3} \right)^{\sum_{i=1}^{n-k+1} \sum_{j=p_i+1}^{n_i} a_j^i} \\ & \prod_{i=1}^{n-k+1} \left(\prod_{j=1}^{p_i} G(a_j^i, c_j^i; i) \right) \left(\prod_{j=p_i+1}^{n_i} G(a_j^i; i) \right), \end{aligned} \quad (4.15)$$

with

$$G(a; i) = \frac{(2a)!}{2^{2a} a!} \sum_{\substack{a_1, \dots, a_{2a-i+1} \geq 0 \\ \sum k a_k = 2a, \sum a_k = i}} \frac{(-1)^i i!}{\prod_k k^{a_k} a_k!},$$

$$G(a, c; i) = \sum_{b=0}^{i-1} (\imath\tau 2\pi)^{i-1-b-c} \frac{i!}{a! b! c! (i-b-c)!} \frac{d^b \Gamma(z)}{dz^b} \Big|_{z=2a+1}. \quad (4.16)$$

2. For $g \in \mathbb{D}_\theta$, the full free energy $W(g, N)$ has the transseries expansion:

$$\begin{aligned} W(g, N) &= \sum_{n \geq 1} \frac{1}{n!} \left(-\frac{N}{2} \right)^n W_n(g) \\ &= \sum_{p \geq 0} e^{\frac{3}{2g}p} \left(\eta \sqrt{2\pi} e^{\imath\tau \frac{\pi}{2}} \left(\frac{e^{\imath\tau \pi} g}{3} \right)^{\frac{1-N}{2}} \right)^p \sum_{l \geq 0} \left(-\frac{2g}{3} \right)^l W_l^{(p)}(N), \end{aligned} \quad (4.17)$$

where

$$\begin{aligned} W_l^{(p)}(N) &= \sum_{\substack{q \geq 0 \\ p+q \geq 1}} (-1)^{p+q-1} \frac{(p+q-1)!}{p!q!} \\ &\quad \times \sum_{\substack{n_1, \dots, n_q \geq 1 \\ m_1, \dots, m_p \geq 0 \\ \sum n_i + \sum m_j = l}} \left(\prod_{i=1}^q \frac{\Gamma(2n_i + N/2)}{2^{2n_i} n_i! \Gamma(N/2)} \right) \left(\prod_{j=1}^p \frac{(-1)^{m_j}}{2^{2m_j} m_j! \Gamma\left(\frac{N}{2} - 2m_j\right)} \right). \end{aligned} \quad (4.18)$$

Proof. See Appendix C.5 □

While the expressions in Proposition 5 are not the most amenable to computations, one feature is striking. Expanding the cumulant $W_n(g)$ into p instanton sectors, we observe that only the first n instantons contribute to W_n , that is the sum in Eq. (4.14) truncates to $p = n$. The n instanton contribution to W_n comes from $n = p = k$ in Eq. (4.15) which implies $n_1 = n$ and all the others 0, hence⁸:

$$W_n^{(n)}(g) \simeq e^{\frac{3}{2g}n} \left(\eta \sqrt{2\pi} \sqrt{\frac{g}{3}} \right)^n (-1)^{n-1} (n-1)! \left(\sum_{q=0}^{\infty} \frac{(2q)!}{q!} \left(\frac{g}{6} \right)^q \right)^n. \quad (4.19)$$

This is genuinely new phenomenon. Usually, for quantities that are interesting for physics, one either deals with functions having only one instanton, like $Z(g, N)$ (or $Z_n(g)$) or with function receiving contributions from all the instanton sectors, like $W(g, N)$. This is, to our knowledge, the first instance when some physically relevant quantity receiving contributions from a finite number of instantons strictly larger than one is encountered. The n instanton contribution comes from $n_1 = n$ and all the others 0, such that effectively:

$$W_n^{(n)}(g) \approx (Z_1(g))^n,$$

and, for all n , $Z_n(g)$ has just a single instanton.

⁸This formula is most easily derived from Eq. (C.74).

4.3. Differential Equations

The exotic behavior of $W_n(g)$ can also be understood in terms of differential equations. By rewriting the partition function as $Z(g, N) = e^{W(g, N)}$, it is straightforward to turn (3.16) into a differential equation for $W(g, N)$, which in turn implies a tower of equations for $W_n(g)$.

Proposition 6. *The function $W(g, N)$ obeys the nonlinear differential equation:*

$$16g^2 W''(g, N) + 16g^2 (W'(g, N))^2 + ((8N + 24)g + 24) W'(g, N) + N(N + 2) = 0. \quad (4.20)$$

The functions $W_n(g)$ obey the tower of differential equations:

$$\begin{aligned} 4g^2 W_1''(g) + 6(g + 1)W_1'(g) - 1 &= 0, \\ 4g^2 W_2''(g) + 6(g + 1)W_2'(g) + 8g^2 (W_1'(g))^2 - 8gW_1'(g) + 2 &= 0, \\ 4g^2 W_n''(g) + 6(g + 1)W_n'(g) + 4g^2 \sum_{k=1}^{n-1} \binom{n}{k} W_{n-k}' W_k' - 4ngW_{n-1}'(g) &= 0. \end{aligned} \quad (4.21)$$

The differential equation for $W_1(g)$ is, unsurprisingly, identical to the one for $Z_1(g)$ (the connected 1-point function equals to the full 1-point function). Note that although the differential equation for $W(g, N)$ is nonlinear, the one for $W_n(g)$ is linear. In fact, since $W_0(g) = 0$, the nonlinear term $(W'(g, N))^2$ produces only source terms in (4.21). The linearity of the equations provides another point of view on why only a finite number of instantons arise in each $W_n(g)$.

Acknowledgements

R. G., H. K. and D. L. have been supported by the European Research Council (ERC) under the European Union's Horizon 2020 research and innovation program (grant agreement No. 818066) and by the Deutsche Forschungsgemeinschaft (DFG, German Research Foundation) under Germany's Excellence Strategy EXC-2181/1-390900948 (the Heidelberg STRUCTURES Cluster of Excellence). We thank Ricardo Schiappa for comments on an early version of this work.

Funding Open Access funding enabled and organized by Projekt DEAL.

Open Access. This article is licensed under a Creative Commons Attribution 4.0 International License, which permits use, sharing, adaptation, distribution and reproduction in any medium or format, as long as you give appropriate credit to the original author(s) and the source, provide a link to the Creative Commons licence, and indicate if changes were made. The images or other third party material in this article are included in the article's Creative Commons licence, unless indicated otherwise in a credit line to the material. If material is not included in the article's Creative Commons licence and your intended use is not permitted by statutory regulation or exceeds the permitted use, you will need to obtain permission directly from

the copyright holder. To view a copy of this licence, visit <http://creativecommons.org/licenses/by/4.0/>.

Publisher's Note Springer Nature remains neutral with regard to jurisdictional claims in published maps and institutional affiliations.

A. Asymptotic Expansions

Analytic continuations of exponential integrals like $Z(g, N)$ can be carried out by deforming the original real integration cycles in the complex plane. Complex Morse theory (Picard–Lefschetz Theory) provides a systematic framework for decomposing the original integration cycle \mathcal{C} into a sum of more convenient cycles \mathcal{J}_i called Lefschetz thimbles:

$$I(g) = \int_{\mathcal{C}} dx e^{\frac{1}{g}f(x)} a(x) = \sum_i \int_{\mathcal{J}_i} dx e^{\frac{1}{g}f(x)} a(x). \quad (\text{A.1})$$

Generically, each thimble intersects one critical (or saddle) point $x_i^* \in \mathbb{C}^m$ and consists of the union of downward flows with respect to the real part of $f(x)$ originating at x_i^* . From a topological point of view $\{\mathcal{J}_i\}$ generate the m 'th relative homology group of the underlying $2m$ -dimensional space. Crucially, the imaginary part of $f(x)$ is constant along each \mathcal{J}_i and the integral along a thimble is absolutely convergent. Since the individual integrals are non-oscillating, it is possible to apply Laplace's method to each term, expanding the integrand around the critical points:

$$I(g) = \sum_i e^{\frac{1}{g}f(x_i^*)} \Phi^{(i)}(g),$$

where $\Phi^{(i)}(g)$ is an asymptotic series, possibly containing logarithms and non-integer powers of g . As g is varied, the thimbles are deformed and the number of thimbles appearing in the decomposition of the original contour \mathcal{C} may vary discontinuously. These discrete changes, happening at values of g for which different thimbles intersect each other, are connected to the so-called Stokes jumps.

Lefschetz thimble techniques are standard tool in resurgence analysis [5, 6, 32] and have many other applications to path integrals [15, 33–37]. More details and a nice pedagogical introduction can be found in [17].

In the following we review the derivation of the asymptotic expansions around the critical points of the zero-dimensional ϕ^4 theory for $N = 1$.

A.1. The ϕ Representation of the Partition Function

The vacuum expansion. Our starting point is the partition function of the model in the ϕ representation. We set $N = 1$ and consider:

$$Z(g) = \int_{-\infty}^{+\infty} [d\phi] e^{-S[\phi]}, \quad S[\phi] = \frac{1}{2}\phi^2 + \frac{g}{4!}\phi^4, \quad (\text{A.2})$$

where again we set $[d\phi] = d\phi/\sqrt{2\pi}$. There are three solutions of the equations of motions, i.e., critical points $S'[\phi_*] = 0$, namely $\phi_0 = 0$ and $\phi_{\pm} = \pm i\sqrt{\frac{6}{g}}$, and each of them has an attached thimble, \mathcal{J}_0 and \mathcal{J}_{\pm} (see Fig. 4). For symmetry reasons it is clear that $Z_{\mathcal{J}_+}(g) = Z_{\mathcal{J}_-}(g)$; thus, there are only two asymptotic expansions.

Equation (A.2) is absolutely convergent if g is in the right half complex plane $\text{Re}(g) > 0$; hence, in this domain it defines an analytic function $Z(g)$. In order to analytically continue this function we turn in the complex plane and parameterize $g = |g|e^{i\varphi}$ but we tilt the contour of integration by $e^{-i\theta}$ to compensate. In detail, we define:

$$Z_{\theta}(g) = \int_{\mathbb{R}e^{-i\theta}} [d\phi] e^{-\frac{1}{2}\phi^2 - \frac{|g|e^{i\varphi}}{4!}\phi^4} = e^{-i\theta} \int_{\mathbb{R}} [d\phi] e^{-\frac{1}{2}\phi^2 e^{-2i\theta} - \frac{|g|e^{i(\varphi-4\theta)}}{4!}\phi^4}, \quad (\text{A.3})$$

which is absolutely convergent if both $\varphi - 4\theta \in (-\pi/2, \pi/2)$ and $-2\theta \in (-\pi/2, \pi/2)$, and is independent of θ as long as it converges. As $Z_0(g) = Z(g)$, it follows that $Z_{\theta}(g)$ is the analytic continuation of $Z(g)$ and it is easy to check that the integral in Eq. (A.3) defines it for all $-3\pi/2 \leq \varphi < 3\pi/2$. We denote:

$$Z_+(g) = Z_{\theta}(g) \text{ for } \theta > 0, \quad Z_-(g) = Z_{\theta}(g) \text{ for } \theta < 0, \quad (\text{A.4})$$

the anticlockwise, respectively clockwise, analytic continuations. Both $Z_+(g)$ and $Z_-(g)$ are defined for any g with $\text{Re}(g) < 0$, but they are not equal. That is $Z_{\theta}(g)$ is a multi-valued function in the complex g -plane, with a branch point at the origin. We chose the range $-\pi < \varphi < \pi$ for the principle Riemann sheet, with a cut along the negative real axis.

For $|\varphi| < \pi$ the integration contour in Eq. (A.3) is homotopic to just the perturbative thimble \mathcal{J}_0 , which at the origin is tangent to the real axis. In this case, the Laplace method applied to $Z_{\mathcal{J}_0}(g)$ amounts to Taylor expanding the quartic interaction and computing the Gaussian integral⁹:

$$\begin{aligned} Z(g) = Z_{\mathcal{J}_0}(g) &= \int_{\mathcal{J}_0} [d\phi] e^{-\frac{1}{2}\phi^2 - \frac{g}{4!}\phi^4} = \sum_{n=0}^{\infty} \frac{1}{n!} \left(-\frac{g}{4!}\right)^n \int_{-\infty}^{\infty} [d\phi] e^{-\frac{1}{2}\phi^2} \phi^{4n} \\ &= \sum_{n=0}^{\infty} \left(-\frac{2}{3}\right)^n \frac{(4n)!}{2^{6n}(2n)!n!} g^n \equiv \sum_{n=0}^{\infty} A_n^{\text{pert.}} g^n. \end{aligned} \quad (\text{A.5})$$

The instanton sector. At $\varphi = \pm\pi$, i.e., at $g < 0$, the perturbative thimble intersects the instanton thimbles. At $|\varphi| > \pi$ they split again, but on the opposite side, so that the perturbative thimble effectively has a jump at $|\varphi| = \pi$, leading to a jump in the decomposition of the original contour \mathcal{C} .

As the evaluation of the integrals along the instanton thimbles, $Z_{\mathcal{J}_{\pm}}$, is well behaved and continuous across the Stokes line at $\varphi = \pi$, for the asymptotic

⁹As explained for example in [16], in the Laplace method we restrict the integration to a small neighborhood of the saddle point, we expand the integrand, keeping only the first nontrivial term in the exponent while expanding the rest, and lastly exchange sum and integral, extending the integration domain to an infinite line along which the integrals are convergent and computable.

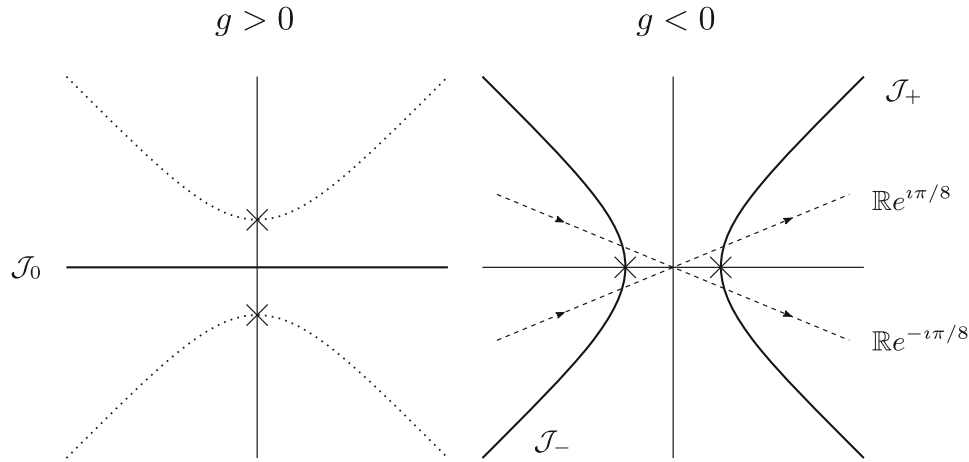


FIGURE 4. Critical points and thimbles (thick lines) in the complex ϕ -plane. The crosses mark the positions of the instantons, and the dashed lines are the tilted contours of Eq. (A.10)

expansion around the instanton, we consider the case $g < 0$. In this case the thimbles \mathcal{J}_{\pm} are described by $\operatorname{Re}(\phi) = \pm \sqrt{(\operatorname{Im}(\phi))^2 + \frac{6}{|g|}}$. Since we know the analytic expression of the thimbles, we take an explicit parametrization of the curve and use it to compute the integral. For example we can choose:

$$\gamma_{\pm} : t \in (-\infty, \infty) \rightarrow \left(\pm \sqrt{t^2 + \frac{6}{|g|}} \right) + \imath t. \quad (\text{A.6})$$

and the integral reads:

$$\begin{aligned} Z_{\mathcal{J}_+} &= \int_{\mathcal{J}_+} [d\phi] e^{-S(\phi)} = \int_{-\infty}^{\infty} [dt] \dot{\gamma}_+(t) e^{-S(\gamma_+(t))} \\ &= \int_0^{\infty} [dt] \dot{\gamma}_+(t) e^{-S(\gamma_+(t))} + \int_0^{\infty} [dt] \dot{\gamma}_+(-t) e^{-S(\gamma_+(-t))}. \end{aligned} \quad (\text{A.7})$$

The imaginary part of the action is zero along the thimbles. Also we have that $\dot{\gamma}_{\pm}(-t) = \frac{\mp t}{\sqrt{t^2 + \frac{6}{|g|}}} + \imath$, and thus, the real parts of the two integrals cancel. In the end we find:

$$Z_{\mathcal{J}_+} = 2\imath \int_0^{\infty} [dt] e^{-\frac{3}{2|g|} - t^2 - \frac{|g|}{6} t^4} = \imath e^{\frac{3}{2g}} \int_{-\infty}^{+\infty} [dt] e^{-t^2 + \frac{g}{6} t^4}. \quad (\text{A.8})$$

Now we can rescale the t by $\frac{1}{\sqrt{2}}$ and find the same integral as for \mathcal{J}_0 but with the opposite sign for g . In the end we have:

$$Z_{\mathcal{J}_{\pm}} = \frac{\imath}{\sqrt{2}} e^{\frac{3}{2g}} \sum_{p=0}^{\infty} (-1)^p A_p^{\text{pert.}} g^p. \quad (\text{A.9})$$

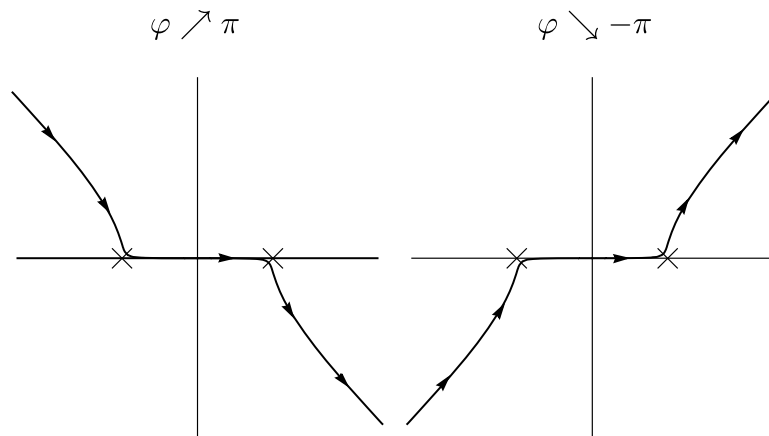


FIGURE 5. The thimble \mathcal{J}_0 for $Z_+(-|g|)$ (left) and $Z_-(-|g|)$ (right) as $|\varphi| \nearrow \pi$

Discontinuity. The discontinuity at the cut can be computed as:

$$Z_-(-|g|) - Z_+(-|g|) = \int_{\mathbb{R}e^{i\pi/8}} \frac{d\phi}{\sqrt{2\pi}} e^{-\frac{1}{2}\phi^2 + \frac{|g|}{4!}\phi^4} - \int_{\mathbb{R}e^{-i\pi/8}} \frac{d\phi}{\sqrt{2\pi}} e^{-\frac{1}{2}\phi^2 + \frac{|g|}{4!}\phi^4}, \quad (\text{A.10})$$

where we tilted the contours by the θ of minimal absolute value which ensures convergence. Each of the two contours can be deformed to the perturbative thimble alone for $|\varphi| < \pi$. However, in the limit of $|\varphi| \nearrow \pi$ the difference of the two perturbative thimbles approaches the sum of the two instanton thimbles (see Fig. 5), leading to the asymptotic expansion in Eq. (3.15), with $N = 1$.

B. A Simple Generalization of the Nevanlinna–Sokal Theorem

Proof of Theorem 1. The proof is an infinitesimal variation of the proof of [27] which deals with the case $\beta = 0$. We parallel the notation of [27].

We first observe that:

$$|a_q| = \lim_{z \rightarrow 0, z \in \text{Disk}_R} \left| \frac{a_q z^q + R_{q+1}(z)}{z^q} \right| = \lim_{z \rightarrow 0, z \in \text{Disk}_R} \frac{|R_q(z)|}{|z|^q} \leq K q! q^\beta \rho^{-q}; \quad (\text{B.1})$$

hence, $B(t)$ is an integer power series which converges in the disk $|t| < \rho$ and defines an analytic function in this domain.

Let us recall Hankel's contour integral representation of the inverse of the Gamma function:

$$\frac{1}{2\pi i} \oint_{\text{Re}(z^{-1})=r^{-1}} dz e^{x/z} z^{k-1} = \frac{1}{2\pi i} \int_{r^{-1}-i\infty}^{r^{-1}+i\infty} dw e^{xw} w^{-k-1} = \frac{x^k}{\Gamma(k+1)}, \quad (\text{B.2})$$

which holds for any $r, x \in \mathbb{R}_+$ and $k \in \mathbb{C}$. We define for $x \in \mathbb{R}_+$ the function:

$$b_0(x) = \frac{1}{2\pi i} \oint_{\text{Re}(z^{-1})=r^{-1}} dz e^{x/z} z^{-1} f(z), \quad (\text{B.3})$$

which is an r independent function for $r < R$ as long as the integral converges because the integration contour is fully contain in Disk_R . Substituting the asymptotic expansion of $f(z)$ up to order q , we obtain:

$$b_0(x) = \sum_{k=0}^{q-1} \frac{a_k}{k!} x^k + \frac{1}{2\pi i} \oint_{\text{Re}(z^{-1})=r^{-1}} dz e^{x/z} z^{-1} R_q(z). \quad (\text{B.4})$$

Changing variables to $w = 1/z$ and using the bound on R_q , the remainder term above is bounded by:

$$K q! q^\beta \rho^{-q} e^{x/r} \int_{-\infty}^{\infty} dv \frac{1}{|r^{-1} + v|^{q+1}} \leq K q! q^\beta \rho^{-q} e^{x/r} r^q \int_{-\infty}^{\infty} dv \frac{1}{(1+v^2)^{\frac{q+1}{2}}}, \quad (\text{B.5})$$

and the integral in the last line is always bounded by the case $q = 1$ in which case it is π and can be absorbed in K . Choosing $r = x/q$ (which is possible for q large enough $q > x/R$) and using the Stirling upper bound on the Gamma function, the reminder is finally bounded by $K q^{\beta+1/2} (x/\rho)^q$ hence goes to zero in the $q \rightarrow \infty$ limit as long as $x < \rho$. It follows that for $0 < x < \rho$, $b_0(x) = B(t)|_{t=x}$.

We now define $b_m(x) = \frac{d^m}{dx^m} b_0(x)$, and using Eq. (B.4) with $q = m + 1$ we get:

$$b_m(x) = a_m + \frac{1}{2\pi i} \oint_{\text{Re}(z^{-1})=r^{-1}} dz e^{x/z} z^{-m-1} R_{m+1}(z), \quad (\text{B.6})$$

and we have the bound $|b_m(x)| \leq K (m+1)! (m+1)^\beta \rho^{-m-1} e^{x/r}$ (note that this bound covers also the term $|a_m| < K m! m^\beta \rho^{-m}$).

The sum $B_x(t) = \sum_{m \geq 0} \frac{(t-x)^m}{m!} b_m(x)$ defines an analytic function in t as long as it converges. As:

$$|B_x(t)| \leq K e^{x/r} \sum_{m \geq 0} (m+1)^{\beta+1} (|t-x|/\rho)^m, \quad (\text{B.7})$$

we conclude that $B_x(t)$ is analytic in a disk of radius ρ centered at x . It is immediate to check that $B_x(t) = B_{x'}(t)$ as long as they both converge; hence, $B_x(t)$ is the analytic continuation of $B(t)$ to the strip $\{t \in \mathbb{C} \mid \text{dist}(t, \mathbb{R}_+) < \rho\}$ and it obeys the appropriate exponential bound. The last point follows by noting that for $z' \in \text{Disk}_r$:

$$\begin{aligned} & \frac{1}{z'} \int_0^\infty dx e^{-x/z'} \frac{1}{2\pi i} \oint_{\text{Re}(z^{-1})=r^{-1}} dz e^{x/z} z^{-1} \\ & f(z) = \frac{1}{2\pi i} \oint_{\text{Re}(z^{-1})=r^{-1}} dz \frac{1}{z-z'} f(z) = f(z'), \end{aligned} \quad (\text{B.8})$$

by Cauchy's theorem. \square

C. Proofs of Propositions

In this appendix we gather the proofs of various propositions in the main body of the paper.

C.1. Properties of $Z(g, N)$

Proof of Proposition 1. The proof of this proposition is linear.

Property 1. This follows by bounding the square root and taking into account that the Gaussian integral is normalized to 1. For $N \geq 0$ and $g = |g|e^{i\varphi}$ with $-\pi < \varphi < \pi$, we have the uniform bound:

$$|1 - i\sqrt{\frac{g}{3}}\sigma| = |e^{-i\frac{\varphi}{2}} - i\sqrt{\frac{|g|}{3}}\sigma| \geq \cos \frac{\varphi}{2}. \quad (\text{C.1})$$

For $N < 0$ we use $|1 - i\sqrt{\frac{g}{3}}\sigma| \leq 1 + \sqrt{\frac{|g|}{3}}|\sigma|$ and splitting the integration interval in regions where $\sqrt{\frac{|g|}{3}}|\sigma| \leq 1$, respectively $\sqrt{\frac{|g|}{3}}|\sigma| \geq 1$, and then re-extending the integration intervals to cover $(-\infty, \infty)$ we get:

$$\begin{aligned} |Z(g, N)| &\leq \int_{-\infty}^{\infty} [d\sigma] e^{-\frac{1}{2}\sigma^2} \left(1 + \sqrt{\frac{|g|}{3}}|\sigma|\right)^{|N|/2} \\ &\leq 2^{|N|/2} + \frac{2^{3|N|/4}}{\sqrt{\pi}} \frac{|g|^{N/4}}{3^{|N|/4}} \Gamma\left(\frac{|N|+2}{4}\right). \end{aligned} \quad (\text{C.2})$$

Property 2. The perturbative expansion is obtained using $(1-x)^{-N/2} = \sum_{q \geq 0} \binom{q+N/2-1}{q} x^q$ and commuting (formally) the sum and integral:

$$\begin{aligned} Z(g, N) &= \sum_{n=0}^{\infty} \binom{2n + \frac{N}{2} - 1}{2n} \left(-\frac{g}{3}\right)^n \int_{\mathbb{R}} [d\sigma] e^{-\frac{1}{2}\sigma^2} \sigma^{2n} \\ &= \sum_{n=0}^{\infty} \frac{\Gamma(2n + N/2)}{2^{2n} n! \Gamma(N/2)} \left(-\frac{2g}{3}\right)^n. \end{aligned} \quad (\text{C.3})$$

For the case $N = 1$ for instance we have $\frac{\Gamma(2n+1/2)}{\Gamma(1/2)} = \frac{(4n)!}{4^{2n}(2n)!}$ (see also Eq. (A.5) in Appendix A).

Property 3. Properties 3, 4, 5 and 6 are closely related and require that we deal carefully with the integration contour. We define:

$$\begin{aligned} Z_{\theta}(g, N) &= \int_{e^{-i\theta}\mathbb{R}} [d\sigma] e^{-\frac{1}{2}\sigma^2} \frac{1}{(1 - i\sqrt{\frac{g}{3}}\sigma)^{N/2}} \\ &= \int_{\mathbb{R}} e^{-i\theta} [d\sigma] e^{-\frac{1}{2}e^{-2i\theta}\sigma^2} \frac{1}{\left(1 - i\sqrt{\frac{|g|}{3}}e^{i\frac{\varphi-2\theta}{2}}\sigma\right)^{N/2}}, \end{aligned} \quad (\text{C.4})$$

which is absolutely convergent if both $\varphi - 2\theta \in (-\pi, \pi)$ and $-2\theta \in (-\pi/2, \pi/2)$. Moreover, as long as it converges, it is independent of θ , as can be verified by noticing that the derivative with respect to θ can be rewritten as the integral of a total derivative in σ . Thus, $Z_{\theta}(g, N)$ is the analytic continuation of $Z(g, N)$ and optimizing on θ the partition function can be continued to the extended Riemann sheet $\mathbb{C}_{3\pi/2}$ with a branch point at 0.

Using a Taylor formula with integral rest, we have $Z_\theta(g, N) - \sum_{k=0}^{q-1} \frac{1}{k!} Z_\theta^{(k)}(0, N) g^k = R_\theta^q(g, N)$ with:

$$\begin{aligned} R_\theta^q(g, N) &= \int_0^1 du \frac{(1-u)^{2q-1}}{(2q-1)!} \int_{\mathbb{R}} e^{-\imath\theta} [d\sigma] e^{-\frac{1}{2}e^{-2\imath\theta}\sigma^2} \left(\frac{d}{du}\right)^{2q} \\ &\quad \times \left(\frac{1}{\left(1 - \imath\sqrt{\frac{|g|}{3}} e^{\imath\frac{\varphi-2\theta}{2}} \sigma u\right)^{N/2}} \right) \\ &= \int_0^1 du \frac{(1-u)^{2q-1}}{(2q-1)!} \int_{\mathbb{R}} e^{-\imath\theta} [d\sigma] e^{-\frac{1}{2}e^{-2\imath\theta}\sigma^2} \frac{\left(-\imath\sqrt{\frac{|g|}{3}} e^{\imath\frac{\varphi-2\theta}{2}} \sigma\right)^n (-1)^n \frac{\Gamma(n+N/2)}{\Gamma(N/2)}}{\left(1 - \imath\sqrt{\frac{|g|}{3}} e^{\imath\frac{\varphi-2\theta}{2}} \sigma u\right)^{\frac{2n+N}{2}}} \Bigg|_{n=2q}, \end{aligned} \quad (\text{C.5})$$

where for $N < 0$ we need to choose $q > -N/4$. Using $|1 - \imath\sqrt{\frac{|g|}{3}} e^{\imath\frac{\varphi-2\theta}{2}} \sigma u| \geq \cos \frac{\varphi-2\theta}{2}$ the rest term is bounded as¹⁰:

$$|R_\theta^q(g, N)| \leq \frac{1}{(\cos(2\theta))^{\frac{1}{2}+q}} \frac{\left(\frac{|g|}{3}\right)^q}{\left(\cos \frac{\varphi-2\theta}{2}\right)^{2q+N/2}} \frac{1}{(2q)!} \frac{\Gamma(2q+N/2)}{\Gamma(N/2)} \frac{(2q)!}{2^q q!}, \quad (\text{C.6})$$

and using the Stirling formula as upper/lower bound for the Γ function¹¹ we have for q large enough (larger than $\max\{1, N\}$):

$$\begin{aligned} \frac{\Gamma(2q + \frac{N}{2})}{2^q q!} &\leq K \frac{(2q + \frac{N}{2} - 1)^{\frac{1}{2}+2q+\frac{N}{2}-1} e^{-(2q+\frac{N}{2}-1)}}{2^q q^{\frac{1}{2}+q} e^{-q}} \\ &\leq K 2^q q^{q+\frac{N}{2}-1} e^{-q} \left(1 + \frac{\frac{N}{2}-1}{2q}\right)^{\frac{4q+N-1}{2}} \leq K q! q^{\frac{N-3}{2}} 2^q, \end{aligned} \quad (\text{C.8})$$

for K some q independent constant.¹² Conveniently, choosing $\theta = \varphi/6$, we get the following bounds on $Z_{\varphi/6}(g, N)$ and $R_{\varphi/6}^q(g, N)$:

$$|R_{\varphi/6}^q(g, N)| \leq \frac{K}{\left(\cos \frac{\varphi}{3}\right)^{\frac{N+1}{2}}} q! q^{\frac{N-3}{2}} \left(\frac{1}{\frac{3}{2} \left(\cos \frac{\varphi}{3}\right)^3}\right)^q |g|^q,$$

¹⁰The factor $1/(\cos(2\theta))^q$ can be improved to 1 by Taylor expanding in the Gaussian measure along the lines of the proof of Proposition 4.

¹¹In detail:

$$1 \leq \frac{\Gamma(x+1)}{\sqrt{2\pi x}(x/e)^x} \leq e^{\frac{1}{12x}} \leq e^{1/12}, \quad x \in [1, \infty). \quad (\text{C.7})$$

¹²Note that $\left(1 + \frac{\frac{N}{2}-1}{2q}\right)^{\frac{4q+N-1}{2}} \leq \exp\left\{\frac{4q+N-1}{2} \ln\left(1 + \frac{\frac{N}{2}-1}{2q}\right)\right\} \leq \exp\left\{\frac{(4q+N-1)(\frac{N}{2}-1)}{4q}\right\} \leq K$ for $q \geq 1$.

$$|Z_{\varphi/6}(g, N)| \leq \frac{1}{\left(\cos \frac{\varphi}{3}\right)^{\frac{N+1}{2}}} . \quad (\text{C.9})$$

Observe that $Z_{\theta}(g, N)$ is independent on θ only as long as φ and θ are independent, but the choice $\theta = \varphi/6$ fixes θ in terms of the argument of g and $Z_{\varphi/6}(g, N)$ depends on φ .

We are now in the position to prove that $Z(g, N)$ is Borel summable along all the directions in the cut plane \mathbb{C}_{π} by verifying the conditions of Theorem 1, Appendix B. This comes about as follows:

- let us fix some $\alpha \in (-\pi, \pi)$. As already noted in Properties 1 and 2, $Z(g, N)$ is analytic in \mathbb{C}_{π} ; hence, in particular at $|g|e^{i\alpha}$ and its asymptotic expansion at 0 is known.
- $Z(g, N)$ is analytically continued to any g in a Sokal disk (with 0 on its boundary) tilted by α , that is $g \in \text{Disk}_R^{\alpha} = \{z \mid \text{Re}(e^{i\alpha}/z) > 1/R\}$ via $Z_{\varphi/6}(g, N)$. Note that this Sokal disk extends up to g with argument $\varphi = \alpha \pm \pi/2$. In the entire Sokal disk the rest term obeys the bound:

$$|R_{\varphi/6}^q(g, N)| \leq K q! q^{\frac{N-3}{2}} |g|^q \max_{\pm} \left\{ \frac{1}{\left(\cos \frac{\alpha \pm \frac{\pi}{2}}{3}\right)^{\frac{N+1}{2}}} \left(\frac{1}{\frac{3}{2} \left(\cos \frac{\alpha \pm \frac{\pi}{2}}{3}\right)^3} \right)^q \right\} . \quad (\text{C.10})$$

For any fixed $\alpha \in (-\pi, \pi)$, $\min_{\pm} \left\{ \frac{3}{2} \left(\cos \frac{\alpha \pm \frac{\pi}{2}}{3}\right)^3 \right\} = \rho > 0$ for some ρ ; hence, the Taylor rest obeys the bound in Eq. (2.4).

Property 4. Although this point is discussed in the main body of the paper, we include it also here for completeness. We denote the analytic continuation of $Z(g, N)$ to the extended Riemann sheet $\mathbb{C}_{3\pi/2}$ by:

$$\theta > 0 : \quad Z_+(g, N) = Z_{\theta}(g, N) , \quad Z_-(g, N) = Z_{-\theta}(g, N) . \quad (\text{C.11})$$

Observe that the factorial bound on the Taylor rest term cannot be satisfied (for any choice of θ) when $\varphi \rightarrow \pm 3\pi/2$. As Borel summability along a direction α requires analytic continuation and bound on the rest term in a Sokal disk centered on that direction, hence extending up to $\alpha \pm \pi/2$, $Z(g, N)$ loses Borel summability at $g \in \mathbb{R}_-$.

We start from Eq. (3.2) which we quote here again:

$$Z(g, N) = \int_{-\infty}^{+\infty} [d\sigma] e^{-\frac{1}{2}\sigma^2} \frac{1}{\left(1 - e^{i\frac{\pi}{2}} \sqrt{\frac{g}{3}} \sigma\right)^{N/2}} , \quad (\text{C.12})$$

and the Lefschetz thimble of the integral is the real axis irrespective of g (comparing to Eq. (A.1), we see that in the present case thimbles are defined by the saddle points of σ^2). As long as $g = |g|e^{i\varphi} \in \mathbb{C}_{\pi}$, the integral converges as the singularity at

$$\sigma_{\star} = -i\sqrt{\frac{3}{g}} = e^{-i\frac{\pi}{2} - i\frac{\varphi}{2}} \sqrt{\frac{3}{|g|}} , \quad (\text{C.13})$$

lies outside the integration contour. Notice that the singularity is a pole for N even, and otherwise it is a branch point with branch cut $\sigma_{\star} \times (1, +\infty)$. We

will discuss in detail the general case with a branch cut, as the case of even N turns out to be readable as a special case of the results at general N .

As g approaches \mathbb{R}_- the branch point hits the contour of integration: for $\varphi \nearrow \pi$ (that is we approach the cut in the g -plane counterclockwise) the branch point hits the real axis at $-\sqrt{3/|g|}$ while for $\varphi \searrow -\pi$ (that is we approach the cut in the g -plane clockwise) the branch point hits the real axis at $\sqrt{3/|g|}$. The analytic continuation $Z_+(g, N)$ (resp. $Z_-(g, N)$) consists in tilting the contour of integration in σ by some clockwise rotation $-\theta < 0$ (resp. counterclockwise, $\theta > 0$) to avoid the collision with the branch point. However, once g passes on the second Riemann sheet $\varphi > \pi$ (resp. $\varphi < -\pi$) the tilted contour is no longer a thimble and in order to derive the asymptotic behavior of $Z_{\pm}(g, N)$ we need to rotate it back to the real axis. This costs us a Hankel contour C along the cut (see Fig. 1):

$$\begin{aligned} Z_{\pm}(g, N)|_{\varphi \gtrless \pi} &= \int_{e^{\mp i\theta}\mathbb{R}} [d\sigma] \frac{e^{-\frac{1}{2}\sigma^2}}{(1 - i\sqrt{\frac{g}{3}}\sigma)^{N/2}} = Z^{\mathbb{R}}(g, N) + Z_{\pm}^C(g, N) \\ Z_{\pm}^C(g, N) &= \int_C [d\sigma] e^{-\frac{1}{2}\sigma^2} \frac{1}{(1 - i\sqrt{\frac{g}{3}}\sigma)^{N/2}}. \end{aligned} \quad (\text{C.14})$$

The integral $Z^{\mathbb{R}}(g, N)$, defined in Eq. (3.4), is absolutely convergent, and hence analytic, in the range $|\varphi| \in (\pi, 3\pi)$, where it is bounded from above as in Eq. (3.6).

The Hankel contour C turns clockwise around the cut $\sigma_{\star} \times (1, +\infty)$, i.e., starting at infinity with argument $\frac{3\pi}{2} - \frac{\varphi}{2}$ and going back with argument $-\frac{\pi}{2} - \frac{\varphi}{2}$ after having encircled the branch point σ_{\star} . We kept a subscript \pm for the contribution of the Hankel contour, because, even though the definition of $Z_{\pm}^C(g, N)$ and C might suggest that it is one single function of g , in fact the integral around the cut is divergent for $|\varphi| < \pi/2$, and therefore, the integrals at $\pi < \varphi < 3\pi/2$ and at $-\pi > \varphi > -3\pi/2$ are not the analytic continuation of each other.

We will now rewrite $Z_{\pm}^C(g, N)$ in a more useful form. With the change of variables $\sigma = e^{-i\frac{\pi}{2} - i\frac{\varphi}{2}} \sqrt{3/|g|} \sigma'$ the contour C becomes a Hankel contour C' turning clockwise around $(1, +\infty)$ and a shift to $\sigma' = 1 + t$ brings C' to C'' , a clockwise oriented Hankel contour around the positive real axis, starting at infinity with argument 2π and going back with vanishing argument after having encircled the origin:

$$\begin{aligned} Z_{\pm}^C(g, N) &= \int_C [d\sigma] e^{-\frac{1}{2}\sigma^2} \frac{1}{(1 - e^{i\frac{\pi}{2}} \sqrt{\frac{g}{3}}\sigma)^{N/2}} = \left(\frac{3}{e^{i\pi}g}\right)^{1/2} \int_{C'} [d\sigma'] e^{\frac{3}{2g}(\sigma')^2} \frac{1}{(1 - \sigma')^{N/2}} \\ &= \frac{1}{\sqrt{2\pi}} \left(\frac{3}{e^{i\pi}g}\right)^{1/2} \int_{C''} dt (e^{-i\pi}t)^{-\frac{N}{2}} e^{\frac{3}{2g}(1+t)^2}, \end{aligned} \quad (\text{C.15})$$

where we have made explicit the choice of branch by expressing minus signs as phases. Notice that the integral converges because for $\pi < |\varphi| < \frac{3\pi}{2}$ the exponent has a negative real part.

Next, we make the change of variables $t = e^{i\tau\pi\frac{g}{3}}u$, with $\tau = -\text{sgn}(\varphi)$ (i.e., $\tau = -$ for $\varphi > \pi$, that is for $Z_+^C(g)$ and $\tau = +$ for $\varphi < -\pi$, i.e., for $Z_-^C(g)$), obtaining:

$$Z_{\pm}^C(g, N) = \frac{e^{i\tau\pi(1-\frac{N}{2})}}{i\sqrt{2\pi}} \left(\frac{g}{3}\right)^{\frac{1-N}{2}} e^{\frac{3}{2g}} \int_{e^{-i\tau\pi-i\varphi}C''} du (e^{-i\pi}u)^{-\frac{N}{2}} e^{-u+\frac{g}{6}u^2}. \quad (\text{C.16})$$

The two choices of τ are dictated by the fact that for $\pi < |\varphi| < 3\pi/2$ the contour of integration should stay in the domain of convergence continuously connected to C'' . The fact that this entails two different choices of τ reflects what we anticipated about the need of keeping a \pm subscript. Lastly, the contour of integration can be deformed back to C'' , where we easily evaluate the discontinuity (for $N < 2$) as¹³:

$$\begin{aligned} Z_{\pm}^C(g, N) &= \frac{e^{i\tau\pi(1-\frac{N}{2})}}{\sqrt{2\pi}} \left(\frac{g}{3}\right)^{\frac{1-N}{2}} e^{\frac{3}{2g}} 2 \sin\left(\pi\frac{N}{2}\right) \int_0^{+\infty} du e^{-u+\frac{g}{6}u^2} u^{-\frac{N}{2}} \\ &= \frac{e^{i\tau\pi(1-\frac{N}{2})}}{\sqrt{2\pi}} \left(\frac{g}{3}\right)^{\frac{1-N}{2}} e^{\frac{3}{2g}} 2^{1+N/2} \sin\left(\pi\frac{N}{2}\right) \int_0^{+\infty} d\rho e^{-\frac{1}{2}\rho^2+\frac{g}{24}\rho^4} \rho^{1-N}. \end{aligned} \quad (\text{C.17})$$

In the last step, we performed the change of variables $u = \rho^2/2$ in order to make explicit that for $N = 1$ we reproduce Eq. (A.8) (times two, because the Hankel contour is only one, while there are two instanton thimbles in the ϕ representation). For general N , the integral resembles that of the $O(N)$ model in polar coordinates, except that in that case we would have the opposite sign for the power of the insertion, i.e., ρ^{N-1} . This also explains the relation between the coefficients of the perturbative and nonperturbative series in Eq. (3.12), which are related by the transformation $N \rightarrow 2 - N$ (up to an area of S^{N-1} of the missing angular integration in Eq. (C.17)).

The integral over u (or ρ) in Eq. (C.17) is convergent as long as $\text{Re}(g) < 0$, i.e., for $\pi/2 < |\varphi| < 3\pi/2$. One can use again the Hubbard–Stratonovich trick to write (for $N < 2$):

$$\begin{aligned} \int_0^{+\infty} du e^{-u+\frac{g}{6}u^2} u^{-\frac{N}{2}} &= \int_{-\infty}^{+\infty} [d\sigma] e^{-\frac{\sigma^2}{2}} \int_0^{+\infty} du e^{-u(1+\sqrt{\frac{g}{3}}\sigma)} u^{-\frac{N}{2}} \\ &= \Gamma(1 - N/2) \int_{-\infty}^{+\infty} [d\sigma] e^{-\frac{\sigma^2}{2}} \left(1 + \sqrt{\frac{g}{3}}\sigma\right)^{\frac{N}{2}-1}, \end{aligned} \quad (\text{C.18})$$

where, in order to ensure uniform convergence of the u integral, we keep $|\varphi| = \pi$. Note that the integral is independent of choice of branch of \sqrt{g} , as a sign

¹³This is obtained by writing, for $\text{Re}(z) < 1$,

$$\begin{aligned} \int_{C''} du e^{-S(u)} (e^{-i\pi}u)^{-z} &= \int_{+\infty}^0 du e^{-S(u)} e^{-z(\ln|u|+i\pi)} + \int_0^{+\infty} du e^{-S(u)} e^{-z(\ln|u|-i\pi)} \\ &= 2i \sin(\pi z) \int_0^{+\infty} du e^{-S(u)} u^{-z}. \end{aligned}$$

can be absorbed in σ . The reader will note that this is proportional to our integral in Eq. (3.4) with arguments $Z^{\mathbb{R}}(-g, 2 - N)$, which is unambiguous as $Z^{\mathbb{R}}(g, N)$ is periodic with period 2π in the argument of g ; hence, one can chose any determination of $-g$. The advantage of the manipulation above is that the integral over σ now converges for $0 < |\varphi| < 2\pi$; hence, it allows us to analytically continue $Z_{\pm}^C(g, N)$ beyond $|\varphi| = 3\pi/2$ up to $|\varphi| \nearrow 2\pi$.

Using Euler's reflection formula, $\Gamma(1 - z) \sin(\pi z) = \pi/\Gamma(z)$, we get¹⁴:

$$\begin{aligned} Z_{\pm}^C(g, N) &= \frac{e^{\imath\tau\pi(1-\frac{N}{2})}}{\sqrt{2\pi}} \left(\frac{g}{3}\right)^{\frac{1-N}{2}} e^{\frac{3}{2g}} \frac{2\pi}{\Gamma(N/2)} \int_{-\infty}^{+\infty} [d\sigma] e^{-\frac{\sigma^2}{2}} \left(1 - \imath\sqrt{\frac{-g}{3}}\sigma\right)^{\frac{N}{2}-1} \\ &= e^{\imath\tau\pi(1-\frac{N}{2})} \left(\frac{g}{3}\right)^{\frac{1-N}{2}} e^{\frac{3}{2g}} \frac{\sqrt{2\pi}}{\Gamma(N/2)} Z^{\mathbb{R}}(-g, 2 - N) \\ &= e^{\imath\tau\pi(1-\frac{N}{2})} \left(\frac{g}{3}\right)^{\frac{1-N}{2}} e^{\frac{3}{2g}} \frac{\sqrt{2\pi}}{\Gamma(N/2)} Z(e^{\imath\tau\pi}g, 2 - N). \end{aligned} \quad (\text{C.19})$$

In the last line above we have chosen a determination of -1 such that $e^{\imath\tau\pi}g$ belongs to the principal sheet of the Riemann surface, where $Z = Z^{\mathbb{R}}$; hence, $Z(e^{\imath\tau\pi}g, 2 - N) = Z^{\mathbb{R}}(e^{\imath\tau\pi}g, 2 - N) = Z^{\mathbb{R}}(-g, 2 - N)$, where in the last equality we used the fact that $Z^{\mathbb{R}}$ is single-valued. We have thus shown that, when going from $|\varphi| < \pi$ to $\pi < |\varphi| < 2\pi$ our analytic continuation of $Z(g, N)$ switches:

$$\begin{aligned} Z(g, N) &\xrightarrow{|\varphi| \nearrow \pi_+} Z^{\mathbb{R}}(g, N) + \frac{\sqrt{2\pi}}{\Gamma(N/2)} e^{\imath\tau\frac{\pi}{2}} e^{\frac{3}{2g}} \left(e^{\imath\tau\pi}\frac{g}{3}\right)^{\frac{1-N}{2}} Z^{\mathbb{R}}(-g, 2 - N) \\ &= Z(e^{\imath(2\tau\pi)}g, N) + \frac{\sqrt{2\pi}}{\Gamma(N/2)} e^{\imath\tau\frac{\pi}{2}} e^{\frac{3}{2g}} \left(e^{\imath\tau\pi}\frac{g}{3}\right)^{\frac{1-N}{2}} Z(e^{\imath\tau\pi}g, 2 - N), \end{aligned} \quad (\text{C.20})$$

where $|\varphi| \nearrow \pi_+$ signifies that the switching takes place when $|\varphi|$ crosses the value π coming from below. In the second line above, for $\pi < |\varphi| < 2\pi$, both arguments $e^{\imath(2\tau\pi)}g$ and $e^{\imath\tau\pi}g$ belong to the principal sheet of the Riemann surface, where $Z(g, N)$ has already been constructed and proven to be analytic.

The first term in Eq. (C.20) is regular up to $|\varphi| = 3\pi$, but the second one has a problem when $e^{\imath\tau\pi}g$ reaches the negative real axis (which is $\varphi \rightarrow -2\tau\pi$). Note that $Z(e^{\imath\tau\pi}g, 2 - N)$ approaches the cut singularity in the principal sheet of the Riemann surface, as its argument is $e^{\imath\tau\pi}g$. But we already know what happens with $Z(g', N')$ when g' traverses the cut singularity in the principal Riemann sheet: a branch point crosses the integration contour, one detaches a Hankel contour, and the analytic continuation switches again:

$$\begin{aligned} Z(e^{\imath\tau\pi}g, 2 - N) &\xrightarrow{|\varphi| \nearrow 2\pi_+} Z(e^{\imath(3\tau\pi)}g, 2 - N) \\ &+ \frac{\sqrt{2\pi}}{\Gamma(1 - N/2)} e^{\imath\tau\frac{\pi}{2}} e^{\frac{3}{2ge^{\imath\tau\pi}}} \left(e^{\imath(2\tau\pi)}\frac{g}{3}\right)^{\frac{N-1}{2}} Z(e^{\imath(2\tau\pi)}g, N), \end{aligned} \quad (\text{C.21})$$

where this time the arguments at which Z is evaluated on the right hand side stay in the principal sheet for $2\pi < |\varphi| < 3\pi$.

¹⁴Notice that this allows us also to analytically continue the result to $N \geq 2$.

We iterate this and build the analytic continuation of $Z(g, N)$ in terms of $Z^{\mathbb{R}}$ on the whole Riemann surface. The first few steps in this continuation are:

$$\begin{aligned}
 |\varphi| < \pi : \quad Z(g, N) &= Z^{\mathbb{R}}(g, N) , \\
 \pi < |\varphi| < 2\pi : \quad Z(g, N) &= Z(e^{i(2\tau\pi)}g, N) + \frac{\sqrt{2\pi}}{\Gamma(N/2)} e^{i\tau\frac{\pi}{2}} e^{\frac{3}{2g}} \\
 &\quad \left(e^{i\tau\pi} \frac{g}{3} \right)^{\frac{1-N}{2}} Z(e^{i\tau\pi}g, 2-N) \\
 &= Z^{\mathbb{R}}(g, N) + \frac{\sqrt{2\pi}}{\Gamma(N/2)} e^{i\tau\frac{\pi}{2}} e^{\frac{3}{2g}} \left(e^{i\tau\pi} \frac{g}{3} \right)^{\frac{1-N}{2}} Z^{\mathbb{R}}(-g, 2-N) , \\
 2\pi < |\varphi| < 3\pi : \quad Z(g, N) &= (1 + \tilde{\tau}) Z(e^{i(2\tau\pi)}g, N) \\
 &\quad + e^{i\tau\pi(N-1)} \frac{\sqrt{2\pi}}{\Gamma(N/2)} e^{i\tau\frac{\pi}{2}} e^{\frac{3}{2g}} \left(e^{i(3\tau\pi)} \frac{g}{3} \right)^{\frac{1-N}{2}} Z(e^{i(3\tau\pi)}g, 2-N) \\
 &= (1 + \tilde{\tau}) Z^{\mathbb{R}}(g, N) \\
 &\quad + e^{i\tau\pi(N-1)} \frac{\sqrt{2\pi}}{\Gamma(N/2)} e^{i\tau\frac{\pi}{2}} e^{\frac{3}{2g}} \left(e^{i(3\tau\pi)} \frac{g}{3} \right)^{\frac{1-N}{2}} Z^{\mathbb{R}}(-g, 2-N) , \quad (\text{C.22})
 \end{aligned}$$

where we denoted:

$$\begin{aligned}
 \tilde{\tau} &= \frac{\sqrt{2\pi}}{\Gamma(N/2)} e^{i\tau\frac{\pi}{2}} e^{\frac{3}{2g}} \left(e^{i\tau\pi} \frac{g}{3} \right)^{\frac{1-N}{2}} \frac{\sqrt{2\pi}}{\Gamma(1-N/2)} e^{i\tau\frac{\pi}{2}} e^{\frac{3}{2ge^{i\tau\pi}}} \left(e^{i(2\tau\pi)} \frac{g}{3} \right)^{\frac{N-1}{2}} \\
 &= 2 \sin\left(\frac{N\pi}{2}\right) e^{i\tau\pi\frac{N+1}{2}} . \quad (\text{C.23})
 \end{aligned}$$

In order to iterate Eq. (C.20), we must make sure that at each step the arguments of the functions Z involved in the analytic continuation are brought back to the principal sheet. We denote the analytic continuation of the partition function to the Riemann surface by:

$$\begin{aligned}
 2k\pi < |\varphi| < (2k+1)\pi : \\
 Z(g, N) &= \omega_{2k} Z(e^{i(2k)\tau\pi}g, N) \\
 &\quad + \eta_{2k} \frac{\sqrt{2\pi}}{\Gamma(N/2)} e^{i\tau\frac{\pi}{2}} e^{\frac{3}{2g}} \left(e^{i(2k+1)\tau\pi} \frac{g}{3} \right)^{\frac{1-N}{2}} Z(e^{i(2k+1)\tau\pi}g, 2-N) , \\
 (2k+1)\pi < |\varphi| < (2k+2)\pi : \\
 Z(g, N) &= \omega_{2k+1} Z(e^{i(2k+2)\tau\pi}g, N) \\
 &\quad + \eta_{2k+1} \frac{\sqrt{2\pi}}{\Gamma(N/2)} e^{i\tau\frac{\pi}{2}} e^{\frac{3}{2g}} \left(e^{i(2k+1)\tau\pi} \frac{g}{3} \right)^{\frac{1-N}{2}} Z(e^{i(2k+1)\tau\pi}g, 2-N) , \quad (\text{C.24})
 \end{aligned}$$

a general recursion relation for the (ω_q, η_q) is obtained from Eq. (C.20) and Eq. (C.21) generalized to the Riemann surface¹⁵:

$$(\omega_0, \eta_0) = (1, 0), \quad \begin{cases} \omega_{2k+1} = \omega_{2k} \\ \eta_{2k+1} = \eta_{2k} + \omega_{2k} \end{cases}, \quad \begin{cases} \omega_{2(k+1)} = \tilde{\tau} \eta_{2k+1} + \omega_{2k+1} \\ \eta_{2(k+1)} = e^{i\tau\pi(N-1)} \eta_{2k+1} \end{cases}. \quad (\text{C.25})$$

The recursion can easily be solved by introducing a transfer matrix:

$$\begin{pmatrix} \omega_{2k} \\ \eta_{2k} \end{pmatrix} = A^k \begin{pmatrix} 1 \\ 0 \end{pmatrix}, \quad A = \begin{pmatrix} 1 + \tilde{\tau} & \tilde{\tau} \\ e^{i\tau\pi(N-1)} & e^{i\tau\pi(N-1)} \end{pmatrix}, \quad (\text{C.26})$$

which leads to Eq. (3.11). Since the eigenvalues of A are $\pm e^{i\tau\pi\frac{N}{2}}$, we have that A^k equals the identity matrix for $k = 4$ if N is odd, and for $k = 2$ if N is even. Therefore, in these two cases we have a monodromy group of order 4 and 2, respectively. More generally, we have a monodromy group of finite order if N is a rational number, and an infinite monodromy otherwise.

Property 5. This follows by combining Property 2, which gives the asymptotic expansion of $Z^{\mathbb{R}}(g, N)$, with Eq. (C.19) using $(1+x)^{N/2-1} = \sum_{q \geq 0} \frac{\Gamma(N/2)}{q! \Gamma(N/2-q)} x^q$:

$$Z_{\pm}^C(g, N) = e^{i\tau\pi(1-\frac{N}{2})} \sqrt{2\pi} \left(\frac{g}{3}\right)^{\frac{1-N}{2}} e^{\frac{3}{2g}} \sum_{q \geq 0} \frac{1}{2^{2q} q! \Gamma(\frac{N}{2} - 2q)} \left(\frac{2g}{3}\right)^q. \quad (\text{C.27})$$

Property 6. In order to compute the discontinuity of the partition function, let us consider g in the complex plane of the coupling constant slightly below the negative real axis, $\text{Re}(g), \text{Im}(g) < 0$. This g can be reached either counterclockwise with Z_+ or clockwise with Z_- . There is a subtlety here: if we denote this point as $g = |g|e^{i\varphi}$ with $\varphi \in (\pi, 3\pi/2)$ in the clockwise direction, it corresponds to $g = |g|e^{i(\varphi-2\pi)}$ in the counterclockwise direction. While only the real axis contributes to $Z_-(g, N)$ (as turning clockwise we do not cross the cut to reach it), $Z_+(g, N)$ has the additional contribution of the Hankel contour (as turning counterclockwise we cross the cut):

$$Z_+(g, N) = Z^{\mathbb{R}}(g, N) + Z_+^C(g, N), \quad Z_-(g, N) = Z^{\mathbb{R}}(e^{-2\pi i} g, N) = Z^{\mathbb{R}}(g, N), \quad (\text{C.28})$$

where we used the fact that $Z^{\mathbb{R}}$ is single-valued. When taking the difference,

¹⁵In detail, we use:

$$\begin{aligned} & Z(e^{i(2k)\tau\pi} g, N) \xrightarrow{|\varphi| \nearrow (2k+1)\pi_+} Z(e^{i(2k+2)\tau\pi} g, N) \\ & + \frac{\sqrt{2\pi}}{\Gamma(N/2)} e^{i\tau\frac{\pi}{2}} e^{\frac{3}{2g}} \left(e^{i(2k+1)\tau\pi} \frac{g}{3}\right)^{\frac{1-N}{2}} Z(e^{i(2k+1)\tau\pi} g, 2-N), \\ & Z(e^{i(2k+1)\tau\pi} g, 2-N) \xrightarrow{|\varphi| \nearrow (2k+2)\pi_+} Z(e^{i(2k+3)\tau\pi} g, 2-N) \\ & + \frac{\sqrt{2\pi}}{\Gamma(1-N/2)} e^{i\tau\frac{\pi}{2}} e^{-\frac{3}{2g}} \left(e^{i(2k+2)\tau\pi} \frac{g}{3}\right)^{\frac{N-1}{2}} Z(e^{i(2k+2)\tau\pi} g, N), \\ & \frac{\sqrt{2\pi}}{\Gamma(N/2)} e^{i\tau\frac{\pi}{2}} e^{\frac{3}{2g}} \left(e^{i(2k+1)\tau\pi} \frac{g}{3}\right)^{\frac{1-N}{2}} \left[\frac{\sqrt{2\pi}}{\Gamma(1-N/2)} e^{i\tau\frac{\pi}{2}} e^{-\frac{3}{2g}} \left(e^{i(2k+2)\tau\pi} \frac{g}{3}\right)^{\frac{N-1}{2}} \right] = \tilde{\tau}. \end{aligned}$$

the $Z^{\mathbb{R}}$ pieces cancel and the discontinuity is given by the Hankel contour contribution, $Z_{-}(g, N) - Z_{+}(g, N) = -Z_{+}^C(g, N)$. In particular, at the negative real axis we have:

$$\text{disc}_{\pi}(Z(g, N)) = \lim_{\varphi \searrow \pi} (Z_{-}(e^{-2\pi i} g, N) - Z_{+}(g, N)) = -Z_{+}^C(e^{i\pi} |g|, N). \quad (\text{C.29})$$

Lastly, notice that the computation done on the other side of the cut, $\lim_{\varphi \nearrow -\pi} (Z_{-}(g, N) - Z_{+}(e^{2\pi i} g, N))$, gives the same result, because $Z_{-}^C(e^{-i\pi} |g|, N) = -Z_{+}^C(e^{i\pi} |g|, N)$.

Property 7. From the intermediate field expression Eq. (3.2) of the partition function, we find straightforwardly that $(N + 4g\partial_g)Z(g, N) = NZ(g, N + 2)$. Applying this twice, we have:

$$(N + 2 + 4g\partial_g)(N + 4g\partial_g)Z(g, N) = N(N + 2)Z(g, N + 4). \quad (\text{C.30})$$

Integrating by parts in Eq. (3.2) with $N \rightarrow N + 4$, we find $N(N + 2)Z(g, N + 4) = -4!Z'(g, N)$, and thus we arrive at the equation:

$$N(N + 2)Z(g, N) + ((8N + 24)g + 24)Z'(g, N) + 16g^2Z''(g, N) = 0. \quad (\text{C.31})$$

This concludes the proof of Proposition 1. \square

C.2. Properties of $Z_n(g)$

Proof of Proposition 2. The proof is similar to the one of Proposition 1.

Property 1. We start from:

$$\begin{aligned} Z_n(g) &= \int_{-\infty}^{+\infty} [d\sigma] e^{-\frac{1}{2}\sigma^2} \left(\ln \left(1 - i\sqrt{\frac{g}{3}}\sigma \right) \right)^n \\ &= \int_{-\infty}^{+\infty} [d\sigma] e^{-\frac{1}{2}\sigma^2} \left(\ln \left(1 - ie^{i\frac{\varphi}{2}} \sqrt{\frac{|g|}{3}}\sigma \right) \right)^n, \end{aligned} \quad (\text{C.32})$$

where we parameterized $g = |g|e^{i\varphi}$ with $\varphi \in (-\pi, \pi)$. For any real x we have $1 + |x| \geq |1 - ie^{i\frac{\varphi}{2}}x| \geq \cos \frac{\varphi}{2}$; hence, we can bound the logarithm as:

$$\begin{aligned} \left| \ln \left(1 - ie^{i\frac{\varphi}{2}}x \right) \right|^2 &\leq \pi^2 + \max \left\{ [\ln(\cos \frac{\varphi}{2})]^2, [\ln(1 + |x|)]^2 \right\} \\ &\leq 2 \left[(|\ln(\cos \frac{\varphi}{2})| + 1) \ln(e^{\pi} + |x|) \right]^2, \end{aligned} \quad (\text{C.33})$$

which implies:

$$|Z_n(g)| \leq \left| 2^{1/2} (|\ln(\cos \frac{\varphi}{2})| + 1) \right|^n \int [d\sigma] e^{-\frac{1}{2}\sigma^2} \left[\ln \left(e^{\pi} + \sqrt{\frac{|g|}{3}}|\sigma| \right) \right]^n. \quad (\text{C.34})$$

We have $\ln(e^{\pi} + \sqrt{\frac{|g|}{3}}|\sigma|) \leq \frac{1}{\varepsilon}(e^{\pi} + \sqrt{\frac{|g|}{3}}|\sigma|)^{\varepsilon}$ for any $\varepsilon > 0$. Cutting the integration interval into regions where $e^{\pi} < \sqrt{\frac{|g|}{3}}|\sigma|$ and regions where $e^{\pi} >$

$\sqrt{\frac{|g|}{3}}|\sigma|$ and extending each piece back to the entire real line, we get a bound:

$$\begin{aligned} |Z_n(g)| &\leq \frac{\left| 2^{1/2} \left(\left| \ln \left(\cos \frac{\varphi}{2} \right) \right| + 1 \right) \right|^n}{\varepsilon^n} \left[(2e^\pi)^{n\varepsilon} + \left(\frac{4|g|}{3} \right)^{\frac{n\varepsilon}{2}} \int [d\sigma] e^{-\frac{1}{2}\sigma^2} |\sigma|^{n\varepsilon} \right] \\ &\leq K^n \frac{\left(\left| \ln \left(\cos \frac{\varphi}{2} \right) \right| + 1 \right)^n}{\varepsilon^n} \left(1 + |g|^{\frac{n\varepsilon}{2}} \Gamma \left(\frac{n\varepsilon+1}{2} \right) \right). \end{aligned} \quad (\text{C.35})$$

Property 2. In order to derive the asymptotic expansion of $Z_n(g)$, we use Faà di Bruno's formula¹⁶: to expand:

$$\left(\ln(1 - i\sqrt{\frac{g}{3}}\sigma) \right)^n = \sum_{m \geq n} \left(i\sqrt{\frac{g}{3}} \right)^m \sigma^m \sum_{\substack{m_1, \dots, m_m \geq 0 \\ \sum k m_k = m, \sum m_k = n}} \frac{(-1)^n n!}{\prod_k k^{m_k} m_k!}, \quad (\text{C.36})$$

and integrate the Gaussian term by term. As a cross check, we can (formally) resum¹⁷

$$\begin{aligned} \sum_{n \geq 0} \frac{1}{n!} \left(-\frac{N}{2} \right)^n Z_n(g) &\simeq \sum_{n \geq 0} \frac{1}{n!} \left(-\frac{N}{2} \right)^n \sum_{m \geq n/2} \left(-\frac{2g}{3} \right)^m \frac{(2m)!}{2^{2m} m!} \\ &\quad \times \sum_{\substack{m_1, \dots, m_{2m} \geq 0 \\ \sum k m_k = 2m, \sum m_k = n}} \frac{(-1)^n n!}{\prod_k k^{m_k} m_k!} \\ &= \sum_{m=0}^{\infty} \left(-\frac{2g}{3} \right)^m \frac{(2m)!}{2^{2m} m!} \sum_{\substack{m_1, \dots, m_{2m} \geq 0 \\ \sum k m_k = 2m}} \prod_{k=1}^{2m} \left(\frac{N}{2k} \right)^{m_k} \frac{1}{m_k!} \\ &= \sum_{m=0}^{\infty} \frac{\Gamma(2m + N/2)}{2^{2m} m! \Gamma(N/2)} \left(-\frac{2g}{3} \right)^m, \end{aligned} \quad (\text{C.37})$$

reproducing the asymptotic expansion of $Z(g, N)$ in Eq. (3.7).

¹⁶Namely, we evaluate the q -th term of the Taylor expansion using the following formula (at $u = 0$)

$$\begin{aligned} \frac{d^q}{du^q} [\ln(1 - ux)]^n &= \sum_{\substack{m_1, \dots, m_q \\ \sum k m_k = q, \sum m_k \leq n}} \frac{q!}{\prod_k m_k! (k!)^{m_k}} \frac{n!}{(n - \sum_k m_k)!} [\ln(1 - ux)]^{n - \sum_k m_k} \\ &\quad \prod_k \left(\frac{-(k-1)! x^k}{(1 - ux)^k} \right)^{m_k}. \end{aligned}$$

¹⁷ In the last step, we use: $\sum_{m_1, m_2, \dots \geq 0} : \prod_{k \geq 1} \frac{1}{m_k!} \left(\frac{N x^k}{2k} \right)^{m_k} = \exp \{ \sum_{k \geq 1} \frac{N x^k}{2k} \} = (1 - x)^{-N/2} = \sum_{m=0}^{\infty} \frac{\Gamma(m + N/2)}{\Gamma(N/2) m!} x^m$.

Property 3. We analytically continue $Z_n(g)$ to the extended Riemann sheet $\mathbb{C}_{3\pi/2}$ as in Property 3, Proposition 2, by turning the integration contour by $e^{-i\theta}$:

$$Z_{n\theta}(g) = \int_{-\infty}^{+\infty} e^{-i\theta} [d\sigma] e^{-\frac{1}{2} e^{-2i\theta} \sigma^2} \left(\ln(1 - i e^{i\frac{\varphi-2\theta}{2}} \sqrt{\frac{|g|}{3}} \sigma) \right)^n. \quad (\text{C.38})$$

Using a Taylor formula with integral rest, the reminder $R_{n\theta}^q(g)$ writes:

$$\begin{aligned} R_{n\theta}^q(g) &= \int_0^1 du \frac{(1-u)^{2q-1}}{(2q-1)!} \int_{\mathbb{R}} e^{-i\theta} [d\sigma] e^{-\frac{1}{2} e^{-2i\theta} \sigma^2} \left(\frac{d}{du} \right)^{2q} \left(\ln \left(1 - i e^{i\frac{\varphi-2\theta}{2}} \sqrt{\frac{|g|}{3}} \sigma u \right) \right)^n \\ &= \int_0^1 du \frac{(1-u)^{2q-1}}{(2q-1)!} \int_{\mathbb{R}} e^{-i\theta} [d\sigma] e^{-\frac{1}{2} e^{-2i\theta} \sigma^2} \frac{\left(i e^{i\frac{\varphi-2\theta}{2}} \sqrt{\frac{|g|}{3}} \sigma \right)^{2q}}{\left(1 - i e^{i\frac{\varphi-2\theta}{2}} \sqrt{\frac{|g|}{3}} \sigma u \right)^{2q}} \\ &\quad \times \sum_{\substack{m_1, \dots, m_q \\ \sum k m_k = 2q, \sum m_k \leq n}} \frac{(2q)!}{\prod_k m_k! k^{m_k}} \frac{(-1)^{\sum m_k} n!}{(n - \sum_k m_k)!} \\ &\quad \times \left(\ln \left(1 - i e^{i\frac{\varphi-2\theta}{2}} \sqrt{\frac{|g|}{3}} \sigma u \right) \right)^{n - \sum_k m_k}. \end{aligned} \quad (\text{C.39})$$

Now $|1 - i \sqrt{\frac{|g|}{3}} e^{i\frac{\varphi-2\theta}{2}} \sigma u| \geq \cos \frac{\varphi-2\theta}{2}$ and:

$$\begin{aligned} &\frac{\left(\ln \left(1 - i e^{i\frac{\varphi-2\theta}{2}} \sqrt{\frac{|g|}{3}} \sigma u \right) \right)^{n - \sum_k m_k}}{\left(1 - i e^{i\frac{\varphi-2\theta}{2}} \sqrt{\frac{|g|}{3}} \sigma u \right)^{2q}} \\ &\leq \frac{\left| 2^{1/2} \left(\left| \ln \left(\cos \frac{\varphi-2\theta}{2} \right) \right| + 1 \right) \ln(e^\pi + |g| |\sigma|) \right|^{n - \sum m_k}}{\left(\cos \frac{\varphi-2\theta}{2} \right)^{2q}}, \end{aligned} \quad (\text{C.40})$$

therefore:

$$\begin{aligned} |R_{n\theta}^q(g)| &\leq \frac{n! 2^{\frac{n}{2}} \left(\left| \ln \left(\cos \frac{\varphi-2\theta}{2} \right) \right| + 1 \right)^n}{\left(\cos \frac{\varphi-2\theta}{2} \right)^{2q}} \left(\frac{|g|}{3} \right)^q \frac{\Gamma(2q + \frac{1}{2})}{(2q)!} \\ &\quad \times \int [d\sigma] e^{-\frac{1}{2} \cos(2\theta) \sigma^2} \sigma^{2q} [\ln(e^\pi + |g| |\sigma|)]^n \\ &\leq K \frac{\left(\left| \ln \left(\cos \frac{\varphi-2\theta}{2} \right) \right| + 1 \right)^n}{\left(\cos \frac{\varphi-2\theta}{2} \right)^{2q}} \left(\frac{|g|}{3} \right)^q \\ &\quad \times \left(\frac{(2q)!}{2^q q! (\cos(2\theta))^{q+1/2}} + 2^q \frac{|g|^{\frac{n\varepsilon}{2}} \Gamma(q + \frac{n\varepsilon+1}{2})}{(\cos(2\theta))^{q+(n\varepsilon+1)/2}} \right), \end{aligned} \quad (\text{C.41})$$

for any ε with (K depending on n and ε). Fixing for example $\varepsilon = 1$ and $\theta = \frac{\varphi}{6}$ yields the desired result as in Property 3, Proposition 1.

Property 4. A slight variation on the bound in Property 1 yields:

$$|Z_{n\theta}(g)| \leq K^n \frac{\left(\left| \ln \left(\cos \frac{\varphi - 2\theta}{2} \right) \right| + 1 \right)^n}{\varepsilon^n} \left(1 + \frac{|g|^{\frac{n\varepsilon}{2}} \Gamma \left(\frac{n\varepsilon+1}{2} \right)}{(\cos(2\theta))^{(n\varepsilon+1)/2}} \right). \quad (\text{C.42})$$

Fixing for convenience $\theta = \frac{\varphi}{6}$, one observes that $\sum_{n \geq 0} \frac{1}{n!} (-N/2)^n Z_{n\theta}(g)$ has infinite radius of convergence in N for any $|\varphi| < 3\pi/2$. Denoting, similarly to the notation we used for $Z(g, N)$, the analytic continuation of $Z_n(g)$ to the extended Riemann sheet $\mathbb{C}_{3\pi/2}$ by:

$$\theta > 0, \quad Z_{n+}(g) = Z_{n\theta}(g), \quad Z_{n-}(g) = Z_{n-\theta}(g), \quad (\text{C.43})$$

we note that the bound on the Taylor rest term in Eq. (C.41) is lost for $\varphi \rightarrow \pm 3\pi/2$; hence, Borel summability is lost for $\varphi \rightarrow \pm\pi$. As in the case of $Z(g, N)$, after g crosses the cut at \mathbb{R}_- , say counterclockwise, in deforming the contour of integration $e^{-i\theta}\mathbb{R}$ back to the steepest-descent contour along the real line, we generate a clockwise-oriented Hankel contour around $\sigma_* \times (1, +\infty)$:

$$\begin{aligned} Z_{n\pm}(g)|_{\varphi \gtrless \pi} &= \int_{e^{\mp i\theta}\mathbb{R}} [d\sigma] e^{-\frac{1}{2}\sigma^2} \left(\ln \left(1 - i\sqrt{\frac{g}{3}}\sigma \right) \right)^n = Z_n^{\mathbb{R}}(g) + Z_{n\pm}^C(g) \\ Z_n^{\mathbb{R}}(g) &= \int_{\mathbb{R}} [d\sigma] e^{-\frac{1}{2}\sigma^2} \left(\ln \left(1 - i\sqrt{\frac{g}{3}}\sigma \right) \right)^n, \\ Z_{n\pm}^C(g) &= \int_C [d\sigma] e^{-\frac{1}{2}\sigma^2} \left(\ln \left(1 - i\sqrt{\frac{g}{3}}\sigma \right) \right)^n. \end{aligned} \quad (\text{C.44})$$

Property 5. We now compute $Z_{n\pm}^C(g)$. As in Proposition 1 this is given by integrating along the clockwise orientated Hankel contour \mathcal{C} . First we change variable to $\sigma = e^{-i\frac{\pi}{2} - i\frac{\varphi}{2}} \sqrt{3/|g|} \sigma'$ and the contour becomes C' clockwise oriented around $(1, \infty)$ and a shift $\sigma' = 1 + t$ brings C' to a clockwise-oriented contour around the positive real axis:

$$\begin{aligned} Z_{n\pm}^C(g) &= \left(\frac{3}{e^{i\pi}g} \right)^{1/2} \int_{C'} [d\sigma'] e^{\frac{3}{2g}(\sigma')^2} [\ln(1 - \sigma')]^n \\ &= \frac{1}{\sqrt{2\pi}} \left(\frac{3}{e^{i\pi}g} \right)^{1/2} \int_{C''} dt e^{\frac{3}{2g}(1+t)^2} [\ln(-t)]^n. \end{aligned} \quad (\text{C.45})$$

A further change of variables $t = e^{i\tau\pi} \frac{g}{3} u$ with $\tau = -\text{sgn}(\varphi)$ yields¹⁸:

$$\begin{aligned} Z_{n\pm}^C(g) &= \frac{e^{i\tau\pi}}{i} \frac{1}{\sqrt{2\pi}} \sqrt{\frac{g}{3}} e^{\frac{3}{2g}} \int_0^\infty du e^{-u + \frac{g}{6}u^2} \left[\left(\ln \left(\frac{e^{i\tau\pi}g}{3} u \right) - i\pi \right)^n - \left(\ln \left(\frac{e^{i\tau\pi}g}{3} u \right) + i\pi \right)^n \right] \\ &= \frac{e^{i\tau\pi}}{i} \frac{1}{\sqrt{2\pi}} \sqrt{\frac{g}{3}} e^{\frac{3}{2g}} \sum_{q \geq 0} \frac{1}{q!} \left(\frac{g}{6} \right)^q \sum_{p=0}^n \binom{n}{p} \end{aligned}$$

¹⁸See comments below Eq. (C.16) for an explanation of the τ -dependence.

$$\times \int_0^\infty du e^{-u} u^{2q} (\ln u)^p \left[\left(\ln \left(\frac{e^{\imath\tau\pi} g}{3} \right) - \imath\pi \right)^{n-p} - \left(\ln \left(\frac{e^{\imath\tau\pi} g}{3} \right) + \imath\pi \right)^{n-p} \right], \quad (\text{C.46})$$

and integrating over u we get

$$Z_{n\pm}^C(g) \simeq \frac{e^{\imath\tau\pi}}{\imath} \frac{e^{\frac{3}{2g}}}{\sqrt{2\pi}} \sqrt{\frac{g}{3}} \sum_{q=0}^\infty \frac{1}{q!} \left(\frac{g}{6} \right)^q \sum_{p=0}^n \binom{n}{p} \frac{d^p \Gamma(z)}{dz^p} \Big|_{z=2q+1} \\ \times \left[\left(\ln \left(\frac{e^{\imath\tau\pi} g}{3} \right) - \imath\pi \right)^{n-p} - \left(\ln \left(\frac{e^{\imath\tau\pi} g}{3} \right) + \imath\pi \right)^{n-p} \right], \quad (\text{C.47})$$

which combined with Property 2 implies the full transseries expansion Eq. (3.26).

A good cross check of the results consist in summing over n :

$$\sum_{n \geq 0} \frac{1}{n!} \left(-\frac{N}{2} \right)^n Z_{n\pm}^C(g) \\ = \frac{e^{\imath\tau\pi}}{\imath} \frac{e^{\frac{3}{2g}}}{\sqrt{2\pi}} \sqrt{\frac{g}{3}} \sum_{q=0}^\infty \frac{1}{q!} \left(\frac{g}{6} \right)^q \sum_{p,k=0}^\infty \frac{1}{p! k!} \left(-\frac{N}{2} \right)^{p+k} \frac{d^p \Gamma(z)}{dz^p} \Big|_{z=2q+1} \\ \times \left[\left(\ln \left(\frac{e^{\imath\tau\pi} g}{3} \right) - \imath\pi \right)^k - \left(\ln \left(\frac{e^{\imath\tau\pi} g}{3} \right) + \imath\pi \right)^k \right] \\ = \frac{e^{\imath\tau\pi}}{\imath} \frac{e^{\frac{3}{2g}}}{\sqrt{2\pi}} \sqrt{\frac{g}{3}} \sum_{q=0}^\infty \frac{1}{q!} \left(\frac{g}{6} \right)^q \Gamma \left(2q + \frac{2-N}{2} \right) \left[e^{\imath \frac{N\pi}{2}} \left(\frac{e^{\imath\tau\pi} g}{3} \right)^{-\frac{N}{2}} - e^{-\imath \frac{N\pi}{2}} \left(\frac{e^{\imath\tau\pi} g}{3} \right)^{-\frac{N}{2}} \right] \\ = \frac{e^{\imath\tau\pi(1-\frac{N}{2})}}{\imath} \frac{e^{\frac{3}{2g}}}{\sqrt{2\pi}} \left(\frac{g}{3} \right)^{\frac{1-N}{2}} \sum_{q \geq 0} \frac{\Gamma(2q + \frac{2-N}{2}) \frac{\sin \frac{N\pi}{2}}{2^{2q} q!} 2\pi \imath}{2^{2q} q!} \left(\frac{2g}{3} \right)^q, \quad (\text{C.48})$$

Which coincides with the instanton part in Eq. (3.12).

Property 6. This follows from $\text{disc}_\pi(Z_n(g)) = -Z_{n+}^C(e^{\imath\pi}|g|)$ combined with Properties 4 and 5.

Property 7. The derivation of Eq. (3.29) is straightforward. We substitute the small- N expansion (3.23), with the condition $Z(g, 0) = 1$, in the partial differential equation for $Z(g, N)$, Eq. (3.16), and collect the terms with the same powers of N .

This concludes the proof of Proposition 2. \square

C.3. The LVE, Analyticity

Proof of Proposition 3. We review here briefly the proof the LVE formula for the free energy. For more details, see [18] and follow-up work. We use the notation of the Gaussian integral as a differential operator (see [38] for a detailed discussion of this notation), as a convenient bookkeeping device for the action of derivatives with respect to matrix elements of the covariance of a Gaussian measure and we denote $V(\sigma) = \ln(1 - \imath\sqrt{g/3}\sigma)$. Equation (3.23) becomes with this notation:

$$Z(g, N) = \sum_{n \geq 0} \frac{1}{n!} \left(-\frac{N}{2} \right)^n Z_n, \quad Z_n(g) = \int [d\sigma] e^{-\frac{1}{2}\sigma^2} [\ln(1 - \imath\sqrt{g/3}\sigma)]^n$$

$$\equiv \left[e^{\frac{1}{2} \frac{\delta}{\delta \sigma} \frac{\delta}{\delta \sigma} V(\sigma)^n} \right]_{\sigma=0}, \quad (\text{C.49})$$

where $\delta/\delta\sigma$ denotes the derivative with respect to σ .

Let us take aside a term $Z_n(g)$. We introduce copies with degenerate covariance and we introduce fictitious interpolating link parameters $x_{kl} = x_{lk} = 1$:

$$Z_n(g) = \left[e^{\frac{1}{2} \sum_{k,l=1}^n \frac{\delta}{\delta \sigma_k} \frac{\delta}{\delta \sigma_l} \prod_{i=1}^n V(\sigma_i)} \right]_{\sigma_i=0} = \left[e^{\frac{1}{2} \sum_{k,l=1}^n x_{kl} \frac{\delta}{\delta \sigma_k} \frac{\delta}{\delta \sigma_l} \prod_{i=1}^n V(\sigma_i)} \right]_{\sigma_i=0, x_{ij}=1}. \quad (\text{C.50})$$

We fix the diagonal elements $x_{ii} = 1$ and use symmetric interpolations $x_{ij} = x_{ji}$ where x_{ij} with $i < j$ are independent parameters. For all $i \neq j$:

$$\frac{\partial}{\partial x_{ij}} \left[e^{\frac{1}{2} \sum_{k,l=1}^n x_{kl} \frac{\delta}{\delta \sigma_k} \frac{\delta}{\delta \sigma_l}} \right] = e^{\frac{1}{2} \sum_{k,l=1}^n x_{kl} \frac{\delta}{\delta \sigma_k} \frac{\delta}{\delta \sigma_l}} \left(\frac{\delta}{\delta \sigma_i} \frac{\delta}{\delta \sigma_j} \right), \quad (\text{C.51})$$

and using Appendix D, we get:

$$\begin{aligned} Z(g, N) &= \sum_{n \geq 0} \frac{\left(-\frac{N}{2}\right)^n}{n!} \sum_{\mathcal{F} \in F_n} \int_0^1 \prod_{(i,j) \in \mathcal{F}} du_{ij} \\ &\quad \times \left[e^{\frac{1}{2} \sum_{k,l} w_{kl}^{\mathcal{F}} \frac{\delta}{\delta \sigma_k} \frac{\delta}{\delta \sigma_l}} \left(\prod_{(i,j) \in \mathcal{F}} \frac{\delta}{\delta \sigma_i} \frac{\delta}{\delta \sigma_j} \right) \prod_{i=1}^n V(\sigma_i) \right]_{\sigma_i=0}, \end{aligned} \quad (\text{C.52})$$

where F_n is the set of all the forests over n labeled vertices.

Observing that the contribution of a forest factors over the trees (connected components) in the forest, the logarithm is trivial: it comes to restricting the sum above to trees over n vertices (hence with $n - 1$ edges):

$$\begin{aligned} W(g, N) &= \sum_{n \geq 1} \frac{\left(-\frac{N}{2}\right)^n}{n!} \sum_{\mathcal{T} \in T_n} \int_0^1 \prod_{(i,j) \in \mathcal{T}} du_{ij} \\ &\quad \times \left[e^{\frac{1}{2} \sum_{k,l} w_{kl}^{\mathcal{T}} \frac{\delta}{\delta \sigma_k} \frac{\delta}{\delta \sigma_l}} \left(\prod_{(i,j) \in \mathcal{T}} \frac{\delta}{\delta \sigma_i} \frac{\delta}{\delta \sigma_j} \right) \prod_{i=1}^n V(\sigma_i) \right]_{\sigma_i=0}. \end{aligned} \quad (\text{C.53})$$

Taking into account that the action of the derivatives on the interaction is:

$$\frac{\delta^d}{\delta \sigma^d} \ln \left(1 - \imath \sqrt{\frac{g}{3}} \sigma \right) = (-1) \frac{(d-1)! \left(\imath \sqrt{\frac{g}{3}} \right)^d}{\left(1 - \imath \sqrt{\frac{g}{3}} \sigma \right)^d}, \quad (\text{C.54})$$

denoting d_i the degree of the vertex i in \mathcal{T} , recalling that $\sum_i d_i = 2(n-1)$ and observing that the terms $n = 1$ is special we get:

$$\begin{aligned} W(g, N) &= -\frac{N}{2} \left[e^{\frac{1}{2} \frac{\delta}{\delta \sigma} \frac{\delta}{\delta \sigma} \ln \left(1 - \imath \sqrt{\frac{g}{3}} \sigma \right)} \right]_{\sigma=0} \\ &\quad - \sum_{n \geq 2} \frac{1}{n!} \left(-\frac{N}{2} \right)^n \left(\frac{g}{3} \right)^{n-1} \sum_{\mathcal{T} \in T_n} \int_0^1 \prod_{(i,j) \in \mathcal{T}} du_{ij} \end{aligned}$$

$$\times \left[e^{\frac{1}{2} \sum_{i,j} w_{ij}^T \frac{\delta}{\delta \sigma_i} \frac{\delta}{\delta \sigma_j}} \prod_i \frac{(d_i - 1)!}{(1 - \imath \sqrt{\frac{g}{3}} \sigma_i)^{d_i}} \right]_{\sigma_i=0}. \quad (\text{C.55})$$

Reinstating the notation of the normalized Gaussian measure as a probability density, we obtain the series in Eq. (4.7), with coefficients (4.5).

Property 1 and 2. In order to determine the domain of convergence of (4.7), let us denote as usual $g = |g|e^{\imath\varphi}$, and take $-\pi < \varphi < \pi$. In this region, we can use the uniform bound $|1 - \imath \sqrt{\frac{g}{3}} \sigma_i| \geq \cos \frac{\varphi}{2}$, remaining with Gaussian integrals over σ_i and integrals over u_{ij} , both bounded by 1. Therefore, for $n \geq 2$, a crude bound on $W_n(g)$ is:

$$|W_n(g)| \leq \left| \frac{g}{3} \right|^{n-1} \frac{(n-2)!}{(\cos \frac{\varphi}{2})^{2(n-1)}} \sum_{d_i \geq 1}^{\sum_{i=1}^n (d_i - 1) = n-2} 1 = \frac{(2n-3)!}{(n-1)!} \left| \frac{g}{3 (\cos \frac{\varphi}{2})^2} \right|^{n-1}, \quad (\text{C.56})$$

where we used the fact that there are $(n-2)! / \prod_i (d_i - 1)!$ trees over n labeled vertices with degree d_i at the vertex i , and that the sum over d_i is the coefficient of x^{n-2} in the expansion of $(1-x)^{-n} = \sum_{q \geq 0} \binom{n-1+q}{n-1} x^q$. Using Stirling's formula for the asymptotics of the factorials, it follows that $W(g, N)$ is convergent in a cardioid domain $|gN| < \frac{3}{2} (\cos \frac{\varphi}{2})^2$.

Property 3. The domain of convergence can be enlarged by turning $\sigma \rightarrow e^{-\imath\theta} \sigma$, which yields a convergent expansion in a subdomain of the extended Riemann sheet $\mathbb{C}_{3\pi/2}$. In order to make this precise, let us define:

$$\begin{aligned} W_\theta(g, N) = & -\frac{N}{2} \int e^{-\imath\theta} [d\sigma] e^{-\frac{1}{2} e^{-2\imath\theta} \sigma^2} \ln \left(1 - \imath \sqrt{\frac{g}{3}} e^{-\imath\theta} \sigma \right) - \sum_{n \geq 2} \frac{1}{n!} \left(-\frac{N}{2} \right)^n \left(\frac{g}{3} \right)^{n-1} \\ & \times \sum_{\mathcal{T} \in T_n} \int_0^1 \prod_{(i,j) \in \mathcal{T}} du_{ij} \int_{\mathbb{R}} \frac{\prod_i e^{-\imath\theta} [d\sigma_i]}{\sqrt{\det w^{\mathcal{T}}}} e^{-\frac{1}{2} e^{-2\imath\theta} \sum_{i,j} \sigma_i (w^{\mathcal{T}})^{-1}_{ij} \sigma_j} \\ & \prod_i \frac{(d_i - 1)!}{\left(1 - \imath \sqrt{\frac{g}{3}} e^{-\imath\theta} \sigma_i \right)^{d_i}}, \end{aligned} \quad (\text{C.57})$$

and implicitly $W_{n\theta}(g)$. It is easy to check that, for g in the cut plane \mathbb{C}_π both $W_\theta(g, N)$ and $W_{n\theta}(g)$ are independent of θ as long as they converge. As θ can be chosen such that the integrals converge for $|\varphi| > \pi$, $W_\theta(g, N)$ and $W_{n\theta}(g)$ analytically extend $W(g, N)$ and $W_n(g)$ to some maximal domain.

Property 4 and 5. We now have the bound $|1 - \imath \sqrt{\frac{g}{3}} e^{-\imath\theta} \sigma_i| \geq \cos \frac{\varphi-2\theta}{2}$ and the Gaussian integral is bounded by:

$$\left| \int \frac{\prod_i e^{-\imath\theta} [d\sigma_i]}{\sqrt{\det w^{\mathcal{T}}}} e^{-\frac{1}{2} e^{-2\imath\theta} \sum_{i,j} \sigma_i (w^{\mathcal{T}})^{-1}_{ij} \sigma_j} \right| \leq \frac{1}{[\cos(2\theta)]^{\frac{n}{2}}}, \quad (\text{C.58})$$

and the combinatorics runs as before leading to:

$$|W_{n\theta}(g)| \leq \frac{(2n-3)!}{(n-1)!} \frac{1}{\sqrt{\cos(2\theta)}} \left| \frac{g}{3 \sqrt{\cos(2\theta)} \left(\cos \frac{\varphi-2\theta}{2} \right)^2} \right|^{n-1}. \quad (\text{C.59})$$

Using again Stirling's formula, we find that $W(g, N)$ is convergent for $|g| < \frac{1}{|N|} \frac{3}{2} \sqrt{\cos(2\theta)} \left(\cos \frac{\varphi - 2\theta}{2} \right)^2$. This concludes the proof of Proposition 3. \square

C.4. Borel Summability of $W_n(g)$ and $W(g, N)$ in \mathbb{C}_π

Proof of Proposition 4.. We focus on $W(g, N)$: for $W_n(g)$ one follows the same steps without summing over n . Our starting point is the expression:

$$W_\theta(g, N) = -\frac{N}{2} \left[e^{\frac{1}{2} e^{2i\theta} \frac{\delta}{\delta\sigma} \frac{\delta}{\delta\sigma}} \ln \left(1 - i\sqrt{\frac{g}{3}} e^{-i\theta} \sigma \right) \right]_{\sigma=0} - \sum_{n \geq 2} \frac{1}{n!} \left(-\frac{N}{2} \right)^n \left(\frac{g}{3} \right)^{n-1} \\ \times \sum_{\mathcal{T} \in T_n} \int_0^1 \left(\prod_{(i,j) \in \mathcal{T}} du_{ij} \right) \left[e^{\frac{1}{2} e^{2i\theta} \sum_{i,j} w_{ij}^{\mathcal{T}} \frac{\delta}{\delta\sigma_i} \frac{\delta}{\delta\sigma_j}} \prod_i \frac{(d_i - 1)!}{(1 - i\sqrt{\frac{g}{3}} e^{-i\theta} \sigma_i)^{d_i}} \right]_{\sigma_i=0}. \quad (\text{C.60})$$

for the analytical continuation $W_\theta(g, N)$ of the free energy.

We are interested in finding a good bound on the Taylor rest term of order q of the expansion of $W(g, N)$. This Taylor rest term consists in two pieces. We denote $Q_\theta^q(g)$ the sum over all the trees having at least q edges:

$$Q_\theta^q(g, N) = - \sum_{n \geq q+1} \frac{1}{n!} \left(-\frac{N}{2} \right)^n \left(\frac{g}{3} \right)^{n-1} \\ \times \sum_{\mathcal{T} \in T_n} \int_0^1 \left(\prod_{(i,j) \in \mathcal{T}} du_{ij} \right) \left[e^{\frac{1}{2} e^{2i\theta} \sum_{i,j} w_{ij}^{\mathcal{T}} \frac{\delta}{\delta\sigma_i} \frac{\delta}{\delta\sigma_j}} \prod_i \frac{(d_i - 1)!}{(1 - i\sqrt{\frac{g}{3}} e^{-i\theta} \sigma_i)^{d_i}} \right]_{\sigma_i=0}. \quad (\text{C.61})$$

Due to the overall g^{n-1} factor, such trees contribute only to orders higher than q in the Taylor expansion of $W_\theta(g, N)$, hence are entirely contained in the Taylor rest term. The trees with less than q edges contribute both to the explicit terms of order lower than q in the Taylor expansion and to the rest term. In order to isolate their contribution to the rest term we perform for each of them a Taylor expansion with integral rest up to an appropriate order. We do this by Taylor expanding the Gaussian measure, which generates loop edges, each of which comes equipped with a g . For a tree with $n - 1$ edges, $n - q$ explicit loop edges need to be expanded. The Taylor rest term coming from such trees writes then:

$$P_\theta^q(g, N) = -\frac{N}{2} \int_0^1 \frac{(1-t)^{q-1}}{(q-1)!} \left(\frac{d}{dt} \right)^q \left[e^{\frac{t}{2} e^{2i\theta} \frac{\delta}{\delta\sigma} \frac{\delta}{\delta\sigma}} \ln \left(1 - i\sqrt{\frac{g}{3}} e^{-i\theta} \sigma \right) \right]_{\sigma=0} \\ - \sum_{n=2}^q \frac{1}{n!} \left(-\frac{N}{2} \right)^n \left(\frac{g}{3} \right)^{n-1} \sum_{\mathcal{T} \in T_n} \int_0^1 \left(\prod_{(i,j) \in \mathcal{T}} du_{ij} \right) \int_0^1 dt \frac{(1-t)^{q-n}}{(q-n)!} \\ \times \left(\frac{d}{dt} \right)^{q-n+1} \left[e^{\frac{t}{2} e^{2i\theta} \sum_{i,j} w_{ij}^{\mathcal{T}} \frac{\delta}{\delta\sigma_i} \frac{\delta}{\delta\sigma_j}} \prod_i \frac{(d_i - 1)!}{(1 - i\sqrt{\frac{g}{3}} e^{-i\theta} \sigma_i)^{d_i}} \right]_{\sigma_i=0}. \quad (\text{C.62})$$

The total rest term of the Taylor expansion of $W_\theta(g, N)$ is the sum $R_\theta^q(g, N) = P_\theta^q(g, N) + Q_\theta^q(g, N)$.

The contribution of large trees. $Q_\theta^q(g, N)$. Using Eq. (4.10), the contribution of large trees is immediately bounded by:

$$|Q_\theta^q(g, N)| \leq \frac{1}{\sqrt{\cos(2\theta)}} \sum_{n \geq q+1} \left| \frac{N}{2} \right|^n \left| \frac{g}{3} \right|^{n-1} \frac{1}{\left[\sqrt{\cos(2\theta)} \left(\cos \frac{\varphi-2\theta}{2} \right)^2 \right]^{n-1}} \frac{1}{n(n-1)} \binom{2n-3}{n-1}, \quad (\text{C.63})$$

and using $\frac{1}{n(n-1)} \binom{2n-3}{n-1} \leq 2^{2n-3}$ we get:

$$\begin{aligned} |Q_\theta^q(g, N)| &\leq \frac{|N|}{4\sqrt{\cos(2\theta)}} \sum_{n \geq q+1} \left(\frac{1}{\frac{3}{2}\sqrt{\cos(2\theta)} \left(\cos \frac{\varphi-2\theta}{2} \right)^2} \right)^{n-1} |Ng|^{n-1} \\ &\leq \frac{\frac{|N|}{4\sqrt{\cos(2\theta)}}}{1 - \frac{|Ng|}{\frac{3}{2}\sqrt{\cos(2\theta)} \left(\cos \frac{\varphi-2\theta}{2} \right)^2}} \left(\frac{1}{\frac{3}{2}\sqrt{\cos(2\theta)} \left(\cos \frac{\varphi-2\theta}{2} \right)^2} \right)^q |Ng|^q. \end{aligned} \quad (\text{C.64})$$

Observe that this bound *does not* have a $q!$ growth. This seems much better than expected. In fact this is not surprising: the factorial growth of the rest term comes from the divergent number of graphs in perturbation theory. As the large trees do not need to be further expanded in graphs, they do not generate a factorial growth. In fact it is the small trees that pose a problem.

The contribution of small trees $P_\theta^q(g, N)$. The contribution of small trees requires more work. We have:

$$\begin{aligned} P_\theta^q(g, N) &= -\frac{N}{2} \int_0^1 \frac{(1-t)^{q-1}}{(q-1)!} \left[e^{\frac{t}{2} e^{2i\theta} \frac{\delta}{\delta\sigma} \frac{\delta}{\delta\sigma}} \left(\frac{1}{2} e^{2i\theta} \right)^q \left(\frac{\delta}{\delta\sigma} \right)^{2q} \ln \left(1 - i\sqrt{\frac{g}{3}} e^{-i\theta} \sigma \right) \right]_{\sigma=0} \\ &\quad - \sum_{n=2}^q \frac{1}{n!} \left(-\frac{N}{2} \right)^n \left(\frac{g}{3} \right)^{n-1} \sum_{\mathcal{T} \in T_n} \int_0^1 \left(\prod_{(i,j) \in \mathcal{T}} du_{ij} \right) \int_0^1 dt \frac{(1-t)^{q-n}}{(q-n)!} \\ &\quad \times \left[e^{\frac{t}{2} e^{2i\theta} \sum_{i,j} w_{ij}^{\mathcal{T}} \frac{\delta}{\delta\sigma_i} \frac{\delta}{\delta\sigma_j}} \left(\frac{1}{2} e^{2i\theta} \sum_{i,j} w_{ij}^{\mathcal{T}} \frac{\delta}{\delta\sigma_i} \frac{\delta}{\delta\sigma_j} \right)^{q-n+1} \right. \\ &\quad \left. \prod_i \frac{(d_i-1)!}{\left(1 - i\sqrt{\frac{g}{3}} e^{-i\theta} \sigma_i \right)^{d_i}} \right]_{\sigma_i=0}. \end{aligned} \quad (\text{C.65})$$

The first term is bounded by:

$$\begin{aligned} &\frac{|N|}{2^{q+1}} \left| \int_0^1 \frac{(1-t)^{q-1}}{(q-1)!} \left[e^{\frac{t}{2} e^{2i\theta} \frac{\delta}{\delta\sigma} \frac{\delta}{\delta\sigma}} \frac{(2q-1)! \left(i\sqrt{\frac{g}{3}} \right)^{2q}}{\left(1 - i\sqrt{\frac{g}{3}} e^{-i\theta} \sigma \right)^{2q}} \right]_{\sigma=0} \right| \\ &\leq \frac{|N|}{2\sqrt{\cos(2\theta)}} \left(\frac{|g|}{6} \right)^q \frac{(2q-1)!}{q!} \frac{1}{\left(\cos \frac{\varphi-2\theta}{2} \right)^{2q}} \end{aligned}$$

$$\leq \frac{|N|}{4\sqrt{\cos(2\theta)}} (q-1)! \left(\frac{1}{\frac{3}{2} \left(\cos \frac{\varphi-2\theta}{2} \right)^2} \right)^q |g|^q. \quad (\text{C.66})$$

Observe that, due to the expansion of the q loop edges, this first term displays a $q!$ growth. Thus already the first term has a worse large-order behavior than the sum over large trees.

We now analyze the contribution to the rest term of the trees with $2 \leq n \leq q$ vertices. Note that a term has initially $\sum d_i = 2(n-1)$ corners (factors $1/(1 - \iota\sqrt{\frac{g}{3}}e^{-\iota\theta}\sigma_i)$) and $2(q-n+1)$ derivatives will act on it. The additional derivatives (corresponding to the loop edges) create each a new corner on which subsequent derivatives can act. In total, for each tree, the loop edges generate exactly:

$$[2(n-1)][2(n-1)+1] \dots [2(n-1)+2(q-n+1)-1] = \frac{(2q-1)!}{(2n-3)!}, \quad (\text{C.67})$$

possible terms, each with $2(n-1) + 2(q-n+1)$ corners (factors $1/(1 - \iota\sqrt{\frac{g}{3}}e^{-\iota\theta}\sigma_i)$). The w 's are bounded by 1 and the sum over trees is done as in Eq. (4.10) leading to the global bound:

$$\begin{aligned} & \sum_{n=2}^q \frac{|N|^n |g|^q}{2^{q+1} 3^q} \frac{(2q-1)!}{(2n-3)!} \frac{1}{(q-n+1)!} \frac{(n-2)!}{n!} \binom{2n-3}{n-1} \left(\frac{1}{\cos \frac{\varphi-2\theta}{2}} \right)^{2q} \frac{1}{[\cos(2\theta)]^{n/2}} \\ & \leq \frac{(2q-1)! |g|^q}{2^{q+1} 3^q \left(\cos \frac{\varphi-2\theta}{2} \right)^{2q}} \sum_{n=2}^q \frac{1}{(q-n+1)! n! (n-1)!} \frac{|N|^n}{[\cos(2\theta)]^{n/2}}. \end{aligned} \quad (\text{C.68})$$

Now, using $(2q-1)! \leq 2^{2q-1} q! (q-1)!$ we get an upper bound:

$$\begin{aligned} & \frac{1}{4} (q-1)! \left(\frac{1}{\frac{3}{2} \left(\cos \frac{\varphi-2\theta}{2} \right)^2} \right)^q |g|^q \sum_{n=2}^q \frac{q!}{(q-n+1)! n! (n-1)!} \frac{|N|^n}{[\cos(2\theta)]^{n/2}} \\ & \leq \frac{1}{4} (q-1)! \left(\frac{1}{\frac{3}{2} \left(\cos \frac{\varphi-2\theta}{2} \right)^2} \right)^q |g|^q 2^q e^{\frac{|N|}{\sqrt{\cos(2\theta)}}}. \end{aligned} \quad (\text{C.69})$$

Adding up Eq. (C.64), (C.66) and (C.69), we get:

$$\begin{aligned} |R_\theta^q(g, N)| & \leq \frac{\frac{|N|}{4\sqrt{\cos(2\theta)}}}{1 - \frac{|Ng|}{\frac{3}{2}\sqrt{\cos(2\theta)} \left(\cos \frac{\varphi-2\theta}{2} \right)^2}} \left(\frac{1}{\frac{3}{2}\sqrt{\cos(2\theta)} \left(\cos \frac{\varphi-2\theta}{2} \right)^2} \right)^q |Ng|^q \\ & \quad + \frac{1}{4} (q-1)! \left(\frac{1}{\frac{3}{2} \left(\cos \frac{\varphi-2\theta}{2} \right)^2} \right)^q |g|^q \left(\frac{|N|}{\sqrt{\cos(2\theta)}} + 2^q e^{\frac{|N|}{\sqrt{\cos(2\theta)}}} \right). \end{aligned} \quad (\text{C.70})$$

We opportunisticly chose $\theta = \frac{\varphi}{6}$ and using some trivial bounds we get

$$|R_\theta^q(g, N)| \leq \frac{\frac{|N|}{4\sqrt{\cos \frac{\varphi}{3}}}}{1 - \frac{|Ng|}{\frac{3}{2}(\cos \frac{\varphi}{3})^{5/2}}} \left(\frac{1}{\frac{3}{2}(\cos \frac{\varphi}{3})^{5/2}} \right)^q |Ng|^q + (q-1)! |g|^q \\ \times \left(\frac{1}{\frac{3}{2}(\cos \frac{\varphi}{3})^2} \right)^q 2^q e^{\frac{|N|}{\cos(\frac{\varphi}{3})^{1/2}}}. \quad (\text{C.71})$$

We are now in the position to prove that $W(g, N)$ is Borel summable along all the directions in the cut plane \mathbb{C}_π by verifying the conditions of Theorem 1, Appendix B. This comes about as follows:

- let us fix some $\alpha \in (-\pi, \pi)$. As we are interested in analyticity and rest bound in some Sokal disk extending up to $\varphi = \alpha \pm \pi/2$, we denote $c = \min\{\cos \frac{\alpha+\pi/2}{3}; \cos \frac{\alpha-\pi/2}{3}\} > 0$ (because as $|\alpha| < \pi$).
- $W(g, N)$ can be analytically continued via $W_{\varphi/6}(g, N)$ ¹⁹ to any g in a Sokal disk (with 0 on its boundary) tilted by α , that is $g \in \text{Disk}_R^\alpha = \{z \mid \text{Re}(e^{i\alpha}/z) > 1/R\}$ provided that $R = \frac{3}{2|N|}c^{5/2}(1-\nu)$ for some fixed $\nu > 0$. In this disk the Taylor rest term obeys the uniform bound:

$$|R_\theta^q(g)| \leq \frac{|N|}{4c^{1/2}\nu} \left(\frac{1}{\frac{3}{2}c^{5/2}} \right)^q |g|^q + (q-1)! |g|^q \left(\frac{2}{\frac{3}{2}c^2} \right)^q e^{|N|/c^{1/2}}. \quad (\text{C.72})$$

Fixing $K = \max\{|N|/(4c^{1/2}\nu), e^{|N|/c^{1/2}}\}$ and $\rho = \min\{3/2 c^{5/2}; 3/4 c^2\}$, we finally obtain uniformly in the Sokal disk:

$$|R_\theta^q(g, N)| \leq K q! \rho^{-q} |g|^q; \quad (\text{C.73})$$

hence, the rest obeys the bound in Eq. (2.4) and from Theorem 1 we conclude that $W(g, N)$ is Borel summable along α .

Note that Borel summability is lost in the $N \rightarrow \infty$ limit.

This concludes the proof of Proposition 4. \square

C.5. Transseries Expansion of $W_n(g)$ and $W(g, N)$

Proof of Proposition 5. An explicit expression for $W_n(g)$ is obtained by combining the Möbis inversion formula in Eq.(4.3) with the transseries expansion of $Z_n(g)$ in Eq. (3.26). In order to prove Proposition 5, we have to use standard sum and product manipulation tricks and factor the powers of the transseries monomial $e^{\frac{3}{2}g}$ in front. Although the manipulations are not complicated, the expressions are very lengthy and we will introduce some bookkeeping notation to keep the formulas readable.

¹⁹Indeed, $W_{\varphi/6}(g, N) = Q_{\varphi/6}^0(g, N)$ and the series defining it converges absolutely in such a disk $|Q_{\varphi/6}^0(g, N)| \leq 1/(4c^{1/2}\nu)$.

Property 1. Combining the Möbis inversion formula (4.3) with the transseries expansion of $Z_n(g)$ in Eq. (3.26) leads to:

$$W_n(g) \simeq \sum_{k=1}^n (-1)^{k-1} (k-1)! \sum_{\substack{n_1, \dots, n_{n-k+1} \geq 0 \\ \sum i n_i = n, \sum n_i = k}} \frac{n!}{\prod_i n_i! (i!)^{n_i}} \prod_{i=1}^{n-k+1} \left(Z_i^{\text{pert.}}(g) + \eta e^{\frac{3}{2g}} Z_i^{(\eta)}(g) \right)^{n_i}, \quad (\text{C.74})$$

with:

$$Z_i^{\text{pert.}}(g) = \sum_{a=0}^{\infty} \left(-\frac{2g}{3} \right)^a G(a; i), \quad G(a; i) = \frac{(2a)!}{2^{2a} a!} \sum_{\substack{a_1, \dots, a_{2a-i+1} \geq 0 \\ \sum k a_k = 2a, \sum a_k = i}} \frac{(-1)^i i!}{\prod_k k^{a_k} a_k!}, \quad (\text{C.75})$$

and:

$$Z_i^{(\eta)}(g) = \frac{\imath}{\sqrt{2\pi}} \sqrt{\frac{g}{3}} \sum_{a=0}^{\infty} \sum_{b=0}^i \frac{1}{a!} \left(\frac{g}{6} \right)^a \binom{i}{b} \frac{d^b \Gamma(z)}{dz^b} \Big|_{z=2a+1} \times \tau \left[\left(\ln \left(\frac{g}{3} \right) \right)^{i-b} - \left(\ln \left(\frac{g}{3} \right) + \tau 2\pi \imath \right)^{i-b} \right], \quad (\text{C.76})$$

where we used $\left[\left(\ln(e^{\imath\tau\pi} \frac{g}{3}) - \imath\pi \right)^{i-b} - \left(\ln(e^{\imath\tau\pi} \frac{g}{3}) + \imath\pi \right)^{i-b} \right] = \tau \left[\left(\ln \left(\frac{g}{3} \right) \right)^{i-b} - \left(\ln \left(\frac{g}{3} \right) + \tau 2\pi \imath \right)^{i-b} \right]$ as $\tau = \pm$. Using now $\tau \left[\left(\ln \left(\frac{g}{3} \right) \right)^n - \left(\ln \left(\frac{g}{3} \right) + \tau 2\pi \imath \right)^n \right] = -\tau \sum_{c=0}^{n-1} \binom{n}{c} \left(\ln \left(\frac{g}{3} \right) \right)^c (\tau 2\pi \imath)^{n-c}$, commuting the sums over b and c , and combining the binomials, this can further be written as:

$$\begin{aligned} Z_i^{(\eta)}(g) &= \frac{\imath}{\sqrt{2\pi}} \sqrt{\frac{g}{3}} \sum_{a=0}^{\infty} \sum_{b=0}^{i-1} \frac{1}{a!} \left(\frac{g}{6} \right)^a \binom{i}{b} \frac{d^b \Gamma(z)}{dz^b} \Big|_{z=2a+1} (-\tau) \\ &\quad \times \sum_{c=0}^{i-1-b} \binom{i-b}{c} \left(\ln \left(\frac{g}{3} \right) \right)^c (\tau 2\pi \imath)^{i-b-c} \\ &= \sqrt{2\pi} \sqrt{\frac{g}{3}} \sum_{a=0}^{\infty} \sum_{c=0}^{i-1} \left(\frac{g}{6} \right)^a \left(\ln \left(\frac{g}{3} \right) \right)^c G(a, c; i), \end{aligned} \quad (\text{C.77})$$

with:

$$G(a, c; i) = \sum_{b=0}^{i-1} (\imath\tau 2\pi)^{i-1-b-c} \frac{i!}{a! b! c! (i-b-c)!} \frac{d^b \Gamma(z)}{dz^b} \Big|_{z=2a+1}, \quad \text{and} \quad Z_0^{(\eta)} = 0. \quad (\text{C.78})$$

First, we pull the transseries monomial to the front in Eq. (C.74):

$$\begin{aligned} W_n(g) &\simeq \sum_{k=1}^n (-1)^{k-1} (k-1)! \sum_{\substack{n_1, \dots, n_{n-k+1} \geq 0 \\ \sum i n_i = n, \sum n_i = k}} \frac{n!}{\prod_i n_i! (i!)^{n_i}} \\ &\quad \prod_{i=1}^{n-k+1} \left(Z_i^{\text{pert.}}(g) + \eta e^{\frac{3}{2g}} Z_i^{(\eta)}(g) \right)^{n_i} \end{aligned}$$

$$\begin{aligned}
&= \sum_{p=0}^n e^{\frac{3}{2g}p} \sum_{\substack{k=p \\ k+p \geq 1}}^n (-1)^{k-1} (k-1)! \sum_{\substack{n_1, \dots, n_{n-k+1} \geq 0 \\ \sum i n_i = n, \sum n_i = k}} \\
&\times \sum_{\substack{\{0 \leq p_i \leq n_i\} \\ i=1, \dots, n-k+1 \\ \sum p_i = p}} \frac{n! \prod_{i=1}^{n-k+1} (Z_i^{\text{pert.}}(g))^{n_i-p_i} (\eta Z_i^{(\eta)}(g))^{p_i}}{\prod_i (n_i - p_i)! p_i! (i!)^{n_i}}. \quad (\text{C.79})
\end{aligned}$$

This is a transseries in g , with $Z_i^{(\eta)}(g)$ carrying also powers of \sqrt{g} and $\ln(g)$. In a second step, we want to make this statement manifest and use the expressions for $Z_i^{\text{pert.}}$ and $Z_i^{(\eta)}$ to calculate:

$$\begin{aligned}
\prod_{i \geq 1} (Z_i^{\text{pert.}}(g))^{n_i-p_i} (\eta Z_i^{(\eta)}(g))^{p_i} &= \prod_{i \geq 1} \left(\sum_{a_1^i, \dots, a_{n_i-p_i}^i \geq 0} \prod_{j=1}^{n_i-p_i} \left(-\frac{2g}{3}\right)^{a_j^i} G(a_j^i; i) \right) \\
&\cdot \left(\left(\eta \sqrt{2\pi} \sqrt{\frac{g}{3}} \right)^{p_i} \sum_{a_1^i, \dots, a_{p_i}^i \geq 0} \sum_{c_1^i, \dots, c_{p_i}^i = 0}^{i-1} \prod_{j=1}^{p_i} \left(\frac{g}{6}\right)^{a_j^i} (\ln(\frac{g}{3}))^{c_j^i} G(a_j^i, c_j^i; i) \right), \\
&= \left(\eta \sqrt{2\pi} \sqrt{\frac{g}{3}} \right)^{\sum_{i \geq 1} p_i} \sum_{\substack{l \geq 0 \\ \sum_i (i-1)p_i \geq l \geq 0}} g^l (\ln(\frac{g}{3}))^{l'} \sum_{\substack{\{a_j^i \geq 0\}_{j=1, \dots, n_i}^{i=1, \dots, n-k+1} \\ \sum_i \sum_j a_j^i = l}} \sum_{\substack{\{i-1 \geq c_j^i \geq 0\}_{j=1, \dots, p_i}^{i=1, \dots, n-k+1} \\ \sum_i \sum_j c_j^i = l'}} \\
&\cdot \left(\frac{1}{6}\right)^{\sum_{i \geq 1} \sum_{j=1}^{p_i} a_j^i} \left(-\frac{2}{3}\right)^{\sum_{i \geq 1} \sum_{j=p_i+1}^{n_i} a_j^i} \prod_{i \geq 1} \left(\prod_{j=1}^{p_i} G(a_j^i, c_j^i; i) \right) \left(\prod_{j=p_i+1}^{n_i} G(a_j^i; i) \right). \quad (\text{C.80})
\end{aligned}$$

Finally, inserting this into Eq. (C.79) we obtain the transseries expansion of $W_n(g)$, organized into instanton sectors:

$$W_n(g) \simeq \sum_{p=0}^n e^{\frac{3}{2g}p} \left(\eta \sqrt{2\pi} \sqrt{\frac{g}{3}} \right)^p \sum_{l \geq 0, n-p \geq l' \geq 0} g^l (\ln(\frac{g}{3}))^{l'} W_{n;l,l'}^{(p)}, \quad (\text{C.81})$$

with

$$\begin{aligned}
W_{n;l,l'}^{(p)} &= \sum_{\substack{k=p \\ k+p \geq 1}}^n (-1)^{k-1} (k-1)! \sum_{\substack{n_1, \dots, n_{n-k+1} \geq 0 \\ x \sum i n_i = n, \sum n_i = k}} \sum_{\substack{\{0 \leq p_i \leq n_i\} \\ i=1, \dots, n-k+1 \\ \sum p_i = p}} \frac{n!}{\prod_i (n_i - p_i)! p_i! (i!)^{n_i}} \\
&\times \sum_{\substack{\{a_j^i \geq 0\}_{j=1, \dots, n_i}^{i=1, \dots, n-k+1} \\ \sum_i \sum_j a_j^i = l}} \sum_{\substack{\{i-1 \geq c_j^i \geq 0\}_{j=1, \dots, p_i}^{i=1, \dots, n-k+1} \\ \sum_i \sum_j c_j^i = l'}} \left(\frac{1}{6}\right)^{\sum_{i=1}^{n-k+1} \sum_{j=1}^{p_i} a_j^i} \\
&\left(-\frac{2}{3}\right)^{\sum_{i=1}^{n-k+1} \sum_{j=p_i+1}^{n_i} a_j^i} \prod_{i=1}^{n-k+1} \left(\prod_{j=1}^{p_i} G(a_j^i, c_j^i; i) \right) \left(\prod_{j=p_i+1}^{n_i} G(a_j^i; i) \right), \quad (\text{C.82})
\end{aligned}$$

as advertised.

Property 2. It remains to transseries expansion for the full free energy $W(g, N)$. In this case, the expressions are simpler because the Z_i have been summed. Starting from the relation between $W(g, N)$ and the $W_n(g)$:

$$\begin{aligned}
 W(g, N) &= \sum_{n \geq 1} \frac{1}{n!} \left(-\frac{N}{2} \right)^n W_n(g) \\
 &\simeq \sum_{n \geq 1} \frac{\left(-\frac{N}{2} \right)^n}{n!} \sum_{k=1}^n (-1)^{k-1} (k-1)! \sum_{\substack{n_1, \dots, n_{n-k+1} \geq 0 \\ \sum i n_i = n, \sum n_i = k}} \frac{n!}{\prod_i n_i! (i!)^{n_i}} \\
 &\quad \prod_{i=1}^{n-k+1} \left(Z_i^{\text{pert.}}(g) + \eta e^{\frac{3}{2g}} Z_i^{(\eta)}(g) \right)^{n_i} \\
 &= \sum_{k \geq 1} (-1)^{k-1} (k-1)! \sum_{\substack{n_1, n_2, \dots \geq 0 \\ \sum n_i = k}} \prod_{i \geq 1} \frac{1}{n_i!} \left(\frac{1}{i!} \left(-\frac{N}{2} \right)^i \left(Z_i^{\text{pert.}}(g) + \eta e^{\frac{3}{2g}} Z_i^{(\eta)}(g) \right) \right)^{n_i},
 \end{aligned} \tag{C.83}$$

which becomes:

$$\begin{aligned}
 &\sum_{k \geq 1} (-1)^{k-1} (k-1)! \frac{1}{k!} \left(\sum_{i \geq 1} \frac{1}{i!} \left(-\frac{N}{2} \right)^i \left(Z_i^{\text{pert.}}(g) + \eta e^{\frac{3}{2g}} Z_i^{(\eta)}(g) \right) \right)^k \\
 &= \sum_{k \geq 1} (-1)^{k-1} (k-1)! \frac{1}{k!} \left((Z^{\text{pert.}}(g, N) - 1 + \eta e^{\frac{3}{2g}} Z^{(\eta)}(g, N)) \right)^k \\
 &= \sum_{k \geq 1} \frac{(-1)^{k-1}}{k} (Z^{\text{pert.}}(g, N) - 1 + \eta e^{\frac{3}{2g}} Z^{(\eta)}(g, N))^k \\
 &= \ln \left(Z^{\text{pert.}}(g, N) + \eta e^{\frac{3}{2g}} Z^{(\eta)}(g, N) \right),
 \end{aligned} \tag{C.84}$$

we unsurprisingly recover, that formally $W(g, N) = \ln(Z(g, N))$. Here, we used the notation (cf. Eq. (3.12)) $Z(g, N) = Z^{\text{pert.}}(g, N) + \eta e^{\frac{3}{2g}} Z^{(\eta)}(g, N)$, with:

$$\begin{aligned}
 Z^{\text{pert.}}(g, N) &= \sum_{n=0}^{\infty} \frac{\Gamma(2n + N/2)}{2^{2n} n! \Gamma(N/2)} \left(-\frac{2g}{3} \right)^n, \\
 Z^{(\eta)}(g, N) &= e^{i\tau\pi(1-\frac{N}{2})} \sqrt{2\pi} \left(\frac{g}{3} \right)^{\frac{1-N}{2}} \sum_{q=0}^{\infty} \frac{1}{2^{2q} q! \Gamma(\frac{N}{2} - 2q)} \left(\frac{2g}{3} \right)^q.
 \end{aligned} \tag{C.85}$$

As before, the expansion into instanton sectors can be made manifest, by pulling the transseries monomials to the front in $W(g, N)$. We start from the second to last line in Eq. (C.84)) that can also be written as:

$$W(g, N) \simeq \sum_{k \geq 1} (-1)^{k-1} (k-1)! \sum_{\substack{p, q \geq 0 \\ p+q=k}} \frac{1}{p!q!} (Z^{\text{pert.}}(g) - 1)^q \left(\eta e^{\frac{3}{2g}} Z^{(\eta)}(g) \right)^p$$

$$= \sum_{p \geq 0} e^{\frac{3}{2g}p} \sum_{\substack{q \geq 0 \\ p+q \geq 1}} (-1)^{p+q-1} \frac{(p+q-1)!}{p!q!} (Z^{\text{pert.}}(g) - 1)^q (\eta Z^{(\eta)}(g))^p. \quad (\text{C.86})$$

Next, we use the expressions for $Z^{\text{pert.}}$ and $Z^{(\eta)}$ to calculate:

$$\begin{aligned} & (Z^{\text{pert.}}(g) - 1)^q (\eta Z^{(\eta)}(g))^p \\ &= \left(\sum_{n=1}^{\infty} \frac{\Gamma(2n+N/2)}{2^{2n} n! \Gamma(N/2)} \left(-\frac{2g}{3}\right)^n \right)^q \left(\eta \sqrt{2\pi} e^{\imath\tau \frac{\pi}{2}} \left(\frac{e^{\imath\tau\pi} g}{3}\right)^{\frac{1-N}{2}} \right)^p \\ & \quad \left(\sum_{m \geq 0} \frac{1}{2^{2m} m! \Gamma(\frac{N}{2} - 2m)} \left(\frac{2g}{3}\right)^m \right)^p \\ &= \left(\eta \sqrt{2\pi} e^{\imath\tau \frac{\pi}{2}} \left(\frac{e^{\imath\tau\pi} g}{3}\right)^{\frac{1-N}{2}} \right)^p \sum_{\substack{n_1, \dots, n_q \geq 1 \\ m_1, \dots, m_p \geq 0}} \left(\prod_{i=1}^q \frac{\Gamma(2n_i + \frac{N}{2})}{2^{2n_i} n_i! \Gamma(\frac{N}{2})} \left(-\frac{2g}{3}\right)^{n_i} \right) \\ & \quad \times \left(\prod_{j=1}^p \frac{1}{2^{2m_j} m_j! \Gamma(\frac{N}{2} - 2m_j)} \left(\frac{2g}{3}\right)^{m_j} \right) \\ &= \left(\eta \sqrt{2\pi} e^{\imath\tau \frac{\pi}{2}} \left(\frac{e^{\imath\tau\pi} g}{3}\right)^{\frac{1-N}{2}} \right)^p \sum_{l \geq 0} \left(-\frac{2g}{3}\right)^l \sum_{\substack{n_1, \dots, n_q \geq 1 \\ m_1, \dots, m_p \geq 0 \\ \sum n_i + \sum m_j = l}} \left(\prod_{i=1}^q \frac{\Gamma(2n_i + \frac{N}{2})}{2^{2n_i} n_i! \Gamma(\frac{N}{2})} \right) \\ & \quad \times \left(\prod_{j=1}^p \frac{(-1)^{m_j}}{2^{2m_j} m_j! \Gamma(\frac{N}{2} - 2m_j)} \right). \quad (\text{C.87}) \end{aligned}$$

Finally, inserting this into Eq. (C.86) we obtain the transseries expansion of the free energy, organized into instanton sectors:

$$\begin{aligned} W(g, N) &= \sum_{p \geq 0} e^{\frac{3}{2g}p} \left(\eta \sqrt{2\pi} e^{\imath\tau \frac{\pi}{2}} \left(\frac{e^{\imath\tau\pi} g}{3}\right)^{\frac{1-N}{2}} \right)^p \sum_{l \geq 0} \left(-\frac{2g}{3}\right)^l \\ & \quad \times \cdot \left(\sum_{\substack{q \geq 0 \\ p+q \geq 1}} (-1)^{p+q-1} \frac{(p+q-1)!}{p!q!} \sum_{\substack{n_1, \dots, n_q \geq 1 \\ m_1, \dots, m_p \geq 0 \\ \sum n_i + \sum m_j = l}} \left(\prod_{i=1}^q \frac{\Gamma(2n_i + N/2)}{2^{2n_i} n_i! \Gamma(N/2)} \right) \right. \\ & \quad \left. \times \left(\prod_{j=1}^p \frac{(-1)^{m_j}}{2^{2m_j} m_j! \Gamma(N/2 - 2m_j)} \right) \right), \quad (\text{C.88}) \end{aligned}$$

which has the desired form

$$W(g) \simeq \sum_{p \geq 0} e^{\frac{3}{2g}p} \left(\eta \sqrt{2\pi} e^{\imath\tau \frac{\pi}{2}} \left(\frac{e^{\imath\tau\pi} g}{3}\right)^{\frac{1-N}{2}} \right)^p \sum_{l \geq 0} \left(-\frac{2g}{3}\right)^l W_l^{(p)}(N), \quad (\text{C.89})$$

and we can read up the coefficients $W_l^{(p)}$.

This concludes the proof of Proposition 5. \square

D. The BKAR Formula

The Brydges-Kennedy-Abdesselam-Rivasseau (BKAR) [39, 40] forest formula is a Taylor formula for functions of several variables. Due to its symmetry and positivity properties it is very well adapted for nonperturbative quantum field theory.

Let us consider a set of n points labeled $i = 1 \dots n$, which we identify with the set of vertices of the complete graph \mathcal{K}_n . The set of unordered pairs of such points has $n(n-1)/2$ elements $e = (i, j)$ for $1 \leq i, j \leq n$, $i \neq j$ and can be identified with the set of edges of \mathcal{K}_n . Let us consider a smooth (and arbitrarily derivable) function $f : [0, 1]^{n(n-1)/2} \rightarrow \mathbb{R}$ depending on the edge variables $x_e \equiv x_{ij}$, $e = (i, j)$.

Theorem 2. [The Forest Formula, [39, 40]] We have (with the convention that empty products are 1):

$$f(1, \dots, 1) = \sum_{\mathcal{F}} \underbrace{\int_0^1 \dots \int_0^1}_{|\mathcal{F}| \text{ times}} \left(\prod_{e \in \mathcal{F}} du_e \right) \left[\left(\prod_{e \in \mathcal{F}} \frac{\partial}{\partial x_e} \right) f \right] \left(w_{kl}^{\mathcal{F}}(u_{\mathcal{F}}) \right), \quad (\text{D.1})$$

where:

- the sum runs over the forests²⁰ \mathcal{F} drawn over the n labeled vertices i , including the empty forest (having no edge). To each edge $e \in \mathcal{F}$, we attribute a variable u_e that is integrated from 0 to 1 and we denote $u_{\mathcal{F}} = \{u_e \mid e \in \mathcal{F}\}$.
- the derivative $\left(\prod_{e \in \mathcal{F}} \frac{\partial}{\partial x_e} \right) f$ is evaluated at the point:

$$w_{kl}^{\mathcal{F}}(u_{\mathcal{F}}) = \inf_{e' \in P_{k-l}^{\mathcal{F}}} \{u_{e'}\}, \quad (\text{D.2})$$

where $P_{k-l}^{\mathcal{F}}$ denotes the unique path in the forest \mathcal{F} joining the vertices k and l , and the infimum is set to zero if such a path does not exist.

Setting by convention $w_{kk}^{\mathcal{F}}(u_{\mathcal{F}}) \equiv 1$, for any assignment of tree edge variables $0 \leq u_{\mathcal{F}} \leq 1$ the symmetric $n \times n$ matrix $W^{\mathcal{F}}(u^{\mathcal{F}}) = (w_{kl}^{\mathcal{F}}(u_{\mathcal{F}}))_{1 \leq k, l \leq n}$ is positive.

The most subtle point in this formula is that $W^{\mathcal{F}}(u^{\mathcal{F}})$ is a positive matrix. To see this we proceeded as follows. A forest \mathcal{F} divides the complete graph \mathcal{K}_n into several connected components (or blocks) corresponding to the trees in the forest. For instance, if \mathcal{F} is the empty forest the blocks are all singletons consisting in a unique vertex per block. For any forest \mathcal{F} , the matrix:

$$B_{kl}^{\mathcal{F}} = \begin{cases} 1, & \text{if } k, l \text{ belong to the same block of } \mathcal{F} \\ 0, & \text{otherwise} \end{cases}, \quad (\text{D.3})$$

²⁰Acyclic edge subgraphs of the complete graph \mathcal{K}_n .

is positive. Indeed, denoting $b \subset \mathcal{F}$ the blocks of \mathcal{F} and $k \in b$ the vertices in the block b :

$$\sum_{k,l} B_{kl}^{\mathcal{F}} a_k a_l = \sum_{b \subset \mathcal{F}} \left(\sum_{k \in b} a_k \right)^2. \quad (\text{D.4})$$

Let us denote the number of edges in \mathcal{F} by $q \equiv |\mathcal{F}|$. We order the edges of \mathcal{F} in decreasing order of their parameters u :

$$1 \geq u_{e_1} \geq u_{e_2} \geq \dots u_{e_q} \geq 0. \quad (\text{D.5})$$

Adding edges one by one starting from the highest edge we obtain a family of subforests of \mathcal{F} :

$$\mathcal{F}^0 = \emptyset, \quad \mathcal{F}^1 = \{e_1\}, \quad \mathcal{F}^2 = \{e_1, e_2\}, \dots, \quad \mathcal{F}^q = \{e_1, \dots, e_q\} = \mathcal{F}, \quad (\text{D.6})$$

and the matrix $W^{\mathcal{F}}(u_{\mathcal{F}})$ writes as:

$$W^{\mathcal{F}}(u_{\mathcal{F}}) = (1 - u_{e_1})B^{\mathcal{F}^0} + (u_{e_1} - u_{e_2})B^{\mathcal{F}^1} + \dots + u_{e_q}B^{\mathcal{F}^q}. \quad (\text{D.7})$$

Indeed, if i and j do not belong to the same block of $\mathcal{F}^q = \mathcal{F}$, then they do not belong to the same block in any of the \mathcal{F}^s , $s \leq q$ and none of the terms above contribute, hence $w_{ij}^{\mathcal{F}}(u_{\mathcal{F}}) = 0$. If, on the other hand, i and j belong to the same block of \mathcal{F} , then:

$$\left[(1 - u_{e_1})B^{\mathcal{F}^0} + (u_{e_1} - u_{e_2})B^{\mathcal{F}^1} + \dots + u_{e_q}B^{\mathcal{F}^q} \right]_{ij} = u_{e_s}, \quad (\text{D.8})$$

where s is such that i and j belong to the same block of \mathcal{F}^s , but belong to two different blocks of \mathcal{F}^{s-1} . As $u_{e_s} \leq u_{e_{s-1}} \leq u_{e_{s-2}} \leq \dots$ it follows that u_{e_s} is the infimum of the u s in the unique path in \mathcal{F}^s joining i and j ; hence, it is also the infimum of the u s in the unique path in \mathcal{F} joining i and j . The matrix $W^{\mathcal{F}}(u_{\mathcal{F}})$ is a convex combination of positive matrices; hence, it is itself positive.

D.1. Feynman Graphs and $W(g, N)$

Each term in the convergent series in Eq. (4.7) can be further expanded in a formal Taylor series in the coupling constant. The series thus obtained is asymptotic to $W(g, N)$ as long as Eq. (4.7) converges hence in a cardioid domain of the cut complex plane \mathbb{C}_{π} (see Proposition 3) which sweeps all the directions in \mathbb{C}_{π} . In this range of g no singularity of the integrand crosses the real axis, which is the steepest-descent contour of the exponentials in Eq. (4.5).

The asymptotic series of $W(g, N)$ in the first Riemann sheet is well known to be the formal sum over connected Feynman graphs of amplitudes. However, due to the presence of the w parameters and the integrals over the u s, it is not exactly transparent how this comes about starting from Eq. (4.7). The fact that Eq. (4.7) does indeed reproduce the Feynman graph expansion has been proven in [41]. We sketch below how this comes about.

Hepp sectors. To any graph G with vertices labeled $i, i = 1, \dots, n$, one can associate a *characteristic* function depending on edge variables $f(x_{ij}) = \prod_{(i,j) \in G} x_{ij}$ where the product runs over the edges of G . The forest formula applied to this function yields:

$$1 = \sum_{\mathcal{F} \subset G} \underbrace{\int_0^1 \dots \int_0^1}_{|\mathcal{F}| \text{ times}} \left(\prod_{(i,j) \in \mathcal{F}} du_{ij} \right) \left[\prod_{(k,l) \notin \mathcal{F}} w_{kl}^{\mathcal{F}}(u_{\mathcal{F}}) \right]. \quad (\text{D.9})$$

Remark that the derivative of the characteristic function is nonzero only if the forest \mathcal{F} is made of edges of G (which we signify by $\mathcal{F} \subset G$). Furthermore, if \mathcal{F} has more than one block, then one of the w s in the product is set to zero. It follows that only trees contribute:

$$1 = \sum_{\mathcal{T} \subset G} \underbrace{\int_0^1 \dots \int_0^1}_{|\mathcal{T}| \text{ times}} \left(\prod_{(i,j) \in \mathcal{T}} du_{ij} \right) \left[\prod_{(k,l) \notin \mathcal{T}} w_{kl}^{\mathcal{T}}(u_{\mathcal{T}}) \right]. \quad (\text{D.10})$$

This formula defines normalized weights associated with the graph G and the spanning trees $\mathcal{T} \subset G$:

$$w(G, \mathcal{T}) = \underbrace{\int_0^1 \dots \int_0^1}_{|\mathcal{T}| \text{ times}} \left(\prod_{(i,j) \in \mathcal{T}} du_{ij} \right) \left[\prod_{(k,l) \notin \mathcal{T}} w_{kl}^{\mathcal{T}}(u_{\mathcal{T}}) \right], \quad \sum_{\mathcal{T} \subset G} w(G, \mathcal{T}) = 1, \quad (\text{D.11})$$

which admit a striking combinatorial interpretation. We define a *Hepp sector* as a total ordering π of the edges of G , that is a bijection $\pi : E(G) \rightarrow \{1, \dots, |E(G)|\}$, where $E(G)$ is the set of edges of G . For any π the *leading spanning tree* in π , denoted $\mathcal{T}(\pi)$, is the tree such that $\sum_{e \in \mathcal{T}(\pi)} \pi(e)$ is minimal. The tree $\mathcal{T}(\pi)$ is obtained by Kruskal's greedy algorithm: at each step one adds the edge $e \in G$ with minimal $\pi(e)$ that does not form a loop.

Lemma 1. *We have:*

$$w(G, \mathcal{T}) = \frac{N(G, \mathcal{T})}{|E(G)|!}, \quad (\text{D.12})$$

where $N(G, \mathcal{T})$ is the number of sectors π such that $\mathcal{T}(\pi) = \mathcal{T}$, that is $w(G, \mathcal{T})$ is the percentage of Hepp sectors in which \mathcal{T} is the leading spanning tree of G .

Proof. Let us define the function:

$$\chi(u_{E(G) \setminus \mathcal{T}} \leq u_{\mathcal{T}}) \begin{cases} 1, & \text{if } \forall (i,j) \in E(G) \setminus \mathcal{T}, \quad u_{ij} \leq \inf_{(k,l) \in P_{i \rightarrow j}^{\mathcal{T}}} u_{kl} \\ 0, & \text{otherwise} \end{cases}. \quad (\text{D.13})$$

On the one hand we have:

$$w(G, \mathcal{T}) = \int_0^1 \left(\prod_{e \in E(G)} du_e \right) \chi(u_{G \setminus \mathcal{T}} \leq u_{\mathcal{T}}), \quad (\text{D.14})$$

as, at any fixed $\{u_e, e \in \mathcal{T}\}$ the integral over the loop edge variable u_{kl} yields $w_{kl}^{\mathcal{T}}(u_{\mathcal{T}})$.

We now split the integration interval according to Hepp sectors. In the sector π corresponding to $u_{\pi^{-1}(1)} > u_{\pi^{-1}(2)} > \dots$ the characteristic function χ tests whether every loop edge (i, j) has smaller u_{ij} than $\inf\{u_{kl}\}$ in the tree path $P_{i \rightarrow j}^{\mathcal{T}}$ connecting i and j . This is true if and only if \mathcal{T} is the leading spanning tree in π :

$$\begin{aligned} & \int_0^1 \left(\prod_{e \in \mathcal{E}(G)} du_e \right) \chi(u_{G \setminus \mathcal{T}} \leq u_{\mathcal{T}}) \\ &= \sum_{\pi} \int_0^1 du_{\pi^{-1}(1)} \int_0^{u_{\pi^{-1}(1)}} du_{\pi^{-1}(2)} \dots \int_0^{u_{\pi^{-1}(|E(G)|-1)}} du_{\pi^{-1}(|E(G)|)} \chi(u_{G \setminus \mathcal{T}} \leq u_{\mathcal{T}}) \\ &= \sum_{\pi, \mathcal{T}(\pi) = \mathcal{T}} \int_0^1 du_{\pi^{-1}(1)} \int_0^{u_{\pi^{-1}(1)}} du_{\pi^{-1}(2)} \dots \int_0^{u_{\pi^{-1}(|E(G)|-1)}} du_{\pi^{-1}(|E(G)|)} \\ &= \frac{1}{|E(G)|!} \sum_{\pi, \mathcal{T}(\pi) = \mathcal{T}} 1. \end{aligned} \quad (\text{D.15})$$

□

Lemma 2 (Asymptotic series [41].) *The asymptotic expansion at zero of the free energy $W(g, N)$ in the cut plane $g \in \mathbb{C}_{\pi}$ is the formal sum over connected Feynman graphs of Feynman amplitudes.*

Proof. Taylor expanding the Gaussian integrals in Eq. (4.7) to infinity yields:

$$\begin{aligned} W(g, N) &\simeq -\frac{N}{2} \left[\sum_{l \geq 0} \frac{1}{l!} \left(\frac{1}{2} \frac{\delta}{\delta \sigma} \frac{\delta}{\delta \sigma} \right)^l \ln \left(1 - \sqrt{\frac{g}{3}} \sigma \right) \right]_{\sigma=0} - \sum_{n \geq 2} \frac{\left(-\frac{N}{2} \right)^n}{n!} \left(\frac{g}{3} \right)^{n-1} \sum_{\mathcal{T} \in T_n} \\ &\quad \int_0^1 \left(\prod_{(i,j) \in \mathcal{T}} du_{ij} \right) \\ &\quad \times \left[\sum_{\{l_i \geq 0\}} \frac{1}{l_i!} \left(\frac{1}{2} \frac{\delta}{\delta \sigma_i} \frac{\delta}{\delta \sigma_i} \right)^{l_i} \sum_{\{l_{ij} \geq 0\}_{i \leq j}} \frac{1}{l_{ij}!} \left(w_{ij}^{\mathcal{T}} \frac{\delta}{\delta \sigma_i} \frac{\delta}{\delta \sigma_j} \right)^{l_{ij}} \prod_i \frac{(d_i-1)!}{\left(1 - \sqrt{\frac{g}{3}} \sigma_i \right)^{d_i}} \right]_{\sigma_i=0} \\ &= \sum_{n \geq 1} \frac{1}{n!} \left(-\frac{N}{2} \right)^n \sum_{\mathcal{T} \in T_n} \sum_{\{l_i \geq 0\}, \{l_{ij} \geq 0\}_{i < j}} \frac{\prod_i (d_i + l_i + \sum_j l_{ij} - 1)!}{(\prod_i 2^{l_i} l_i!) (\prod_{i < j} l_{ij}!)} \\ &\quad \left[\int_0^1 \left(\prod_{(i,j) \in \mathcal{T}} du_{ij} \right) \left(\prod_{(i,j)} w_{ij}^{\mathcal{T}} \right)^{l_{ij}} \right] \left(-\frac{g}{3} \right)^{n-1 + \sum_i l_i + \sum_{i < j} l_{ij}}. \end{aligned} \quad (\text{D.16})$$

The additional derivatives with respect to σ generate loop edges decorating the tree \mathcal{T} : l_{ij} is the multiplicity of the loop edge between i and j and l_i the number of tadpole edges (or self loops) at the vertex i . We denote the graph consisting in \mathcal{T} decorated by such extra loop edges by G . Of course, \mathcal{T} is a spanning tree of G which we denote $G \supset \mathcal{T}$. From Lemma 1, the integral over u in Eq. (D.16) is:

$$w(G, \mathcal{T}) = \underbrace{\int_0^1 \dots \int_0^1}_{|\mathcal{T}| \text{ times}} \left(\prod_{(i,j) \in \mathcal{T}} du_{ij} \right) \left[\prod_{(k,l) \notin \mathcal{T}} w_{kl}^{\mathcal{T}}(u_{\mathcal{T}}) \right] = \frac{N(G, \mathcal{T})}{|E(G)|!},$$

(D.17)

yields the percentage of Hepp sectors in which \mathcal{T} is the leading spanning tree of G . Collecting the coupling constants and the symmetry factor in the amplitude $A(G)$ of the graph G , we write:

$$W(g) = \sum_{n \geq 1} \frac{1}{n!} \sum_{\mathcal{T} \in \mathcal{T}_n} \sum_{G \supset \mathcal{T}} w(G, \mathcal{T}) A(G), \quad (\text{D.18})$$

that is for each tree \mathcal{T} we resum the amplitudes of the graphs in which \mathcal{T} is a spanning tree with a weight given by the percentage of Hepp sectors of G in which \mathcal{T} is the leading tree. Denoting G_n the set of connected graphs over n vertices, we commute the sums over trees \mathcal{T} and graphs G and using $\sum_{\mathcal{T} \subset G} w(G, \mathcal{T}) = 1$ we get:

$$W(g) = \sum_{n \geq 1} \frac{1}{n!} \sum_{G \in G_n} A(G), \quad (\text{D.19})$$

which is the familiar perturbative expansion of the free energy in connected graphs. \square

References

- [1] Écalle, J.: Les fonctions résurgentes. Vol. I-III, Université de Paris-Sud, Département de Mathématique, Orsay (1981)
- [2] Sauzin, D.: Resurgent functions and splitting problems. arXiv:0706.0137
- [3] Mariño, M.: Lectures on non-perturbative effects in large N gauge theories, matrix models and strings. Fortsch. Phys. **62**, 455 (2014). [arXiv:1206.6272]
- [4] Dorigoni, D.: An Introduction to Resurgence, Trans-Series and Alien Calculus. Annals Phys. **409**, 167914 (2019). [arXiv:1411.3585]
- [5] Dunne, G.V., Ünsal, M.: What is QFT? Resurgent trans-series, Lefschetz thimbles, and new exact saddles. PoS LATTICE2015, 010 (2016). arXiv:1511.05977
- [6] Aniceto, I., Basar, G., Schiappa, R.: A primer on resurgent transseries and their asymptotics. Phys. Rept. **809**, 1 (2019). [arXiv:1802.10441]
- [7] Di Vecchia, P., Kato, M., Ohta, N.: Double scaling limit in $O(N)$ vector models. Nucl. Phys. B **357**, 495 (1991)
- [8] Di Francesco, P., Ginsparg, P.H., Zinn-Justin, J.: 2-D gravity and random matrices. Phys. Rept. **254**, 1 (1995). [arXiv:hep-th/9306153]
- [9] Gurau, R.: Random Tensors. Oxford University Press, Oxford (2016)
- [10] Fauvet, F., Menous, F., Quéva, J.: Resurgence and holonomy of the ϕ^{2k} model in zero dimension. J. Math. Phys. **61**, 092301 (2020). [arXiv:1910.01606]
- [11] Jaffe, A.: Constructive quantum field theory. Math. Phys. **2000**, 111 (2000)
- [12] Rivasseau, V.: From Perturbative to Constructive Renormalization, vol. 46. Princeton University Press (2014)
- [13] Rivasseau, V.: Constructive field theory in zero dimension. Adv. Math. Phys. **2009**, 180159 (2009). [arXiv:0906.3524]
- [14] Bersini, J., Maiezza, A., Vasquez, J.C.: Resurgence of the renormalization group equation. Ann. Phys. **415**, (2020). arXiv:1910.14507

- [15] Tanizaki, Y.: Lefschetz-thimble techniques for path integral of zero-dimensional $O(n)$ sigma models. *Phys. Rev. D* **91**, 036002 (2015). [arXiv:1412.1891]
- [16] Bender, C.M., Orszag, S.A.: *Advanced Mathematical Methods for Scientists and Engineers I*, 1st edn. Springer, New York (1999). <https://doi.org/10.1007/978-1-4757-3069-2>
- [17] Witten, E.: Analytic continuation of Chern–Simons theory. *AMS/IP Stud. Adv. Math.* **50**, 347 (2011). [arXiv:1001.2933]
- [18] Rivasseau, V.: Constructive matrix theory. *JHEP* **09**, 008 (2007). [arXiv:0706.1224]
- [19] Magnen, J., Rivasseau, V.: Constructive ϕ^4 field theory without tears. *Annales Henri Poincaré* **9**, 403 (2008). [arXiv:0706.2457]
- [20] de Gennes, P.: Exponents for the excluded volume problem as derived by the Wilson method. *Phys. Lett. A* **38**, 339 (1972)
- [21] Slade, G.: Self-avoiding walk, spin systems, and renormalization. *Proc. R. Soc. Lond. A* **475**, 20180549 (2019). [arXiv:1808.04476]
- [22] Baldino, S., Schiappa, R., Schwick, M., Vega, R.: Resurgent Stokes Data for Painleve Equations and Two-Dimensional Quantum (Super) Gravity. arXiv:2203.13726
- [23] Hikami, S., Brezin, E.: Large-order behaviour of the $1/N$ expansion in zero and one dimensions. *J. Phys. A: Math. General* **12**, 759 (1979)
- [24] Di Pietro, L., Mariño, M., Sberveglieri, G., Serone, M.: Resurgence and $1/N$ expansion in integrable field theories. *J. High Energy Phys.* **2021**, 166 (2021). [arXiv:2108.02647]
- [25] Ferdinand, L., Gurau, R., Perez-Sanchez, C.I., Vignes-Tourneret, F.: Borel summability of the $1/N$ expansion in quartic $O(N)$ -vector models. arXiv:2209.09045
- [26] Gurau, R., Rivasseau, V., Sfondrini, A.: Renormalization: an advanced overview, arXiv:1401.5003
- [27] Sokal, A.D.: An improvement of Watson’s theorem on Borel summability. *J. Math. Phys.* **21**, 261 (1980)
- [28] NIST Digital Library of Mathematical Functions.’ <https://dlmf.nist.gov/>. Release 1.1.9 of 2023-03-15
- [29] Hubbard, J.: Calculation of partition functions. *Phys. Rev. Lett.* **3**, 77 (1959)
- [30] Stratonovich, R.L.: On a method of calculating quantum distribution functions. *Soviet Phys. Doklady* **2**, 416 (1957)
- [31] Watson, G.N.: *A Treatise on the Theory of Bessel Functions*. Cambridge University Press, Cambridge (1944)
- [32] Sternin, B.Y., Shatalov, V.E.: Saddle-point method and resurgent analysis. *Math. Notes* **61**, 227 (1997)
- [33] Witten, E.: A new look at the path integral of quantum mechanics. arXiv:1009.6032
- [34] Fujii, H., Honda, D., Kato, M., Kikukawa, Y., Komatsu, S., Sano, T.: Hybrid Monte Carlo on Lefschetz thimbles - a study of the residual sign problem. *JHEP* **10**, 147 (2013). [arXiv:1309.4371]

- [35] Aarts, G., Bongiovanni, L., Seiler, E., Sexty, D.: Some remarks on Lefschetz thimbles and complex Langevin dynamics. *JHEP* **10**, 159 (2014). [arXiv:1407.2090]
- [36] Bluecher, S., Pawłowski, J.M., Scherzer, M., Schlosser, M., Stamatescu, I.-O., Syrkowski, S., et al.: Reweighting Lefschetz thimbles. *SciPost Phys.* **5**, 044 (2018). [arXiv:1803.08418]
- [37] Tanizaki, Y., Nishimura, H., Verbaarschot, J.J.M.: Gradient flows without blow-up for Lefschetz thimbles. *JHEP* **10**, 100 (2017). [arXiv:1706.03822]
- [38] Bauerschmidt, R., Brydges, D.C., Slade, G.: Introduction to a Renormalisation Group Method, vol. 2242. Springer Nature (2019)
- [39] Brydges, D.C., Kennedy, T.: Mayer expansions and the Hamilton–Jacobi equation. *J. Stat. Phys.* **48**, 19 (1987)
- [40] Abdesselam, A., Rivasseau, V.: Trees, forests and jungles: A Botanical garden for cluster expansions. *Lect. Notes Phys.* **446**, 7 (1995). [arXiv:hep-th/9409094]
- [41] Rivasseau, V., Wang, Z.: How to resum Feynman graphs. *Annales Henri Poincaré* **15**, 2069 (2014). [arXiv:1304.5913]

Dario Benedetti and Razvan Gurau
CPHT, CNRS, Ecole Polytechnique, Institut Polytechnique de Paris
Route de Saclay
91128 Palaiseau
France
e-mail: dario.benedetti@polytechnique.edu;
gurau@thphys.uni-heidelberg.de

Razvan Gurau, Hannes Keppler and Davide Lettera
Heidelberg University, Institut für Theoretische Physik
Philosophenweg 19
69120 Heidelberg
Germany
e-mail: keppler@thphys.uni-heidelberg.de;
lettera@thphys.uni-heidelberg.de

Communicated by Abdelmalek Abdesselam.

Received: July 12, 2023.

Accepted: April 1, 2024.

Coupling renormalization flow in the strongly interacting regime of an asymptotically free quantum field theory in four dimensions

Authors: Jürgen Berges, Răzvan Gurău, Hannes Keppler and
Thimo Preis

Published in *Phys. Rev. D* **110** (2024) 3, 036007. DOI: 10.1103/PhysRevD.110.036007.

Licensed under CC BY 4.0. Reproduced with permission. Hyperlink colors removed.

Also available as e-print: arXiv 2405.08153 [hep-th].

The original idea was developed jointly by J. Berges, R. Gurău, and T. Preis. The initial version of the numerical code was written by T. Preis, and later substantially extended by H. Keppler; this final version was used to solve the equations. H. Keppler and T. Preis contributed equally to the data analysis, and T. Preis created all figures for the publication. While T. Preis proposed and drafted Sections I–IV, including the Introduction and Conclusions, Sections V, VI, VII, and the Appendix were initially written by H. Keppler. All authors contributed to the manuscript through corrections and suggestions.

Coupling renormalization flow in the strongly interacting regime of an asymptotically free quantum field theory in four dimensions

Jürgen Berges, Razvan Gurau[✉], Hannes Keppeler[✉], and Thimo Preis^{✉*}

Institut für Theoretische Physik, Universität Heidelberg, 69120 Heidelberg, Germany



(Received 30 May 2024; accepted 5 July 2024; published 9 August 2024)

We consider a scalar quantum field theory with global $O(N)^3$ symmetry in four Euclidean dimensions and solve it numerically in closed form in the large- N limit. For imaginary tetrahedral coupling the theory is asymptotically free, with stable and real quantum effective action. We demonstrate the dynamical build-up of a strong interaction as the correlation length increases in a regime where the coupling renormalization flow remains well defined in the infrared. This is in contrast to perturbative results of asymptotically free theories, which predict that the coupling becomes ill defined in the infrared, like in quantum chromodynamics. These properties make the model an important laboratory for the study of strong-coupling phenomena in quantum field theory from first principles.

DOI: 10.1103/PhysRevD.110.036007

I. INTRODUCTION AND OVERVIEW

Asymptotically free quantum field theories are a cornerstone in the fundamental description of nature. A prominent example is the theory of quantum chromodynamics (QCD) in the Standard Model of particle physics [1,2]. While the high-momentum (ultraviolet) behavior of the theory is perturbatively accessible, the scale-dependent (“running”) coupling increases toward low momenta and becomes ill defined in the infrared. The divergence of the coupling at a finite infrared momentum predicted by perturbation theory illustrates the dynamical generation of a nonperturbative scale by quantum fluctuations. Such behavior is characteristic for the perturbative analysis of asymptotically free theories, and it would be highly valuable to establish a nonperturbative example where the coupling is well-defined and can be followed all the way from the weakly coupled high-momentum regime to the strongly interacting infrared.

In this work we investigate the large- N limit of a four dimensional scalar quantum field theory with global $O(N)^3$ symmetry introduced in Ref. [3]. The model has three independent quartic couplings, whose perturbative renormalization flow, which encodes how the physical couplings change with the momentum scale due to quantum corrections, has been analyzed in Refs. [3–5]. In four Euclidean dimensions the couplings exhibit asymptotic freedom in a

regime governed by the flow of an imaginary tetrahedral coupling $ig(p)$ [3]. In turn, the tetrahedral coupling diverges in perturbation theory at a finite infrared momentum scale μ_{pert}^* . A corresponding perturbative behavior is found, in particular, also for the running coupling in quantum chromodynamics [1,2]. The perturbative scale-dependence of the squared coupling of our model is represented by the dashed curve in Fig. 1.

This is to be contrasted with the nonperturbative large- N renormalization flow of the coupling we obtain in this work, which is displayed by the solid (colored) curves for various values of the renormalized mass in Fig. 1. Contrary to the perturbative prediction, the full coupling is found to

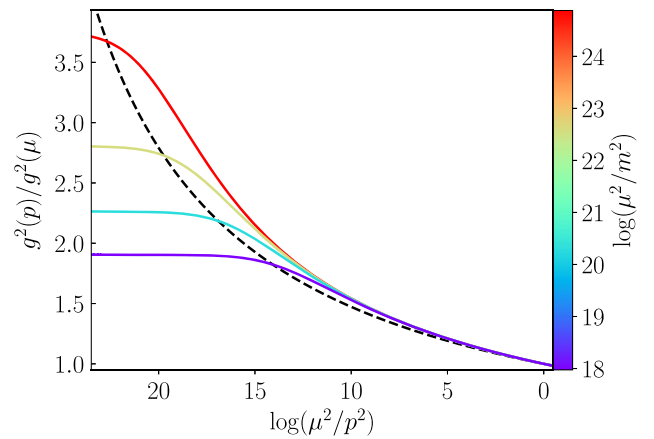


FIG. 1. Flow of the squared tetrahedral coupling g^2 with momentum p for various renormalized masses m^2 (color scale), with $g(\mu) = 20$ at the renormalization scale μ . The two-loop perturbative running is mass independent and represented as dashed.

*Contact author: preis@thphys.uni-heidelberg.de

Published by the American Physical Society under the terms of the Creative Commons Attribution 4.0 International license. Further distribution of this work must maintain attribution to the author(s) and the published article's title, journal citation, and DOI. Funded by SCOAP³.

depend on the renormalized mass or, equivalently, the inverse correlation length. Our results show the generation of a strong interaction by quantum fluctuations, which builds up as the correlation length is increased. The running coupling remains well-defined and finite in the infrared for renormalized masses above a threshold value m^* . Approaching this threshold from above, the growth behavior of the running coupling defines a strong-interaction scale μ^* , which plays the role of a nonperturbative generalization of μ_{pert}^* . We find μ^* to be larger than the scale determined from two-loop perturbation theory. While masses above m^* allow us to investigate the running coupling in a controlled way for momenta even below μ^* , we emphasize that the two scales should not be identified, and we find m^* to be significantly smaller than μ^* . Disentangling these scales allows one to follow the coupling flow from an ultraviolet Gaussian fixed point to a strongly interacting but well-defined infrared in quantum field theory, opening up a new pathway for the investigation of strong-coupling phenomena in four dimensions from first principles.

II. $O(N)^3$ SYMMETRIC TENSOR FIELD THEORY

Following Ref. [3], we consider a scalar (under rotations) field $\bar{\varphi}_{\mathbf{a}=(a^1,a^2,a^3)}$ with $a^{i=1,2,3} = 1, \dots, N$ transforming as a real 3-index tensor in the trifundamental representation of $O(N)^3$ [4,6,7]. The model is defined by the bare (classical) action

$$S[\bar{\varphi}] = \int d^4x \left\{ \frac{1}{2} \bar{\varphi}_{\mathbf{a}}(x) (-\partial^2 + \bar{m}^2) \bar{\varphi}_{\mathbf{a}}(x) + \frac{1}{4} \left(\bar{g}_1 \hat{P}_{\mathbf{ab};\mathbf{cd}}^{(1)} + \bar{g}_2 \hat{P}_{\mathbf{ab};\mathbf{cd}}^{(2)} + i\bar{g} \hat{\delta}_{\mathbf{abcd}}^t \right) \times \bar{\varphi}_{\mathbf{a}}(x) \bar{\varphi}_{\mathbf{b}}(x) \bar{\varphi}_{\mathbf{c}}(x) \bar{\varphi}_{\mathbf{d}}(x) \right\} \quad (1)$$

in four Euclidean dimensions. Here \bar{m} is the bare mass parameter, and we take the bare quartic couplings \bar{g}_1 , \bar{g}_2 and \bar{g} to be real such that $i\bar{g}$ in Eq. (1) is purely imaginary. The three interaction terms in the action stem from the three $O(N)^3$ invariant contraction patterns (“pillow,” “double-trace” and “tetrahedral”)

$$\begin{aligned} \hat{\delta}_{\mathbf{ab};\mathbf{cd}}^p &= \frac{1}{3N^2} \sum_{i=1}^3 \delta_{a^i c^i} \delta_{b^i d^i} \prod_{j \neq i} \delta_{a^j b^j} \delta_{c^j d^j}, \\ \hat{\delta}_{\mathbf{ab};\mathbf{cd}}^d &= N^{-3} \prod_{i=1}^3 \delta_{a^i b^i} \prod_{j=1}^3 \delta_{c^j d^j}, \\ \hat{\delta}_{\mathbf{abcd}}^t &= N^{-3/2} \delta_{a^1 b^1} \delta_{c^1 d^1} \delta_{a^2 c^2} \delta_{b^2 d^2} \delta_{a^3 d^3} \delta_{b^3 c^3}, \end{aligned} \quad (2)$$

which relate to the orthonormal projectors $\hat{P}^{(1)} = 3(\hat{\delta}^p - \hat{\delta}^d)$ and $\hat{P}^{(2)} = \hat{\delta}^d$ appearing in Eq. (1).

III. RENORMALIZED CORRELATION FUNCTIONS

Physical observables can be obtained from the renormalized large- N quantum field theory [8–15]. We aim to compute correlation functions representing expectation values of products of quantum fields, specifically the renormalized two-point correlation function or full propagator $G_{\mathbf{ab}}(x, y)$. In the tensor field theory this computation can be achieved in closed form in the large- N limit. By contrast, in asymptotically free theories like quantum chromodynamics a resummation of the large- N planar Feynman diagrams [16,17] is out of reach. This gives us unique access also to the nonperturbative infrared behavior of our large- N theory.

The renormalized field correlation functions are obtained after imposing renormalization conditions. Two of them concern the full propagator and we write

$$G^{-1}(0) = m^2, \quad \frac{G^{-1}(\mu) - G^{-1}(0)}{\mu^2} = 1. \quad (3)$$

The first condition fixes the renormalized mass m at zero momentum. The second one specifies the wave function renormalization

$$Z(p) = \frac{G^{-1}(p) - G^{-1}(0)}{p^2}, \quad (4)$$

at some high momentum scale μ (the renormalization scale) to $Z(\mu) = 1$. Three additional renormalization conditions fix the three couplings at the same renormalization scale μ ; in particular, the tetrahedral coupling is fixed to a given $g(\mu)$, and the results for the running coupling are presented as a ratio as in Fig. 1. In the large- N limit the running of the renormalized tetrahedral coupling is entirely encoded in the scale dependence of the wave function renormalization (4) as (see also the Appendix) [5]

$$g(p) = \frac{g(\mu)}{Z^2(p)}. \quad (5)$$

With these renormalization conditions the full large- N propagator in the $O(N)^3$ -symmetric regime, where $G_{\mathbf{ab}} = G\delta_{\mathbf{ab}}$, is determined in momentum space by

$$\begin{aligned} G^{-1}(p) &= p^2 + m^2 + g^2(\mu) \int \frac{d^4q}{(2\pi)^4} \frac{d^4k}{(2\pi)^4} G(q)G(k) \\ &\times \left[G(p+q+k) - G(q+k) \right. \\ &\left. - \frac{p^2}{\mu^2} \left(G(\mu+q+k) - G(q+k) \right) \right]. \end{aligned} \quad (6)$$

The self-consistent solution of this equation may be viewed as resumming infinitely many perturbative contributions in

the quartic couplings. It is remarkable that Eq. (6) contains in closed form all the relevant phenomena in the asymptotically free regime and in the strongly interacting infrared we are addressing. The solution for the nonperturbative propagator $G(p)$ determines the wave function renormalization $Z(p)$ and the coupling $g(p)$ according to Eqs. (4) and (5). The behavior of the other couplings g_1 and g_2 does not enter the solution of Eq. (6). Their running is in turn dictated by the momentum dependence of $g(p)$ and has been shown to be perturbatively already well defined in the infrared in Ref. [3]. Even at next-to-leading order in the large- N expansion one only encounters further tadpole corrections which are compensated by the mass renormalization [3].

We iteratively solve Eq. (6) until convergence is observed (see details in the Appendix). We verified that the relevant physical results are insensitive to changes in the momentum discretization for the numerical parameters explored in this work.

IV. PERTURBATION THEORY

We first summarize the two-loop perturbative results as detailed in the Appendix, which predict [see Eq. (A10)]

$$g_{\text{pert}}^2(p) = \frac{g^2(\mu)}{1 + \frac{2g^2(\mu)}{(4\pi)^4} \log\left(\frac{p^2}{\mu^2}\right)}. \quad (7)$$

This perturbative result exhibits a pole at the finite infrared momentum scale

$$\mu_{\text{pert}}^* = \mu e^{-(4\pi)^4/(4g^2(\mu))}. \quad (8)$$

This behavior may be contrasted with the perturbative coupling flow of a familiar scalar quantum field theory with single-component field ϕ and quartic interaction term $\lambda\phi^4$ in four dimensions. In that case the renormalization flow is described by the beta-function $\beta_\lambda \sim \lambda^2$, leading to the scale-dependent coupling $\lambda(p) = \lambda(\mu)(1 - K\lambda(\mu) \log(p^2/\mu^2))^{-1}$ for some constant $K > 0$. Comparing to Eq. (7), one observes that a sign flip in the denominator transforms the UV Landau pole of the ϕ^4 model into an IR pole of an asymptotically free theory—a well known feature of the ϕ^4 -model with negative coupling, $\lambda < 0$ [18,19]. However, such a model with repulsive interaction has classically an unbounded spectrum and is therefore considered unstable. Recently this conclusion has been reinvestigated in the context of \mathcal{PT} -symmetry [20–22]. In contrast, our theory is bounded from below due to the two additional (positive semidefinite) quartic couplings and, importantly, the two-loop beta-function $\beta_{g_{\text{real}}} \sim g_{\text{real}}^3$ changes sign for an imaginary coupling $g_{\text{real}} \rightarrow ig$, not a negative one. The beta-function of our tensor field theory starts at cubic order in the tetrahedral coupling because its flow is driven solely by the wavefunction renormalization.

V. NONPERTURBATIVE FLOW OF THE TETRAHEDRAL COUPLING

The running of the tetrahedral coupling is controlled by the wave function renormalization and, gathering Eqs. (4) and (5), we obtain

$$\frac{g^2(\mu)}{g^2(p)} = Z(p)^4 = \left[\frac{G^{-1}(p) - G^{-1}(0)}{p^2} \right]^4. \quad (9)$$

The full large- N result for the scale-dependent coupling is given for a wide range of renormalized masses (see color code) in Figs. 1 and 2. In Fig. 2, we plot its inverse on a logarithmic momentum scale for a broader range of masses to illustrate the deviation from the perturbative result (7), which is represented by a strictly straight dashed line. At large momenta, the perturbative and nonperturbative solutions agree increasingly well, consistent with the prediction of asymptotic freedom. However, the slope of the nonperturbative flow becomes steeper toward the IR such that the coupling grows faster than the perturbative one at intermediate scales.

While the perturbative result is insensitive to the renormalized mass, the full coupling is seen to depend on it. The coupling reaches a mass-dependent finite value in the deep infrared for masses above a threshold value. As we decrease the renormalized mass, the limiting value of the tetrahedral coupling grows, as depicted in Fig. 3 [23]. The observed behavior suggests that, for any given $g(\mu)$, there exist a finite mass m^* for which the tetrahedral coupling diverges at a finite IR momentum scale μ^* . We stress that the mass scale m^* should not be identified with the dynamically generated scale μ^* . We can estimate m^* from Fig. 3 and the momentum scale μ^* by extrapolating the envelope of the curves in Fig. 2. We find that the dynamically generated scale μ^* is significantly larger than the mass scale m^* , which in turn is much larger than the perturbative scale μ_{pert}^* .

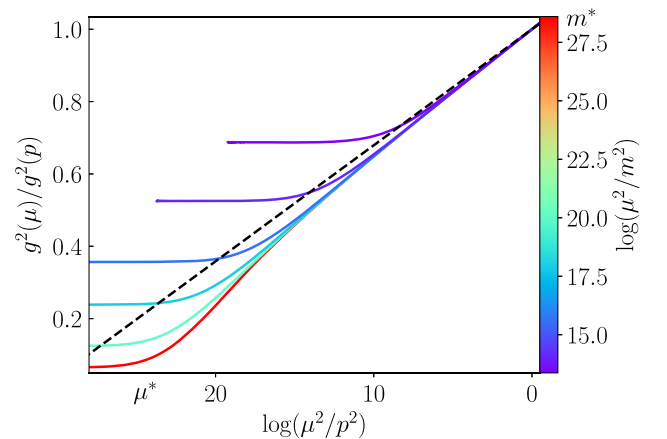


FIG. 2. Inverse of the squared tetrahedral coupling for different renormalized masses (color scale). The perturbative result is displayed as a black dashed line.

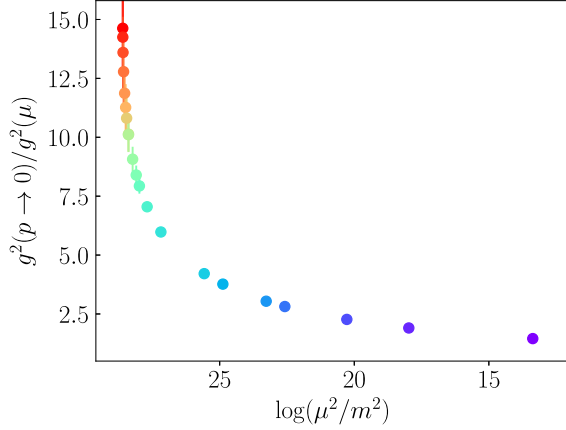


FIG. 3. Limiting value of the squared tetrahedral coupling in the infrared for varying mass.

[24]. These values of m^* and μ^* are highlighted in Fig. 2. For completeness, the corresponding results for the propagator are discussed in the Appendix.

VI. RELATION TO OTHER TENSOR FIELD THEORIES

In order to put our results into context, we compare to similar tensor models in the literature. First, one can consider the $O(N)^3$ model in $4 - \epsilon$ dimensions [4]. This model has a nontrivial (so-called “melonic”) fixed point with couplings of order $\sqrt{\epsilon}$. However, while the tetrahedral coupling is real, the pillow and double trace couplings are imaginary at the fixed point, and the resulting conformal field theory is unstable as it has a primary operator in the principal series [25,26]. Alternatively, one can consider a long-range version of the $O(N)^3$ model in $d < 4$ dimensions [5,27]. Picking the marginal scaling for the propagator and an imaginary tetrahedral coupling, one obtains a line of infrared fixed points (indexed by the exactly marginal tetrahedral coupling), which are stable and correspond to well-defined (and presumably unitary [28]) large- N conformal field theories. More generally, the renormalization group fixed points for tensor field theories give rise to a new family of conformal “melonic” field theories which can be studied analytically [29–36] (see also [37–41] for reviews and references therein) [42].

We stress that the behavior we encounter here is of a very different nature. The infrared regime we identify does not correspond to a renormalization group fixed point: although the (classically marginal) tetrahedral coupling flows to a fixed value, the renormalized mass is nonzero and larger than a threshold value.

VII. REAL TETRAHEDRAL COUPLING

If one considers the $O(N)^3$ model with a real tetrahedral coupling in exactly four dimensions, the melonic fixed

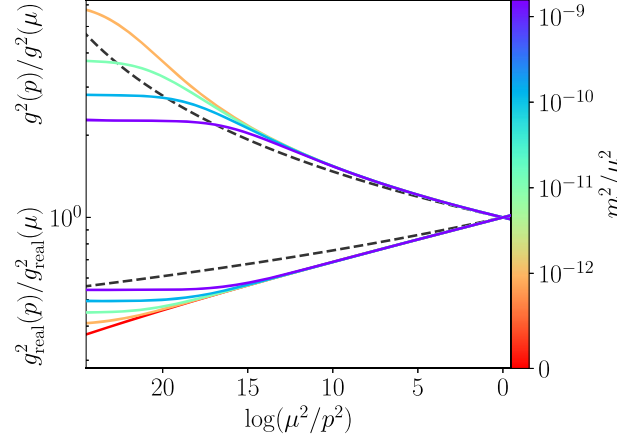


FIG. 4. Comparison of real vs imaginary tetrahedral coupling for different renormalized masses and $|g(\mu)| = |g_{\text{real}}(\mu)|$. The corresponding perturbative predictions are shown as dashed black lines. For real tetrahedral coupling also the solution at vanishing renormalized mass is shown (red curve).

point of order $\sqrt{\epsilon}$ coincides with the trivial Gaussian fixed point. The perturbative computation, Eq. (7) with the sign in the denominator flipped, shows that the tetrahedral coupling vanishes in the IR like $g^2(p) \sim \log(\mu^2/p^2)^{-1}$ and displays a UV Landau pole at a finite scale. It is not known whether this flow is completed by some nontrivial UV fixed point. In Fig. 4 we contrast the running in the real and imaginary case obtained by solving Eq. (6) with $g^2 \rightarrow -g_{\text{real}}^2$. The corresponding two-point functions are discussed in the Appendix. For a real tetrahedral coupling we are able to obtain a self-consistent solution for the propagator with vanishing renormalized mass. This solution exhibits a vanishing coupling for $p \rightarrow 0$ (red curve in Fig. 4). The self-consistent running decreases faster toward the IR than predicted by perturbation theory (dashed). Similar to the imaginary tetrahedral coupling case, the self-consistent solution with real tetrahedral coupling is sensitive to the presence of a nonvanishing renormalized mass, whereas the perturbative solution is not.

VIII. DISCUSSION AND OUTLOOK

Our results show that for an asymptotically free massive scalar field theory in four dimensions quantum fluctuations can generate a strong coupling that remains well defined in the infrared. The phenomenon is captured in closed form by the equation for the scalar field two-point correlator in the large- N limit. The wave function renormalization determines the growth of the running coupling toward the infrared. In contrast to the standard perturbative behavior, as long as the mass is above a threshold value, the full nonperturbative coupling remains finite in the infrared. By varying the mass over several orders of magnitude, we find that the infrared value of the coupling grows as the mass is decreased, and exceeds the perturbative estimate.

It is very interesting to consider these results in view of other asymptotically free theories such as QCD, where the nonperturbative generation of a strong-interaction scale by quantum fluctuations is known to have striking phenomenological consequences such as confinement [43]. The gluons in QCD are massless, which is protected by local gauge symmetry, and only gauge-invariant quantities are observable. In particular, in QCD the perturbative notion of a (gauge-variant) coupling ceases to hold in the infrared, where it diverges at the confinement scale Λ_{QCD} . Comparing this to the asymptotically free scalar field theory, the role of Λ_{QCD} is played by the scale μ_{pert}^* in the perturbative tensor model. However, the scalar field theory allows one to vary the mass scale and investigate the dynamical build-up of a strong-interaction as the correlation length increases in a regime where the nonperturbative coupling remains well defined and its infrared value determines the physical interaction strength.

ACKNOWLEDGMENTS

We thank J. Horak, I. Klebanov, T. Krajewski, T. Muller, J. Pawłowski, F. Popov, P. Romatschke, F. Sattler,

A. Tanasa, G. Tarnopolsky, R. Venugopalan, and J. Wessely for useful discussions and comments on the draft. The authors acknowledge support by the state of Baden-Württemberg through bwHPC and the German Research Foundation (DFG) through grant no INST 40/575-1 FUGG (JUSTUS 2 cluster), the Heidelberg STRUCTURES Excellence Cluster under Germany's Excellence Strategy EXC2181/1-390900948, the DFG under the Collaborative Research Center SFB 1225 ISOQUANT (Project-ID 273811115), and the European Research Council (ERC) under the European Union's Horizon 2020 research and innovation program (Grant Agreement No. 818066). T.P. acknowledges partial support from the Simons Foundation under Award number 994318 (Simons Collaboration on Confinement and QCD Strings) and thanks Stony Brook University and Brookhaven National Laboratory for their hospitality.

APPENDIX

1. Renormalization and two-loop perturbation theory

The renormalized action of the model writes in terms of the renormalized field φ_a as:

$$S[\varphi] = \int d^4x \left\{ \frac{\tilde{Z}}{2} \varphi_a(x) (-\partial^2) \varphi_a(x) + \frac{1}{2} (m^2 + \delta m^2) \varphi_a(x) \varphi_a(x) + \frac{1}{4} \left((g_1 + \delta g_1) \hat{P}_{ab;cd}^{(1)} + (g_2 + \delta g_2) \hat{P}_{ab;cd}^{(2)} + i(g + \delta g) \hat{\delta}_{abcd}^t \right) \varphi_a(x) \varphi_b(x) \varphi_c(x) \varphi_d(x) \right\}, \quad (\text{A1})$$

where the wave function renormalization constant is $\tilde{Z} = 1 + \delta\tilde{Z}$. The bare and renormalized quantities are related by $\bar{\varphi}_a = \tilde{Z}^{1/2} \varphi_a$, $\bar{m}^2 = \tilde{Z}^{-1} (m^2 + \delta m^2)$, $\bar{g} = \tilde{Z}^{-2} (g + \delta g)$, $\bar{g}_{1,2} = \tilde{Z}^{-2} (g_{1,2} + \delta g_{1,2})$ and the counterterms $\delta\tilde{Z}$, δm^2 , δg and $\delta g_{1,2}$ ensure that the renormalized correlations are free of divergences. The counterterms are fixed by the renormalization conditions:

$$G^{-1}(0) = m^2, \quad Z(\mu) = \frac{G^{-1}(\mu) - G^{-1}(0)}{\mu^2} = 1, \quad \Gamma^{(4,t)}(p_1, p_2, p_3, p_4)|_{p_i^2=\mu^2} = \delta \left(\sum_{i=1}^4 p_i \right) g(\mu), \quad (\text{A2})$$

where $G_{ab}(x, y) = \langle \varphi_a(x) \varphi_b(y) \rangle = G(x, y) \delta_{ab}$ is the renormalized two-point function and $\Gamma^{(4,t)}$ is the tetrahedral channel of the renormalized four-point function. The four-point functions in the $\hat{P}^{(1)}$ and $\hat{P}^{(2)}$ channel are fixed similarly.

The function $Z(\mu)$ arising in the renormalization condition above is related to $\tilde{Z} = \tilde{Z}(\mu)$, the renormalization constant in the renormalized action. The renormalized propagator is $G^{-1}(p) = \tilde{Z}(\mu) G_b^{-1}(p)$ with G_b^{-1} the resummed

propagator computed in the bare theory, hence $Z(p) = \tilde{Z}(\mu) f_b(p)$ for f_b some function which depends parametrically on the bare parameters. This function is of course divergent, that is it exhibits $1/\epsilon$ poles in $d = 4 - \epsilon$, or logarithmic divergences with the ultraviolet momentum cutoff Λ at $d = 4$. Fixing $Z(\mu) = 1$ yields $\tilde{Z}(\mu) = 1/f_b(\mu)$ which in turn implies $Z(p) = \tilde{Z}(\mu)/\tilde{Z}(p)$. The renormalized two-point function at large- N respects the Schwinger-Dyson equation:

$$G^{-1}(p) = \tilde{Z} p^2 + m^2 + \delta m^2 + (g_2 + \delta g_2) \int \frac{d^4 q}{(2\pi)^4} G(q) + (g + \delta g)^2 \int \frac{d^4 q}{(2\pi)^4} \frac{d^4 k}{(2\pi)^4} G(q) G(k) G(p + q + k). \quad (\text{A3})$$

Imposing the renormalization conditions and taking into account that in the large N limit $\delta g = 0$, see Ref. [5], we obtain Eq. (6) of the main text.

Keeping the renormalization scale μ fixed, we are interested in the momentum dependence of the physical couplings of the theory, that is the local parts of the effective action at a symmetric point

$$\Gamma^{(n)}(p_i)|_{p_i^2=p^2} = \delta \left(\sum_i p_i \right) Z(p)^{n/2} g^{(n)}(p). \quad (\text{A4})$$

As $\delta g = 0$ at large- N , the momentum dependent tetrahedral coupling is entirely driven by the wave function,

$Z^2(p)g(p) = g(\mu)$. The renormalized propagator $G(p)$ is determined self-consistently by Eq. (6), which in turn fixes the wave function renormalization $Z(p)$ and the running coupling $g(p)$. The running of g_1 and g_2 is dictated by the running of g and can be extracted from their corresponding Bethe-Salpeter equations, which we will address in future work.

Two loops. The renormalization group flow at two-loops is obtained using dimensional regularization and minimal subtraction in $d = 4 - \epsilon$ and setting $\epsilon = 0$. At two loops and after mass renormalization, Eq. (A3) reads (where we denote the renormalization scale with s here for convenience)

$$G_{\text{pert}}^{-1}(p) = \tilde{Z}p^2 + m^2 + g^2 s^{2\epsilon} \int \frac{d^d q}{(2\pi)^d} \frac{d^d k}{(2\pi)^d} \frac{1}{(q^2 + m^2)(k^2 + m^2)} \left(\frac{1}{(p+q+k)^2 + m^2} - \frac{1}{(q+k)^2 + m^2} \right), \quad (\text{A5})$$

and the sunset (melon) diagram evaluates in a Laurent series in ϵ [44]

$$\begin{aligned} & g^2 s^{2\epsilon} \int \frac{d^d q}{(2\pi)^d} \frac{d^d k}{(2\pi)^d} \frac{1}{(q^2 + m^2)(k^2 + m^2)((p+q+k)^2 + m^2)} \\ &= -\frac{g^2 m^2}{(4\pi)^4} \left\{ \frac{6}{\epsilon^2} + \frac{6}{\epsilon} \left[\frac{3}{2} - \gamma + \log \left(\frac{4\pi s^2}{m^2} \right) \right] + \frac{p^2}{2m^2 \epsilon} + O(\epsilon^0) \right\}. \end{aligned} \quad (\text{A6})$$

Up to order $1/\epsilon$ the full propagator at two loops is $G_{\text{pert}}^{-1}(p) = \tilde{Z}p^2 + m^2 - p^2 \frac{g^2}{(4\pi)^4 2\epsilon}$. In the minimal subtraction scheme, renormalization is performed by requiring that at the renormalization scale s both the tetrahedral counterterm δg and the wave function counterterm $\delta \tilde{Z}$ are pure divergences. As $\delta g = 0$ we have

$$g(s) = g, \quad \tilde{Z}(s) = 1 + \frac{g^2}{(4\pi)^4 2\epsilon}, \quad (\text{A7})$$

where the first equation signifies that the coupling constant g in the renormalized action is exactly the physical four point function (in the tetrahedral channel) at the renormalization scale s .

We note that the minimal subtraction prescription differs from imposing the renormalization conditions in Eq. (3) by finite terms, but the beta functions up to two loops are prescription independent [45,46]. The bare tetrahedral coupling writes $\bar{g} = s^\epsilon g(s) \tilde{Z}^{-2}(s)$. Taking the s derivative at fixed \bar{g} , at two loops we obtain

$$\beta(g) = s \partial_s g(s) = -\epsilon g(s) - \frac{2g^3(s)}{(4\pi)^4}, \quad \eta = s \partial_s \log(\tilde{Z}(s)) = \frac{\beta(g) \partial_g \tilde{Z}(s)}{\tilde{Z}(s)} = -\frac{g^2(s)}{(4\pi)^4}. \quad (\text{A8})$$

We emphasize that we obtained a scale-dependent coupling despite $\delta g = 0$, as the flow is driven by the wavefunction renormalization $\tilde{Z}(s)$, which is nontrivial already at leading order in the large- N expansion. This features sets melonic tensor field theories, such as $O(N)^3$ at large- N , apart from the more standard $O(N)$ vector models at large- N . We set $\epsilon = 0$ and integrate the flow down from some reference scale μ in the UV to find

$$g_{\text{pert}}^2(s) = \frac{g^2(\mu)}{1 + \frac{2g^2(\mu)}{(4\pi)^4} \log \left(\frac{s^2}{\mu^2} \right)}, \quad \tilde{Z}_{\text{pert}}(s) = e^{-\int_{g(s)}^{g(\mu)} \frac{\eta(g') dg'}{\beta(g')}} \tilde{Z}(\mu) = \left[1 + \frac{2g^2(\mu)}{(4\pi)^4} \log \left(\frac{s^2}{\mu^2} \right) \right]^{-\frac{1}{4}} \tilde{Z}(\mu). \quad (\text{A9})$$

Taking into account the relation between $Z(p)$ and $\tilde{Z}(p)$, we get

$$Z_{\text{pert}}(p) = \left[1 + \frac{2g^2(\mu)}{(4\pi)^4} \log \left(\frac{p^2}{\mu^2} \right) \right]^{\frac{1}{4}}. \quad (\text{A10})$$

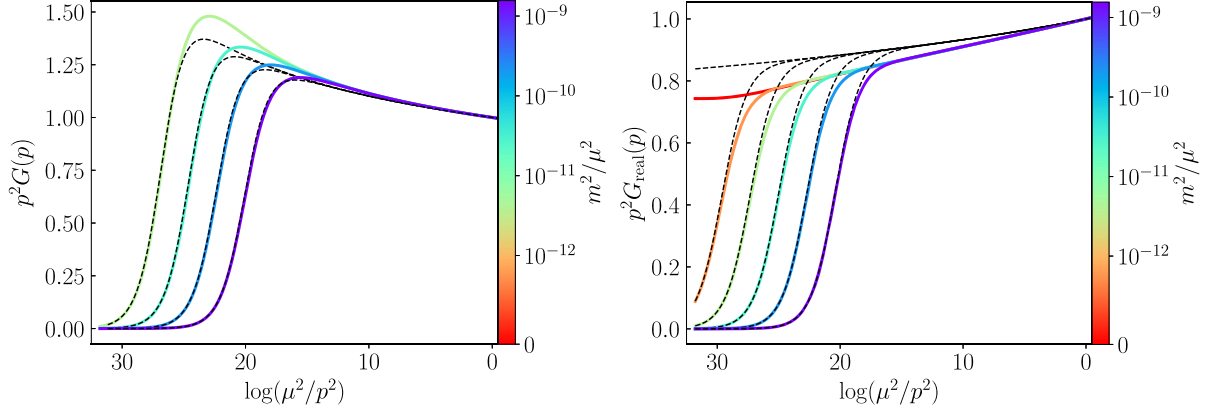


FIG. 5. Propagator with $1/p^2$ momentum dependence scaled out respectively for the case of imaginary tetrahedral coupling (left) and real tetrahedral coupling (right) displayed for various renormalized masses (color scale). The two loop results correspond to the black dashed lines.

2. Full propagator

In Fig. 5 we display the renormalized self-consistent propagator for different renormalized masses with the trivial $1/p^2$ momentum dependence scaled out. The flow of couplings discussed in Fig. 4 in the main text was obtained from the propagators depicted here.

The case with imaginary tetrahedral coupling is shown on the left. Due to the Gaussian UV fixed point, all the solutions asymptote to 1 at high momenta. As we decrease p toward the IR, $p^2 G(p)$ increases until the presence of a nonvanishing renormalized mass m^2 eventually suppresses the momentum dependence and $p^2 G(p) \sim p^2/m^2$ drops to zero. If we decrease m^2 , we extend the range of scales over which $p^2 G(p)$ grows and we observe an increasingly prominent bump at intermediate momentum scales with associated increasing deviations from the two-loop perturbation theory result

$$p^2 G_{\text{pert}}(p) \simeq \frac{p^2}{m^2 + p^2 \left[1 + \frac{2g^2(\mu)}{(4\pi)^4} \log\left(\frac{p^2}{\mu^2}\right) \right]^{\frac{1}{4}}}, \quad (\text{A11})$$

which is displayed in dashed black. Observe that Eq. (A11) is only valid for momenta $p^2 \geq (\mu_{\text{pert}}^*)^2$ with $\mu_{\text{pert}}^* = \mu \exp[-(4\pi)^4/(4g^2(\mu))]$ since the term in square brackets becomes negative for $p \leq \mu_{\text{pert}}^*$.

The case with real tetrahedral coupling is shown on the right in Fig. 5. In contrast to the imaginary case, the propagator is more suppressed for low momenta and we were able to obtain a solution for vanishing mass. In the perturbative two-loop result for the propagator in Eq. (A11) only the sign in front of $g^2(\mu)$ changes. This makes the perturbative result well defined for all momenta $p \leq \mu_{\text{pert}}^*$. These differences are not surprising as for real tetrahedral coupling the Gaussian fixed point is IR attractive. In contrast to the imaginary tetrahedral case, for real coupling it is not known whether there exists a nontrivial UV fixed point and consequently the theory might not exist without a UV cutoff.

3. Numerical implementation

Implementing the renormalization conditions (3) amounts to subtracting the sunset integral evaluated at zero external momentum respectively at the renormalization scale μ . The mass and wave function counterterms are

$$\delta m^2 = -(g_2 + \delta g_2) \int \frac{d^4 q}{(2\pi)^4} G(q) - g^2(\mu) \int \frac{d^4 q}{(2\pi)^4} \frac{d^4 k}{(2\pi)^4} G(q) G(k) G(q+k), \quad (\text{A12})$$

$$\delta \tilde{Z} = -\frac{g^2(\mu)}{\mu^2} \int \frac{d^4 q}{(2\pi)^4} \frac{d^4 k}{(2\pi)^4} G(q) G(k) [G(\mu+q+k) - G(q+k)], \quad (\text{A13})$$

leading to the renormalized version of the Schwinger-Dyson equation in Eq. (6)

$$G^{-1}(p) = p^2(1 + \delta \tilde{Z}) + m^2 + g^2(\mu) I(G; p), \quad (\text{A14})$$

with

$$I(G; p) = \int \frac{d^4 q}{(2\pi)^4} \frac{d^4 k}{(2\pi)^4} G(q) G(k) [G(p+q+k) - G(q+k)], \quad (\text{A15})$$

and $\delta \tilde{Z} = -g^2(\mu)/\mu^2 I(G; \mu)$.

We discretize by using a logarithmic p^2 grid with 7000 points and IR/UV cutoffs, respectively $\Lambda_{\text{IR}}/\mu = 1.25 \times 10^{-7}$ and $\Lambda/\mu = 1.25$, which regularize the integral.

a. Algorithm

We solve the renormalized Schwinger-Dyson equation for the propagator via fixed-point iteration. The algorithm proceeds as follows:

- (1) We initiate the solver by providing the arbitrary renormalization scale μ , chosen for convenience to lie in the UV with $\mu/\Lambda = 0.8$, and the renormalized parameters m^2 and $g(\mu)$.
- (2) Due to asymptotic freedom [3], we can and do choose the initial ansatz for the propagator to coincide with the classical one $[G^{-1}(p)]^{i=0} = p^2 + m^2$. Here the superscript i denotes the iteration step.
- (3) We calculate the integral $I([G]^i; p)$ in Eq. (A15). This requires some interpolation and extrapolation for p^2 values that are not elements of the grid (see next paragraph).
- (4) We determine $\delta\tilde{Z}$ from $I([G]^i; \mu)$.
- (5) We evaluate the right hand side of Eq. (A14) as $[\text{RHS}]^{i+1} = p^2(1 - g^2(\mu)/\mu^2 I([G]^i, \mu)) + m^2 + g^2(\mu)I([G]^i, p)$ and set $[G^{-1}]^{i+1} = \alpha[\text{RHS}]^{i+1} +$

$(1 - \alpha)[G^{-1}]^i$ with mixing parameter $\alpha = 0.2$ to improve the convergence of the algorithm.

- (6) We repeat steps 3–5 until apparent convergence is achieved. This is quantified by confirming that the grid-point-wise relative deviation of $[G^{-1}]^i$ and $[G^{-1}]^{i+1}$ averaged over all grid points is below a predefined threshold, 10^{-7} in our case.

We tested the insensitivity of all displayed results by varying the resolution of the grid and the cutoffs over four orders of magnitude.

b. Integration

We use hyperspherical coordinates $(r, \theta, \psi, \phi) \in [0, \infty) \times [0, \pi] \times [0, \pi] \times [0, 2\pi]$ and denote $z = \cos(\theta)$, $y = \cos(\psi)$, such that the integral measure on \mathbb{R}^4 can be written as $d^4p = \frac{1}{2}p^2\sqrt{1-z^2}d(p^2)dzdyd\phi$. Due to spherical symmetry all functions only depend on the invariant p^2 . We make use of the fact that the sunset integral:

$$M(p) = \int \frac{d^4q}{(2\pi)^4} \frac{d^4k}{(2\pi)^4} G(q)G(k)G(p+q+k), \quad (\text{A16})$$

can be written as two nested convolutions. First, we define:

$$F(p) = \int \frac{d^4k}{(2\pi)^4} G(p+k)G(k) = \frac{1}{(2\pi)^3} \int_{\Lambda_{\text{IR}}^2}^{\Lambda^2} dk^2 \int_{-1}^1 dz k^2 \sqrt{1-z^2} G(p^2 + k^2 + |p||k|z)G(k^2), \quad (\text{A17})$$

and, second, we notice that $I(p) = M(p) - M(0)$ can be computed as:

$$I(p) = \int \frac{d^4q}{(2\pi)^4} (F(p+q) - F(q))G(q) = \int_{\Lambda_{\text{IR}}^2}^{\Lambda^2} \frac{dq^2}{(2\pi)^3} \int_{-1}^1 dz q^2 \sqrt{1-z^2} G(q^2)[F(p^2 + q^2 + |p||q|z) - F(q^2)]. \quad (\text{A18})$$

The angular z -integrals are performed via a Gauss-Chebyshev quadrature with 64 points and for the q^2 -integrals we use Gauss-Legendre quadrature [47] with 7000 points.

Momenta probed in the convolution range from 0 to 2Λ , such that $G^{-1}(p)$ and $F(p)$ need to be extrapolated. For $|p| < \Lambda_{\text{IR}}$ we set both functions to be equal to their values at Λ_{IR} . For $\Lambda < |p| < 2\Lambda$ we make use of asymptotic

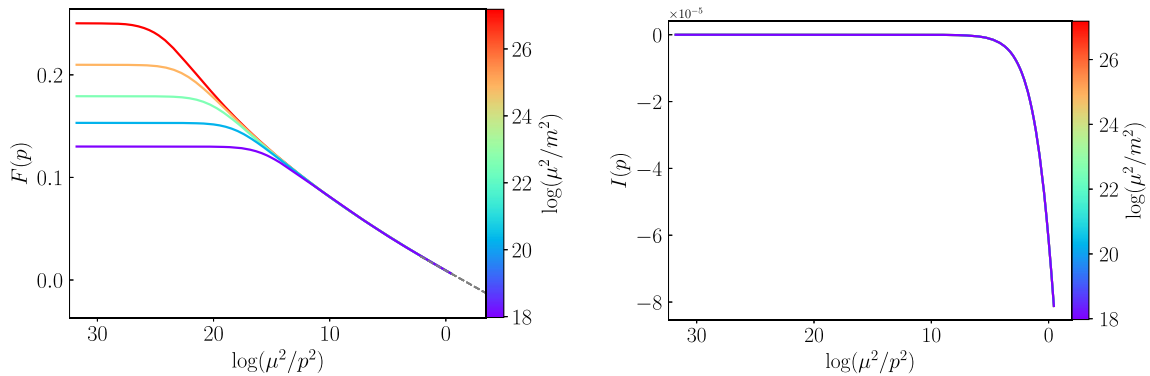


FIG. 6. Left: Numerical results for the convolution of two propagators $F(p) = \int \frac{d^4k}{(2\pi)^4} G(p+k)G(k)$ together with the prescribed extrapolation functions (A19). The extrapolation for $\Lambda < p \leq 2\Lambda$ is shown in dashed gray. Right: Numerical results for the melon integral with subtracted local part (A15). The individual lines for different masses are not distinguishable in this plot.

freedom and extrapolate with the momentum dependence inferred from perturbation theory [48]:

$$G_{\text{pert}}^{-1}(p) = m^2 + p^2 \left[1 + \frac{2g^2(\mu)}{(4\pi)^4} \log\left(\frac{p^2}{\mu^2}\right) \right]^{\frac{1}{4}},$$

$$F_{\text{pert}}(p) = F(\Lambda) \left[1 + \log\left(\frac{\Lambda^2}{p^2}\right) \right]. \quad (\text{A19})$$

The validity of these extrapolations is tested by varying the cutoffs and comparing to the numerical result at high and low momenta. The corresponding numerical result for the convolution $F(p) = \int \frac{d^4k}{(2\pi)^4} G(p+k)G(k)$ and the sunset integral with subtracted local part (A15) are shown in Fig. 6.

-
- [1] D. J. Gross and F. Wilczek, Phys. Rev. Lett. **30**, 1343 (1973).
- [2] H. D. Politzer, Phys. Rev. Lett. **30**, 1346 (1973).
- [3] J. Berges, R. Gurau, and T. Preis, Phys. Rev. D **108**, 016019 (2023).
- [4] S. Giombi, I. R. Klebanov, and G. Tarnopolsky, Phys. Rev. D **96**, 106014 (2017).
- [5] D. Benedetti, R. Gurau, and S. Harribey, J. High Energy Phys. 06 (2019) 053.
- [6] S. Carrozza and A. Tanasa, Lett. Math. Phys. **106**, 1531 (2016).
- [7] I. R. Klebanov and G. Tarnopolsky, Phys. Rev. D **95**, 046004 (2017).
- [8] J.-P. Blaizot, E. Iancu, and U. Reinosa, Nucl. Phys. **A736**, 149 (2004).
- [9] J. Berges, S. Borsanyi, U. Reinosa, and J. Serreau, Ann. Phys. (Amsterdam) **320**, 344 (2005).
- [10] J. Berges, S. Borsanyi, U. Reinosa, and J. Serreau, Phys. Rev. D **71**, 105004 (2005).
- [11] G. Aarts and J. M. Martinez Resco, J. High Energy Phys. 02 (2004) 061.
- [12] U. Reinosa and J. Serreau, J. High Energy Phys. 07 (2006) 028.
- [13] G. Fejos, A. Patkos, and Z. Szep, Nucl. Phys. **A803**, 115 (2008).
- [14] J.-P. Blaizot, J. M. Pawłowski, and U. Reinosa, Phys. Lett. B **696**, 523 (2011).
- [15] J.-P. Blaizot, J. M. Pawłowski, and U. Reinosa, Ann. Phys. (Amsterdam) **431**, 168549 (2021).
- [16] G. 't Hooft, Nucl. Phys. **B72**, 461 (1974).
- [17] E. Brezin, C. Itzykson, G. Parisi, and J. B. Zuber, Commun. Math. Phys. **59**, 35 (1978).
- [18] K. Symanzik, Commun. Math. Phys. **23**, 49 (1971).
- [19] K. Symanzik, Lett. Nuovo Cimento **6S2**, 77 (1973).
- [20] C. M. Bender and S. Boettcher, Phys. Rev. Lett. **80**, 5243 (1998).
- [21] S. Lawrence, H. Oh, and Y. Yamauchi, Phys. Rev. D **106**, 114503 (2022).
- [22] P. Romatschke, arXiv:2310.03815.
- [23] The numerical error is estimated by using once $G^{-1}(0) = m^2$ and once $G^{-1}(\Lambda_{\text{IR}})$, with Λ_{IR} the numerical IR cutoff, to subtract the momentum independent part in Eq. (9).
- [24] For $g(\mu) = 20$, as employed for the figures, we find $\log(\mu^2/(\mu^*)^2) \simeq 25.2$, $\log(\mu^2/(m^*)^2) \simeq 28.6$ and $\log(\mu^2/(\mu_{\text{pert}}^*)^2) \simeq 31.2$.
- [25] J. Kim, I. R. Klebanov, G. Tarnopolsky, and W. Zhao, Phys. Rev. X **9**, 021043 (2019).
- [26] D. Benedetti, J. High Energy Phys. 05 (2021) 004.
- [27] D. Benedetti, R. Gurau, and S. Harribey, Phys. Rev. D **103**, 046018 (2021).
- [28] D. Benedetti, R. Gurau, S. Harribey, and K. Suzuki, J. High Energy Phys. 02 (2020) 072; 08 (2020) 167(E).
- [29] D. Benedetti and R. Gurau, J. High Energy Phys. 05 (2018) 156.
- [30] D. Benedetti, N. Delporte, S. Harribey, and R. Sinha, J. High Energy Phys. 06 (2020) 065.
- [31] D. Benedetti, R. Gurau, S. Harribey, and D. Lettera, J. High Energy Phys. 02 (2022) 147.
- [32] S. Prakash and R. Sinha, J. High Energy Phys. 02 (2018) 086.
- [33] D. Benedetti, S. Carrozza, R. Gurau, and A. Sfondrini, J. High Energy Phys. 01 (2018) 003.
- [34] S. Giombi, I. R. Klebanov, F. Popov, S. Prakash, and G. Tarnopolsky, Phys. Rev. D **98**, 105005 (2018).
- [35] E. Witten, J. Phys. A **52**, 474002 (2019).
- [36] R. Gurau, Nucl. Phys. **B916**, 386 (2017).
- [37] S. Harribey, Renormalization in tensor field theory and the melonic fixed point, Ph.D. thesis, Heidelberg University, 2022.
- [38] D. Benedetti, Proc. Sci. CORFU2019 (2020) 168 [arXiv:2004.08616].
- [39] R. G. Gurau, Ann. Inst. H. Poincaré D Comb. Phys. Interact. **9**, 159 (2022).
- [40] I. R. Klebanov, F. Popov, and G. Tarnopolsky, Proc. Sci. TASI2017 (2018) 004 [arXiv:1808.09434].
- [41] N. Delporte, Tensor field theories: Renormalization and random geometry, Ph.D. thesis, University Paris-Saclay, 2020.
- [42] It should be noted that, similar to our Eq. (6), such analytic solutions always start by solving self-consistently a large- N Schwinger-Dyson equation for the two point function.
- [43] K. G. Wilson, Phys. Rev. D **10**, 2445 (1974).
- [44] H. Kleinert and V. Schulte-frohlinde, *Critical Properties of Phi4- Theories* (World Scientific Publishing Company, Singapore, 2001).

-
- [45] J. Zinn-Justin, *Quantum Field Theory and Critical Phenomena*, International Series of Monographs on Physics (Clarendon Press, New York, 2002).
- [46] S. Weinberg, *The Quantum Theory of Fields. Vol. 2: Modern Applications* (Cambridge University Press, Cambridge, England, 2013).
- [47] W. H. Press, S. A. Teukolsky, W. T. Vetterling, and B. P. Flannery, *Numerical Recipes*, 3rd ed. (Cambridge University Press, Cambridge, England, 2007).
- [48] The second equation stems from the integral $\int_{\Lambda_{\text{IR}} < |k| < \Lambda} \frac{d^4 k}{(p+k)^2 k^2} = \frac{(2\pi)^2}{4} [1 - \Lambda_{\text{IR}}^2/p^2 + \log(\Lambda^2/p^2)]$.

Discussion and Outlook

The purpose of this chapter is to place the research presented in this thesis in relation to the broader research on tensor models and in other fields. At the end, some directions for future research are mentioned.

8.1 Orthogonal and symplectic random tensor models

The motivation to study tensor models with symplectic symmetry stems from two main aspects. First, the relevance of field theories with $Sp(N)$ symmetry and N to $-N$ relations; and second, the aim to generalize known results on tensor models to different symmetry groups. In the following, both motivations will be explained in more detail, and then the relevance of the work presented in Chapters 3–5 will be described.

The initial motivation to study tensor models with $Sp(N)$ symmetry came from theories of so-called symplectic fermions. Their action is

$$S(\chi) = \int d^d x \left[\frac{1}{2} \partial_\mu \chi^a \omega_{ab} \partial^\mu \chi^b + \frac{g}{4!} \left(\chi^a \omega_{ab} \chi^b \right)^2 \right], \quad (8.1.1)$$

where χ is an N (N even) component vector of anticommuting Grassmann variables and ω is the antisymmetric symplectic form. The action is invariant under $Sp(N)$ transformations of χ . The field is fermionic because its components anticommute, but it is a scalar with respect to Lorentz transformations, respectively $SO(d)$ rotations in Euclidean signature. The case $N = 2, d = 2$ is a two-dimensional CFT used to describe polymers [225]; in $2 < d < 4$ dimensions, the model was considered in the context of critical phenomena [212, 213]; and for $d = 3$, as a holographic dual [226] to Vasiliev's higher spin gravity [227] in four-dimensional de Sitter (dS) space.

The correlation functions of these models are related to the correlation functions of an analogous bosonic $O(N)$ vector model by the replacement $N \rightarrow -N$. This relation plays an important role in the mentioned works. The beta function [213] of the model reads

$$\beta(g) = (d - 4)\tilde{g} + \frac{8 - N}{6}\tilde{g}^2 + \frac{3N - 14}{12}\tilde{g}^3 + O(\tilde{g}^4), \quad \tilde{g} = \frac{g}{(4\pi)^{d/2}\Gamma(d/2)}, \quad (8.1.2)$$

which is exactly the beta function of the $O(N)$ vector model after continuing $N \rightarrow -N$ (see, e.g., [228]). The beta function has a nontrivial infrared fixed point $\tilde{g}_* = 6/(8 - N)\epsilon + O(\epsilon^2)$ in $d = 4 - \epsilon$ (with $\epsilon > 0$) dimensions, which can be viewed as a fermionic version of the Wilson–Fisher fixed point. For $N < 8$ the fixed point is at positive values of the coupling, while for $N > 8$ it is at

negative coupling. Note that a negative coupling is not necessarily a problem, as the fields are fermionic.²⁹

The relation with the $O(N)$ vector model for negative N is also the primary reason why the $Sp(N)$ model is relevant in the context of dS/CFT holography [229]. The central proposal of this conjectural kind of holographic duality is, that a quantum gravity theory in d -dimensional de Sitter space has a dual description given by a CFT on a Euclidean $(d-1)$ -dimensional sphere. This would be a wide generalization of the better-known AdS/CFT correspondence between a quantum gravity theory in d -dimensional anti-de Sitter (AdS) space and a CFT in \mathbb{R}^d with Lorentzian signature. In this context the three-dimensional critical $O(N)$ vector model is proposed to be the dual of Vasiliev's higher spin gravity in four-dimensional AdS [230]. The first concrete model of a dS/CFT correspondence, presented in [226], was the proposed duality between that higher spin gravity in four-dimensional dS space and the fermionic $Sp(N)$ vector model in Eq. (8.1.1). The main reason to consider the $Sp(N)$ vector model is that $N \sim 1/(\Lambda G_N)$, where Λ is the cosmological constant and G_N Newton's gravitational constant in the higher spin gravity theory. Thus, changing the sign of the cosmological constant³⁰ amounts to changing the sign of N on the CFT side.

Random tensor models generate, in a diagrammatic expansion à la Feynman, the necessary combinatorial data to describe gluings of simplices in any dimension. In this sense, and after assigning, e.g., a side length to the simplices, they can be used to generate ensembles of discrete random geometric spaces. Among the most studied tensor models are those with an action that is invariant under a $U(N_1) \otimes \cdots \otimes U(N_D)$ symmetry [45]. In these models the tensors are complex and the only allowed contractions are between a tensor and its complex conjugate. The Feynman graphs of these models are therefore bipartite, i.e., their vertices fall into two classes: black and white. Edges connect only black to white vertices, and never vertices of the same class. This ensures that the dual simplicial complexes are orientable. Inspired by the methodology in QFT, where one carefully studies all classes of graphs instead of restricting to just a subclass of diagrams, there arose a wish for tensor models that generate a more general class of diagrams. As an intermediate step, the so-called multi-orientable random tensor models [231] break the $U(N)^3$ symmetry to $U(N) \otimes O(N) \otimes U(N)$, and enlarge the class of diagrams to include certain non-bipartite graphs.³¹ Some years later, tensor models with $O(N_1) \otimes \cdots \otimes O(N_D)$ symmetry [96] were introduced, and these generate a very large class of Feynman diagrams, which includes the graphs of the $U(N_1) \otimes \cdots \otimes U(N_D)$ and multi-orientable models. In particular, the simplicial complexes dual to the Feynman graphs of these models can be nonorientable. In contrast to the other models mentioned, the models with orthogonal symmetry work with real tensors.

The research on $Sp(N)$ random tensor models presented in this thesis continues the study of tensor models with different symmetry groups. It establishes the intimate relation between these models and those with orthogonal symmetry and can be viewed as an explicit example of the formal relationship $O(-N) \simeq Sp(N)$ in the tensor setting. This means that many results on $O(N)$ tensor models, e.g., the classification and combinatorics of their Feynman graphs, can be straight-

²⁹ For the reader interested in renormalization, we note that a version of the symplectic fermion model with a long-range kinetic term was studied in [134] and serves to demonstrate a method for rigorous nonperturbative renormalization.

In this paper a non-Gaussian fixed point of order ϵ in $d = 1, 2, 3$ was constructed.

³⁰ $\Lambda > 0$ corresponds to dS and $\Lambda < 0$ to AdS.

³¹ With this symmetry it is possible to include the tetrahedral interaction which is crucial in many tensor models and also in Chapter 7.

forwardly generalized to $Sp(N)$. In particular Chapter 5 allows to extend the results of [61, 68, 124] on bosonic tensors of order three and five, transforming in irreducible representations of $O(N)$ to fermionic tensor models transforming in the dual (obtained by exchanging symmetrization and antisymmetrization) representation of $Sp(N)$. For example, as mentioned in the summary, the symmetric traceless, respectively antisymmetric, $O(N)$ tensor model is related to the fermionic tensor model transforming in the antisymmetric traceless, respectively symmetric, representation of $Sp(N)$. However, one should be careful when applying the N to $-N$ duality to the $1/N$ expansion of tensor models. In order to obtain such an expansion, the coupling constants of the model must have an explicit dependence on N . For example, the conventional scaling, suitable for a $1/N$ expansion, of the invariant associated with the left graph in Fig. 2.1 in an $O(N)^3$ tensor model would be N^{-3} . These additional factors of N are introduced by hand and do not change sign automatically when the symmetry group is changed. In actual calculations, it is probably advisable to separate the factors of N arising from the tensor model Feynman graphs and are the ones that show the $N \rightarrow -N$ relation, from the explicit scaling with N of the coupling constants, which is needed for a well-defined large N limit.

In the field theory context, the research presented in this thesis lays the foundation for the construction of new CFTs in $d < 4$ dimensions, which could arise at RG fixed points of these theories. For example, considering a fermionic $Sp(N_1) \otimes Sp(N_2) \otimes Sp(N_3)$ theory, the authors of [112] studied fixed points and critical exponents of the corresponding bosonic $O(N_1) \otimes O(N_2) \otimes O(N_3)$ model. In particular, the critical exponents would be of great interest in order to determine whether the CFTs with symplectic symmetry constitute new universality classes. Many very different physical systems often fall into the same universality class, and are thus described by the same CFT when they are at criticality. This universality is probably the most promising way in which tensor field theories could be used as models of certain physical systems.

A remarkable property of tensor models with symplectic or mixed symplectic-orthogonal symmetry is their ability to generate a plethora of fermionic theories. In connection to the SYK model, fermionic tensor models have been considered in $d = 1$ in [91, 92, 104, 116] and in [232–234] even with some symplectic symmetry. However, in more than one dimension, research on fermionic tensor models is sparse, the exception being a tensorial generalization of the Gross–Neveu model [118, 120] in two and three dimensions, and d -dimensional complex tensor models with $U(N) \otimes O(N) \otimes U(N)$ symmetry [117]. A more thorough and systematic understanding of fermionic tensor models would be valuable, as they could unveil phases or critical phenomena that are absent in purely bosonic systems. By mixing fermionic and bosonic degrees of freedom, these models could provide simplified frameworks to study supersymmetry and its potential breaking, or they might give rise to novel statistical physics models—similar to the way self-avoiding walks can be described by a supersymmetric vector model [235, 236] (see also [203] and references therein).

In total, fermionic tensor models could serve as valuable tools in theoretical physics and may offer new perspectives on the behavior of more complex field theories.

8.2 Zero-dimensional $O(N)$ model: constructive expansions and transseries

The work presented in Chapter 6 has established rigorous results on Borel summability and transseries expansions in the zero-dimensional $O(N)$ vector model, by using techniques from constructive

field theory—most notably the LVE and the intermediate field representation.

This part is somewhat separate from the rest of the thesis, as it does not deal with tensors. Furthermore, the model is zero-dimensional and no large N techniques are employed. However, the techniques used in that chapter have been chosen to allow, in principle, a generalization to higher-dimensional or lattice field theory. For example, we did not make use of special functions that appear solely because of the particular model and the fact that the zero-dimensional path integral is merely an ordinary integral.

On the one hand, the zero-dimensional ϕ^4 model, and more generally ϕ^{2k} models for $k \geq 2$, have been extensively studied (see the review [223] and [237]). From a physics perspective, much of the current mathematical literature on resurgence focuses primarily on these zero-dimensional models. On the other hand, the rigorous study of Borel summability in (higher-dimensional) QFT is the object of constructive field theory. The generalization of resurgence results to higher-dimensional field theory is mostly an open topic. In higher dimensions, the partition function does not obey a simple ordinary differential equation, but much more involved integro-differential equations. Moreover, the series coefficients arise from ultraviolet divergent Feynman amplitudes that must be renormalized, which leads to running couplings.

With this background, Chapter 6 revisited the zero-dimensional $O(N)$ model and employed techniques from constructive field theory, most importantly the LVE. These techniques helped gain analytic control of, e.g., the free energy even in the zero-dimensional setting and can be generalized more directly. A novel contribution of this work is the new perspective it provides on the origin of instanton contributions in this model by using the intermediate field representation, where a singularity crosses the integration path and detaches a Hankel contour.

At least two possible ways might be considered to extend the rigorous study of transseries expansions to the physically relevant case of QFT in higher dimensions: One way would be to place the theory on a finite spacetime lattice. In this case, the methods used in Chapter 6 can in principle be applied directly. The integrals become high (but finite) dimensional, which increases the technical complexity of the problem. In the end one would be interested in the limit of large and very fine lattices. Another possibility would be to work directly with renormalizable models in higher dimensions. To treat such models a multiscale version of the LVE was developed in [238] (see also the book [130]). Regarding Borel summability, some progress was made in [192], where it was proven by means of the LVE that the connected correlation functions of a four-dimensional ϕ^4 theory are Borel summable in a RG slice (with fixed cutoffs). The authors of [239] considered a two-dimensional vector model with quartic interaction and proved that the free energy is analytic and Borel summable in a cardioid domain. A lesson to be learned from the work in this thesis is to consider the convergent small N series and the respective moments $Z_n(g)$ and cumulants $W_n(g)$ as intermediate steps to access the free energy $W(g, N)$ also in the higher-dimensional case.

It is not yet clear how the results obtained with the help of a small N expansion interplay with nonperturbative effects that have been studied in the large N expansion of this model (see [240] and [241] for a more recent point of view). An important remark is that the relation between the small and large N expansions involves a rescaling of the coupling constant to g/N . This changes the N dependence of the partition function and the free energy. In addition, the large N expansion is asymptotic and the small N series convergent.

In summary, the results presented in that chapter not only rigorously validate formal transseries

manipulations but could also pave the way for extending these techniques to higher-dimensional quantum field theories, where similar divergence and resurgence phenomena occur.

8.3 Four-dimensional asymptotically free tensor field theory

Asymptotically free QFTs play a fundamental role in our current understanding of nature. A well-known example is QCD, where the coupling is small at high momenta but grows towards the infrared. The divergence of the coupling at a finite infrared scale, predicted by perturbation theory, signals the dynamical generation of a strong interaction scale due to quantum fluctuations. Such behavior is characteristic of asymptotically free theories, and gaining a deeper understanding of this phenomenon—tracking the coupling from the ultraviolet to the strongly correlated infrared regime—in four spacetime dimensions remains a central challenge in QFT. The aim of the work reproduced in Chapter 7 was to establish an example of a theory that is solvable and can be understood all the way from the asymptotically free ultraviolet to the strongly correlated infrared regime.

The model is a tensor field theory invariant under the trifundamental action of $O(N)^3$. In [96] it was established that the theory admits a nontrivial large N limit. This limit allows, in principle, to solve the model in terms of a few closed self-consistent equations for the full propagator (Schwinger–Dyson equation) and the four-point functions (Bethe–Salpeter equation). These equations are most conveniently derived using the 2PI effective action, applied first to tensor models in [99, 119]. The $O(N)^3$ tensor field theory has been studied in $d = 4 - \epsilon$ dimensions in [97] and gives rise to a nontrivial RG fixed point with couplings of order $\sqrt{\epsilon}$. While the model with a short-range propagator in $d < 4$ leads to an unstable CFT at the fixed point [98, 105] a long-range version of the model generates a line of stable infrared fixed points [99, 100, 112]. The situation in exactly four dimensions is different and the known nontrivial fixed points merge with the Gaussian fixed point. Nevertheless it was noticed in [103] that a purely imaginary tetrahedral coupling causes the Gaussian fixed point to be ultraviolet attractive and therefore defines an asymptotically free theory. The analysis in that paper was purely perturbative and could not describe the strongly correlated infrared behavior. The work in Chapter 7 takes a first step in this direction by solving the Schwinger–Dyson equation for the full propagator for a wide range of momentum scales. We emphasize that all solutions require a finite renormalized mass, which eventually stops the renormalization group flow, and thus do not correspond to a renormalization group fixed point in the infrared.

At first sight, the most unconventional property of the model is the purely imaginary tetrahedral coupling that renders the theory non-unitary. However, the tetrahedral interaction

$$\sum_{a,b,c,d,e,f=1}^N \phi_{abc}\phi_{ade}\phi_{fbc}\phi_{fde} \quad (8.3.1)$$

is unbounded below and above, whereas the other two $O(N)^3$ invariant interactions (pillow and double-trace) are positive definite. Thus, as a purely Euclidean QFT the imaginary coupling is required to ensure a bounded path integral. Moreover, because of the large N limit only the square of the tetrahedral coupling contributes and the effective action, as well as all correlation functions, are real. At next-to-leading order in $1/N$ the tetrahedral coupling still receives no direct quantum cor-

rections, but a tadpole with the imaginary tetrahedral interaction is added to the Schwinger–Dyson equation. This tadpole only shifts the bare mass and does not affect the results on the renormalized propagator. Nevertheless, the other two couplings of the model, which will be discussed below, receive small imaginary corrections at next-to-leading order in $1/N$. Thus, beyond leading order, the complex nature of the field theory is no longer hidden by the large N limit. Nevertheless, it appears that the pure large N theory may be a well-defined QFT in which the standard condition of Hermiticity is relaxed. In this way the theory circumvents a no-go theorem by Coleman and Gross for asymptotically free scalar field theories in four dimensions [242]. In general, complex and non-unitary field theories are of their own interest [243, 244], e.g., in condensed matter and statistical physics.

One of the most intriguing results is the observation of a threshold mass m^* , such that only solutions with renormalized mass $m > m^*$ could be obtained. We think that this is not due to a lack of computational capabilities, because we could clearly observe how the running coupling grows larger and larger in the infrared and eventually diverges as $m \searrow m^*$ (Fig. 2.6). One possible interpretation of this result is that it signals an instability of the effective action that wants to transition to a new stable vacuum. Investigating the possibilities of symmetry breaking and bound state formation, which will be discussed below, may shed more light on this scenario and may provide a physical interpretation.

The main motivation for this research is to study an example of an asymptotically free theory that becomes strongly correlated in the infrared, and in this respect the model shares some similarities with QCD. However, it is important to highlight several differences: First, the model does not have a gauge symmetry and related gauge fields. Thus it does not feature effects like color confinement, but avoids the problem to define gauge independent observables. Second, being a scalar under spacetime rotations and translations, the tensor field can generically be massive, unlike a gauge field. Varying the mass allows to investigate the dynamical build-up of strong correlations.

A newly emerging perspective, that was not taken in the paper reproduced in Chapter 7, is to interpret the model’s behavior primarily in terms of the propagator. This is appropriate as the momentum dependence of the running coupling in Eq. (2.3.6) is due solely to $Z(p)$ and thus to a propagator effect. In this view, asymptotic freedom is due to an additional logarithmic decrease of the propagator for high momenta, which effectively suppresses loop (quantum) effects. In turn, the strong correlations in the infrared are caused by stronger loop effects due to the enhanced propagator.

The work in Chapter 7 focused on the propagator and the tetrahedral coupling. The main reason for this is that they are decoupled from the rest of the theory, and the preceding perturbative study in [103] showed that they also drive asymptotic freedom in the other two couplings: g_1 and g_2 . There it was also shown, that although the tetrahedral coupling diverges, g_1 and g_2 attained finite and positive values in the infrared. Nevertheless, a full understanding of the infrared dynamics of the model requires a nonperturbative study of these couplings. The large N limit allows to derive a closed (Bethe–Salpeter) equation that determines the full four-point functions of the g_1 and g_2 interactions. Diagrammatically, it can be represented as a ladder expansion

$$\text{Diagram} = 2g_2 \text{Diagram}_1 + 2g^2 \text{Diagram}_2 - g_2 \text{Diagram}_3 - g^2 \text{Diagram}_4, \quad (8.3.2)$$

where the big four-valent vertex represents the (1PI) four-point function of either the g_1 or g_2 interaction, and edges with a filled bivalent vertex represent again G . For small masses, the renormalized propagator is significantly modified compared to a classical propagator, and this should manifest itself by enhancing loop effects in the above equation. The numerical solution of these equations is being explored in ongoing research by the author and collaborators.

So far, we have only considered the case of unbroken $O(N)^3$ symmetry, in which the vacuum expectation value $\langle\phi_{abc}\rangle$ and all odd correlation functions vanish. On physical grounds, strong correlations could trigger symmetry breaking in the infrared and lead to a non-vanishing vacuum expectation value. Also, as shown in the introduction, the 2PI method is applicable to theories in a symmetry-broken phase. Unfortunately, the large N techniques used here are currently limited to the symmetric regime, since one would need an ansatz for the large N structure of $\langle\phi_{abc}\rangle$. Without a priori knowledge of the specific symmetry breaking pattern, the situation is rather challenging, as the large symmetry group could allow for a plethora of symmetry breaking patterns, and because the tensor valued equations of motion are notoriously hard to solve. See [109] for an example where $O(N)^3$ is broken to $SO(3)$ (in the model with real tetrahedral coupling); [245] for a symmetry breaking pattern of a complex tensor model designed to yield effective matrix theories; and [105] for an SYK-like model.

Another direction for future research is the study of bound state formation due to the strong infrared correlations. Such bound states could appear in the four-point functions of the g_1 and g_2 interactions. In Lorentzian signature, bound states would appear as poles in scattering amplitudes, whereas in the Euclidean setting they would be characterized by factorization of the correlation functions in certain momentum channels. They are of special interest because they could provide a reformulation of the effective degrees of freedom in the deep infrared—analogue to how hadrons emerge as effective degrees of freedom in QCD.

Finally, it would be interesting to study the theory at subleading orders in $1/N$ or at finite N and compare it to the pure large N results. As discussed above, at next-to-leading order only one new diagram contributes and the g_1 and g_2 couplings are expected to get small imaginary parts. Including only the tetrahedral interaction, the next-to-next-to and next-to-next-to-next-to leading order diagrams have been identified in [246]. These subleading orders exhibit an infinite family of diagrams, such that in practice the $1/N$ expansion has to be amended with, e.g., a loop expansion. Nevertheless, the $1/N$ expansion provides a systematic framework for further analysis. The perturbative beta functions, up to next-to-next-to leading order in $1/N$ and three loops have been obtained in [112]. At this order the beta function of the tetrahedral interaction acquires a term quadratic in the couplings, but suppressed in $1/N$. This additional term can lead to new RG fixed points and may eventually spoil the ultraviolet attractiveness of the Gaussian fixed point at relatively small N .

Acknowledgments

First of all, I want to thank my PhD supervisor Răzvan Gurău. He guided me through my doctoral studies, showed me so many wonderful aspects of mathematical physics, and always took the time to share his knowledge with me. We had many lively discussions and I will remember his attitude of always insisting and asking questions until you really understood something. I would also like to thank Johannes Walcher for being referee of this thesis, and the other committee members Lauriane Chomaz and Matthias Bartelmann for their commitment.

Many thanks to the tensor model community for being so welcoming. In particular, I would like to thank Dario Benedetti, Thomas Muller, Thomas Krajewski and Adrian Tanasa with whom I enjoyed a fruitful collaboration. Thanks to Sabine, Davide, Carlos, Luca, and all the other past and present members of our Heidelberg group for bringing some life to Albert-Ueberle-Straße. From the other corners of Philosophenweg, I especially want to thank Björn, Simon and Ruben, as well as my co-authors Thimo and Jürgen Berges. In general, I am deeply grateful to all the people at the ITP and the cluster of excellence STRUCTURES for creating this familial and stimulating atmosphere at the Philosophenweg. This includes of course the secretaries Anja, Besma, Christine, Melanie, Sonja, Ms. Böhmer and Ms. Heinzelmännchen who were always very helpful.

Außerdem danke ich meiner Familie, insbesondere meinen Eltern, für ihre jahrelange Unterstützung, für die Sicherheit die sie mir gegeben haben und dafür, dass sie meine vielen Interessen gefördert haben. Vielen Dank auch an alle meine guten Studienfreunde aus Heidelberg für viele so unvergesslich schöne Jahre. Zu guter Letzt möchte ich meiner Frau Sophie danken, für ihre Liebe, für ihre Unterstützung und dafür, dass sie zusammen mit unserer kleinen Sonja so viel Freude in mein Leben bringt.

Bibliography

1. Gurau, R. & Keppler, H. Duality of orthogonal and symplectic random tensor models. *Ann. Inst. Henri Poincaré D: Comb. Phys. Interact.* **12** (2025), no. 2, 319–362. arXiv: 2207.01993 [math-ph].
2. Keppler, H. & Muller, T. Duality of orthogonal and symplectic random tensor models: general invariants. *Lett. Math. Phys.* **113** (2023), no. 4, article no. 83. arXiv: 2304.03625 [hep-th].
3. Keppler, H., Krajewski, T., Muller, T. & Tanasa, A. Duality of $O(N)$ and $Sp(N)$ random tensor models: tensors with symmetries. *J. Phys. A* **56** (2023), no. 49, 495206. arXiv: 2307.01527 [math-ph].
4. Benedetti, D., Gurau, R., Keppler, H. & Lettera, D. The small- N series in the zero-dimensional $O(N)$ model: constructive expansions and transseries. *Annales Henri Poincaré* **25** (2024), 5367–5428. arXiv: 2210.14776 [hep-th].
5. Berges, J., Gurau, R., Keppler, H. & Preis, T. Coupling renormalization flow in the strongly interacting regime of an asymptotically free quantum field theory in four dimensions. *Phys. Rev. D* **110** (2024), no. 3, 036007. arXiv: 2405.08153 [hep-th].
6. Ambjørn, J., Durhuus, B. & Jonsson, T. Three-dimensional simplicial quantum gravity and generalized matrix models. *Mod. Phys. Lett. A* **6** (1991), 1133–1146.
7. Sasakura, N. Tensor model for gravity and orientability of manifold. *Mod. Phys. Lett. A* **6** (1991), 2613–2624.
8. Gross, M. Tensor models and simplicial quantum gravity in > 2 -D. *Nucl. Phys. B Proc. Suppl.* **25** (1992), 144–149.
9. Di Francesco, P., Ginsparg, P. H. & Zinn-Justin, J. 2-d gravity and random matrices. *Phys. Rept.* **254** (1995), 1–133. arXiv: hep-th/9306153.
10. Wishart, J. The generalised product moment distribution in samples from a normal multivariate population. *Biometrika* **20A** (1928), no. 1-2, 32–52.
11. Wigner, E. P. Characteristic vectors of bordered matrices with infinite dimensions. *Ann. Math.* **62** (1955), no. 3, 548–564.
12. 't Hooft, G. A planar diagram theory for strong interactions. *Nucl. Phys. B* **72** (1974), 461.
13. Tutte, W. T. A census of planar maps. *Can. J. Math.* **15** (1963), 249–271.
14. Schaeffer, G. Bijective census and random generation of Eulerian planar maps with prescribed degrees. *Electron. J. Comb.* **4** (1997).
15. Cori, R. & Schaeffer, G. Description trees and Tutte formulas. *Theor. Comput. Sci.* **292** (2003), 165–183.

16. Chapuy, G., Marcus, M. & Schaeffer, G. A bijection for rooted maps on orientable surfaces. *SIAM J. Discrete Math.* **23** (2009), no. 3, 1587–1611.
17. Brezin, E., Itzykson, C., Parisi, G. & Zuber, J. B. Planar diagrams. *Commun. Math. Phys.* **59** (1978), 35.
18. Eynard, B. *Counting Surfaces. CRM Aisenstadt Chair lectures* Birkhäuser Basel, 2016.
19. David, F. Planar diagrams, two-dimensional lattice gravity and surface models. *Nucl. Phys. B* **257** (1985), 45.
20. Kazakov, V. A., Migdal, A. A. & Kostov, I. K. Critical properties of randomly triangulated planar random surfaces. *Phys. Lett. B* **157** (1985), 295–300.
21. Ambjørn, J., Durhuus, B. & Fröhlich, J. Diseases of triangulated random surface models, and possible cures. *Nucl. Phys. B* **257** (1985), 433–449.
22. Kazakov, V. A. Bilocal regularization of models of random surfaces. *Phys. Lett. B* **150** (1985), 282–284.
23. Le Gall, J.-F. Uniqueness and universality of the Brownian map. *Ann. Probab.* **41** (2013), no. 4, 2880–2960.
24. Miermont, G. The Brownian map is the scaling limit of uniform random plane quadrangulations. *Acta Mathematica* **210** (2013), no. 2, 319–401.
25. Duplantier, B. & Sheffield, S. Liouville quantum gravity and KPZ. *Invent. Math.* **185** (2011), no. 2, 333–393. arXiv: 0808.1560 [math.PR].
26. Miller, J. & Sheffield, S. Liouville quantum gravity and the Brownian map I: The QLE(8/3,0) metric. *Invent. math.* **219** (2020), 75–152. arXiv: 1507.00719 [math.PR].
27. Duplantier, B. & Sheffield, S. Schramm–Loewner evolution and Liouville quantum gravity. *Phys. Rev. Lett.* **107** (2011), 131305. arXiv: 1012.4800 [math-ph].
28. Sheffield, S. What is a random surface? *Proc. Int. Cong. Math.* (2022), 1202–1258. arXiv: 2203.02470 [math.PR].
29. Kazakov, V. A. Ising model on a dynamical planar random lattice: exact solution. *Phys. Lett. A* **119** (1986), 140–144.
30. David, F. Conformal field theories coupled to 2d gravity in the conformal gauge. *Mod. Phys. Lett. A* **3** (1988), 1651.
31. Kazakov, V. A. The appearance of matter fields from quantum fluctuations of 2d gravity. *Mod. Phys. Lett. A* **4** (1989), 2125.
32. Ambjørn, J., Jurkiewicz, J. & Makeenko, Y. M. Multiloop correlators for two-dimensional quantum gravity. *Phys. Lett. B* **251** (1990), 517–524.
33. Brezin, E., Douglas, M. R., Kazakov, V. & Shenker, S. H. The Ising model coupled to 2-D gravity: a nonperturbative analysis. *Phys. Lett. B* **237** (1990), 43–46.
34. Dijkgraaf, R., Verlinde, H. L. & Verlinde, E. P. Loop equations and Virasoro constraints in nonperturbative 2-D quantum gravity. *Nucl. Phys. B* **348** (1991), 435–456.

35. Fukuma, M., Kawai, H. & Nakayama, R. Continuum Schwinger–Dyson equations and universal structures in two-dimensional quantum gravity. *Int. J. Mod. Phys. A* **6** (1991), 1385–1406.
36. Makeenko, Y. Loop equations and Virasoro constraints in matrix models. In: *25th International Ahrenshoop Symposium on the Theory of Elementary Particles* 1991. arXiv: hep-th/9112058.
37. Knizhnik, V. G., Polyakov, A. M. & Zamolodchikov, A. B. Fractal structure of 2d quantum gravity. *Mod. Phys. Lett. A* **3** (1988), 819.
38. Gross, D. J. & Migdal, A. A. Nonperturbative two-dimensional quantum gravity. *Phys. Rev. Lett.* **64** (1990), 127.
39. Douglas, M. R. & Shenker, S. H. Strings in less than one-dimension. *Nucl. Phys. B* **335** (1990), 635.
40. Brezin, E. & Kazakov, V. A. Exactly solvable field theories of closed strings. *Phys. Lett. B* **236** (1990), 144–150.
41. Gurau, R. Colored Group Field Theory. *Commun. Math. Phys.* **304** (2011), 69–93. arXiv: 0907.2582 [hep-th].
42. Gurau, R. The $1/N$ expansion of colored tensor models. *Ann. Henri Poincaré* **12** (2011), 829–847. arXiv: 1011.2726 [gr-qc].
43. Gurau, R. & Rivasseau, V. The $1/N$ expansion of colored tensor models in arbitrary dimension. *EPL* **95** (2011), no. 5, 50004. arXiv: 1101.4182 [gr-qc].
44. Bonzom, V., Gurau, R., Riello, A. & Rivasseau, V. Critical behavior of colored tensor models in the large N limit. *Nucl. Phys. B* **853** (2011), 174–195. arXiv: 1105.3122 [hep-th].
45. Bonzom, V., Gurau, R. & Rivasseau, V. Random tensor models in the large N limit: uncoloring the colored tensor models. *Phys. Rev. D* **85** (2012), 084037. arXiv: 1202.3637 [hep-th].
46. Gurau, R. The complete $1/N$ expansion of colored tensor models in arbitrary dimension. *Ann. Henri Poincaré* **13** (2012), 399–423. arXiv: 1102.5759 [gr-qc].
47. Gurau, R. The $1/N$ expansion of tensor models beyond perturbation theory. *Commun. Math. Phys.* **330** (2014), 973–1019. arXiv: 1304.2666 [math-ph].
48. Gurau, R. *Random Tensors* 1st ed. Oxford University Press, Oxford, 2017.
49. Gurau, R. Lost in Translation: Topological Singularities in Group Field Theory. *Class. Quant. Grav.* **27** (2010), 235023. arXiv: 1006.0714 [hep-th].
50. Aldous, D. The continuum random tree. I. *Ann. Probab.* **19** (1991), no. 1, 1–28.
51. Gurau, R. & Ryan, J. P. Melons are branched polymers. *Ann. Henri Poincaré* **15** (2014), no. 11, 2085–2131. arXiv: 1302.4386 [math-ph].
52. Kamiński, W., Oriti, D. & Ryan, J. P. Towards a double-scaling limit for tensor models: probing sub-dominant orders. *New J. Phys.* **16** (2014), 063048. arXiv: 1304.6934 [hep-th].
53. Gurau, R. & Schaeffer, G. Regular colored graphs of positive degree. *Ann. Inst. Henri Poincaré Comb. Phys. Interact. A* **3** (2016), no. 3, 257–320. arXiv: 1307.5279 [math.CO].

54. Dartois, S., Gurau, R. & Rivasseau, V. Double scaling in tensor models with a quartic interaction. *JHEP* **09** (2013), 088. arXiv: 1307.5281 [hep-th].
55. Bonzom, V., Gurau, R., Ryan, J. P. & Tanasa, A. The double scaling limit of random tensor models. *JHEP* **09** (2014), 051. arXiv: 1404.7517 [hep-th].
56. Gurau, R., Tanasa, A. & Youmans, D. R. The double scaling limit of the multi-orientable tensor model. *EPL* **111** (2015), no. 2, 21002. arXiv: 1505.00586 [hep-th].
57. Bonzom, V., Nador, V. & Tanasa, A. Double scaling limit for the $O(N)^3$ -invariant tensor model. *J. Phys. A* **55** (2022), no. 13, 135201. arXiv: 2109.07238 [hep-th].
58. Gurau, R. Universality for random tensors. *Ann. Inst. H. Poincaré Probab. Statist.* **50** (2014), no. 4, 1474–1525. arXiv: 1111.0519 [math.PR].
59. Benedetti, D., Carrozza, S., Toriumi, R. & Valette, G. Multiple scaling limits of $U(N)^2 \times O(D)$ multi-matrix models. *Ann. Inst. H. Poincaré D Comb. Phys. Interact.* **9** (2022), no. 2, 367–433. arXiv: 2003.02100 [math-ph].
60. Carrozza, S., Ferrari, F., Tanasa, A. & Valette, G. On the large D expansion of Hermitian multi-matrix models. *J. Math. Phys.* **61** (2020), no. 7, 073501. arXiv: 2003.04152 [hep-th].
61. Carrozza, S. & Harribey, S. Melonic large N limit of 5-index irreducible random tensors. *Commun. Math. Phys.* **390** (2022), no. 3, 1219–1270. arXiv: 2104.03665 [math-ph].
62. Gurau, R. A generalization of the Virasoro algebra to arbitrary dimensions. *Nucl. Phys. B* **852** (2011), 592–614. arXiv: 1105.6072 [hep-th].
63. Gurau, R. The Schwinger Dyson equations and the algebra of constraints of random tensor models at all orders. *Nucl. Phys. B* **865** (2012), 133–147. arXiv: 1203.4965 [hep-th].
64. Dartois, S., Rivasseau, V. & Tanasa, A. The $1/N$ expansion of multi-orientable random tensor models. *Ann. Henri Poincaré* **15** (2014), no. 5, 965–984.
65. Gurau, R. The $1/N$ expansion of tensor models with two symmetric tensors. *Commun. Math. Phys.* **360** (2018), no. 3, 985–1007. arXiv: 1706.05328 [hep-th].
66. Ferrari, F., Rivasseau, V. & Valette, G. A new large N expansion for general matrix–tensor models. *Commun. Math. Phys.* **370** (2019), no. 2, 403–448. arXiv: 1709.07366 [hep-th].
67. Klebanov, I. R. & Tarnopolsky, G. On large N limit of symmetric traceless tensor models. *JHEP* **10** (2017), 037. arXiv: 1706.00839 [hep-th].
68. Benedetti, D., Carrozza, S., Gurau, R. & Kolanowski, M. The $1/N$ expansion of the symmetric traceless and the antisymmetric tensor models in rank three. *Commun. Math. Phys.* **371** (2019), no. 1, 55–97. arXiv: 1712.00249 [hep-th].
69. Bonzom, V. Another proof of the $1/N$ expansion of the rank three tensor model with tetrahedral interaction. (2019). arXiv: 1912.11104 [math-ph].
70. Bonzom, V., Delepouve, T. & Rivasseau, V. Enhancing non-melonic triangulations: A tensor model mixing melonic and planar maps. *Nucl. Phys. B* **895** (2015), 161–191. arXiv: 1502.01365 [math-ph].
71. Ambjørn, J. & Loll, R. Causal dynamical triangulations: gateway to nonperturbative quantum gravity. (2024). arXiv: 2401.09399 [hep-th].

72. Lionni, L. & Marckert, J.-F. Iterated foldings of discrete spaces and their limits: candidates for the role of Brownian map in higher dimensions. *Math. Phys. Anal. Geom.* **24** (2021), no. 4, 39. arXiv: 1908.02259 [math.PR].
73. Budd, T. & Lionni, L. A family of triangulated 3-spheres constructed from trees. (2022). arXiv: 2203.16105 [math.CO].
74. Carrozza, S. Tensor models and group field theories: combinatorics, large N and renormalization. In: *Encyclopedia of Mathematical Physics (2nd ed.)* Academic Press, Oxford, 2025, 578–594. arXiv: 2404.07834 [math-ph].
75. Oriti, D. The microscopic dynamics of quantum space as a group field theory. In: *Foundations of Space and Time: Reflections on Quantum Gravity* Cambridge University Press, 2011, 257–320. arXiv: 1110.5606 [hep-th].
76. Krajewski, T. Group field theories. In: *Proceedings of 3rd Quantum Gravity and Quantum Geometry School — PoS(QGQGS 2011)* **140**. 2013, 005.
77. Boulatov, D. V. A model of three-dimensional lattice gravity. *Mod. Phys. Lett. A* **7** (1992), 1629–1646. arXiv: hep-th/9202074.
78. Ooguri, H. Topological lattice models in four-dimensions. *Mod. Phys. Lett. A* **7** (1992), 2799–2810. arXiv: hep-th/9205090.
79. Baratin, A., Carrozza, S., Oriti, D., Ryan, J. & Smerlak, M. Melonic phase transition in group field theory. *Lett. Math. Phys.* **104** (2014), 1003–1017. arXiv: 1307.5026 [hep-th].
80. Ben Geloun, J. & Rivasseau, V. A renormalizable 4-dimensional tensor field theory. *Commun. Math. Phys.* **318** (2013), 69–109. arXiv: 1111.4997 [hep-th].
81. Rivasseau, V. Quantum gravity and renormalization: the tensor track. *AIP Conf. Proc.* **1444** (2012), no. 1, 18–29. arXiv: 1112.5104 [hep-th].
82. Sachdev, S. & Ye, J. Gapless spin fluid ground state in a random, quantum Heisenberg magnet. *Phys. Rev. Lett.* **70** (1993), 3339. arXiv: cond-mat/9212030.
83. Kitaev, A. *A simple model of quantum holography*. Talks 1 and 2 at KITP (2015).
84. Teitelboim, C. Gravitation and Hamiltonian structure in two space-time dimensions. *Phys. Lett. B* **126** (1983), 41–45.
85. Jackiw, R. Lower dimensional gravity. *Nucl. Phys. B* **252** (1985), 343–356.
86. Maldacena, J. & Stanford, D. Remarks on the Sachdev-Ye-Kitaev model. *Phys. Rev. D* **94** (2016), no. 10, 106002. arXiv: 1604.07818 [hep-th].
87. Maldacena, J., Stanford, D. & Yang, Z. Conformal symmetry and its breaking in two dimensional nearly anti-de-Sitter space. *PTEP* **2016** (2016), no. 12, 12C104. arXiv: 1606.01857 [hep-th].
88. Stanford, D. & Witten, E. Fermionic localization of the Schwarzian theory. *JHEP* **10** (2017), 008. arXiv: 1703.04612 [hep-th].
89. Maldacena, J., Shenker, S. H. & Stanford, D. A bound on chaos. *JHEP* **08** (2016), 106. arXiv: 1503.01409 [hep-th].

90. Mertens, T. G. & Turiaci, G. J. Solvable models of quantum black holes: a review on Jackiw–Teitelboim gravity. *Living Rev. Rel.* **26** (2023), no. 1, 4. arXiv: 2210.10846 [hep-th].
91. Witten, E. An SYK-like model without disorder. *J. Phys. A* **52** (2019), no. 47, 474002. arXiv: 1610.09758 [hep-th].
92. Klebanov, I. R. & Tarnopolsky, G. Uncolored random tensors, melon diagrams, and the Sachdev–Ye–Kitaev models. *Phys. Rev. D* **95** (2017), no. 4, 046004. arXiv: 1611.08915 [hep-th].
93. Gurau, R. The complete $1/N$ expansion of a SYK-like tensor model. *Nucl. Phys. B* **916** (2017), 386–401. arXiv: 1611.04032 [hep-th].
94. Gurau, R. G. Notes on tensor models and tensor field theories. *Ann. Inst. H. Poincaré D: Comb. Phys. Interact.* **9** (2022), no. 1, 159–218. arXiv: 1907.03531 [hep-th].
95. Benedetti, D. The melonic large- N limit in quantum field theory. Habilitation à diriger des recherches (Institut Polytechnique de Paris, 2023). HAL Id: tel-04040245.
96. Carrozza, S. & Tanasa, A. $O(N)$ random tensor models. *Lett. Math. Phys.* **106** (2016), no. 11, 1531–1559. arXiv: 1512.06718 [math-ph].
97. Giombi, S., Klebanov, I. R. & Tarnopolsky, G. Bosonic tensor models at large N and small ϵ . *Phys. Rev. D* **96** (2017), no. 10, 106014. arXiv: 1707.03866 [hep-th].
98. Benedetti, D. Instability of complex CFTs with operators in the principal series. *JHEP* **05** (2021), 004. arXiv: 2103.01813 [hep-th].
99. Benedetti, D., Gurau, R. & Harribey, S. Line of fixed points in a bosonic tensor model. *JHEP* **06** (2019), 053. arXiv: 1903.03578 [hep-th].
100. Benedetti, D., Gurau, R., Harribey, S. & Suzuki, K. Hints of unitarity at large N in the $O(N)^3$ tensor field theory. *JHEP* **02** (2020). [Erratum: JHEP 08, 167 (2020)], 072. arXiv: 1909.07767 [hep-th].
101. Benedetti, D., Gurau, R. & Suzuki, K. Conformal symmetry and composite operators in the $O(N)^3$ tensor field theory. *JHEP* **06** (2020), 113. arXiv: 2002.07652 [hep-th].
102. Harribey, S. Renormalization in tensor field theory and the melonic fixed point. PhD thesis (Heidelberg U., 2022). arXiv: 2207.05520 [hep-th].
103. Berges, J., Gurau, R. & Preis, T. Asymptotic freedom in a strongly interacting scalar quantum field theory in four Euclidean dimensions. *Phys. Rev. D* **108** (2023), no. 1, 016019. arXiv: 2301.09514 [hep-th].
104. Peng, C., Spradlin, M. & Volovich, A. A supersymmetric SYK-like tensor model. *JHEP* **05** (2017), 062. arXiv: 1612.03851 [hep-th].
105. Kim, J., Klebanov, I. R., Tarnopolsky, G. & Zhao, W. Symmetry breaking in coupled SYK or tensor models. *Phys. Rev. X* **9** (2019), no. 2, 021043. arXiv: 1902.02287 [hep-th].
106. Pakrouski, K., Klebanov, I. R., Popov, F. & Tarnopolsky, G. Spectrum of Majorana quantum mechanics with $O(4)^3$ symmetry. *Phys. Rev. Lett.* **122** (2019), no. 1, 011601. arXiv: 1808.07455 [hep-th].
107. Popov, F. K. Supersymmetric tensor model at large N and small ϵ . *Phys. Rev. D* **101** (2020), no. 2, 026020. arXiv: 1907.02440 [hep-th].

108. Benedetti, D., Delporte, N., Harribey, S. & Sinha, R. Sextic tensor field theories in rank 3 and 5. *JHEP* **06** (2020), 065. arXiv: 1912.06641 [hep-th].
109. Benedetti, D. & Costa, I. $SO(3)$ -invariant phase of the $O(N)^3$ tensor model. *Phys. Rev. D* **101** (2020), no. 8, 086021. arXiv: 1912.07311 [hep-th].
110. De Mello Koch, R., Gossman, D., Hasina Tahiridimbisoa, N. & Mahu, A. L. Holography for tensor models. *Phys. Rev. D* **101** (2020), no. 4, 046004. arXiv: 1910.13982 [hep-th].
111. Benedetti, D. & Delporte, N. Remarks on a melonic field theory with cubic interaction. *JHEP* **04** (2021), 197. arXiv: 2012.12238 [hep-th].
112. Benedetti, D., Gurau, R. & Harribey, S. Trifundamental quartic model. *Phys. Rev. D* **103** (2021), no. 4, 046018. arXiv: 2011.11276 [hep-th].
113. Harribey, S. Sextic tensor model in rank 3 at next-to-leading order. *JHEP* **10** (2022), 037. arXiv: 2109.08034 [hep-th].
114. Jepsen, C. & Oz, Y. RG flows and fixed points of $O(N)^r$ models. *JHEP* **02** (2024), 035. arXiv: 2311.09039 [hep-th].
115. Bulychева, K., Klebanov, I. R., Milekhin, A. & Tarnopolsky, G. Spectra of operators in large N tensor models. *Phys. Rev. D* **97** (2018), no. 2, 026016. arXiv: 1707.09347 [hep-th].
116. Choudhury, S., Dey, A., Halder, I., Janagal, L., Minwalla, S. & Poojary, R. Notes on melonic $O(N)^{q-1}$ tensor models. *JHEP* **06** (2018), 094. arXiv: 1707.09352 [hep-th].
117. Prakash, S. & Sinha, R. A complex Fermionic tensor model in d dimensions. *JHEP* **02** (2018), 086. arXiv: 1710.09357 [hep-th].
118. Benedetti, D., Carrozza, S., Gurau, R. & Sfondrini, A. Tensorial Gross-Neveu models. *JHEP* **01** (2018), 003. arXiv: 1710.10253 [hep-th].
119. Benedetti, D. & Gurau, R. 2PI effective action for the SYK model and tensor field theories. *JHEP* **05** (2018), 156. arXiv: 1802.05500 [hep-th].
120. Benedetti, D. & Delporte, N. Phase diagram and fixed points of tensorial Gross-Neveu models in three dimensions. *JHEP* **01** (2019), 218. arXiv: 1810.04583 [hep-th].
121. Klebanov, I. R., Milekhin, A., Popov, F. & Tarnopolsky, G. Spectra of eigenstates in fermionic tensor quantum mechanics. *Phys. Rev. D* **97** (2018), no. 10, 106023. arXiv: 1802.10263 [hep-th].
122. Giombi, S., Klebanov, I. R., Popov, F., Prakash, S. & Tarnopolsky, G. Prismatic large N models for bosonic tensors. *Phys. Rev. D* **98** (2018), no. 10, 105005. arXiv: 1808.04344 [hep-th].
123. Gurau, R. & Rivasseau, V. Quantum gravity and random tensors. (2024). arXiv: 2401.13510 [hep-th].
124. Carrozza, S. Large N limit of irreducible tensor models: $O(N)$ rank-3 tensors with mixed permutation symmetry. *JHEP* **06** (2018), 39. arXiv: 1803.02496 [hep-th].
125. Osterwalder, K. & Schrader, R. Axioms for Euclidean Green's functions. *Commun. Math. Phys.* **31** (1973), 83–112.
126. Osterwalder, K. & Schrader, R. Axioms for Euclidean Green's Functions. 2. *Commun. Math. Phys.* **42** (1975), 281.

127. Wightman, A. S. & Gøarding, L. Fields as operator-valued distributions in relativistic quantum theory. *Arkiv f. Fysik, Kungl. Svenska Vetenskapsak* **28** (1964), 129–189.
128. Streater, R. F. & Wightman, A. S. *PCT, Spin and Statistics, and All That* Princeton University Press, 1989.
129. Jaffe, A. Constructive quantum field theory. In: *Mathematical Physics 2000* Imperial College Press, 111–127. eprint: <https://arthurjaffe.com/Assets/pdf/CQFT.pdf>.
130. Rivasseau, V. *From Perturbative to Constructive Renormalization* Princeton University Press, 2014.
131. Gawedzki, K. & Kupiainen, A. Massless lattice φ_4^4 theory: a nonperturbative control of a renormalizable model. *Phys. Rev. Lett.* **54** (1985), 92–94.
132. Feldman, J., Magnen, J., Rivasseau, V. & Seneor, R. Construction and Borel summability of infrared ϕ_4^4 by a phase space expansion. *Commun. Math. Phys.* **109** (1987), 437–480.
133. Aizenman, M. & Duminil-Copin, H. Marginal triviality of the scaling limits of critical 4D Ising and ϕ_4^4 models. *Annals Math.* **194** (2021), no. 1, 163. arXiv: 1912.07973 [math-ph].
134. Giuliani, A., Mastropietro, V. & Rychkov, S. Gentle introduction to rigorous renormalization group: a worked fermionic example. *JHEP* **01** (2021), 026. arXiv: 2008.04361 [hep-th].
135. Kupiainen, A. Rigorous renormalization group. *Nature Phys.* **19** (2023), no. 11, 1539–1541.
136. Wilson, K. G. Renormalization group and critical phenomena. 1. Renormalization group and the Kadanoff scaling picture. *Phys. Rev. B* **4** (1971), 3174–3183.
137. Wilson, K. G. Renormalization group and critical phenomena. 2. Phase space cell analysis of critical behavior. *Phys. Rev. B* **4** (1971), 3184–3205.
138. Wilson, K. G. & Kogut, J. B. The Renormalization group and the epsilon expansion. *Phys. Rept.* **12** (1974), 75–199.
139. Wilson, K. G. The renormalization group: critical phenomena and the Kondo problem. *Rev. Mod. Phys.* **47** (1975), 773.
140. Kadanoff, L. P. Scaling laws for Ising models near $T(c)$. *Physics Physique Fizika* **2** (1966), 263–272.
141. Weinberg, S. *The Quantum Theory of Fields. Vol. 2: Modern Applications* Cambridge University Press, 2013.
142. Gross, D. J. & Wilczek, F. Ultraviolet behavior of nonabelian gauge theories. *Phys. Rev. Lett.* **30** (1973), 1343–1346.
143. Politzer, H. D. Reliable perturbative results for strong interactions? *Phys. Rev. Lett.* **30** (1973), 1346–1349.
144. Workman, R. L. *et al.* Review of Particle Physics. *PTEP* **2022** (2022). (Particle Data Group), 083C01.
145. Achard, P. *et al.* Measurement of the running of the electromagnetic coupling at large momentum-transfer at lep. *Phys. Lett. B* **623** (2005). (L3 Collaboration), 26–36. arXiv: hep-ex/0507078.

146. Gawedzki, K. & Kupiainen, A. Exact renormalization for the Gross–Neveu model of quantum fields. *Phys. Rev. Lett.* **54** (1985), 2191–2194.
147. Gawedzki, K. & Kupiainen, A. Gross–Neveu model through convergent perturbation expansions. *Commun. Math. Phys.* **102** (1985), 1.
148. Feldman, J., Magnen, J., Rivasseau, V. & Seneor, R. Massive Gross–Neveu model: a rigorous perturbative construction. *Phys. Rev. Lett.* **54** (1985), 1479–1481.
149. Feldman, J., Magnen, J., Rivasseau, V. & Seneor, R. A renormalizable field theory: the massive Gross–Neveu model in two-dimensions. *Commun. Math. Phys.* **103** (1986), 67–103.
150. Disertori, M. & Rivasseau, V. Continuous constructive fermionic renormalization. *Annales Henri Poincaré* **1** (2000), 1–57. arXiv: hep-th/9802145.
151. Salmhofer, M. & Wieczorkowski, C. Construction of the renormalized $\text{GN}_{2-\epsilon}$ trajectory. *Math. Phys. Electron. J.* **6** (2000), 1–18.
152. Aizenman, M. Proof of the triviality of ϕ_D^4 field theory and some mean field features of Ising models for $d > 4$. *Phys. Rev. Lett.* **47** (1981), 1–4.
153. Aizenman, M. Geometric analysis of ϕ^4 fields and Ising models (parts 1 & 2). *Commun. Math. Phys.* **86** (1982), 1.
154. Fröhlich, J. On the triviality of $\lambda\phi_d^4$ theories and the approach to the critical point in $d \geq 4$ dimensions. *Nucl. Phys. B* **200** (1982), 281–296.
155. Witten, E. & Jaffe, A. Quantum Yang–Mills theory. (2000).
156. Douglas, M. R. Report on the status of the Yang–Mills millenium prize problem. (2004).
157. Faddeev, L. D. Mass in quantum Yang–Mills theory: comment on a Clay millenium problem. (2009). arXiv: 0911.1013 [math-ph].
158. Witten, E. Topological quantum field theory. *Commun. Math. Phys.* **117** (1988), 353.
159. Cornwall, J. M., Jackiw, R. & Tomboulis, E. Effective Action for Composite Operators. *Phys. Rev. D* **10** (1974), 2428–2445.
160. Berges, J. N-particle irreducible effective action techniques for gauge theories. *Phys. Rev. D* **70** (2004), 105010. arXiv: hep-ph/0401172.
161. Berges, J., Borsanyi, S., Reinosa, U. & Serreau, J. Nonperturbative renormalization for 2PI effective action techniques. *Annals Phys.* **320** (2005), 344–398. arXiv: hep-ph/0503240.
162. Blaizot, J.-P., Iancu, E. & Reinosa, U. Renormalization of Φ -derivable approximations in scalar field theories. *Nucl. Phys. A* **736** (2004), 149–200. arXiv: hep-ph/0312085.
163. Blaizot, J.-P., Pawłowski, J. M. & Reinosa, U. Exact renormalization group and Φ -derivable approximations. *Phys. Lett. B* **696** (2011), 523–528. arXiv: 1009.6048 [hep-ph].
164. Berges, J. & Serreau, J. Progress in nonequilibrium quantum field theory. In: *5th International Conference on Strong and Electroweak Matter* 2003, 111–126. arXiv: hep-ph/0302210.
165. Berges, J. & Serreau, J. Progress in nonequilibrium quantum field theory II. In: *6th International Conference on Strong and Electroweak Matter* 2005, 102–116. arXiv: hep-ph/0410330.

166. Berges, J. Introduction to nonequilibrium quantum field theory. *AIP Conf. Proc.* **739** (2004), no. 1, 3–62. arXiv: hep-ph/0409233.
167. Berges, J. Controlled nonperturbative dynamics of quantum fields out-of-equilibrium. *Nucl. Phys. A* **699** (2002), 847–886. arXiv: hep-ph/0105311.
168. Aarts, G., Ahrensmeier, D., Baier, R., Berges, J. & Serreau, J. Far from equilibrium dynamics with broken symmetries from the 2PI - $1/N$ expansion. *Phys. Rev. D* **66** (2002), 045008. arXiv: hep-ph/0201308.
169. Salpeter, E. E. Wave functions in momentum space. *Phys. Rev.* **84** (1951), 1226–1231.
170. Salpeter, E. E. & Bethe, H. A. A relativistic equation for bound state problems. *Phys. Rev.* **84** (1951), 1232–1242.
171. Poland, D., Rychkov, S. & Vichi, A. The conformal bootstrap: theory, numerical techniques, and applications. *Rev. Mod. Phys.* **91** (2019), 015002. arXiv: 1805.04405 [hep-th].
172. Carrington, M. E., Fu, W.-J., Mikula, P. & Pickering, D. Four-point vertices from the 2PI and 4PI effective actions. *Phys. Rev. D* **89** (2014), no. 2, 025013. arXiv: 1310.4352 [hep-ph].
173. Aoyama, T., Hayakawa, M., Kinoshita, T. & Nio, M. Tenth-order QED contribution to the electron $g-2$ and an improved value of the fine structure constant. *Phys. Rev. Lett.* **109** (11 2012), 111807.
174. Volkov, S. Calculation of the total 10th order QED contribution to the electron magnetic moment. *Phys. Rev. D* **110** (3 2024), 036001.
175. Aoyama, T., Hayakawa, M., Hirayama, A. & Nio, M. Verification of the tenth-order QED contribution to the anomalous magnetic moment of the electron from diagrams without fermion loops. *Phys. Rev. D* **111** (3 2025), L031902.
176. Le Guillou, J. C. & Zinn-Justin, J. Critical exponents for the n -vector model in three dimensions from field theory. *Phys. Rev. Lett.* **39** (2 1977), 95–98.
177. Kompaniets, M. V. & Panzer, E. Minimally subtracted six-loop renormalization of $O(n)$ -symmetric ϕ^4 theory and critical exponents. *Phys. Rev. D* **96** (3 2017), 036016.
178. Heisenberg, W. & Euler, H. Consequences of Dirac’s theory of positrons. *Z. Phys.* **98** (1936), no. 11-12, 714–732. arXiv: physics/0605038.
179. Schwinger, J. S. On gauge invariance and vacuum polarization. *Phys. Rev.* **82** (1951), 664–679.
180. Affleck, I. K., Alvarez, O. & Manton, N. S. Pair Production at Strong Coupling in Weak External Fields. *Nucl. Phys. B* **197** (1982), 509–519.
181. Tanasa, A. *Combinatorial physics. combinatorics, quantum field theory, and quantum gravity models* 1st ed. Oxford University Press, Oxford, 2021.
182. Borel, É. Mémoire sur les séries divergentes. *Ann. Sci. Éc. Norm. Supér.* **3 16** (1899), 9–131.
183. Caliceti, E., Meyer-Hermann, M., Ribeca, P., Surzhykov, A. & Jentschura, U. D. From useful algorithms for slowly convergent series to physical predictions based on divergent perturbative expansions. *Phys. Rept.* **446** (2007), 1–96. arXiv: 0707.1596 [physics.comp-ph].
184. Sokal, A. D. An improvement of Watson’s theorem on Borel summability. *J. Math. Phys.* **21** (1980), 261–263.

185. Nevanlinna, F. Zur Theorie der asymptotischen Potenzreihen. *Ann. Acad. Sci. Fenn. Ser. A* **12** (1916), no. 3, 81.
186. Grecchi, V. & Maioli, M. Borel summability beyond the factorial growth. *Ann. Inst. Henri Poincaré, Phys. Théor.* **41** (1984), 37–47.
187. Grecchi, V. & Maioli, M. Generalized logarithmic Borel summability. *J. Math. Phys.* **25** (1984), no. 12, 3439–3443.
188. Witten, E. Analytic continuation of Chern–Simons theory. *AMS/IP Stud. Adv. Math.* **50** (2011), 347–446. arXiv: 1001.2933 [hep-th].
189. Dunne, G. & Ünsal, M. What is QFT? Resurgent trans-series, Lefschetz thimbles, and new exact saddles. In: *Proceedings of The 33rd International Symposium on Lattice Field Theory — PoS(LATTICE 2015)* **251**. 2016, 010.
190. Brydges, D. C. & Kennedy, T. Mayer expansions and the Hamilton-Jacobi equation. *Journal of Statistical Physics* **48** (1987), 19–49.
191. Abdesselam, A. & Rivasseau, V. Trees, forests and jungles: a botanical garden for cluster expansions. *Lect. Notes Phys.* **446** (1995), 7. arXiv: hep-th/9409094.
192. Magnen, J. & Rivasseau, V. Constructive ϕ^4 field theory without tears. *Annales Henri Poincaré* **9** (2008), 403–424. arXiv: 0706.2457 [math-ph].
193. Rivasseau, V. & Wang, Z. Loop vertex expansion for Φ^{2k} theory in zero dimension. *J. Math. Phys.* **51** (2010), 092304. arXiv: 1003.1037 [math-ph].
194. Rivasseau, V. & Wang, Z. Constructive renormalization for Φ_2^4 theory with loop vertex expansion. *J. Math. Phys.* **53** (2012), 042302. arXiv: 1104.3443 [math-ph].
195. Rivasseau, V. & Wang, Z. Corrected loop vertex expansion for Φ_2^4 theory. *J. Math. Phys.* **56** (2015), no. 6, 062301. arXiv: 1406.7428 [math-ph].
196. Rivasseau, V. Constructive matrix theory. *JHEP* **09** (2007), 008. arXiv: 0706.1224 [hep-th].
197. Magnen, J., Noui, K., Rivasseau, V. & Smerlak, M. Scaling behaviour of three-dimensional group field theory. *Class. Quant. Grav.* **26** (2009), 185012. arXiv: 0906.5477 [hep-th].
198. Delepouve, T. & Rivasseau, V. Constructive tensor field theory: the T_3^4 model. *Commun. Math. Phys.* **345** (2016), no. 2, 477–506. arXiv: 1412.5091 [math-ph].
199. Gurau, R. G. & Krajewski, T. Analyticity results for the cumulants in a random matrix model. *Ann. Inst. H. Poincaré D Comb. Phys. Interact.* **2** (2015), no. 2, 169–228. arXiv: 1409.1705 [math-ph].
200. Krajewski, T., Rivasseau, V. & Sazonov, V. Constructive matrix theory for higher order interaction. *Annales Henri Poincaré* **20** (2019), no. 12, 3997–4032. arXiv: 1712.05670 [math-ph].
201. Krajewski, T., Rivasseau, V. & Sazonov, V. Constructive matrix theory for higher order interaction II: Hermitian and real symmetric cases. *Annales Henri Poincaré* **23** (2022), no. 10, 3431–3452. arXiv: 1910.13261 [math-ph].
202. Gurau, R., Rivasseau, V. & Sfondrini, A. Renormalization: an advanced overview. (2014). arXiv: 1401.5003 [hep-th].

203. Bauerschmidt, R., Brydges, D. C. & Slade, G. *Introduction to a Renormalisation Group Method* arXiv: 1907.05474 [math-ph]. Springer, 2019.
204. King, R. C. The dimensions of irreducible tensor representations of the orthogonal and symplectic groups. *Can. J. Math.* **23** (1971), no. 1, 176–188.
205. King, R. C. Modification rules and products of irreducible representations of the unitary, orthogonal, and symplectic groups. *Journal of Mathematical Physics* **12** (1971), no. 8, 1588–1598.
206. Cvitanović, P. & Kennedy, A. D. Spinors in negative dimensions. *Phys. Scripta* **26** (1982), 5.
207. Parisi, G. & Sourlas, N. Random magnetic fields, supersymmetry, and negative dimensions. *Phys. Rev. Lett.* **43** (11 1979), 744–745.
208. Ramgoolam, S. Comment on two-dimensional $O(N)$ and $Sp(N)$ Yang–Mills theories as string theories. *Nuclear Physics B* **418** (1994), no. 1, 30–44. arXiv: 9307085 [hep-th].
209. Cvitanović, P. *Group Theory. Birdtracks, Lie’s, and Exceptional Groups* Princeton University Press, Princeton, N.J., 2008.
210. Mkrtchyan, R. L. & Veselov, A. P. On duality and negative dimensions in the theory of Lie groups and symmetric spaces. *Journal of Mathematical Physics* **52** (2011), no. 8, 083514.
211. Mkrtchian, R. L. The equivalence of $Sp(2N)$ and $SO(-2N)$ gauge theories. *Phys. Lett. B* **105** (1981), 174–176.
212. LeClair, A. Quantum critical spin liquids, the 3D Ising model, and conformal field theory in 2+1 dimensions. (2006). arXiv: cond-mat/0610639.
213. LeClair, A. & Neubert, M. Semi-lorentz invariance, unitarity, and critical exponents of symplectic fermion models. *JHEP* **10** (2007) . arXiv: 0705.4657 [hep-th].
214. Bond, A. D., Litim, D. F. & Steudtner, T. Asymptotic safety with Majorana fermions and new large N equivalences. *Phys. Rev. D* **101** (4 2020) . arXiv: 1911.11168 [hep-th].
215. Mulase, M. & Waldron, A. Duality of orthogonal and symplectic matrix integrals and quaternionic feynman graphs. *Commun. Math. Phys.* **240** (2003), 553–586. arXiv: math-ph/0206011.
216. Dunne, G. V. Negative-dimensional groups in quantum physics. *Journal of Physics A: Mathematical and General* **22** (1989), no. 11, 1719.
217. Brauer, R. On algebras which are connected with the semisimple continuous groups. *Annals of mathematics* **38** (1937), no. 4, 857–872.
218. Bulgakova, D. V., Goncharov, Y. O. & Helpin, T. Construction of the traceless projection of tensors via the Brauer algebra. *arXiv e-prints* (2022) . arXiv: 2212.14496 [math.RT].
219. Écalle, J. *Les fonctions résurgentes. Vol. I-III* 247. Université de Paris-Sud, Département de Mathématique, Orsay, 1981.
220. Zinn-Justin, J. Perturbation series at large orders in quantum mechanics and field theories: application to the problem of resummation. *Phys. Rept.* **70** (1981), 109.
221. Mariño, M. Lectures on non-perturbative effects in large N gauge theories, matrix models and strings. *Fortsch. Phys.* **62** (2014), 455–540. arXiv: 1206.6272 [hep-th].

222. Dorigoni, D. An introduction to resurgence, trans-series and alien calculus. *Annals Phys.* **409** (2019), 167914. arXiv: 1411.3585 [hep-th].
223. Aniceto, I., Basar, G. & Schiappa, R. A primer on resurgent transseries and their asymptotics. *Phys. Rept.* **809** (2019), 1–135. arXiv: 1802.10441 [hep-th].
224. Rivasseau, V. & Wang, Z. How to resum feynman graphs. *Annales Henri Poincaré* **15** (2014), no. 11, 2069–2083. arXiv: 1304.5913 [math-ph].
225. Saleur, H. Polymers and percolation in two-dimensions and twisted N=2 supersymmetry. *Nucl. Phys. B* **382** (1992), 486–531. arXiv: hep-th/9111007.
226. Anninos, D., Hartman, T. & Strominger, A. Higher spin realization of the dS/CFT correspondence. *Class. Quant. Grav.* **34** (2017), no. 1. arXiv: 1108.5735 [hep-th].
227. Vasiliev, M. A. Consistent equation for interacting gauge fields of all spins in (3+1)-dimensions. *Phys. Lett. B* **243** (1990), 378–382.
228. Zinn-Justin, J. *Quantum Field Theory and Critical Phenomena* Oxford University Press, 2002.
229. Strominger, A. The dS/CFT correspondence. *JHEP* **10** (2001), 034. arXiv: hep-th/0106113.
230. Klebanov, I. R. & Polyakov, A. M. AdS dual of the critical $O(N)$ vector model. *Phys. Lett. B* **550** (2002), 213–219. arXiv: hep-th/0210114.
231. Tanasa, A. Multi-orientable group field theory. *J. Phys. A* **45** (2012), 165401. arXiv: 1109.0694 [math.CO].
232. Gubser, S. S., Heydeman, M., Jepsen, C., Parikh, S., Saberi, I., Stoica, B. & Trundy, B. Melonic theories over diverse number systems. *Phys. Rev. D* **98** (2018), no. 12. arXiv: 1707.01087 [hep-th].
233. Gubser, S. S., Jepsen, C., Ji, Z. & Trundy, B. Higher melonic theories. *JHEP* **09** (2018), 049. arXiv: 1806.04800 [hep-th].
234. Carrozza, S. & Pozsgay, V. SYK-like tensor quantum mechanics with $Sp(N)$ symmetry. *Nucl. Phys. B* **941** (2019), 28–52. arXiv: 1809.07753 [hep-th].
235. McKane, A. J. Reformulation of $n \rightarrow 0$ models using anticommuting scalar fields. *Phys. Lett. A* **76** (1980), 22–24.
236. Parisi, G. & Sourlas, N. Self avoiding walk and supersymmetry. *J. Physique Lett.* **41** (17 1980), 403–405.
237. Fauvet, F., Menous, F. & Quéva, J. Resurgence and holonomy of the ϕ^{2k} model in zero dimension. *J. Math. Phys.* **61** (2020), no. 9, 092301. arXiv: 1910.01606 [math-ph].
238. Gurau, R. & Rivasseau, V. The multiscale loop vertex expansion. *Annales Henri Poincaré* **16** (2015), no. 8, 1869–1897. arXiv: 1312.7226 [math-ph].
239. Erbin, H., Lahoche, V. & Tamaazousti, M. Constructive expansion for vector field theories I. Quartic models in low dimensions. *J. Math. Phys.* **62** (2021), no. 4, 043501. arXiv: 1904.05933 [hep-th].
240. Hikami, S. & Brezin, E. Large-order behaviour of the $1/N$ expansion in zero and one dimensions. *Journal of Physics A: Mathematical and General* **12** (1979), no. 6, 759.

- 241. Di Pietro, L., Mariño, M., Sberveglieri, G. & Serone, M. Resurgence and $1/N$ expansion in integrable field theories. *Journal of High Energy Physics* **2021** (2021), no. 10, 166, 166. arXiv: 2108.02647 [hep-th].
- 242. Coleman, S. R. & Gross, D. J. Price of asymptotic freedom. *Phys. Rev. Lett.* **31** (1973), 851–854.
- 243. Fisher, M. E. Yang–Lee edge singularity and ϕ^3 field theory. *Phys. Rev. Lett.* **40** (1978), 1610–1613.
- 244. Gromov, N., Kazakov, V. & Korchemsky, G. Exact correlation functions in conformal fishnet theory. *JHEP* **08** (2019), 123. arXiv: 1808.02688 [hep-th].
- 245. Diaz, P. & Rosabal, J. A. Spontaneous symmetry breaking in tensor theories. *JHEP* **01** (2019), 094. arXiv: 1809.10153 [hep-th].
- 246. Bonzom, V., Nador, V. & Tanasa, A. Diagrammatics of the quartic $O(N)^3$ -invariant Sachdev–Ye–Kitaev-like tensor model. *J. Math. Phys.* **60** (2019), no. 7, 072302. arXiv: 1903.01723 [hep-th].